AKADEMIE DER WISSENSCHAFTEN DER DDR

ZfK

ZENTRALINSTITUT FÜR KERNFORSCHUNG
ROSSENDORF BEI DRESDEN

ZfK – 638

ANNUAL REPORT 1987 ON NUCLEAR PHYSICS ACTIVITIES AND APPLICATIONS

Zentralinstitut für Kernforschung, Rossendorf
Technische Universität, Dresden
Karl-Marx-Universität, Leipzig
Humboldt-Universität, Berlin
Bergakademie Freiberg

Edited by K. Hohmuth
Edditorial staff: H. W. Barz, F. Dönau, F. Flagmeyer, M. Friedrich, W. D. Fromm, H. Märten, K. Möller, J. Mösner, F. Naehring, S. Unterricker, G. Winter

April 1988

ISSN 0138-2950

Postanschrift: Akademie der Wissenschaften der DDR
Zentralinstitut für Kernforschung Rossendorf
Postschließfach 19
Dresden
8051
Deutsche Demokratische Republik

Diese Publikation wurde in der Abteilung Information des Zentralinstitutes für Kernforschung hergestellt

III-12-12 J 1339/88

INDC/GDR/-053/G

AKADEMIE DER WISSENSCHAFTEN DER DDR

Z E N T R A L I N S T I T U T F Ü R K E R N F O R S C H U N G
R O S S E N D O R F B E I D R E S D E N

ZfK - 638

ANNUAL REPORT 1987
ON NUCLEAR PHYSICS ACTIVITIES AND APPLICATIONS

Zentralinstitut für Kernforschung, Rossendorf

Technische Universität, Dresden

Karl-Marx-Universität, Leipzig

Humboldt-Universität, Berlin

Bergakademie Freiberg

Edited by K. Hohmuth

Edditorial staff: H.W. Barz, F. Dönau, F. Flagmeyer, M. Friedrich, W.D. Fromm, H. Märten, K. Möller, J. Mösner, F. Naehring, S. Unterricker, G. Winter

April 1988

CONTENTS

	page
Nuclear Reactions	1
Nuclear Spectroscopy	19
Theory	27
Applied Methods	43
Accelerators	93
Nuclear Electronics and Methods	96
Computational Methods and Codes	115
List of Publications, Academic Promotions, Lectures and Conference Contributions, Scientific Meetings, Patents and Awards of Honour	118

INHALTSVERZEICHNIS

	Seite
Kernreaktionen	1
Kernspektroskopie	19
Kern- und Festkörpertheorie	27
Anwendungsorientierte Arbeiten	43
Beschleuniger	93
Elektronik und methodische Arbeiten	96
Rechenprogramme	115
Liste der Veröffentlichungen, Diplomarbeiten, Promotionen, Vorträge, Veranstaltungen, Patente, wissenschaftliche Preise und Auszeichnungen	118

СОДЕРЖАНИЕ

	стр
Ядерные реакции	I
Ядерная спектроскопия	I9
Теория	27
Прикладные методы ядерной физики	43
Ускорители	93
Ядерная электроника и методы измерения	96
Вычислительный центр и программное обеспечение	II5
Список публикаций и докладов	II8

CONTRIBUTIONS

NUCLEAR REACTIONS

page

Deuteron fragmentation at relativistic energies
H. Müller 1

Alpha-proton diffraction scattering at 8.9 GeV/c
V.G. Ableev, B. Naumann, A.A. Nomofilov, N.M. Piskunov, V.I. Sharov, I.M. Sitnik, E.A. Strokovsky, L.N. Strunov, S.A. Zaporozhets, S. Dshemuchadse, S. Tesch 2

A measurement of the forward differential cross section of the reaction $H(n,d)\gamma$ at E_n = 25.6 MeV
P. Michel, K. Möller, J. Mösner, G. Schmidt 3

On the evolution of the mass asymmetry in damped heavy-ion collisions
P. Gippner, K.D. Schilling, F. Stary, E. Will, K. Heidel, S.M. Lukyanov, Yu.E. Penionzhkevich, V.S. Salamatin, H. Sodan, G.G. Chubarian, R. Schmidt 4

Description of heavy-ion collisions by use of trajectory-model calculations
G. Zwicker 5

Yield measurement of long-range alpha particle (LRA) accompanied fission of ^{238}U and ^{232}Th induced by 13.5 MeV deuterons
R. Kotte, D. Wohlfarth 6

Correlation measurement of alpha particle accompanied fission induced in the reaction 13.5 MeV d + ^{238}U
R. Kotte, E. Hentschel, H.-G. Ortlepp, K.-D. Schilling, W. Seidel, F. Stary, G. Zwicker 7

Angular distributions of prompt γ-rays accompanying the "ternary" fission of ^{252}Cf
W. Pilz, W. Neubert, K. Arnold, D. Lucas, H. Märten 9

The neutron spectrum from neutron-induced fission of ^{232}Th
H. Märten, D. Richter, A. Ruben, D. Seeliger, G.N. Lovchikova, S.E. Sukhikh, A.M. Trufanov 10

Theoretical interpretation of $^{252}Cf(sf)$ neutron data
H. Märten 11

Semi-empirical description of fission fragment mass yield curves
D. Lucas, H. Märten 12

Differential neutron-emission cross-sections of ^{238}U bombarded with 14 MeV neutrons
T. Elfruth, T. Hehl, H. Kalka, H. Märten, H. Payrovan, A. Ruben, D. Seeliger, K. Seidel, S. Unholzer 13

SMD/SMC-model for practical application
H. Kalka, M. Torjman, D. Seeliger 14

Determination of the parameters of U-235 fission-foils
K. Merla 15

Optimization of the fission cross-section measurement of ^{238}U at 5 MeV neutron energy using the TCAPM
U. Todt, C.-M. Herbach 16

page

Absolute measurement of the ^{238}U fission cross-section at 5 MeV neutron energy using the TCAPM
C.-M. Herbach, K. Merla, G. Musiol, H.-G. Ortlepp, G. Pausch, R. Perez, U. Todt, I.D. Alkhasov, E.A. Ganza, V.A. Kalinin, O.I. Kostochkin, L.L. Solin, P.S. Soloshenkov, S.M. Solovjev 17

The influence of neutron inelastic scattering anisotropy on the neutron leakage spectrum of a lead sphere
M. Toepfer, B. Böhmer, C. Reiche 18

NUCLEAR SPECTROSCOPY

Evidence for a new isomer in the doubly-odd nucleus ^{84}Rb
J. Döring, G. Winter, L. Funke, L. Käubler, W. Wagner 19

A new isomer in ^{83}Br excited in the ^{82}Se ($^{7}Li,\alpha$ 2n) reaction
G. Winter, R. Schwengner, L. Funke, E. Will 20

A new three-particle isomer in ^{85}Kr
G. Winter, R. Schwengner, L. Funke, J. Döring 21

A strongly retarded E2 transition in ^{86}Kr
G. Winter, J. Döring, L. Funke, H. Prade 22

High-spin states in the N=48 nucleus ^{86}Sr
A.E. Zobov, A.S. Mishin, H. Rotter, G. Winter, L. Funke, H. Prade 23

A new three-quasiparticle isomer in ^{117}Sb
L.K. Kostov, L.G. Kostova, W. Andrejtscheff, H. Prade, J. Döring, R. Schwengner 24

In-beam study of ^{142}Nd
H. Prade, J. Döring, W. Enghardt, L. Funke, L. Käubler, R. Schwengner, G. Winter 25

Shell-model description of ^{142}Nd
H. Prade, J. Döring, W. Enghardt, L. Funke, L. Käubler, J. Blomqvist 26

THEORIE

On the canonical realization of a finite-dimensional Lie algebra
G. Flach, D. Kirschbaum 27

The effective axial-charge formfactor of the nucleon in neutron-rich nuclei
M. Kirchbach 28

Nuclear stopping power and the two-fluid hydrodynamics
H.W. Barz, B. Kämpfer 30

The concept of the formation length in the intranuclear cascade model
H. Iwe 31

Hypernuclear production by the (π^+,K^+) reaction
R Wünsch, J. Zofka 32

Percolation approach for atomic and molecular cluster formation
O. Knospe, R. Schmidt, G. Seifert 33

page

First stages of matter growth in a dynamical percolation model
J. Knoll, O. Knospe, R. Schmidt 34

Preferential emission of fast particles to negative angles within the two-stage model
M. Biedermann, P. Mädler 35

Particle escape from time-dependent mean fields
B. Milek, R. Reif 36

Gamow states in an explicitly time-dependent model
B. Milek, G. Mutschke, R. Reif 37

Order out of chaos in atomic nuclei
I. Rotter 38

Computer experiments of the lateral solid phase transformation of Si-layers for SOI
H.-J. Müller, K.-H. Heinig 40

Electronic stopping cross-sections for the MeV implantation of B^+ and P^+ into silicon
M. Posselt, W. Skorupa 41

Determination of splitting parameter functions for neutron shielding calculations based on non-analogue Monte Carlo method
G.-R. Jaenisch, F. Seidel 42

APPLIED METHODS

Standard functions in the case of fibre textures
S. Matthies, K. Helming, T. Steinkopff, K. Kunze 43

A nearly isometric representation of the space of Eulerian angles (G-space)
K. Helming, S. Matthies, G.W. Vinel 44

Numerical aspects of the normal distribution in the orientation space
S. Matthies, G.W. Vinel 45

Discrete statistical treatment of texture development
T. Steinkopff, S. Matthies 46

Partial structure functions for amorphous $Fe_{83}B_{17}$
W. Matz, A.V. Serebryakov, Yu.A. Levin 47

A method for the variation of the neutron scattering length density in solvating materials
F. Eichhorn, F. Häußler 48

Secondary extinction in texture analysis by neutron diffraction
A. Mücklich, P. Klimanek 49

Determination of damage profiles by PIXE measurements
C. Ascheron, R. Flagmeyer, J. Vogt, G. Otto, A. Schindler 50

A comparative positron study of the production of vacancy defects in particle irradiated GaP, InP and Si single crystals
C. Ascheron, G. Dlubek, R. Krause, H. Erhard 51

page

Extended defects in hydrogen implanted GaP single crystals
C. Ascheron, H. Bartsch 52

Relation between microhardness and damage density in ion bombarded GaP
C. Ascheron, H. Neumann, G. Otto, V.N. Bugrov, S.A. Karamyan 53

Proton bombardment induced volume changes and lattice disorder in InP, GaAs, GaP, Ge and Si
C. Ascheron, A. Schindler, R. Flagmeyer, G. Otto 54

Lattice stress and detrimental effects of high-fluence hydrogen implantation
C. Ascheron, A. Schindler, A. Setzer 55

RBS/channeling study of (In,Ga)As/GaAs single strained-layer heterostructures
R. Flagmeyer, M. Höricke 56

Determination of strain in (In,Ga)As/GaAs strained-layer superlattices by ion channeling
R. Flagmeyer, K. Lenkeit, Yu.O. Kanter, A.A. Fjodorov 57

Method for gettering of fast diffusing impurities in device structures
C. Ascheron, H. Klose, W. Frentrup 58

A simple device for elemental analysis of samples with an external proton beam
D. Lehmann, B. Krause, U. Lehmann, R. Wipper 59

Fluorine profiling applied to dental practice
H.-E. Zschau, F. Plier, G. Otto, C. Wyrwich, A. Treide 60

Elemental analysis of lignite samples by means of PIXE
J. Vogt, G. Otto, C. Wischnewski 61

PIXE and RBS elemental analysis of coal liquids
W. Knolle, G. Otto 62

Hydrogen analysis by means of the nuclear reaction $^{1}H(^{15}N,\alpha)^{12}C$
D. Grambole, F. Herrmann, W. Rudolph 63

Investigation of pieco ceramics with the Rossendorf nuclear microprobe
F. Herrmann, D. Grambole, W. Rudolph 64

Hydrogen depth profiling on Hf-sputtered Cr-Si resistance layers
C. Neelmeijer, D. Grambole, C. Heiser, F. Herrmann, R. Grötzschel, W. Rudolph, G. Sobe, H. Schreiber, G. Weise, H. Grießmann, A. Heinrich 65

Application of the Bragg ionization chamber for ERD
E. Hentschel, R. Kotte, H.-G. Ortlepp, F. Stary, D. Wohlfarth 66

An experimental arrangement for ^{35}Cl-induced ERD-analysis at the 5 MV Tandem accelerator
C. Neelmeijer, H. Böhme, K. Brankoff, L. Kumpf, W. Rudolph 67

Nondestructive analysis of paintings by a 4 MeV external proton beam
C. Neelmeijer, H. Matthes, W. Pfestorf, H.-P. Schramm 68

page

Determination of the content of natural activities in shielding materials by the intensity of X-ray fluorescent peaks
S. Unterricker, Kim Jung Ho, W. Stolz 69

Moessbauer investigations of dioctahedral pegmatitic micas
C. Pietzsch, W. Schmidt 70

Standardization problems of CPAA measurements in geological samples
D. Degering, S. Unterricker, W. Stolz 71

Application of thin layer activation (TLA) on investigation of cavitation processes
K. Eichhorn, E. Richter 72

Semiconductor secondary electron detector for imaging with ion microbeam
L. Bischoff, F.K. Naehring, M. Deutscher 73

A MOSFET-based sensor for detection of low energy electrons and ions
M. Teichfuß 74

Analysis of Ar ion beam etching induced surface damage of GaAs by means of ^{64}Cu adsorption/autoradigraphy and RBS/channeling - angular dependence and rapid thermal annealing
A. Schindler, R. Fechner, R. Flagmeyer, D. Panknin, F. Bigl 75

Nitrogen and oxygen profiles of ion beam synthesized silicon oxynitride layers determined by elastic recoil detection
W. Skorupa, E. Hentschel, R. Kotte, F. Stary, K. Wollschläger 77

Electrical activation of boron implanted silicon during the early stage of rapid thermal annealing
R. Kögler, E. Wieser, A. Armigliato, E. Landi, S. Solmi 78

The effect of oxygen on electrical activation and diffusion of arsenic in silicon by RTA
R. Kögler, E. Wieser 79

Electrical activation of arsenic atoms in ion beam recrystallized silicon layers
M. Voelskow, W. Skorupa, J. Matthäi 80

Patterning of the underlaying SiO_2-layer as a method of producing grain boundary free silicon stripes on insulating substrates
J. Matthäi, M. Voelskow, K.-H. Stegemann 81

Silicon and chromium distribution in implanted and short time annealed GaAs
D. Panknin, Ya.B. Fattachov, C.E. Richter, M. Gericke 82

Short time threshold for electrical activation of implanted and annealed GaAs
D. Panknin, E. Wieser, Ya.B. Fattachov, I.B. Khaibullin 83

The structure of probe environments in implanted tetrahedrally coordinated semiconductors
S. Unterricker 84

The electrophysical properties of anodic silicon oxide films using Ar^+ implanted starting material
G. Mende, F. Fenske, H. Flietner 85

page

Mathematical modelling of the capacitance characteristics and the threshold voltage of a MOS structure on a thin silicon substrate
N. Sieber, G. Otto 86

Controlling the width of the melting zone in an equipment for lateral zone melting
K. Wollschläger, J. Matthäi, K. Butter, M. Voelskow 87

Data files for photon mass attenuation coefficients in the energy range up to 150 keV
S. Fritzsche, G. Zschornack 88

Detection ratio calculations of a Johansson type crystal spectrometer with mosaic crystals
M. Schneider, A. Reichmann, G.Zschornack, M. Schiekel 89

Nd, Yb, Au and U L-subshell ionization probabilities by 92 MeV Ar impact
H. Schmidt-Böcking, A. Skutlartz, W. Schadt, M. Wassermann, G. Nolte, N. Roller, G. Zschornack 90

A method for ionization cross section evaluation from X-ray spectra
P. Neumann, F. Stefan, G. Zschornack, M. Schiekel 92

ACCELERATORS

Operation and improvement of the cyclotron U-120
B. Anders, R. Brückner, H. Büttig, H. Guratzsch, P. Hartmann, G. Kerber, H. Odrich, S. Preusche, H. Tyrroff, J. Weißig 93

Operation of the electrostatic accelerators in 1987
W. Bürger, S. Turuc 94

An improved extraction system for a RF ion source
M. Friedrich, S. Turuc 95

NUCLEAR ELECTRONICS AND METHODS

Investigation of low-pressure grid avalance counters
W. Seidel, H.-G. Ortlepp 96

Real time digital processing of Bragg ionization chamber signals
A. Romaguera, W.D. Fromm, H.-G. Ortlepp 97

Test experiments with a detector system consisting of a DGAC and a large solid angle BIC
A. Matthies, R. Kotte, H.-G. Ortlepp, W. Seidel 98

Application of Bragg curve spectroscopy to charge identification in nuclear fragmentation
L.N. Andronenko, A.A. Kotov, V.I. Panichev, L.A. Vaishnene, W. Neubert 99

Test of read-out methods with delay lines
W. Neubert, J. Hutsch 100

Cs(Tl) scintillation detector with photodiode readout
R. Schwengner, Th. Scholz, G. Winter, J. Rüdiger, U. Lorenz 101

page

Energy dependence of the prompt reference in γ - r.f. coincidence experiments
L.G. Kostova, L. Käubler, H. Prade, G. Winter 102

Electronic developments of the KFL group
H.-G. Ortlepp, E. Schuster, A. Rink 103

Electronic developments of the KFM-group
W.D. Fromm, F. Schwarzenberg 104

Compact multi-channel analyser ZfK 5193
W.D. Fromm, H. Angermann, H.-G. Ortlepp 105

Dynamic studies at the Rossendorf gamma-camera
W.D. Fromm, R. Bergmann 106

A stationary positron camera with high-density avalanche chambers
W. Enghardt, W.D. Fromm, P. Manfraß, M. Sobiella 107

The processing of the stationary positron camera data
W. Enghardt, W.D. Fromm, P. Manfraß 108

In-vivo imaging with the stationary positron camera
W. Enghardt, P. Manfraß, D. Wohlfarth, R. Bergmann, G.J. Beyer, J. Steinbach, R. Bauer, K. Günther 109

An investigation of the uranium distribution in reactor fuel elements
G. Winter, W.D. Fromm, W. Schulze, Th. Scholz, M. Freitag, R. Schwengner 110

Neutron leakage from an uranium sphere fed with 14 MeV neutrons
T. Elfruth, T. Hehl, M. Töpfer, D. Seeliger, K. Seidel, S. Unholzer, G. Streubel, D. Albert, W. Hansen, C. Reiche, W. Vogel, D.V. Markovskij, G.E. Shatalov 111

Optimal neutron shielding by an iron-water assembly
E. Rodriguez, K. Seidel, K. Noack 112

Test of a tritium adsorption system for a high flux neutron generator
U. Gohs 113

Mylar foil as an exit window for an external beam
D. Lehmann 114

COMPUTATIONAL METHODS AND CODES

OS/8 FORTRAN IV routines for use with CAMAC
U. Katesscenka, G. Pausch 115

Personal computer program package for ion-optical problems
J. Teichert, D. Janssen, M.A. Tiunov 116

BASCIC program to modelling of RBS spectra on the microcomputer of the EDR 184
F. Plier, H.-E. Zschau 117

NUCLEAR REACTIONS

DEUTERON FRAGMENTATION AT RELATIVISTIC ENERGIES

H. Müller
Zentralinstitut für Kernforschung Rossendorf, Bereich KF

Recently the proton spectra at 0° from the reactions C(d,p)X (ref. /1/) and p(d,p)X (ref. /2/) at 9 GeV/c have been measured almost until the kinematical limit. Around 300 MeV/c momentum the proton yield is clearly underestimated by model calculations /1/ based on Glauber theory and known deuteron wave functions where the argument is expressed in terms of light cone variables. According to ref. /1/ this discrepancy reflects the presence of a six-quark admixture in the deuteron wave function and by adjusting the corresponding parameters the spectrum could be described in the whole momentum region measured.

Here, another approach is proposed which differs mainly in the following two points. Instead of light cone variables we employ the usual treatment with an off-shell participant and the argument of the wave function given by the spectator momentum. To describe the participant-target interaction a model for hadronic collisions /3/ is used which takes into account practically all possible final channels. This turnes out to be essential because the various channels are connected with different upper limits of the spectator momentum. The summation over all channels reproduces the characteristic deformation of the momentum spectrum observed in the experiment. As shown in fig. 1 the whole spectrum is satisfactorily described by using the Paris deuteron wave function /4/. There are no free parameters in the calculations, since the yields are normalized to the elastic and inelastic nucleon-nucleon cross sections and the parameters of model /3/ are adjusted to proton-proton data.

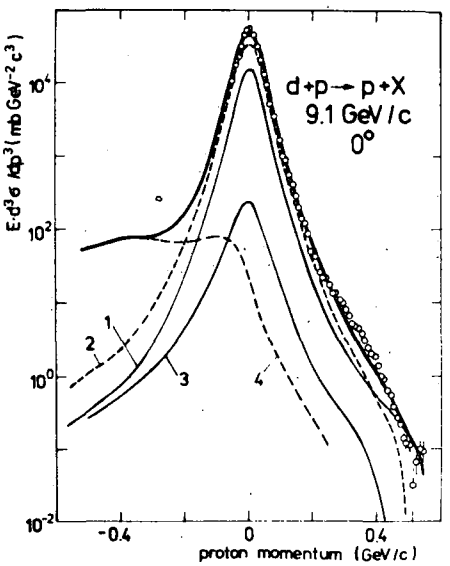

Fig. 1
Invariant cross section versus proton momentum in the deuteron rest frame. Curve 1 (2) represents spectator, curve 3 (4) participant contributions coming from quasi-elastic (quasi-free inelastic) collisions. Data are from ref. /2/.

R e f e r e n c e s

/1/ Ableev, V.G. et al., Nucl. Phys. A393 (1983) 491

/2/ Zaporozhets, S.A. et al., Proceedings of the VIII. Int. Seminar on High Energy Physics Problems, Dubna 1986, JINR report D1, 2-86-668, p. 341

/3/ Barz. H.W., Müller, H., Schulz, H., NBI Preprint NBI-87-34 (1987)

/4/ Lacombe, M. et al., Phys. Lett. 101B (1981) 139

ALPHA-PROTON DIFFRACTION SCATTERING AT 8.9 GeV/c

V.G. Ableev, B. Naumann, A.A. Nomofilov, N.M. Piskunov, V.I. Sharov, I.M. Sitnik, E.A. Strokovsky, L.N. Strunov and S.A. Zaporozhets
Joint Institute for Nuclear Research, Dubna, USSR
S. Dshemuchadse and S. Tesch
Zentralinstitut für Kernforschung, Rossendorf, Bereich KF

It is known that model calculations within the Glauber-Sitenko multiple scattering theory agree rather well with experimental data of high-energy hadron-nucleus diffraction scattering. However, when going into details- e.g. looking for the absolute values of differential cross sections or the position of the diffraction minimum- then clear discrepancies can be seen even if one takes into account very carefully shadowing effects and the realistic wavefunction of the nucleus. So, the authors of ref./1/ were forced to introduce quark degrees of freedom to describe $p\,^4He$ and $\pi\,^4He$ data. On the contrary, in ref./2/ it was shown that one has necessarily to consider the complicated structure of the nucleon-nucleon scattering amplitude to reproduce $p\alpha$ data of a large energy range.

In this situation new data of the diffractive scattering of composite particles may help to clarify the theoretical situation. In ref./3/ we published differential cross sections of alpha diffractive scattering using C, Al, Cu and Pb targets. Here we present new data of the $\alpha\,^1H$ scattering obtained with the magnet spectrometer "ALPHA". The external beam of α particles with momentum of 8.9 GeV/c of the JINR synchrophasotron was incident on a cryogenic hydrogen target (thickness 2.5 g/cm^2). About 280000 triggers have been recorded with momentum resolution of 0.7% and angular resolution of 0.8 mrad. The raw data set has been corrected with respect to the geometrical properties of the set-up, absorption effects along the spectrometer axis and multiple Coulomb scattering in the target. The details of the experiment and the procedure of off-line analysis can be found in ref./3/.

The experimental result is given in table 1. The range of the four-momentum transfer squared $|t|$ covered is presented in fig.1, where one can compare our new data with earlier $\alpha\,^1H$ Dubna measurements at $\sqrt{s}$ = 7.0 GeV (see ref./4/) and SPS /FNAL/ ISR data at very high c.m. energies.

References

/1/ Dakhno L.G. and Nikolaev N.N.; Nucl. Phys. A436 (1985) 653
/2/ Jenkovszky L.L. et al.; report ITP-87-37E, Kiev 1987
/3/ Ableev V. G. et al.; report ZfK-607 (1986)
/4/ Ableev V.G. et al.; Acta Phys. Pol. B16 (1985) 913

$\|t\|$ (GeV/c)^2	$d\sigma/dt$ (b/(GeV/c)^2)	$\|t\|$ (GeV/c)^2	$d\sigma/dt$ (b/ (GeV/c)^2)
0.00446	0.992 ± 0.046	0.0437	0.282 ± 0.010
0.00572	0.855 ± 0.035	0.0475	0.267 ± 0.010
0.00715	0.798 ± 0.030	0.0515	0.225 ± 0.009
0.00873	0.788 ± 0.021	0.0556	0.200 ± 0.0089
0.0105	0.729 ± 0.017	0.0599	0.1888 ± 0.0086
0.0124	0.728 ± 0.016	0.0643	0.1690 ± 0.0084
0.0144	0.700 ± 0.015	0.0689	0.1402 ± 0.0077
0.0167	0.686 ± 0.014	0.0737	0.1240 ± 0.0073
0.0190	0.623 ± 0.013	0.0786	0.1037 ± 0.0069
0.0216	0.576 ± 0.013	0.0837	0.0837 ± 0.0062
0.0243	0.490 ± 0.012	0.0889	0.0744 ± 0.0061
0.0271	0.462 ± 0.012	0.0943	0.0552 ± 0.0053
0.0301	0.411 ± 0.011	0.103	0.0431 ± 0.0035
0.0333	0.383 ± 0.011	0.114	0.0264 ± 0.0029
0.0366	0.356 ± 0.011	0.127	0.01337 ± 0.00215
0.0401	0.300 ± 0.010	0.140	0.01301 ± 0.00328

Table 1 Absolute differential cross sections of $\alpha\,^1H$ diffractive scattering at beam momentum 8.9 GeV/c

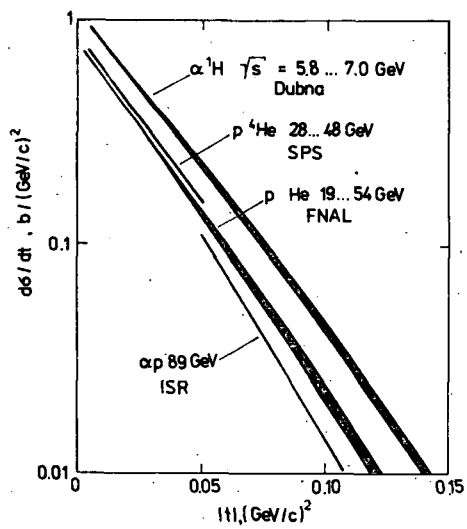

Fig.1 Alpha-proton diffractive scattering cross section at different energies. References of CERN and FNAL data can be found in /1,2/

A MEASUREMENT OF THE FORWARD DIFFERENTIAL CROSS SECTION OF THE REACTION $H(n,d)\gamma$ AT E_n=25.6 MeV

P. Michel, K. Möller, J. Mösner and G. Schmidt
Zentralinstitut für Kernforschung, Rossendorf, Bereich KF

The forward differential cross section of the deuteron photodisintegration or its inverse, the radiative neutron-proton capture, is a sensitive probe for studying the spin dependent part of the NN and N-photon interaction. The disagreement between the theoretical "standard" calculation by Partovi /1/ and a lot of experimental data triggered several theoretical efforts to improve the calculations. Meson exchange corrections (MEC), relativistic effects and more modern NN-potentials have been included. A review on the situation in deuteron photodisintegration at low and medium energies and its connection to other radiative reactions in the two nucleon system was given by Fearing /2/. In the present paper we report on a new measurement in this field. Using the charged particle spectrometer described in detail in ref./3/, we measured the neutron proton capture reaction at the Rossendorf tandem accelerator and determined the differential cross section at extreme forward angles at E_n= 25.6 MeV, corresponding to E_γ= 15 MeV for the inverse reaction.
In order to take into account multiple scattering, energy loss, angular and energy distribution of the collimated neutron beam, detector efficiencies and geometry of the setup we used a Monte Carlo simulation code. We obtained a c.m. differential cross section at 0° and E_γ^{lab} = 15 MeV of

$$(d\sigma / d\Omega)_{0^o,\ disint.} = (5.8 \pm 2.3)\ \mu b/sr.$$

The error consists of statistical and systematic part, but the main contribution (2.1 µb/sr) comes from the statistical one. Our result is compared with other data and some theoretical calculations in fig.1. The new data point is in line with the photodisintegration data obtained in Gent (1987) and Mainz (1985). Considering fig.1 it can be stated that more experimental work will be needed before the data can be used to confirm or the exclude one of the more modern calculations. In our opinion precise measurements of the zero degree cross section should be made using the photodisintegration instead of the capture reaction, especially at low energies the former is favoured to yield smaller error limits at comparable expense.

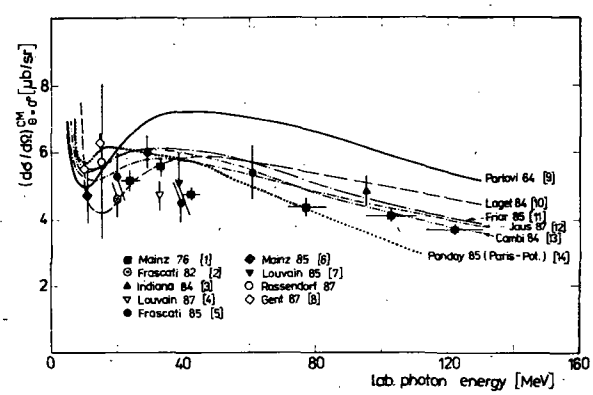

Fig.1 The $^2H(\gamma,p)n$ c.m. differential cross section at 0°

References

/1/ Partovi, F.; Ann. Phys. 27 (1964) 79
/2/ Fearing, H.W.; Czechoslovak Journal of Physics, B36 (1986) 263
/3/ Michel, P.; Dissertation A

ON THE EVOLUTION OF THE MASS ASYMMETRY IN DAMPED HEAVY-ION COLLISIONS

P. Gippner, K.D. Schilling, F. Stary and E. Will
Zentralinstitut für Kernforschung Rossendorf, Bereich KF
K. Heidel, S.M. Lukyanov, Yu.E. Penionzhkevich, V.S. Salamatin and H. Sodan
Joint Institute for Nuclear Research Dubna, Laboratory of Nuclear Reactions
G.G. Chubarian
Yerevan Physics Institute, Yerevan
R. Schmidt
Technische Universität Dresden, Sektion Physik

In order to study the influence of nuclear structure effects on the energy dissipation and the mass drift behaviour in damped nuclear reactions /1/, total kinetic energy (TKE) vs. fragment mass distributions have been measured with the spectrometer DEMAS /2/ in reactions of ^{64}Zn projectiles with ^{114}Sn (Z=50, N=64), ^{139}La (N=82) and ^{nat}Ag (non-magic) nuclei at incidence energies of 20 - 50 % above the Coulomb barrier.

Fig. 1 shows the contour plots of relative yields for the collision system ^{64}Zn + ^{114}Sn as a function of the TKE and the fragment mass. The observed TKE values cover a continuous spectrum extending far below the Coulomb energy V_{CB} of two spheres in the entrance channel (arrows in fig. 1). The experimentally established phenomenon of the existence of a bump in the cross section for strongly relaxed events in certain collision systems /1/ is also observed in the present case. This particular shape of the energy loss distribution as well as the qualitative differences between different collision systems have not yet been understood in detail /1/. Remarkable is the lack of mass drift associated with a large dissipation of relative kinetic energy (TKE). Contrary to the Zn + Sn system, the TKE vs. mass distributions for the collision systems ^{64}Zn + ^{139}La and ^{64}Zn + ^{nat}Ag exhibit a continuous decrease of the reaction yields with increasing TKEL values associated with a simultaneous mass drift towards symmetry. Fig. 2 displays two typical TKE spectra, in which only events with masses between 56 and 72 amu are included. As the sensitivity of damped collisions to the structure of the colliding nuclei could already be demonstrated /3/, one cannot exclude that the characteristic differences in the TKE spectra and in the mass drift behaviour may result from the shell structure of the collision partners.

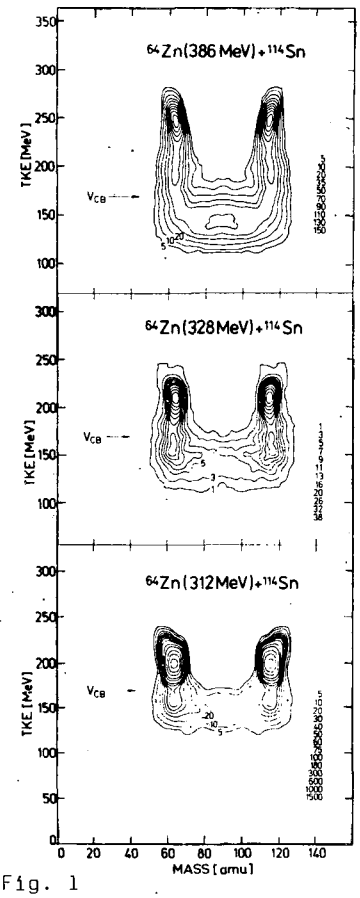

Fig. 1

On the other hand, total lack of mass drift observed in collision systems without shell-stabilized reaction partners can be well understood within the framework of the modified diffusion model /4/.

Therefore, further detailed investigations are required in order to draw definite conclusions on the influence of the internal structure of the involved nuclei on the evolution of the mass-asymmetry degree of freedom.

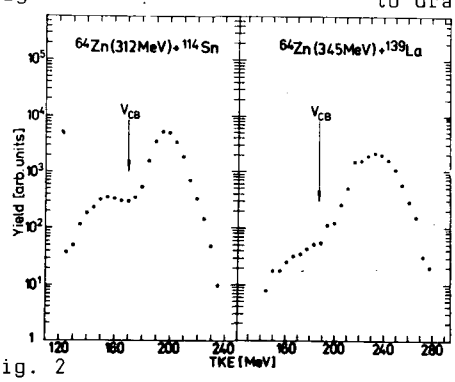

Fig. 2

References

/1/ Schröder, W.U. and Huizenga, J.R.; Treatise on heavy-ion science, vol. 2, ed. Bromley, D.A. (New York, London, 1984) p. 115

/2/ Schilling, K.D. et al.; Nucl. Instrum. Methods A257 (1987) 197

/3/ Hildenbrand, K.D. et al.; Nucl. Phys. A405 (1983) 179

/4/ Schmidt, R.; Z. Phys. A320 (1985) 413; Nucl. Phys. A445 (1985) 534

DESCRIPTION OF HEAVY-ION COLLISIONS BY USE OF TRAJECTORY-MODEL CALCULATIONS

G. Zwicker

Zentralinstitut für Kernforschung, Rossendorf, Bereich KF

In the recent time data for the reactions ^{40}Ar (206 MeV, 220 MeV, 302 MeV) + ^{232}Th /1/ obtained with the spectrometer DEMAS at the cyclotron U-300 at the JINR Dubna were analyzed in the framework of a refined trajectory model which pays special attention to the description of mass transport phenomena. This model includes three shape degrees of freedom and the dissipation processes are described in terms of the one-body approach. The nuclear potential is given by an Yukawa-type potential, shell corrections are not taken into account. The corresponding computer code HICOL used for the present investigations has been placed at disposal by Feldmeier /2/. When calculating the mass distributions for the individual reactions only trajectories leading to such scattering angles which could be observed in the concrete experiments were considered. In spite of the neglection of shell effects it was possible to reproduce the gross features of the mass distributions measured for the lower incident, and consequently, excitation energies how it is shown in figs. 1 and 2. The events answering nearly symmetric fragmentation may be the result of a fission-like process which becomes more and more predominant for increasing bombarding energy. In the case of E_{Lab} = 302 MeV the experimental curve can be explained satisfactorily by a superposition of two parts resulting from the DIC dynamics and from the assumption of a fission process described in terms of a diffusion model on the basis of a Fokker-Planck equation /3/. These findings allow the conclusion that not only for the highest incident energy where shell effects surely have been washed out but also in the other cases the shell structure of the colliding system may not play the most important role for the dynamics of such reaction processes which is determined in first line by the mass transport due to dissipative forces.

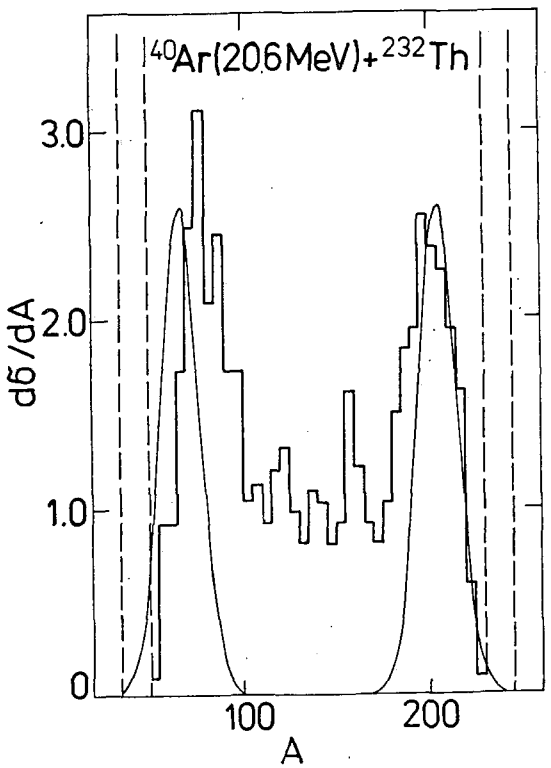

Fig. 1: Mass distribution for ^{40}Ar(206 MeV)+^{232}Th. The thick line shows the experimental data in arb. units. The thin line results from calculation.

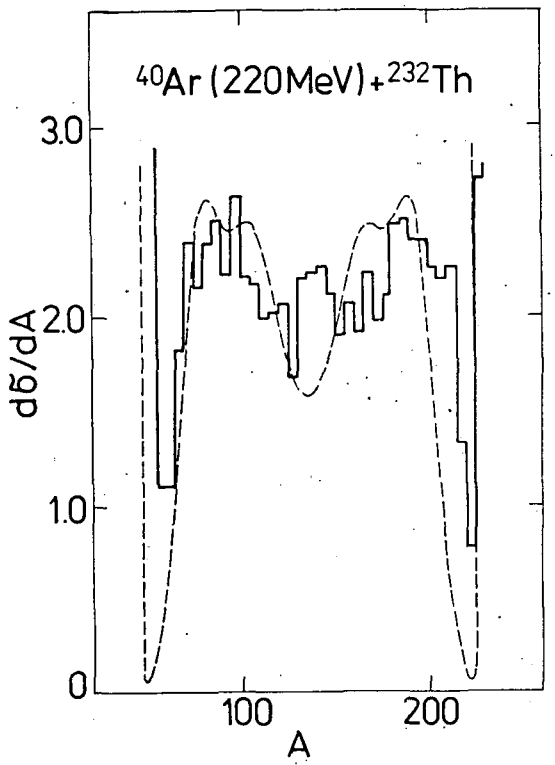

Fig. 2: Mass distribution for ^{40}Ar(220 MeV)+^{232}Th. The thick line shows the measured data in arb. units. The dashed line refers to the calculation

References:

/1/ Gippner P. et al.; Z. Phys. A 325 (1986) 335

/2/ Feldmeier H.; GSI-Report GSI-87-14, Darmstadt, 1987

/3/ Saupe G. et al.; JINR-Report E4-87-409, Dubna, 1987

YIELD MEASUREMENT OF LONG-RANGE ALPHA PARTICLE (LRA) ACCOMPANIED FISSION OF ^{238}U AND ^{232}Th INDUCED BY 13.5 MeV DEUTERONS

R. Kotte and D. Wohlfarth
Zentralinstitut für Kernforschung, Rossendorf, Bereich KF

The detailed investigation of deuteron induced ternary fission of ^{238}U is described in ref. /1/. Because of the unstable detector efficiency of the start-PPAC for α-particles, the yield value deduced from the correlation measurement is not certain. For this reason, the time-of-flight-energy techniques used for light charged particle (lcp) identification was replaced by $\Delta E/E$-techniques. The telescope consisting of a diaphragm of 4 mm diameter, a 45 µm thick ion-implanted silicon detector (12 mm Ø) and a 1 mm thick lithium drifted silicon detector (8 mm Ø) was installed 40 mm apart from the targed centre. The $\Delta E/E$-distributions were recorded into a two-dimensional analyzer with a 256 x 256 channel memory. A coincidence signal was delivered from a 4 x 4 cm^2 parallel-plate avalanche counter (PPAC) triggering on fission fragments (ff) only. It was arranged in such a way that the whole angular distribution of equatorial ternary α-particles was covered. The angular interval determining the geometric (coincidence) efficiency was measured to $\Delta\varphi = 90° \pm 4°$. The ff-PPAC was operated with 3 torr n-heptane. A 10 - 30 nA beam of 13.5 MeV deuterons was focused (2 mm Ø) on nat. UO_2 and ThO targets of 100 - 400 $\mu g \cdot cm^{-2}$ thickness. The targets were produced by vacuum evaporation onto 20 $\mu g \cdot cm^{-2}$ carbon layers and fixed on 40 $\mu g \cdot cm^{-2}$ Formvar foils. Single counting rates of ~20.000/s, ~10.000/s and 4.000/s from the E-, ΔE- and ff-detectors, respectively, had to be handled in order to collect a sufficient number of true lra accompanied fission events. This resulted in a ratio of random (generally scattered deuterons) to true coincidences of ~40. However, the portion of random coincidences contained in that part of the α-particle spectrum of interest was estimated to be less than 4 percent. In order to get the number of fission fragments N_{ff} entering the solid angle of the telescope, a single ff spectrum well separated from the lcp spectrum was derived from the ΔE-detector signals and summed up after the measurements were stopped. The dead-time of the experimental apparatus was estimated to ε_{dead} = 10 %. Energy calibration was performed with the help of known α-lines from ^{241}Am and ThC/C' sources. The lra-energy spectra were fitted to Gaussian distributions and integrated. The ratio of binary to equatorial lra accompanied fission was evaluated with the formula

$$\sigma_{binary}/\sigma_{lra} = \frac{\pi}{\Delta\varphi} \cdot \frac{N_{ff}/2 - N_{lra}}{N_{lra}} \cdot \left(1 - \varepsilon_{dead}\right) .$$

Finally, the following values were deduced and compared with results from ternary fission induced by fast neutrons.

fission induced by	target	$\sigma_{binary}/\sigma_{lra}$	ref.
13.5 MeV d	^{238}U	720 ± 80	this work
14.0 MeV n		795 ± 35	/2/
13.5 MeV d	^{232}Th	950 ± 110	this work
14.0 MeV n		1044 ± 96	/2/

The large errors of our measurements result mainly from the uncertainty in the determination of the angular interval $\Delta\varphi$ and the small number of collected lra events amounting to $N_{lra} \approx 300$ and 100 for uranium and thorium, respectively.

In both cases the lra energy distributions show the shape and position known from ternary fission investigations of various actinides, actually mean values of $\bar{E} \approx 16$ MeV and dispersions of $\Delta E \approx 10$ MeV (FWHM).

References

/1/ Kotte, R. et al.; this report p. 7

/2/ Nagy, L. et al.; Soviet Journ. Nucl. Phys. 8 (1969) 257; Yad. Fiz. 8 (1968) 443

CORRELATION MEASUREMENT OF ALPHA PARTICLE ACCOMPANIED FISSION INDUCED IN THE REACTION 13.5 MeV d + ^{238}U

R. Kotte, E. Hentschel, H.-G. Ortlepp, K.-D. Schilling, W. Seidel, F. Stary and G. Zwicker
Zentralinstitut für Kernforschung, Rossendorf, Bereich KF

Fission accompanied by long-range α-particles (lra) has been investigated by irradiating a natural uranium target with 13.5 MeV deuterons. The experimental arrangement (fig. 1) based on the simple set up of ref. /1/ has been developed for the study of different fission fragment (ff) - alpha correlations. The orientation of the ff axis with respect to the α-particle direction is measured with a large area double-grid avalanche counter (DGAC). The energy and angular distributions of the investigated equatorial α-particles do not differ from those observed in spontaneous or thermal neutron induced fission /2,3/. The angle between α-particles and light fragments has a most probable value of $\bar{\vartheta}_{lf-\alpha}$ = 82.1° ± 0.6° and a dispersion of $\Delta\vartheta$(FWHM) = 18.4° ± 1.2°. From the α-energy distribution, an average value of $\bar{E}_\alpha$ = 14.8 ± 1.0 MeV and a width of ΔE(FWHM) = 9.1 ± 1.2 MeV were derived. The relative stability of the mean values and widths over a wide range of fissioning systems indicates that lra emission is a unique process in the fission of the actinides, which is mainly determined by the Coulomb repulsion. The systematic increase of the mean lra emission angle when moving from uranium to californium is well understood in terms of small variations of the focusing Coulomb field in the result of the shell stabilized heavy fragments /4/. The ff mass distributions for different α-energies are shown in fig. 2 together with that of binary fission. Despite the limited mass resolution (δM = 15 - 20 amu), a remarkable increase of the peak-to-valley ratio (PVR) with increasing E_α is observed. From binary fission investigations of various actinides, it is well known that the symmetric component of the double-humped mass distribution increases with increasing excitation energy. This is due to the reduced influence of the shell corrections leading to asymmetric fission. The present PVR increase indicates that the α-particle arising from ternary fission cools down the fissioning system leaving it with lower free energy (deformation + internal heating) than in binary fission. This observation is confirmed by direct measurements of the (ff+α)-total kinetic energy for $^{235}U(n_{th},f)$ by Theobald et al. /5/. The dependence of the most probable value and the dispersion of the angular distribution on the ff mass ratio are shown in fig. 3 together with the corresponding data observed in $^{235}U(n_{th},f)$. Obviously, there is a drastic increase of the angular width for near-symmetric fragmentation. This finding supports the multi-channel-fission model of Brosa et al. /6/ predicting three different paths in the fission of ^{236}U and leading to a superposition of several lra angular distributions in the overlap region of the individual fission-channel mass distributions. The increase of the mean lra emission angle with decreasing mass ratio is easily understood as result of the different Coulomb forces acting on the α-particles originating from the neck region. The correlations investigated in addition will be published elsewhere /7/. For more details see also ref. /8/.

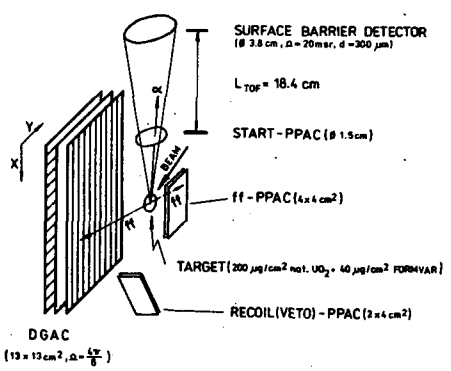

Fig. 1
Experimental arrangement
The α-particles are identified by time-of-flight (TOF)-energy-techniques. All the parallel-plate avalanche counters (PPAC) and the position-sensitive double-grid avalanche counter (DGAC) are commonly supplied with 4 torr n-pentane by a gas flowing-through system.

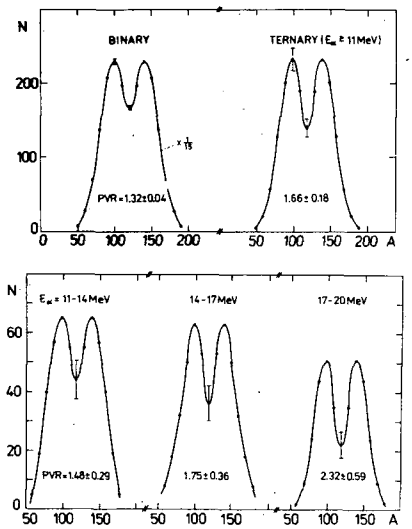

Fig. 2

Mass distribution of the deuteron induced binary and ternary fission of ^{238}U (upper part). Ternary fission mass distribution for different α-particle energy bins (lower part). PVR is the peak-to-valley ratio taken simply from the displayed experimental points.

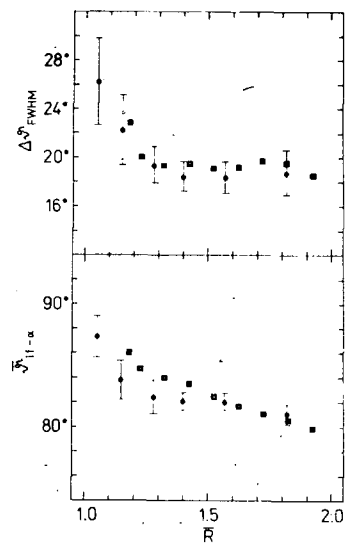

Fig. 3

Mean angle (lower part) and width (upper part) of the lra angular distribution as function of the fragments' mass ratio (averaged over mass intervals of 16 amu). Squares: $^{235}U(n_{th},f)$ data taken from /5/
Circles: this work, $^{238}U(d,f)$

R e f e r e n c e s

/1/ Kotte, R. et al.; ZfK Rossendorf annual report 1985, ZfK-584 (1986) 3

/2/ Guet, C. et al.; Nucl. Phys. A314 (1979) 1

/3/ Tsuji, K. et al.; Proc. Conf. Phys. and Chem. of Fission, Rochester 1973, IAEA-SM-174/16

/4/ Vandenbosch, R. and J.R. Huizenga; "Nucl. Fission", Academic Press, New York 1973, 316

/5/ Theobald, J.P.; TH Darmstadt report IKDA 8735 (1987)

/6/ Brosa, U. et al.; GSI Darmstadt report GSI-08-87 (1987)

/7/ Kotte, R. et al.; to be published in Z. Phys.

/8/ Kotte, R. et al.; Short Note to Z. Phys. A 328 (1987) 495

ANGULAR DISTRIBUTIONS OF PROMPT γ-RAYS ACCOMPANYING THE "TERNARY" FISSION OF ^{252}Cf

W. Pilz and W. Neubert
Zentralinstitut für Kernforschung, Rossendorf, Bereich KF
K. Arnold, D. Lucas and H. Märten
Technische Universität Dresden, Sektion Physik, WB Kernphysik

Double-differential γ-emission probabilities $W(\vartheta,E_\gamma)$ were measured to study possible correlations between light charged particle (LCP) emission and the predicted bending mode of fissioning nuclei /1/. Large NaJ(Tl) detectors were used for γ-registration and position-sensitive parallel plate avalanche counters for fragment registration, both in coincidence with LCP (detected with Si detectors) /2/. About $1{,}44\times10^5$ ternary events were stored during a run of 1.5 months by using a ^{252}Cf source which delivered about 10^4 fission fragments per second. The soft-ware system for recording the events was already described in /3/.
For checks, angular distributions of γ-rays from the binary fission of ^{252}Cf were also measured under the same experimental conditions. In this run, additionally the n/γ-TOF was measured as the fourth parameter. The results of this experiment agree with previous data /4,5/.
Another check of the reliability of our experimental set-up and data acquisition system was performed by an off-line shift of the window in the n/γ-TOF branch. An energy range for neutrons from 2 MeV to 5 MeV was accepted by it. The obtained angular distribution of neutrons is also in agreement with our earlier experimental data /6/ as shown in fig.1.
Fig.2 shows a comparison of the binary and ternary angular distributions of γ- rays for 2 bins of the γ-response amplitude. The anisotropy of both distributions is similar, but a simple comparison of the 0/90 degree ratios cannot be applied. The observed anisotropies show that the alignment of the angular momentum is not destroyed by the LCP emission. However, the shapes of the binary and ternary gamma angular distributions are significantly different.

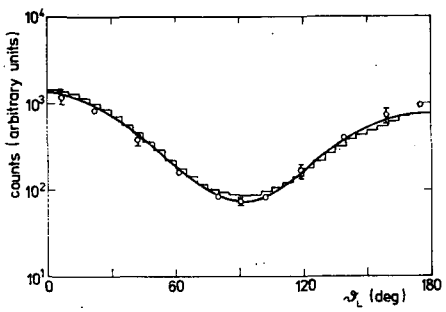

Fig.1 Neutron angular distribution for binary fission (histogram -/6/, Φ - present work, smooth line-theory /6/.

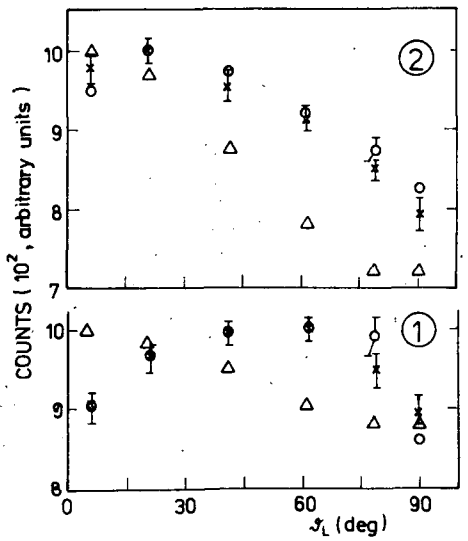

Fig.2 γ-angular distributions, if a light fragment was registered
△ binary fission
○ ternary fission (backward NaJ-detector)
× ternary fission (forward NaJ-detector)
1 $E_{\gamma,response}$=(200-430)keV,
2 $E_{\gamma,response}$=(430-1130)keV
(all distributions are normalized to a maximum hight of 1000)

References

/1/ Zielinska-Pfabé M. and Dietrich K.; Phys. Lett. 49B, 2 (1974) 123
/2/ Bondar N.F., Neubert W. and Pilz W.; Annual Report ZfK-621 (1986) 136
/3/ Fromm W.D.; Annual Report ZfK-621 (1986) 137
/4/ Skarsvåg K.; Phys. Rev. C22 (1980) 638
/5/ Neubert W., Pilz W. and Märten H.; Annual Report ZfK-621 (1986) 4
/6/ Märten H. et al.; Annual Report ZfK-621 (1986) 7

THE NEUTRON SPECTRUM FROM NEUTRON-INDUCED FISSION OF ^{232}Th

H. Märten, D. Richter, A. Ruben, and D. Seeliger
Technische Universität Dresden, Sektion Physik, WB Kernphysik
G.N. Lovchikova, S.E. Sukhikh, and A.M. Trufanov
Institute for Physics and Power Engineering, Obninsk, USSR

The prompt neutron spectrum from ^{232}Th fission induced by 7.3-MeV neutrons has been measured at the Rossendorf tandem facility by the use of a multi-plate fission chamber in conjunction with the three-dimensional-data analysis of neutron time-of-flight, scintillator (NE 213) light output, and pulse shape amplitude (n/γ-discrimination). This type of neutron spectroscopy enables a rather accurate particle discrimination without detector efficiency losses and the application of the sliding bias method based on a two-dimensional efficiency matrix as a function of neutron energy and bias (Monte Carlo calculation). The final spectrum obtained with reference to a ^{252}Cf(sf) neutron spectrum measurement is shown in fig. 1 in comparison with the calculation in the framework of the generalized Madland-Nix model (GMNM) /1/. This statistical-model approach to prompt fission neutron emission is combined with a scission-point model (TSM) /2/ to describe the energy partition (excitation energy, kinetic energy) in fission. In the case of multiple-chance fission reactions (as at 7.3-MeV incidence energy), the theoretical analysis is done for all possible chances. The neutron spectrum from ^{232}Th fission by 7.3-MeV neutrons (fig. 1) is not influenced by pre-fission neutrons above 1 MeV neutron energy. The GMNM (adjusted on the basis of the ^{252}Cf(sf) standard spectrum /1/) describes the measured Th spectrum without any further adjustments. The effect of multiple-chance fission on the average energy of fission neutrons E is shown in fig. 2 in comparison with few experimental points.

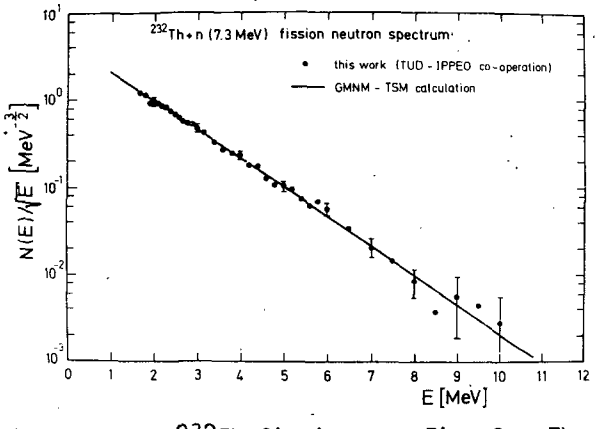

Fig. 1 The ^{232}Th fission neutron spectrum at 7.3-MeV incidence energy

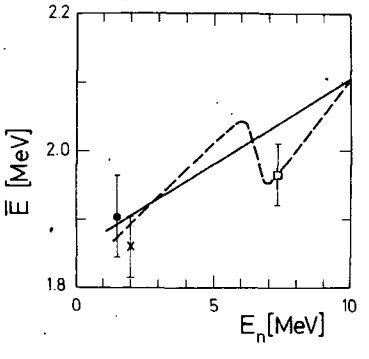

Fig. 2 The average energy of the neutron spectrum from ^{232}Th fission as a function of incidence energy En (• - /3/, x - /4/, □ - this work, —— ENDF/B-IV, --- GMNM-TSM)

The experimental and theoretical investigation of Th fission neutron emission has shown that GMNM-TSM provides the basis for the consistent description of fission neutron data in a wide range of fissioning nuclei.

REFERENCES

/1/ Märten, H. and Seeliger, D.; Nucl. Sci. Eng. 93 (1986) 370
Märten, H. et al.; Proc. Int. Conf. Neutron Physics, Kiev, 1987 (in press)

/2/ Märten, H. et al.; Proc. Int. Conf. Nucl. Phys., Gaussig, 1987 (in press)

/3/ Sukhikh, S.E. et al.; Yad. Const. 3 (1986) 34

/4/ Hirakawa, N. et al.; Radiation Effects 93 (1986) 229

THEORETICAL INTERPRETATION OF ^{252}Cf(sf) NEUTRON DATA

H. Märten
Technische Universität Dresden, Sektion Physik, WB Kernphysik

The complex cascade evaporation model /1/, i.e. a statistical-model approach (SMA) to prompt fission neutron emission from highly excited, rapidly moving fragments represented by an intricate occurence probability function in nucleon numbers, excitation energy, kinetic energy, and angular momentum, has been applied to multiple-differential ^{252}Cf(sf) neutron data measured in Dresden /2/. Energy and angular distributions are well reproduced; see examples in the figures. Special care has been pointed to the description of the crucial polar regions at lab. frame energies close to the kinetic energy of the fragments per nucleon. These regions correspond to very small centre-of-mass frame energy. In addition to the consideration of n/γ-competition of fragment de-excitation, the optical potential used for the calculation of neutron transmission coefficients has a remarkable influence on the shape of emission probability function. The best agreement with measured data has been obtained on the basis of Holmqvist's potential /3/.
No significant indication of secondary mechanisms could be found. Considering experimental as well as theoretical uncertainties the upper limit of a central-component yield /4/ has been estimated to be 5 %. Conclusions concerning the SMA application for practical purposes (data evaluation) are outlined in Ref. /5/.

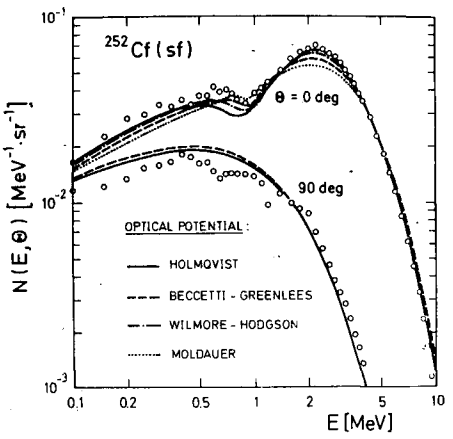

Fig. 1
Differential energy spectra of ^{252}Cf(sf) neutrons at 0° and 90° (with reference to light-fragment direction) in comparison with SMA calculations based on different optical potentials as indicated.

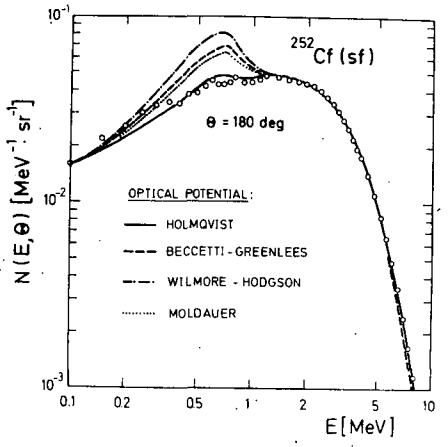

Fig. 2
As for Fig. 1, but for 180°.

References

/1/ H. Märten, D. Seeliger; J. Phys. G 10 (1984) 349
P. Krimmling, H. Märten; ZfK-621 (1987) 8

/2/ H. Märten, D. Richter, D. Seeliger, W. Neubert, A. Lajtai; Nucl. Instr. Meth., in press

/3/ B. Homqvist, Arkiv Fysik 38 (1968) 403

/4/ H.R. Bowman et al.; Phys. Rev. 126 (1962) 2120

/5/ H. Märten, Proc. IAEA Advisory Group Meeting on Nuclear Theory for Fast Neutron Nuclear Data Evaluation, Beijing, 1987, in press

SEMI-EMPIRICAL DESCRIPTION OF FISSION FRAGMENT MASS YIELD CURVES

D. Lucas, H. Märten
Technische Universität Dresden, Sektion Physik, WB Kernphysik

For several fission data calculations, the adequate description of fragment mass yield Y(A) is required. The 5-Gaussian approximation theoretically predicted by Brosa and Grossmann /1/ and previously used to reproduce yield curves for neutron-induced fission of ^{238}U /2/ and ^{235}U /3/ has been applied to Th-Pu fission for incidence energies below 20 MeV. In the case of multiple-chance fission, we account for the partial yield curves for all chances energetically allowed in connection with the statistical-model analysis of the partial fission cross sections (code STAPRE /4/). The qualitative dependence of Gaussian parameters (position, width, and weight) on the excitation energy E of the fissioning nucleus has been assumed as in Refs. /2/ and /3/. Parameters have been adjusted on the basis of experimental data. The ratio of the weight of Gaussians corresponding to asymmetric fission (fission path' standard I and II /1/) has been found to depend on the mass number of the fissioning nucleus.
The weight of the symmetric component is strongly E-dependent. However, its exponential increase /2,3/ has been confirmed for $E \lesssim 15$ MeV. At higher E, the dependence has to be reduced.

The present method is suitable to reproduce mass yield curves for the fission reactions mostly important for practical applications. The accuracy of the predictions are in the order of 5 - 15 % in the fragment mass regions corresponding to considerable yields. For symmetric and extremely asymmetric fission, the uncertainties are higher (10 - 50 %).

References

/1/ Brosa, U., Grossmann, S., Müller, A.; Proc. Int. Symp. Nucl. Phys., Gaussig, 1986, ZfK-610 (1986) 162
/2/ Nagy, S. et al.; Nucl. Sci. Eng. 88 (1984)
/3/ Straede, C.A.; Thesis, CBNM Geel (1985)
/4/ Uhl, M., Strohmaier, B.; Report IRK-76 (1976)

DIFFERENTIAL NEUTRON-EMISSION CROSS-SECTIONS OF ^{238}U BOMBARDED WITH 14 MEV NEUTRONS

T. Elfruth, T. Hehl, H. Kalka, H. Märten, H. Payrovan[x]), A. Ruben, D. Seeliger, K. Seidel, and S. Unholzer
Technische Universität Dresden, Sektion Physik, WB Kernphysik

Neutron-emission cross-sections of ^{238}U are needed for fission and fusion (hybrid) reactor calculations. The accuracy required for these data /1/ is higher, than those achieved in previous experiments. A new measurement with an improved time-of-flight spectrometer /2/ at the pulsed neutron generator /3/ of the Technical University shall contribute to enhance the accuracy.
The angle-integrated emission spectrum is shown in Fig. 1. Contributions to the spectrum arise from neutron scattering in the precompound and in the compound nucleus stage, from (n,2n), (n,3n) and fission neutrons. For a theoretical analysis the following scheme was used:

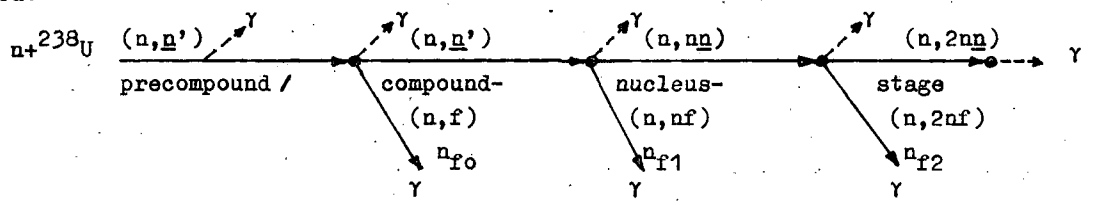

The (n,n') contributions were calculated with the code EXIFON /4/ which takes into account statistical one- and two-step direct single-particle as well as collective interactions and solves the master equation for the preequilibrium and the equilibrium stage. The strength of the other channels and the spectra of the second and third neutrons in (n,2n) and (n,3n) reactions respectively were calculated with the code STAPRE /5/ based on the statistical Hauser-Feshbach theory extended in the level continuum. The spectral shapes of fission neutrons were calculated with the GMNN formalism /6/.
As first step of a spectrum analysis, a calculation was done with parameters representing the mean behaviour of nuclei; non of the model parameters was fitted. The agreement with the experimental spectrum is surprisingly good. A more detailed analysis is in progress.

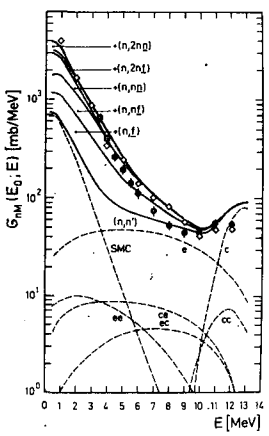

Fig. 1
Angle-integrated neutron emission spectrum from ^{238}U at 14.1 MeV incidence energy. Experimental data of the present work (o) and from Ref. /7/ (◇) are compared with a calculated spectrum (▬) composed of the indicated contributions (——). The (n,n') component consists of direct collective (c), direct single-particle (e) and statistical multistep compound (SMC) contributions (---).

References

/1/ World Request List for Nuclear Data, IAEA Vienna 1981, INDC(SEC)-78/URSF
/2/ Dietz, V. et al.; Gemeinsamer Jahresbericht 1980, p. 196
/3/ Helfer, H. et al.; Gemeinsamer Jahresbericht 1983, p. 126
/4/ Kalka, H.; XVIIth Int. Symp. Nuclear Physics, Gaußig (GDR) 1987
/5/ Uhl, M. and Strohmaier, B., IRK-76, 1976
/6/ Märten, H. and Seeliger, D.; Nucl. Sci. Eng. 93 (1986) 370
/7/ Kammerdiener, J.L.; Ph. D. Thesis University of California, 1972, UCRL-51232

[x]) Fellowship of the IAEA, from I.R. Iran

SMD/SMC-MODEL FOR PRACTICAL APPLICATION

H. Kalka, M. Torjman, and D. Seeliger
Technische Universität Dresden, Sektion Physik, WB Kernphysik

For the theoretical description of nucleon-nucleus reactions at bombarding energies between 5 and 30 MeV a simple model /1,2/ was derived from first principles (Green's function formalism; Gaussian Ensembles). This model which describes energy and angular distributions (for nuclear technology) consists of a statistical multistep direct (SMD) and a statistical multistep compound part (SMC),

$$\frac{d^2\sigma_{\alpha\beta}(\varepsilon)}{d\varepsilon' d\Omega'} = \frac{1}{4\pi}\left[\frac{d\sigma^{SMD}_{\alpha\beta}(\varepsilon)}{d\varepsilon'}\sum_L (2L+1)\, a_L(\varepsilon')\, P_L(\cos\theta') + \frac{d\sigma^{SMC}_{\alpha\beta_c}(\varepsilon)}{d\varepsilon'}\right]. \qquad (1)$$

Within the SMD-part besides the excitation of particle-hole states (excitons) also the direct excitation of collective modes (surface vibrations) are considered. The coefficients a_L for the angular distributions are taken from the systematics of Kalbach and Mann /3/. For the SMC-part which was calculated for (exciton number) $n \geq 5$ isotropy is assumed. In contrast to the phenomenological exciton model the SMC-part in (1) is free of mean square matrix elements (they cancel), and inverse cross sections. Whereas the mean square matrix element of the direct particle-hole excitation (in the SMD-part) is estimated from the optical-model reaction cross section the deformation parameters β_λ of the collective excitations are taken from nuclear data tables /4,5/. In this way calculations of (n,n') are performed parameter-free in a broad range of incidence energy and mass number A. A fairly agreement with experimental data was achieved /2/. An example is given in the Figs. The dashed-dotted line refer to the SMD-contribution. The full line is the sum of SMD and SMC.

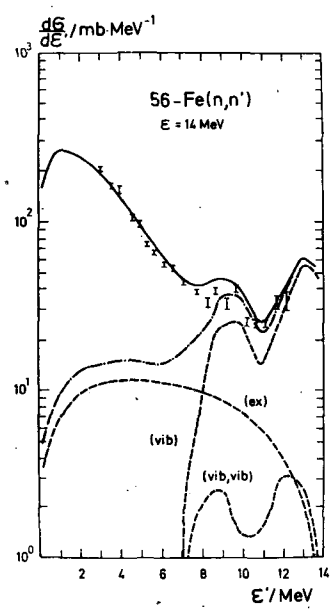

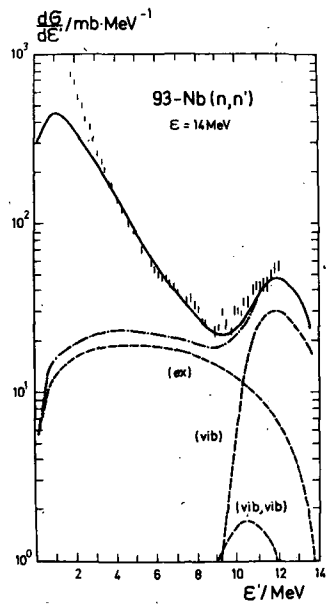

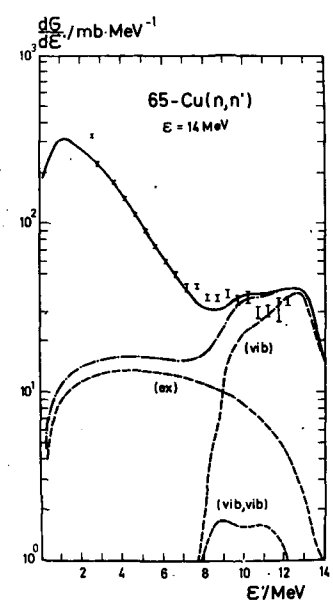

REFERENCES:

/1/ Kalka, H., Zhivopistsev, F.A., Seeliger, D.; will be published in Z. Phys. A
/2/ Kalka, H.; Proc. XVII-th Intern. Symp. on Nucl. Phys., Gaussig (GDR) 1987
/3/ Kalbach, C., Mann, F.M.; Phys. Rev. C23 (1981) 112
/4/ Bohr, A., Mottelson, B.R.; Nuclear Structure, Vol. II, Benjamin, New York (1975)
/5/ Raman, S. et al.; At. Data and Nucl. Data Tabl., 36 (1987) 1

DETERMINATION OF THE PARAMETERS OF U-235 FISSION-FOILS

K. Merla
Technische Universität Dresden, Sektion Physik, WB Angewandte Kernphysik

All fission-foils used in hitherto carried out U-235 fission cross-section measurements by the TUD/KRI collaboration were prepared at the KRI Leningrad by HF-sputtering. The published cross-section results base all on values for the layers areal densities and inhomogeneities determined at the KRI with typical total errors of $\gtrsim 1$ %. Now independent measurements of these foil-parameters at the TUD were finished.
Areal densities were determined by a low geometry α-counter ($\Omega = 6.4335 \cdot 10^{-3} \pm 0.46$ %) already used in /1/. At the spectra corrections for background pulses (0.99 - 2.70 %), admixtures of U-234 and U-236 (3.15 %, measured by mass- and α-spectrometry) and spectra extrapolation to pulse height zero (0.06 - 0.28 %) were considered. The values for areal density base on halfe-life periods from /2/ ($T_{1/2}$ (U-235) = $7.037 \cdot 10^8$ y $\pm$ 0.15 %). Besides the given error components by Ω and $T_{1/2}$ furthermore these by the corrections at the spectra (0.28 - 0.33 %), statistics (0.31 - 0.44 %) and scattering processes (0.27 %) were taken into account. Results of the measurements confirm to the KRI ones obtained in 1977-79 (formerly used for 3 foils) within the error limits. Newer KRI-results from 1980-81 (formerly used for 3 other foils) differ from the determined ones up to 3 % and are systematically higher. This may be caused by systematical errors in the KRI-measurements at the correction of the background raised in consequence of Cf-252 contamination of the equipement.
Changes of the amount of fissionable material of fission-chamber arrangements used in the σ_f-experiments are of special interest because reflecting in changes of the cross-section value directly. These differences are given in table.
Redeterminations of inhomogeneity were performed

- by α-scanning using apertures of 8 mm in diameter corresponding to the neutron cone extend in the σ_f-experiment /3/,
- by Rutherford-Backscattering measurements at the CINR Rossendorf with measuring areals 3 mm in diameter /4/.

Although not completely corresponding measuring points results show good correspondence. Resulting values for inhomogeneity of fission-chamber arrangements in σ_f-experiments are also given in table.
The new values for areal densities and layers inhomogeneities will be implemented in a revise of ascertained cross-section values after finishing experimental investigations of the individual absorption parameters of all foils.

Measurement E_n /MeV	Number of foils used	Areal density new value /ug/cm^2	± %	Diff.of formerly used KRI-value /%	Inhomogeneity new value /%	formerly used /%
14.7	1	258.35	0.70	- 0.64	0.29	1.00
2.6	2	674.75	0.99	+ 0.50	0.98	0.90
8.4	5	1714.36	0.82	+ 1.41	1.06	0.71
4.45/18.8	5	1747.23	0.72	+ 1.51	1.12	0.72

REFERENCES:

/1/ K. Merla et al., ZfK-584 (1986), p. 115
/2/ A. Lorenz (ed.), INDC(NDS)-149/NE, 1983
/3/ C.-M. Herbach et al., INDC(GDR)-036/G, 1985
/4/ K. Merla, R. Grötzschel, ZfK-584 (1986), p. 116

OPTIMIZATION OF THE FISSION CROSS-SECTION MEASUREMENT OF ^{238}U AT 5 MEV NEUTRON ENERGY USING THE TCAPM

U. Todt, C.-M. Herbach
Technische Universität Dresden, Sektion Physik, WB Angewandte Kernphysik

A careful optimization of the experimental system for the fission cross-section measurement of ^{238}U within the neutron energy range of 4-5 MeV became necessary for reaching a statistical uncertainty below 1 % /1/.

Supposing a fixed neutron energy E_n, incidence energy E_d is the only optional parameter. Optimization of E_d is found to be an intricate problem because E_d is connected with all features of the experimental system directly or by means of kinematics as shown in fig. /2/.

A lot of contrary conditions and requests has to be taken into account:

- Reaching a statistical error of 1 % in 100 hours effective measuring time demands an averaged AP-rate $\dot{N}_{AP}$ of about 6000 s^{-1} but it is connected with a rate of scattered deuterons $\dot{N}_d$ of 2.5 - 3.$10^5 s^{-1}$.
- The ratio $\dot{N}_{AP}/\dot{N}_d$ increases with raising E_n but E_n is limited to 5 MeV by reason of energy dependence of ^{238}U cross-section.
- AP-rate requests a large AP-cone $\Delta\Omega_{AP}$ and a sufficient $(CD_2)_n$-target foil thickness n_T leading to large energy spread of AP and background (from $^{12}C(d,\alpha)^{10}B$) by means of kinematics and energy loss inside the foil in contrast to registration of AP with low background.
- Reaching a good AP-detection efficency requires a high AP-energy E_{AP} too, because the ΔE-detector limiting minimum E_{AP} has to be thicker than ~10 µm for solving requests to homogeneity and resolution. This agrees with high E_n, e.g. high E_d.
- The energy loss ΔE_d of the deuterons penetrating $(CD_2)_n$-foil decreases with raising E_d lessen thermic stress of the foil and energy spread of neutrons, AP and α-background. On the other hand the distance between AP and α_0-group of background lowers from 1 MeV at E_n = 4 MeV to nearly 200 keV at 5 MeV.
- The deuteron scattering rate of more than 2.$10^5 s^{-1}$ demands to shorten the LAR output pulse length from 0.5 to 0.25 µs allowing $\dot{N}_d$ up to 3·$10^5 s^{-1}$ /2,4/. This stresses the requirements to the ΔE-detector properties strongly.

Since the background correction is based on particle significant spectrum /2,3,4/ the ΔE-detector has to be very homogeneous. But it must be also large for reaching a large AP-cone. Hence the realization of optimum system for the measurement at E_n = 5 MeV is connected with the availability of a ΔE-detector with a diameter of more than 9 mm and a homogeneity better than 200 keV. If this detector is not thicker than 13 µm, background normalisation by means of monitoring the α_1-group is possible /3/. Results of optimization and measurement are given in /1/.

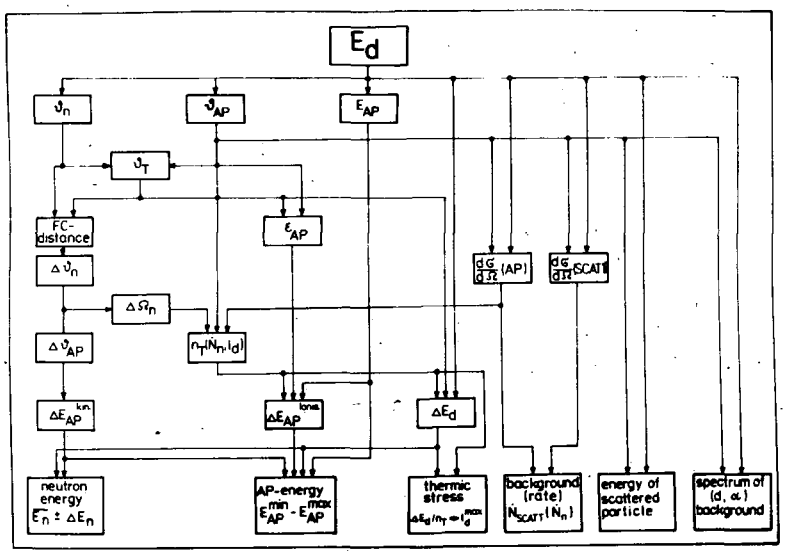

REFERENCES:

/1/ C.-M. Herbach et al., this report, p. 17

/2/ C.-M. Herbach, Forschungsbericht TUD (1987)

/3/ C.-M. Herbach et al., ZfK-621 (1987), p. 18

/4/ C.-M. Herbach et al., Preprint TUD 05-07-85 (1985)

ABSOLUTE MEASUREMENT OF THE ^{238}U FISSION CROSS-SECTION AT 5 MEV NEUTRON ENERGY USING THE TCAPM

C.-M. Herbach, K. Merla, G. Musiol, H.-G. Ortlepp[x)], G. Pausch, R. Perez, U. Todt
Technische Universität Dresden, Sektion Physik, WB Angewandte Kernphysik
[x)] since 1984 CINR Rossendorf

I.D. Alkhasov, E.A. Ganza, V.A. Kalinin, O.I. Kostochkin, L.L. Solin, P.S. Soloshenkov, S.M. Solovjev
Khlopin Radium Institute Leningrad

Absolute measurements of the ^{238}U fission cross-section were finished by a long-time run at 5 MeV neutron energy. A statistical uncertainty of 0.88 % was reached, the preliminary result of $(0.542 \pm 0.011) \cdot 10^{-24} cm^2$ agrees with ENDF/B-V-evalutation $(0.533 \cdot 10^{-24} cm^2)$. Final results at all measured energies /1-4/ will be elaborated after a careful investigation of properties of used fission foils, expecially fragment absorption within the layer /5,6/.

Since cross-section of ^{238}U at 4.5 to 5 MeV is low compared with other nuclei, achieving a sufficient high fission-rate was the main problem. Using the 9-plate fission chamber well optimized in /1/ (^{238}U-inventory 3.372 mg/cm^2), the neutron flux had to be increased about two times in contrast to /1,7/. Therefore a very careful optimization of neutron production and associated particle (AP) identification system was accomplished /8/.

The optimization within the neutron energy range of 4-5 MeV resulted in deuteron energy $E_d = 6.4$ MeV, AP-angle $\vartheta_{AP} = 35.5^o$, $(CD_2)_n$-target thickness $n_T = 0.4$ mg/cm^2, target angle $\vartheta_T = 54.5^o$, AP-apertur of 9 mm in a distance of 136 mm and a LAR output pulse length of 250 ns. That means neutron energy $E_n = 5$ MeV, correlated neutron angle $\vartheta_n = 76.2^o$, $\Delta\Omega_{AP} = 3.44$ msr, $\Delta\Omega_n = 12.4$ msr. Energy distributions are 4.50 - 5.45 MeV for neutrons, 3.83 - 5.08 MeV for AP, 3.83 - 4.47 MeV for α_o - group and 3.10 - 3.81 MeV for the α_1-group of $^{12}C(d,\alpha)^{10}B$. A ratio of neutron rate N_n to scattered deuteron rate N_d of 0.024 - 0.031 was expected refering to AP-detection efficency $\varepsilon_{AP} = 0.7 - 0.9$. AP-rate of more than 6000 s^{-1} should be obtained using a deuteron beam current of 500 nA.

Since a ΔE-detector with a diameter of more than 9 mm and best homogeneity (220 keV spread measured by α-transmission) was only with a thickness of 15 μm available, the α_1-group was not detected completely and monitoration of the α_1-group for background normalisation was impossible /1,9/. Using new $(CD_2)_n$-foils we obtained up to 7100 AP/s and $N_n/N_d = 0.03$ in experiment. Under best conditions an average of 40 hours led to $\dot{N}_{AT} = 5559\ s^{-1}$ and $\dot{N}_d = 2.15 \cdot 10^5 s^{-1}$, e.g. $\dot{N}_n/\dot{N}_d = 0.026$. Also energy distribution expected above was observed. Even AP-background decreased to 0.5 - 2 % and if all control spectra are available an error contribution of less then 0.3 % was obtained.

REFERENCES:

/1/ K. Merla et al., preprint TUD 05-02-87 (1987)
/2/ C.-M. Herbach et al., ZfK-621 (1987), p. 17
/3/ C.-M. Herbach et al., ZfK-584 (1986), p. 5
/4/ R. Arlt u.a., ZfK-408 (1980), S. 25
/5/ C.-M. Herbach et al., ZfK-621 (1987), p. 19
/6/ C.-M. Herbach, G. Pausch, ZfK-584 (1986), p. 114
/7/ C.-M. Herbach, Forschungsbericht TUD (1987)
/8/ U. Todt et al., this report, p. 16
/9/ C.-M. Herbach et al., ZfK-621 (1987), p. 18

THE INFLUENCE OF NEUTRON INELASTIC SCATTERING ANISOTROPY ON THE NEUTRON LEAKAGE SPECTRUM OF A LEAD SPHERE

M. Toepfer
Technische Universität Dresden, Sektion Physik, WB Kernphysik
B. Böhmer, C. Reiche
AdW der DDR, Zentralinstitut für Kernforschung, Rossendorf, Bereich RPT

An important effect of the interaction of 14 MeV neutrons, emerging from fusion reaction between Deuterium and Tritium, with heavy nuclei is the anisotropy of the preequilibrium neutron emission. The new evaluation of the fusion reactor blanket candidate material lead by TUD /1/ was done with special regard to this effect. The strong coupling of angle and energy dependence of the double-differential cross section for the neutron emission from preequilibrium states required its representation in the proposed ENDF/B-VI nuclear data format /2/. A new code SIXFIL had to be created to compile the (n,n')-cross section of this new representation into the transfer matrix for this reaction type. MINX /3/ was used to get group cross sections and the transfer matrices for the elastic scattering and (n,2n), (n,3n) processes. The anisotropy of the inelastic neutron scattering was taken into account up to P_4. The produced group cross section dataset was the basis for neutron transport calculations carried out by the use of ANISN /4/.
Fig. 1 shows the expected effect on neutron leakage spectrum of a Pb sphere shell for a 14 MeV point source in the centre. The forward peaked angular distribution causes deeper penetration of inelastic scattered neutrons. Fig. 2 gives the fractional ratio of the different leakage spectra in dependence on the sphere shell thickness. It must be mentioned that the anisotropy effect in the energy range between 7 and 12 MeV has the same order of magnitude as the experimental uncertainties for a Pb-sphere benchmark experiment /5/.

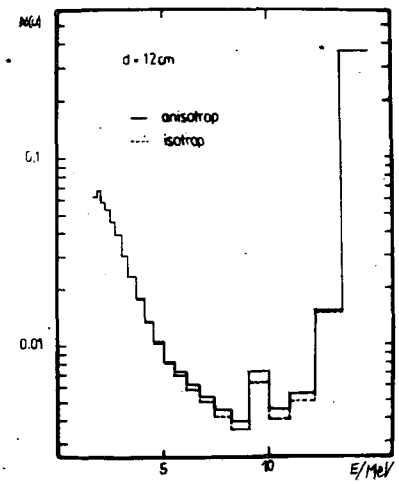

Fig. 1:
Comparison of calculated neutron leakage spectra (dashed line: isotropic (n,n')-cross section; d:thickness of sphere shell)

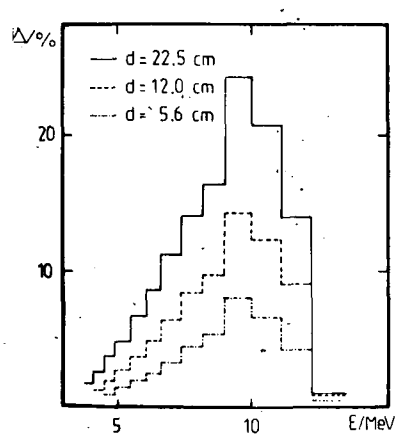

Fig. 2:
Fractional ratio of anisotropy effect for different sphere shell thicknesses

References

/1/ Hermsdorf, D.; INDC(GDR)-39/G, Wien, 1985
/2/ Mac Farlane, R.E.; LA-UR-84 1026 (Revise 1984)
/3/ Weisbin, C.R. et al.; MINX ...; LA-6486-MS/ENDF-237 (1976)
/4/ Engle, W.W.; Jr.: ANISN, A.E.C. Research and Development Report K-1693 (1967)
/5/ Elfruth, T. et al. ; Atomenergie Kerntechnik, Vol. 49 (1987) No. 3

NUCLEAR SPECTROSCOPY

EVIDENCE FOR A NEW ISOMER IN THE DOUBLY-ODD NUCLEUS ^{84}Rb

J. Döring, G. Winter, L. Funke, L. Käubler and W. Wagner
Zentralinstitut für Kernforschung, Rossendorf, Bereich KF

The structure of doubly-odd nuclei in the vicinity of the ^{88}Sr core, i.e. near the neutron shell closure at N = 50 and the proton subshell closure at Z ≈ 38, gives a sensitive test of shell model calculations within a relatively small configuration space. For this purpose the investigation of the nucleus ^{84}Rb with one proton hole and three neutron holes in the respective closed shells has been initiated.

Up to now only little information is available on medium and high spin states in ^{84}Rb. The ground state is known /1/ to be a 2^- state. Furthermore, a state at 248.1 keV with $I^\pi = 3^-$ is excited during the decay of the well-known long-lived 6^- isomeric state at 463.7 keV /1-3/. In connection with the irradiation of a natural NaBr target with 27 MeV α-particles we searched for in-beam γ-rays belonging to ^{84}Rb. An inspection of the beam-on and beam-off singles γ-ray spectra has shown that besides the dominating ^{79,81}Br(α,2n)^{81,83}Rb reaction channels also the ^{79,81}Br(α,n)^{82,84}Rb channels are present. The coincidence spectrum gated by the 248.1 keV γ-ray shows in addition to the known 215.5 keV γ-ray a clear 224.7 keV γ-ray peak. Therefore, a new level at 472.8 keV is introduced. On the other hand, the placement of the 80.6 keV γ-line on top of the 6^- isomer is suggested from the γ-ray intensities measured in the ^{82}Se(^{6}Li,4n) and ^{80}Se(^{7}Li,3n)^{84}Rb reactions. In the relevant γ-ray spectra the lines of the decaying 6^- isomer as well as new γ-rays at energies of 46.7, 80.6, 83.8, 224.7 and 631.0 keV are very strong and have roughly the same intensity relations. The strongest of the new lines at 80.6 keV is assumed to feed the 6^- isomer directly and thus a new level at 544.2 keV is established. The energy difference between this level and the 472.8 keV level fits to a weak 71.4 keV γ-ray (see fig. 1).

Using the pulsed-beam γ-ray timing method time distributions have been measured during the irradiation of a NaBr-target with 27 MeV α-particles. Furthermore, delayed energy spectra have been measured during the bombardment of a target consisting of ^{82}Se (92 %) and ^{80}Se (5 %) with 35 MeV ^{7}Li ions. In both measurements the intensity of the 80.6 keV γ-ray shows a delayed behaviour. From the slope of the background-corrected time distribution (see fig. 2) a half-life of $T_{1/2}$ = 11(1) ns is deduced and assigned to the new level at 544.2 keV. Also the 71.4 keV γ-ray shows a delayed behaviour with roughly the same half-life supporting the existence of the new level. Since the angular distribution coefficients of the 71.4, 80.6 and 224.7 keV γ-rays have not yet been measured we conclude only from systematic considerations that the most probable spin and parity values for the level at 472.8 keV are 4^- or 5^- and for the new isomer 5^- or 6^+. In ^{82}Rb /1/ containing two neutrons less than ^{84}Rb the 5^- state is a long-lived isomeric state, whereas in ^{82}Br /1/ with two protons less than ^{84}Rb the ground state has a 5^- assignment.

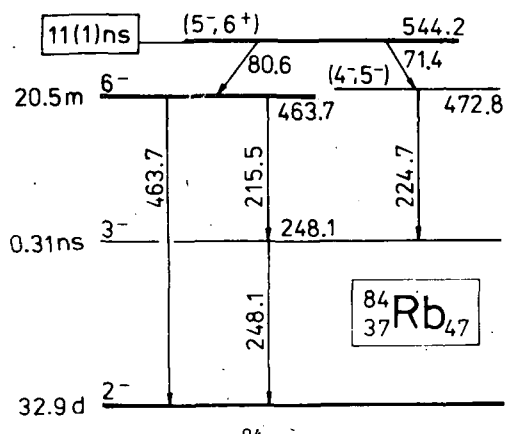

Fig. 1 Level scheme of ^{84}Rb

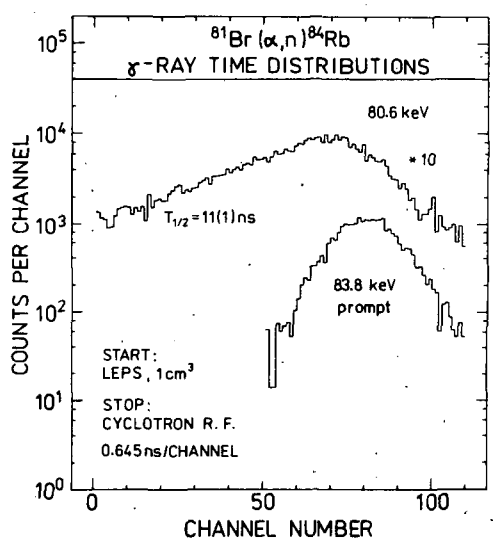

Fig. 2 Background-corrected time distribution of the 80.6 keV γ-ray deexciting the new isomer in ^{84}Rb. For comparison the time distribution of a prompt 83.8 keV γ-ray is given which belongs very likely also to the same nucleus.

References

/1/ Lederer, C.M. et al.; Table of Isotopes, 7th Edn., New York, Wiley 1978
/2/ Ekström, C. et al.; Nucl. Phys. A311 (1978) 269
/3/ Lakshminarayana, V. et al.; J. Phys. G10 (1984) 247

A NEW ISOMER IN ^{83}Br EXCITED IN THE ^{82}Se (^{7}Li,α2n) REACTION

G. Winter, R. Schwengner, L. Funke and E. Will
Zentralinstitut für Kernforschung, Rossendorf, Bereich KF

Excited states in some nuclei around ^{84}Kr have been populated by bombarding ^{82}Se with the 35 MeV ^{7}Li beam that is now available from the Rossendorf cyclotron. The spectra of γ-rays which are delayed with respect to the beam bursts revealed several transitions arising from isomeric decays and led us to establish new isomers in ^{83}Br, ^{85}Rb /1/, ^{85}Kr /2/ and ^{86}Kr /3/. The time distributions /3/ measured for the γ-rays deexciting the 3070 keV level /4/ in ^{83}Br indicated, however, that the lifetime of this isomer is much longer than the repetition time of the beam bursts (104 ns). In order to determine the lifetime in ^{83}Br that is excited by the (^{7}Li,α2n) reaction a particle - gamma coincidence measurement has been carried out. For recording the charged particles emitted in the reaction two silicon detectors with diameters of 42 mm and 150 μm effective thickness were mounted at distances of 2.5 cm from the beam spot on the target. In this way about 30 % of the total solid angle were covered. Proton - gamma and alpha - gamma coincidences could be separated from each other by setting gates in the energy spectrum of the silicon detectors /5/. Coincident events were stored event by event in form of three addresses (particle energy, γ-ray energy, time between particle and γ-ray detection) on magnetic tape and sorted off-line in two-dimensional matrices (E_γ, time), separately for protons and α-particles. Spectra of prompt and delayed γ-rays were then formed by setting gates in the time address. From the intensities of the lines at 303, 1065, 610 and 357 keV in the spectra of delayed events an average value for the half-life of the new isomer in ^{83}Br of $T_{1/2}$ = 0.6 $\pm$ 0.2 μs has been derived. This comparatively long lifetime explains why in the previous in-beam study /4/ based on ^{7}Li bombardment the 303 and 1065 keV γ-rays were found with almost isotropic angular distributions that give no information on the multipolarity of these transitions. These γ-rays of ^{83}Br have also been observed during the irradiation of ^{82}Se with 42 MeV α-particles /6/ but also in the (α,p2n) reaction an isotropic angular distribution was found for the 1065 keV line indicating that the corresponding level is predominantly populated via the isomer. Relative excitation functions for the γ-rays in ^{83}Br have been determined in the ^{7}Li induced reaction and in the (α,p2n) reaction. In the ^{7}Li experiment the γ-ray intensities of the transitions at 303, 1065 and 610 keV increase relative to the intensity of the 514 keV line of ^{85}Rb by factors of 1.39(12), 1.06(9) and 0.93(5), respectively, when the bombarding energy is increased from 30 to 35 MeV. Related to the intensity of the 1122 keV transition in ^{83}Kr /6/ the intensities of the three lines in ^{83}Br increase by factors of 5.1(2), 4.6(2) and 3.8(2), respectively, when the α-particle energy is increased from 36 to 45 MeV. Based on these tendencies we suppose increasing spin values for the corresponding levels (see figure 1) where the spin of the isomer might be 19/2 or 21/2. From empirical considerations one might expect $19/2^-$ or $21/2^-$ isomers resulting from the coupling of a $p_{3/2}$ or $f_{5/2}$ proton to the $(g_{9/2})^{-2}$ neutron excitation that is known as an isomer in several doubly even N = 48 nuclei. The coupling of a $g_{9/2}$ proton to the $(f_{5/2}^{-1}, p_{3/2}^{-1})$ two-proton excitation is an other candidate for the isomer although in this case only the spin $17/2^+$ can be reached.

A comparison of the reduced transition probability of the 303 keV transition (assuming different multipolarities) with known values in other nuclei /7/ shows that the experimental value would be for E1 and M1 extremely small ($2\cdot10^{-8}$ W u or $1.3\cdot10^{-6}$ W u , respectively), for E2 rather small ($1.7\cdot10^{-2}$ W u) or for M2 extremely large (1.0 W u).

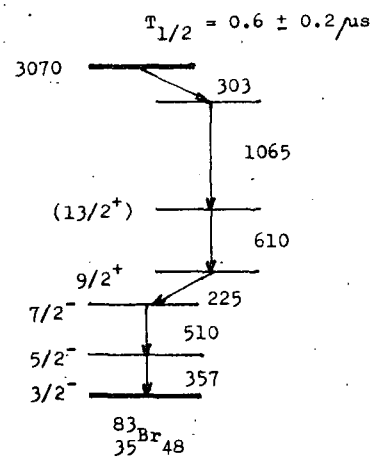

Figure 1. Decay scheme of the new isomer in ^{83}Br

References:
/1/ Käubler, L. et al.; Annual report 1986, ZfK-621 (1987) 29
/2/ Winter, G. et al.; this report p. 21
/3/ Winter, G. et al.; this report p. 22
/4/ Zell, K. O. et al.; Phys. Rev. C25 (1982) 1379
/5/ Funke, L. et al.; Z. Phys. A324 (1986) 127
/6/ Kemnitz, P. et al.; Nucl. Phys. A456 (1986) 89
/7/ Endt, P. M.; Atomic Data and Nuclear Data Tables 23 (1979) 547

A NEW THREE - PARTICLE ISOMER IN ^{85}Kr

G. Winter, R. Schwengner, L. Funke and J. Döring
Zentralinstitut für Kernforschung, Rossendorf, Bereich KF

During the irradiation of ^{82}Se targets with ^{7}Li ions /1,2,3/ a delayed emission of the 1931 keV γ-ray relative to the beam bursts has been observed. This transition is known /4/ to deexcite the $13/2^+$ level in ^{85}Kr. The time distribution /3/ recorded for this γ-ray contains a prompt and a long-lived component indicating that the delayed behaviour of the 1931 keV γ-ray is caused by a new isomeric level that decays via the 1931 keV level with a half-life being much longer than the repetition time of the beam bursts (104 ns). On the basis of a $\gamma\gamma$-coincidence experiment performed in connection with the (α,n) reaction on ^{82}Se a 60.3 keV γ-ray was identified as the isomeric transition. From an intensity balance in the spectrum of delayed γ-rays observed in the (α,n) reaction the total conversion coefficient of the 60.3 keV transition was estimated to be 7^{+3}_{-2}. The lifetime of the isomer was determined in a proton-gamma coincidence experiment /2/ in connection with ^{7}Li bombardment of ^{82}Se. From the intensities of the 1931 keV line in the spectra of delayed proton - γ coincidences a half-life of $T_{1/2} = 1.2^{+1.0}_{-0.4}$ μs has been estimated for the new isomer at 1991 keV in ^{85}Kr. The conversion coefficient of the 60.3 keV transition together with the half-life allow us to assign the multipolarity E2 to the 60.3 keV transition. For the new isomer we propose $I^{\pi} = (17/2^+)$ that is supported by the relative excitation functions of the 60.3 and 1931 keV γ-rays in the (α,n) reaction at bombarding energies between 13 and 21 MeV. The half-life of the $(17/2^+)$ level corresponds to a B(E2) value of $B(E2, 17/2^+ \rightarrow 13/2^+) = 3.8^{+1.8}_{-1.8}$ W u. For the E2 transition from the $13/2^+$ to the $9/2^+$ ground state a value of $B(E2, 13/2^+ \rightarrow 9/2^+) = 2.8^{+0.4}_{-0.3}$ W u has been derived from a lifetime measurement on the basis of the Doppler shift of the 1931 keV γ-ray /4/. Comparing these B(E2) values in ^{85}Kr with those determined for the 4^+ and 2^+ yrast states in /3/ ^{86}Kr (0.05 and 11.2 W u, respectively) it seems very unlikely that the $9/2^+$, $13/2^+$ and $17/2^+$ levels in ^{85}Kr result from a simple coupling of a $g_{9/2}$ neutron hole to the 0^+, 2^+ and 4^+ yrast states, respectively, in ^{86}Kr. In that case the B(E2) values between the states in ^{85}Kr should be approximately the same as those between the corresponding core states /5/. The B(E2) values observed in ^{85}Kr and ^{86}Kr led us to suggest that the simple coupling exists only for the $9/2^+$ and the $17/2^+$ level whereas the $13/2^+$ level contains in addition to the 2^+ core state also a strong component arising from the 4^+ core state. This assumption is supported by the close lying excitation energies of the $13/2^+$ and $17/2^+$ levels in ^{85}Kr. Due to this mixing the $17/2^+$ to $13/2^+$ transition would proceed via the 4^+ component and an angular momentum recoupling where in neighbouring nuclei B(E2) values of a few W u are observed. The $13/2^+$ to $9/2^+$ transition might be understood as a transition between the 2^+ component in the $13/2^+$ level to the 0^+ ground state. With respect to the corresponding transition in ^{86}Kr the B(E2) value in ^{85}Kr is considerably reduced in accordance with the assumed configuration mixing in the $13/2^+$ level.

References:

/1/ Käubler, L. et al.; Annual report 1986, ZfK-621 (1987) 29
/2/ Winter, G. et al.; this report p. 20
/3/ Winter, G. et al.; this report p. 22
/4/ Zobov, A.E. et al.; Reports on 36. Conference on Nuclear Spectroscopy and Nuclear Theory, Kharkov, USSR, 1986, 72
/5/ Ludziejevski, J. et al.; Physica Scripta 14 (1976) 133

A STRONGLY RETARDED E2 TRANSITION IN ^{86}Kr

G. Winter, J. Döring, L. Funke and H. Prade
Zentralinstitut für Kernforschung, Rossendorf, Bereich KF

In-beam studies in connection with ^{7}Li irradiations of ^{82}Se targets /1,2,3/ revealed a delayed emission of the 685 and 1565 keV γ-rays deexciting the 4^+ and 2^+ yrast levels, respectively, in ^{86}Kr. Time distributions have been recorded for various γ-ray energies using a time-to-pulse-height converter that was started by pulses from a Ge(Li) detector and stopped by the radio frequency signal of the cyclotron oscillator. An inspection of the centroids of the time distributions (after correction for contributions arising from the γ-ray continuum) showed that the 685 and 1565 keV transitions are emitted in the decay of an isomer with a half-life of $T_{1/2} = 3.1 \pm 0.6$ ns. This half-life is ascribed to the 4^+ yrast level at 2250 keV in ^{86}Kr and implies a strongly retarded E2 transition to the 2^+ yrast level with a reduced transition probability of $B(E2, 4^+ \rightarrow 2^+) = 0.054 \,^{+0.013}_{-0.009}$ Weisskopf units (W u). For comparison, the reduced E2 transition probability from the 2^+ level to the ground state has been determined in Coulomb excitation experiments /4/ resulting in $B(E2, 2^+ \rightarrow 0^+) = 11.2$ W u. On the basis of particle transfer reaction studies the 4^+ yrast state is interpreted /5/ as the two-proton configuration $(f_{5/2}^{-1}, p_{3/2}^{-1})$. In this nucleus containing a closed neutron shell (N = 50) the strong retardation of the E2 transition probability of the 4^+ yrast level should be connected with the almost completely filled configuration space of the valence protons $(f_{5/2}, p_{3/2})$ allowing 4^+ as the maximum spin for two-proton excitations. A similar retardation is also observed for some nuclei containing the N = 82 closed neutron shell (e.g. ^{138}Ba, ^{142}Nd) where the valence protons are distributed over the $(g_{7/2}, d_{5/2})$ orbitals. In that case the maximum spin for two-proton excitations is 6^+ and the E2 transitions deexciting the 6^+ yrast state to the 4^+ yrast state in ^{138}Ba and ^{142}Nd reveal reduced transition probabilities of $B(E2, 6^+ \rightarrow 4^+) = 0.05$ and 0.02 W u, respectively, while much larger values of $B(E2, 2^+ \rightarrow 0^+) = 10.0$ and 12.0 W u, respectively, are observed for the decay of the 2^+ yrast state /4,6/. In shell model calculations /7/ this retardation depends critically on the values of model parameters, e.g. on the energy separation between $g_{7/2}$ and $d_{5/2}$ orbitals.

References:

/1/ Käubler, L. et al.; Annual report 1986, ZfK-621 (1987) 29
/2/ Winter, G. et al.; this report p. 20
/3/ Winter, G. et al.; this report p. 21
/4/ Raman, S. et al.; Atomic Data and Nuclear Data Tables 36 (1987) 1
/5/ Tucker, A. B. et al.; Phys. Rev. C6 (1972) 2075
/6/ Lederer, C. M. and V. S. Shirley, Table of Isotopes, 7 th Edn., New York: John Wiley 1978
/7/ Prade, H. et al.; Nucl. Phys. A472 (1987) 381

HIGH-SPIN STATES IN THE N=48 NUCLEUS ^{86}Sr

A.E. Zobov, A.S. Mishin
Physico-Technical Institute "A.F. Joffe", Leningrad, USSR

H. Rotter, G. Winter, L. Funke, H. Prade
Zentralinstitut für Kernforschung, Rossendorf, Bereich KF

As a continuation of our recent study /1/ of high-spin states in the N=48 nucleus ^{84}Kr we have initiated the investigation of the heavier isotone ^{86}Sr which has been excited in different reactions. Whereas the reaction $^{76}Ge(^{13}C,3n\gamma)^{86}Sr$ at beam energies up to 42 MeV has been used /2/ at the cyclotron in Leningrad to measure excitation functions, prompt γ-γ coincidences, angular distributions and lifetimes (DSA and plunger method), the reaction $^{84}Kr(\alpha,2n\gamma)^{86}Sr$ at beam energies up to 27 MeV has been applied at the Rossendorf cyclotron for some complementary experiments. In this case a plastic cell of 1.2 cm diameter x 1.8 cm length /3/ with 1.8 mg/cm^2 mylar foils as entrance and exit windows was filled with Kr gas (enriched to 93.6 % in ^{84}Kr) at a pressure of 1 atmosphere. Thus the thickness of the gaseous target amounted to about 6 mg/cm^2.

From the experiments with the ^{13}C beam a level scheme of ^{86}Sr containing numerous new levels up to about 8 MeV and (15 - 16)$\hbar$ has been constructed. However, there were some uncertainties in the level scheme above the well-known 8^+ isomer at 2956 keV. For instance, the transitions of the cascade 1753-1126-227-130 keV (refs. /4,5/) have been placed in a different sequence in former papers /2,6/. On the basis of a delayed γ-γ coincidence experiment performed in the α-particle induced reaction and by taking into account the results of an excitation function measurement between 21 and 27 MeV α-particle energy some of these questions could be solved.

In the delayed γ-γ coincidence experiment the γ-rays preceding the 8^+ isomer (τ =0.66 μs) have been measured by using a 5 % efficiency Ge(Li) detector (start signal for a TAC) and a NaJ(Tl) detector of 7.5 cm length x 7.5 cm diameter (stop signal for the TAC). The delayed γ-ray spectra (3 subsequent time windows of 200 ns each) offer some new γ-rays, e.g. a weak 356 keV transition that fits the sum of the 227 and 130 keV transitions. This fact and the excitation function data confirm the transition sequence mentioned before in agreement with refs. /4,5/.

Furthermore, from lifetime measurements applying the pulsed-beam γ-timing method as well as the Doppler shift attenuation method in connection with the gaseous target, a value of τ =2.1(2) ns could be determined for the 5^- level at 2673 keV. No counterpart of the 12^+ isomer found /1/ in ^{84}Kr has been observed in ^{86}Sr with filled proton $p_{3/2}$ and $f_{5/2}$ subshells. Further experiments, as e.g. linear polarization measurements, are necessary to make firm spin and parity assignments to the high-spin states of ^{86}Sr as a precondition for the interpretation of these excitations.

R e f e r e n c e s :

/1/ Zobov, A.E. et al., Proc. 35th Conf. on nuclear spectroscopy and nuclear structure, Leningrad, 1985 (Nauka, Leningrad, 1985) p.68 ; Rotter, H. et al., Phys. Lett. 163B(1985)323 and to be published
/2/ Zobov, A.E. et al., Proc. 37th Conf. on nuclear spectroscopy and nuclear structure, Jurmala, 1987 (Nauka, Leningrad, 1987) p.65
/3/ Walzog, D. et al., Rossendorf annual report 1981, ZfK-488(1982) p.208
/4/ Fields, C.A. et al., Nucl. Phys. A398(1983)512
/5/ Warburton, E.K. et al., J. Phys. G 12(1986)1017
/6/ Bucurescu, D. et al., Annual report 1984/85 Department of Heavy Ion Physics, Institute of Physics and Nuclear Engineering, Bucharest, 1986, p. 21

A NEW THREE-QUASIPARTICLE ISOMER IN ^{117}Sb

L.K. Kostov, L.G. Kostova and W. Andrejtscheff
Institute for Nuclear Research and Nuclear Energy, Sofia, Bulgaria

H. Prade, J. Döring and R. Schwengner
Zentralinstitut für Kernforschung, Rossendorf, Bereich KF

The odd-mass Sb isotopes with A = 113 - 119 have been the subject of intensive in-beam γ-ray investigations /1-4/. In these studies long-lived high-lying isomers were found in ^{115}Sb /2,4/ and ^{117}Sb /1,3/ having spin and parity assignments of $25/2^+$. Shory et al. /2/ suggested that many of the high-spin states excited during the decay of these isomers can be described by two-neutron one-proton configurations. Comparing the energy spacings of levels in $^{113-119}$Sb with those of the corresponding core levels they have interpreted the lowest $19/2^-$ and $15/2^-$ levels in $^{113-119}$Sb as the coupling of a $d_{5/2}$ proton to two-neutron core excitations in the (A-1) Sn nucleus. This could be confirmed in ^{115}Sb /2,4/ by lifetime and g-factor measurements of the $19/2^-$ level. On the other hand, no information on the lifetime of the $19/2^-$ state in ^{117}Sb has been available until now.

Levels in ^{117}Sb were excited by means of the ^{115}In(α,2n) reaction using the 27 MeV α-particle beam of the Rossendorf cyclotron. We measured γ - r.f. coincidences and analysed the experimental time distributions according to the generalized centroid-shift method. The experimental set-up and details of the data analysis are described e.g. in /5/. The $19/2^-$ state decays via two transitions with energies of 254.6 and 456.9 keV to the $17/2^-$ and $15/2^-$ levels, respectively (see fig. 1). From the centroids of the corresponding time distributions an average half-life of

$$T_{1/2}(2779.8 \text{ keV}) = 0.6 \pm 0.2 \text{ ns}$$

has been determined. For the E2 transition deexciting this isomeric state we derived a reduced transition probability of B(E2, $19/2^- \rightarrow 15/2^-$) = 0.4 W.u.. This value is similar to that for the corresponding $7^- \rightarrow 5^-$ core transition /6/. Although the experimental errors are relatively large this result reveals the core-coupled structure of the $19/2^-$ and $15/2^-$ levels in ^{117}Sb.

We note also that the value of B(M1, $19/2^- \rightarrow 17/2^-$) in ^{117}Sb is close to the B(M1, $7^- \rightarrow 6^-$) value in ^{116}Sn (see fig. 1).

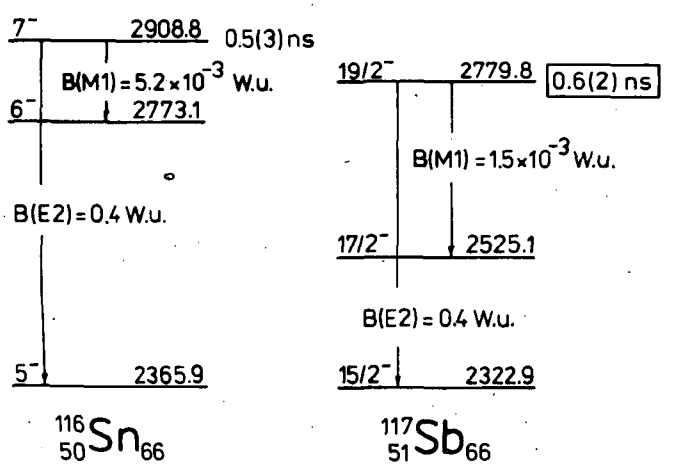

Fig. 1

Partial level schemes of ^{116}Sn and ^{117}Sb according to /2,6/ and this work.

References

/1/ Fromm, W.D. et al.; Nucl. Phys. A243 (1975) 9

/2/ Shory, R.E. et al.; Phys. Rev. C19 (1979) 1324

/3/ Ionescu-Bujor, M. et al.; Nucl. Phys. A466 (1987) 317

/4/ Bron, J. et al.; Nucl. Phys. A279 (1977) 365

/5/ Kostov, L.K. et al.; Nucl. Phys. A376 (1982) 451

/6/ van Poelgeest, A. et al.; Nucl. Phys. A346 (1980) 70

IN-BEAM STUDY OF ^{142}Nd

H. Prade, J. Döring, W. Enghardt, L. Funke, L. Käubler, R. Schwengner and G. Winter
Zentralinstitut für Kernforschung, Rossendorf, Bereich KF

An (α,2n$_\gamma$) in-beam study of excited states in ^{142}Nd revealed 27 new levels on top of the 6^+ isomer. Nanosecond lifetimes were found for three levels. States in ^{142}Nd have been populated by bombarding enriched $^{140}CeO_2$ targets with 20 - 27 MeV α-particles at the Rossendorf cyclotron. The level scheme of ^{142}Nd shown in figure 1 is based on measurements of singles γ-ray spectra, excitation functions, prompt and delayed $\gamma\gamma$-coincidences, angular distributions and linear polarization of γ-rays as well as γ - RF time distributions. The statistical accuracy of the angular distribution coefficients and of the polarization values is similar or better than in the case of our recent ^{140}Ce experiments /1/ and in connection with the excitation function it allows numerous spin and parity assignments for levels in ^{142}Nd.

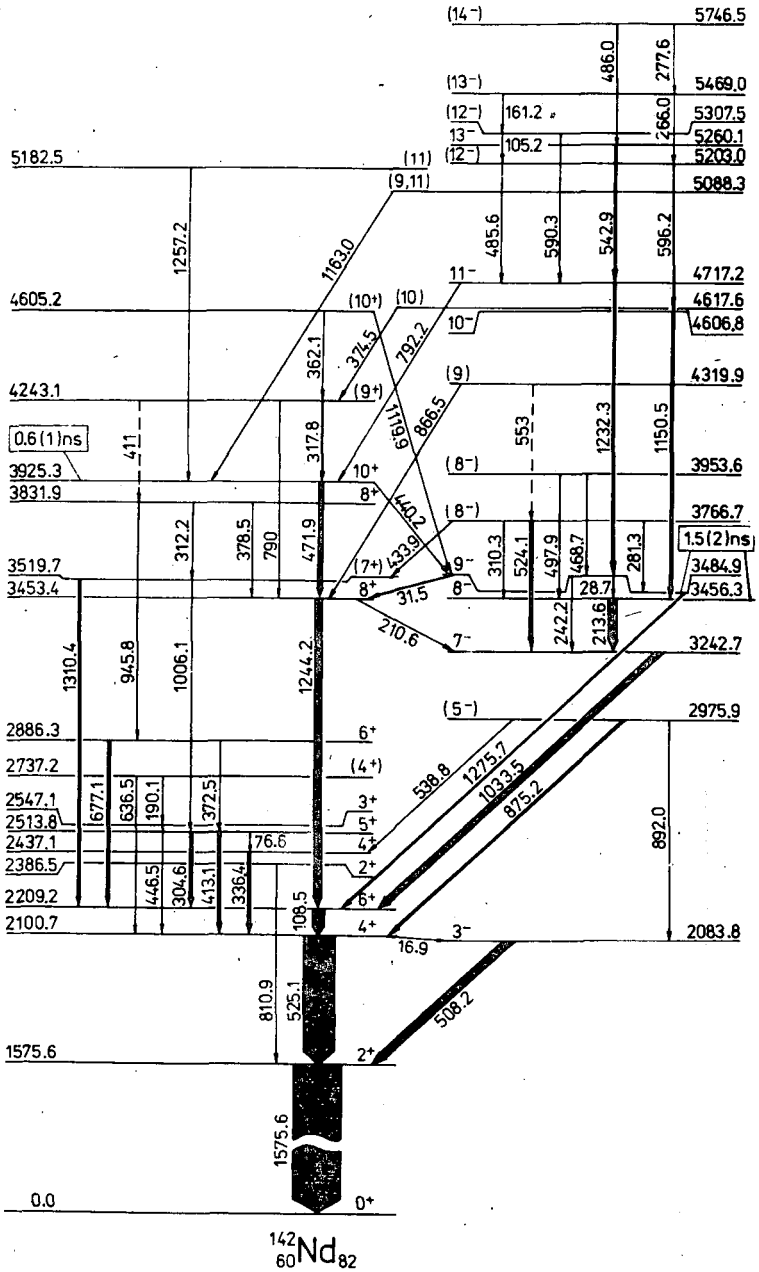

$^{142}_{60}Nd_{82}$

Positive-parity states have been identified up to spin J = 10 $\hbar$, while negative-parity states have been established up to J = (14) $\hbar$. In analogy to the lighter N = 82 nuclei ^{138}Ba /2/ and ^{140}Ce /1/, the 9_1^- and 10_1^+ states were found to be isomeric. Furthermore, for the 8_1^- level a lifetime could be deduced:

$T_{1/2}$(8^-, 3456.3 keV) = 1.5(2) ns,

$T_{1/2}$(9^-, 3484.9 keV) = 1.5(1) ns

and $T_{1/2}$(10^+, 3925.3 keV) = 0.6(1) ns.

In addition to the experimental information given in figure 1 further 13 levels at excitation energies of 3009.6, 3086.0, 3244.4, 3295.8, 3413, 3439.6, 3448, 3860.7, 4070.0, 5315.8, 5437.8, 5513.6 and 5650.8 keV have been established on the basis of our $\gamma\gamma$-coincidence data, but at present no spin and parity assignments can be proposed for these levels. The states at 4016.8, 4995.1, 5364.8, 5571.1, 5965.8 and 6736.5 keV observed in an earlier (α,2n) study /3/ could not be confirmed in this investigation.

Fig. 1
Level scheme of ^{142}Nd

References

/1/ Enghardt W. et al.; Nucl. Phys. A449 (1986) 417
/2/ Prade H. et al.; Nucl. Phys. A472 (1987) 381
/3/ De Geer L.-E. et al.; Nucl. Phys. A246 (1975) 104

SHELL-MODEL DESCRIPTION OF ^{142}Nd

H. Prade, J. Döring, W. Enghardt, L. Funke and L. Käubler
Zentralinstitut für Kernforschung, Rossendorf, Bereich KF

J. Blomqvist
Research Institute of Physics, Stockholm, Sweden

The measured excitation energies of ^{142}Nd states /1/ have been compared with spherical shell-model predictions obtained from suitable truncated model spaces. Thus, excitation energies of positive-parity states have been calculated by applying the shell model with configuration mixing (SCM) to the configuration space /2/ $(g_{7/2}, d_{5/2})^{Z-50}$; $(g_{7/2}, d_{5/2})^{Z-51}(d_{3/2}, s_{1/2})^{1}$. To treat the negative-parity states, an approach /3/ has been used, where an $h_{11/2}$ proton is coupled to low-lying $\pi = +1$ states of ^{141}Pr considered as the core. The core is descibed within the SCM. This concept is capable of describing negative-parity states in N = 82 nuclei, c.f. e.g. /4,5/, since the addition of one $h_{11/2}$ proton will only slightly disturb the states formed by protons on the $\pi = +1$ subshells. In both model spaces the same Hamiltonian containing the modified delta interaction /2/ has been diagonalized. In fig. 1 the experimental level energies are compared with the model predictions.

Though the level energies are generally predicted a bit too small (except the collective 3^- and the probable second 8^- states), the sequence and the spacings of the levels are well reproduced. For all positive-parity states configurations of the type $(g_{7/2}, d_{5/2})^{10}$ are found to dominate the wave functions. The two-proton $(h_{11/2}, d_{5/2})$ and $(h_{11/2}, g_{7/2})$ multiplets provide negative-parity levels up to spin 9, while the states with $9^- \leq J^{\pi} \leq 14^-$ can be interpreted as seniority-four states.

Regarding the level scheme of ^{146}Gd /6/ one may expect $(h_{11/2})^2$ proton excitations, which are outside our SCM configuration space, at level energies of $E_x \gtrsim 4$ MeV. Using empirical values for the one- and two-body interactions, which are derived from the excitation energies of pertinent levels in N = 82 nuclei with $58 \leq Z \leq 64$ and from the respective ground state masses, the energy of the maximum aligned $(h_{11/2})^2_{10^+}$ state has been calculated (for the method see /7/). This two-proton excitation is expected to lie at E_x = 4584 keV. Therefore, the levels at 4605.2 and 4617.6 keV appear to be candidates for a two-proton excitation to the $1h_{11/2}$ shell, where the first is the more likely one due to its deexcitation to the 9^-_1 state in analogy to ^{146}Gd /6/.

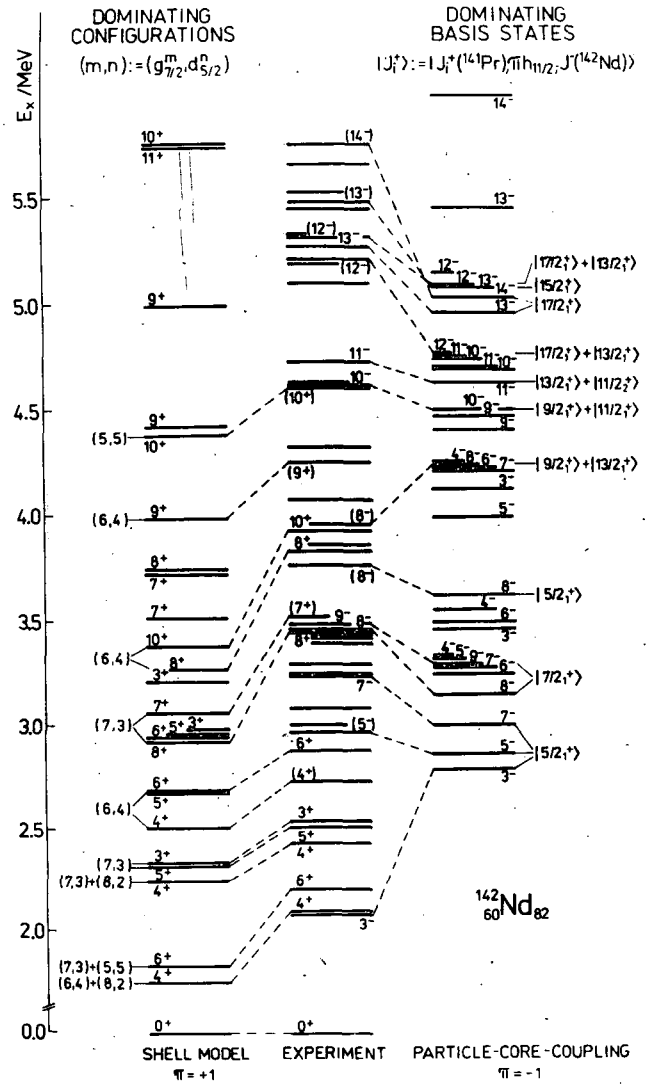

Fig. 1

Comparison between experimental and theoretical spectra of ^{142}Nd. For each value of J^{π} only the three lowest states with $E_x \lesssim$ 6 MeV and $J \geq 3$ are displayed. The main components of the wave functions providing a contribution of more than 50 % are given for the states experimentally found.

References

/1/ Prade H. et al.; this report p. 25
/2/ Wildenthal B.H.; Phys. Rev. Lett. 22 (1969) 1118
/3/ Enghardt W. and Jäger H.U.; Nucl. Phys. A438 (1985) 141
/4/ Prade H. et al.; Nucl. Phys. A472 (1987) 381
/5/ Enghardt W. et al.; Nucl. Phys. A449 (1986) 417
/6/ Kleinheinz P. et al.; Z. Physik A290 (1979) 279
/7/ Blomqvist J. et al.; Z. Physik A312 (1983) 27

THEORY

ON THE CANONICAL REALIZATION OF A FINITE-DIMENSIONAL LIE ALGEBRA.

G. Flach and D. Kirschbaum[+]
Zentralinstitut für Kernforschung, Rossendorf, Bereich KF[+]

We investigated the structure of the derivation algebra in classical Hamiltonian mechanics. This infinite-dimensional Lie algebra k(2n,R) of generators of canonical transformations was obtained as algebraic closure of two finite-dimensional Lie subalgebras /1/. The first one is the Lie algebra sp(2n,R) of generators of the symplectic group, while the second one (pcg) belongs to a projective canonical group and has been derived from point transformations. The algebra pcg and the related Lie group seems not been used so far in the analysis of classical mechanical systems but it has some interesting properties which may be useful for physical investigations.
The essential content of the above mentioned structural relations may be summarized in the following scheme

$$k(2n,R) = sp(2n,R) \cup pcg \qquad (1)$$
$$u(n) = sp(2n,R) \cap pcg ,$$

where u(n) is the symmetry algebra of the n-dimensional harmonic oscillator. We derived the explicit expressions of elements for the pcg algebra and proved furthermore /2/ that a) the algebra pcg is the largest finite-dimensional algebra of point transformations in the algebra k(2n,R), b) the algebra pcg acts transitively on functions f(q) defined on the configuration space and intransitively on functions h(q,p) defined on the phase space.
Having in mind future applications to physical systems (e.g. to systems of oscillators) we sharpen the results of /2/ in the present note.
Remember that any generator L_f as element of the derivation algebra k(2n,R) is determined by use of the Poisson bracket operation as follows

$$L_f = \frac{\partial f}{\partial p^i}\frac{\partial}{\partial q_i} - \frac{\partial f}{\partial q_i}\frac{\partial}{\partial p^i} \qquad (2)$$

with f = f(q,p). The generating functions f of the pcg algebra have been determined in /1,2/, they are p^i, $q_j \cdot E_o^o$, $q_i \cdot p^j$ ($E_o^o = q_i p^i$, i,j = 1,..,n). We derived the pcg algebra starting from the projective transformation group in Q_n. Now we extend theorem a) as follows: There exists no similar projective group in phase space Γ_{2n} = (q,p) giving rise to a finite-dimensional Lie algebra k of canonical generators (2) including the pcg algebra. Such subgroup contains definitely special conformal transformations of the canonical variables (q,p) as follows (q,p) $\longrightarrow$ (q'p'):

$$(q_i') = (\alpha^\mu q_\mu + \beta_\nu p^\nu + 1)^{-1}(q_i) \quad , \quad (p^{i\prime}) = (\alpha^\mu q_\mu + \beta_\nu p^\nu + 1)^{-1}(p^i). \qquad (3)$$

The transformations (3) determine maximal 2n one-parameter subgroups and corresponding vector fields L_f. Using standard techniques the vector fields corresponding to single parameters α^μ or β_ν are calculated to be $q_i q_j \partial q_j$, $q_i p^j \partial q_j$, $p^i p^j \partial p_j$, $q_i p^j \partial p_j$. Using (2), we find the following generating monomials f = f(q,p) corresponding to L_f: $q_i q_j p^j$, $q_i p^j p^j$, $p^i p^j q_j$, $q_i p^j q_j$. The algebra k must contain some generating elements corresponding to the symplectic algebra sp(2n,R). Using the theorem proved in /1/ it follows, that in the set of generating functions of k any elements of third degree in (q,p) are contained and, furthermore, monomials of any degree in (q,p). Therefore a projective Lie algebra k $\supset$ pcg is an infinite-dimensional algebra, this proves our new result concerning theorem a). We sharpen the theorem b) as follows: The pcg algebra acts transitively on any of the following subsets of functions h(q,p) defined on phase space: $P^{(\nu)} \cdot f(q)$ ($P^{(\nu)}$ - the set of monomials of fixed degree ν in p^i(i = 1, ...,n), f(q) on Q_n). Theorem b) results if $\nu = 0$.
The proof is trivial for vector fields L_f corresponding to generating functions (p^i,$q_i p^j$) - the monomials $P^{(\nu)}$ and functions f(q) are separately invariant. Applying the special conformal generators $L_{qi} \cdot E_o^o$ to the monomials $P^{(\nu)}$, we get certain elements $P^{(\nu)} \cdot q$, now using that u(n) $\subset$ pcg then any element $P^{(\nu)} f(g)$ of first degree in q results. Taking use of repeated generators $L_{qi} \cdot E_o^o$ and L_{qip^j} one gets the desired result, i.e. we get any function of the type $P^{(\nu)}$ f(q).

/1/ Kirschbaum, D. Journal of Physics A(1988), in press
/2/ Flach, G., Kirschbaum, D. Annalen der Physik (1988), accepted for publication

THE EFFECTIVE AXIAL-CHARGE FORMFACTOR OF THE NUCLEON IN NEUTRON-RICH NUCLEI

M.Kirchbach
Central Institute for Nuclear Research Rossendorf, 8051 Dresden,
POB 19, GDR

The mesonic exchange current (MEC) inside the nucleus leads to a strong renormalization of the matrix element of the axial-charge (AC) density operator ($AC=g_A\,\vec{\sigma}\cdot\vec{p}/M\,\tau_{\mp}$, $g_A=1.25$) and in this way to an effective nucleon axial formfactor ($g_A^{AC} = g_A(1+\delta)$). The latter can be deduced from the transition rates of 0^+-0^- ß-decays. Extensive theoretical work on the $0^+ \rightleftarrows 0^-$, $\Delta T=1$ -weak transitions in the A=16- nuclei (see refs. /1-2/ for reviews) has shown that the effective axial formfactor of the nucleon in these light nuclei is larger by about 50% than the bare one ($g_A^{AC} \approx 1.5 g_A$). Alternatively, the value of g_A can be obtained by studying the spin-isospin response of nuclei excited by charge-exchange reactions. There, the relevant transition-operator (so called Gamow-Teller (GT) operator) is $GT= g_A\,\vec{\sigma}\,\tau_{\mp}$. In contrast to g_A^{AC} , the apparent axial formfactor of the bound nucleon obtained from the GT-transitions is quenched relative to its value deduced from the free-nucleon ß-decay ($g_A^{GT} \approx \eta_A\, g_A$, $\eta_A < 1$). The studies on the GT-excitations in several nuclei via the (p,n)-reaction have lead to the conclusion that g_A is quenched by at least 20-30% throughout the periodic system ($\eta_A \approx 0.8$) /3/. One necessary step for understanding the g_A^{AC} - g_A^{GT} -puzzle should be to extend the studies on the 0^+-0^- ß-transitions, which so far have been restricted to light nuclei, to heavier nuclei. For this aim, the renormalization parameter δ of the AC-density by the MEC-operator has been calculated along the line of ref. /4/ where the approximation of an inert core has been used (see fig. 1). From fig.1 it is seen that g_A^{AC} decreases with mass-number. The decrease found is due to the fact that the evolution of δ with A is roughly described by

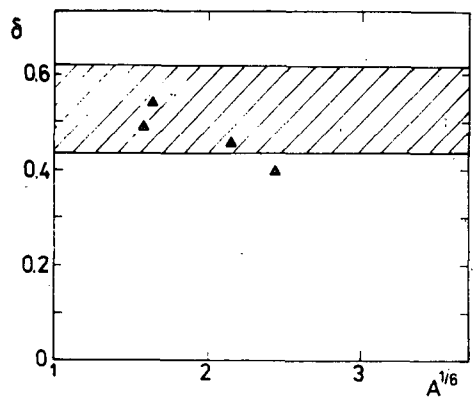

FIGURE 1

The A-dependence of the renormalization parameter The dashed band represents the possible nuclear-matter values of δ as calculated in ref./7/.

$$\delta \sim 1/b f_\pi \sim \sqrt{M\hbar\omega}/f_\pi \sim M^{1/2}\, A^{-1/6}, \qquad (1)$$

$$b=(\hbar/\omega M)^{1/2}\ ,\ \hbar\omega \approx 41\ A^{-1/3}.$$

This result is easy obtained by noticing that the oscillator-length parameter b enters the MEC-operator as $m_\pi^2/f_\pi M(b\, m_\pi)^2$ (its radial dependence being determined by an first-order Yukawa function) , whereas the one-body operator scales like 1/bM. This decrease which is compensated to a large extent by the shell-effects becomes more pronounced if the bare nucleon mass M in eq.(1) is replaced by the effective one as obtained e.g. in relativistic mean-field theory where typically $M^* \approx (0.6\text{-}0.8)$ M is found. In this case the kinetic energy of the decaying $3p_{1/2}$-valence neutron in the A=206-nuclei is larger by about 20-30% as compared to that of the corresponding 2s-nucleon in the light systems. As it is known from current-algebra results, the contribution of the Goldstone bosons (the pions) to the low-energy sum rules is frame dependent and decreases if the nucleon is moving faster. Due to an idea of Rho /5/, the axial-vector strength measured in the GT-transitions corresponds to an infinite momentum of the nucleon, whereas the axial-charge formfactor is deduced within a finite (low-) momentum frame. Our studies indicate that in the asymptotics g_A^{AC} should eventually approach g_A^{GT} (a fact which has been pointed to us by Rho). Furthermore, from eq.(1) it follows that the one-body decay rate increases like (M/M^*) but not like $(M/M^*)^2$ as it has been stated in ref /6/ where the use of $M^* \approx 0.6M$ has been viewed as a mechanism sufficient for enhancing the AC-density

up to the size required by the data. From our studies it follows that effective masses combined with meson-exchange current corrections lead to theoretical results which are compatible with the experimental findings. Preliminary results indicate that the log ft-values in the A=206-nuclei are well reproduced by using an effective nucleon mass of $M^* \approx 0.8M$ which corresponds to renormalization parameter $\delta \approx 0.35$.

References:

/1/ M.Kirchbach, E.Truhlik, Sov.J.Part.Nucl. 17 (1986) 224

/2/ I.S.Towner, Ann.Rev.Nucl.Part.Sci. 36 (1986) 115

/3/ C.D.Goodman,S.D.Bloom, in "Spin Excitations in Nuclei" ed by Petrovich et al (Plenum Press, N.Y. 1984) p.143

/4/ M.Kirchbach, H.Reinhardt, preprint NBI-87-79

/5/ M.Rho, in "Spin Excitations in Nuclei" ed by Petrovich et al (Plenum Press,N.Y. 1984) p.111

/6/ G.Do Dang, M.Jaminon, N. Van Giai, Phys.Lett. 153B (1985) 17

/7/ J.Delorme, Nucl.Phys. A374 (1982) 541c

NUCLEAR STOPPING POWER AND THE TWO-FLUID HYDRODYNAMICS

H. W. Barz and B. Kämpfer
Zentralinstitut für Kernforschung Rossendorf, Bereich KF

Heavy ions colliding with ultra-relativistic energies are expected to penetrate one another. This assumption is based on the observation that high energy protons lose roughly 2.4 units of rapidity when traversing a large nucleus. Therefore the one-fluid model seems to be not adequate to describe heavy ion reactions with several tens of GEV per nucleon. Here we apply now the two-fluid model to investigate the properties of the target and the fragmentation region. The two nuclei are represented by two perfect fluids which are described by the energy momentum tensor $T^{ij} = (e+p)\, u^i u^j + p\, g^{ij}$, where u^i is the four velocity of the fluid and energy density and pressure are functions of the baryon number density n and the temperature. Now, the equations of motion are coupled locally as introduced in ref./1/:

$$T^{ij}_{,j} = -Dn\bar{n}(u^i - \bar{u}^i) - Q\frac{n}{n_0} e_{therm} u^i \; ; \quad \bar{T}^{ij}_{,j} = -Dn\bar{n}(\bar{u}^i - u^i) - Q\frac{\bar{n}}{n_0} \bar{e}_{therm} \bar{u}^i ,$$

where the (un)barred quantities refer to the target(projectile) fluid. The friction term ($\sim$D) is well studied by investigating collisions at lower energy. This term is responsible for the excitation and deceleration of the fluid. The energy leak-out term ($\sim$Q) was introduced in ref./1/ and was assumed to be proportional to the thermal part of the energy density. The quantity Q measures the leak-out rate of energy into the midrapidity region. Further we take a finite phase transition time τ (for details see ref./2/). We carried out one-dimensional calculations of the collision of two slabs with thicknesses 4.9 and 12 fm using different values of Q and τ, while D was fixed to 3 $GeVfm^2$ which gives roughly a rapidity loss of 2.2 units. From fig.1 we see that the rapidity loss rises with increasing velocity of the phase transition and increasing energy leak-out. Further we observe that the projectile fragments are distributed over a wide range of rapidity.

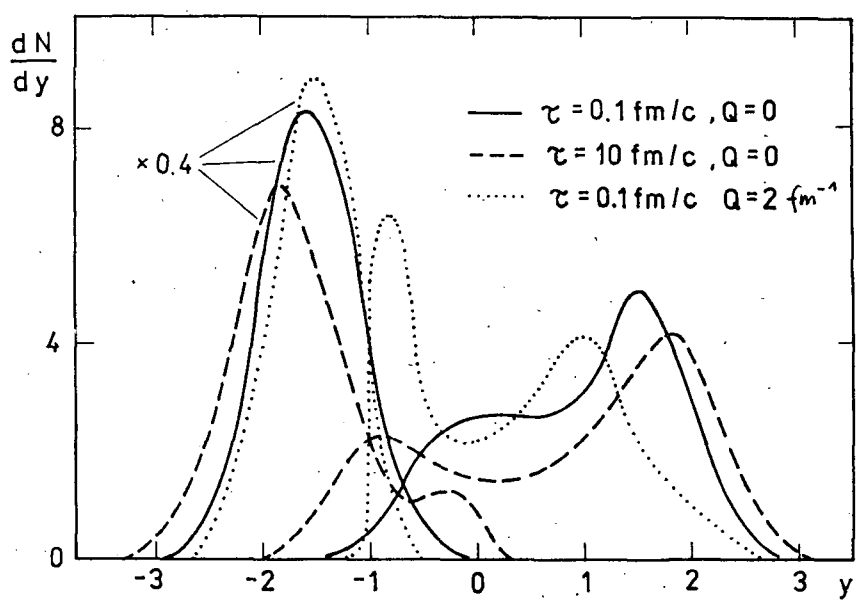

Fig.1. Baryon rapidity distribution for the projectile(right curves) and the target slab for different tansformation times in the equal-velocity system.

References

/1/ Barz,H.W. and Kämpfer, B., Dubna preprint E2-87-794(1987)
/2/ Barz,H.W., Kämpfer,B., Csernai,L. and Lukacs,B., Nucl. Phys. A465(1987)743

THE CONCEPT OF THE FORMATION LENGTH IN THE INTRANUCLEAR CASCADE MODEL

H. Iwe
Zentralinstitut fuer Kernforschung, Rossendorf, Bereich KF

In recent years, the intranuclear cascade model (INC) has been applied successfully for describing different characteristics of secondaries from reactions involving nuclei. It obviously reflects the fact that the cascade model can bring out the essentials of the multiparticle production process in nuclei at energies below 3-5 A GeV. It has been shown that the model is even successful in predicting production rates as the strangeness production [1]. The basic premises of more or less all INC models is that the heavy-ion collision is replaced by a sequence of space-time well-separated binary collision between on-shell hadrons proceeding as in free space. The elementary interactin is assumed to be point-like in space and time.

In modern QCD based models concerning the fragmentation of quarks and partons, the finiteness of the formation length for hadrons corresponds to a finite fragmentation in space and time. Secondary hadrons in the collisions are not formed instantaneously. In their rest frame they need a certain average time τ_0 which is called the hadronic formation time, before they are present as complete hadronic states. These hadrons should have a reduced probability for hadronic interactions inside the nucleus because of the absence of the soft components in the hadronic states. In this picture it appears to be quite natural, that the fast secondaries created in nuclear collisions have a reduced possibility for secondary interactions inside the nucleus. The time interval τ_0 is a characteristic time of the strong interaction ($\tau_0 \approx 1$fm/c). The products of the interaction fly apart. Because of the relativistic time dilatation they are created after the duration of the strong interaction $\tau = \gamma\ \tau_0$. Starting from these qualitative and phenomenological arguments here a procedure is proposed to take into account the finiteness of the interaction time and space. The free cross section σ^0_{hh} is modified by $\sigma = \sigma^0_{hh}(1-\exp(-\tau/\tau_0))$. Here it is assumed that the secondary hadron starts to interact hadronically in its rest frame with an exponentially growing factor depending on the ratio $\tau/\tau_0 = m_0/\hbar c * t/\gamma$. The constant m_0 plays the role of an empirical parameter lying in the range of (0.4-0.9) GeV. Therefore two cascade particles would have the modified free cross section
$\sigma^0_{hh}(1-\exp(-a_1 t_1/\gamma_1))(1-\exp(-a_2 t_2/\gamma_2))$.

The scheme proposed was taken to follow the INC for all low energy hadrons created in turn in the secondary collisions and so on. Fig. 1 shows the distributin function of the time elapsing between two successive collisions without and with consideration of the formation length concept.

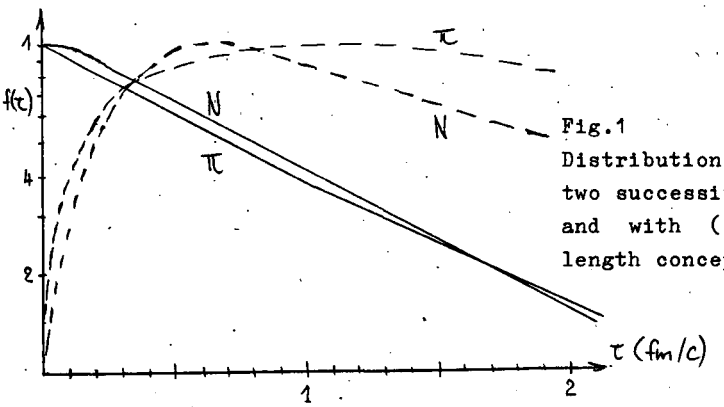

Fig.1
Distribution function of the time elapsing between two successive elementary interactions without(——) and with (.....) consideration of the formation length concept for nucleons and pions.

References:

[1] H.W. Barz and H. Iwe, Nucl. Phys. A453(1986)728

HYPERNUCLEAR PRODUCTION BY THE (π^+,K^+) REACTION

R. Wünsch
Zentralinstitut für Kernforschung Rossendorf, Bereich KF

J. Žofka
Nuclear Physics Institute, Czech. Acad. Sci., Řež/Prague, Czechoslovakia

Production of Λ and Σ hypernuclei has been performed mostly by the (K^-,π^-) reactions with the incident K^- meson in-flight [1] or stopped [2]. The momentum of the K^- in flight has been chosen to approximately satisfy the recoilless condition, so that the substitutional states have been preferably populated in the produced hypernuclei. In the stopped K^- experiment, the produced hyperon gets a momentum comparable with the nucleon Fermi momentum in the nucleus ($p_F \approx 280$ MeV/c) and therefore non-substitutonal states are strongly populated as well.
In addition to the K^--induced reaction, the feasibility of the (π^+,K^+) reaction was theoretically argued [3] and actually proven by the first $^{12}C(\pi^+,K^+)^{12}_{\Lambda}C$ experiment done at Brookhaven [4]. With the pion momentum p_π=1050 MeV/c chosen, the recoil momentum of the Λ hyperon amounts to q≈340 MeV/c, which tends to favour the excitation of non-substitutional and high angular momentum configurations. The quasi-free mechanism (production of hyperons in unbound scattering states) accounts for a considerable part of the total reaction probability.
The (π^+,K^+) reaction is now going to be applied at KEK and BNL for more extensive and advanced studies of Λ and hopefully Σ hypernuclear production. Interests are not only in the structure of light hypernuclei but also in the deep hyperon orbits in heavy hypernuclei. Also, some experiments are planned, investigating the magnetic moment of the hyperon in nuclei and the production of polarized hypernuclei by measuring the angular correlation of their weak decay products.
The experimental progress requires an adequate theoretical analysis. Since many of the interesting states are observed above the hyperon emission threshold, a strong interference between the genuine hypernucleus production and the quasi-free ejection of a hyperon takes place. In order to obtain a realistic excitation spectrum for hypernuclear production, it is necessary to evaluate both resonant and quasi-free processes. For this purpose we have applied our version [5] of the continuum shell model to the (π^+,K^+) reaction on the target nuclei ^{12}C, ^{16}O, ^{28}Si, ^{40}Ca and ^{56}Fe. Fig. 1 shows the curves obtained for ^{28}Si. The ^{56}Fe results are published in ref.[6]

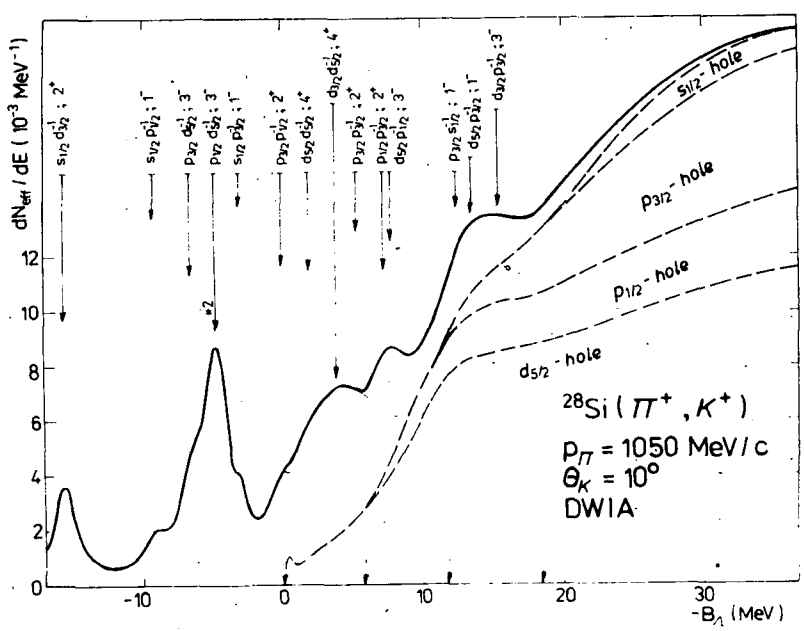

Fig. 1:
Calculated hypernuclear excitation spectrum (effective nucleon number dN_{eff}/dE) for the (π^+,K^+) reaction on ^{28}Si at p_π =1050 MeV/c and Θ_K=10°. The broken lines show the quasi-free contributions in the indicated channels. The resonant contributions have been spread by an additional 2 MeV Breit-Wigner shape. The arrows above the resonances are proportional to their excitation strengths. Multipolarity and dominating configurations are indicated.

R e f e r e n c e s
[1] Proc. Int. Symp. on Hypernuclear and Kaon Physics, ed. R. Chrien, Nucl. Phys. A450 (1986)
[2] Yamazaki T. et al.; Phys. Lett. 144B (1984) 177; Phys. Rev. Lett. 54 (1985) 102
[3] Dover C. B., Ludeking L. and Walker G.; Phys. Rev. C22 (1980) 2073
[4] Milner C. et al.; Phys. Rev. Lett. 54 (1985) 1237
[5] H. W. Barz, Rotter I. and Höhn J.; Nucl. Phys. A275 (1977) 111
[6] Motoba T. et al.; submitted to Phys. Rev. D

PERCOLATION APPROACH FOR ATOMIC AND MOLECULAR CLUSTER FORMATION

O. Knospe, R. Schmidt and G. Seifert
TU Dresden, Sektion Physik, Wissenschaftsbereich Theoretische Physik

Investigations of the formation kinetics as well as the structure of atomic and molecular microclusters are of increasing interest (see e.g. /1/). At present there is no rigorous theory, which could predict experimental size distributions obtained under certain conditions.

We applied a percolation approach for the theoretical analysis of mass spectra of microclusters obtained by adiabatic expansion technique /2/. A similar percolation model was used for the interpretation of mass spectra in nuclear fragmentation processes /3/. The evolution of the shape of the experimental size distributions as function of stagnation pressure and temperature are well reproduced by varying the percolation parameter (see fig. 1). In addition, the even-odd-alternation as well as the "magic" shell structure in metallic secondary ion mass spectra /4/ are investigated by introducing statistical weights for the formation probabilities (see fig. 2). Shell corrections energies of atomic clusters as function of cluster size are deduced from the experimental data /5/. These shell correction energies behave very similarly to those observed in atomic nuclei.

References

/1/ K. Sattler, in "Current Topics in Material Science" Vol. 12, ed. E. Kaldis, Elsevier Science Pub. 1985
/2/ E. Recknagel, Ber. Bunsenges. Phys. Chemie 88 (1984) 2o1
/3/ O. Knospe, R. Schmidt, H. Schulz, Phys. Lett. 182B (1986) 293
/4/ I. Katakuse et al., Int. J. Mass Spectrom. Ion Processes 67 (1985) 229
/5/ O. Knospe, R. Schmidt, G. Seifert, GSI-preprint 87-80 and to be published

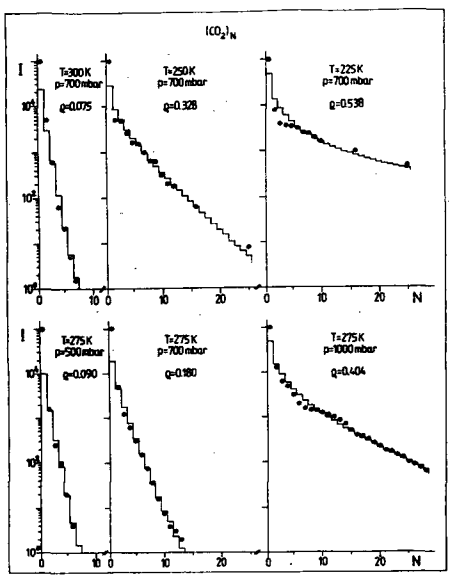

Fig. 1 Mass spectra of $(CO_2)_N$-clusters of ref. /2/ (dots) compared to the prediction of the percolation approach (lines)

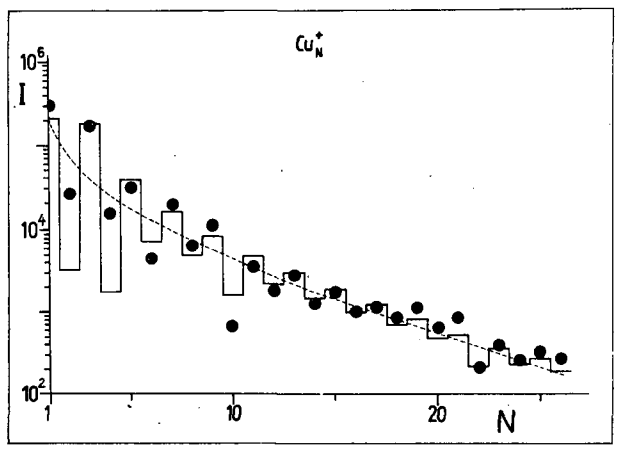

Fig. 2 Mass spectrum of Cu_N^+-clusters of ref. /4/ (dots)

FIRST STAGES OF MATTER GROWTH IN A DYNAMICAL PERCOLATION MODEL

J. Knoll
GSI Darmstadt
O. Knospe and R. Schmidt
TU Dresden, Sektion Physik, Wissenschaftsbereich Theoretische Physik

Growth of matter in its first stages is characterized by nucleation and coagulation processes. At the very beginning monomer addition is the leading process, gradually changing to the fusion of clusters when the density of clusters is high enough.

The nucleation mechanism is characterized by a typical steeply, roughly exponentially falling size distribution. It has been successfully described in a random site-percolation model /1/ where the monomer addition is simulated on a two-dimensional square lattice, the sites of which are occupied randomly.

Cluster-cluster coagulation leads to a log-normal size distribution. This type of distributions has been successfully investigated by solving kinetic equations for all cluster-cluster reactions /2/ neglecting all types of evaporation.

In this work we present an attempt to generalize the percolation approach /1/ to include the nucleation as well as the coagulation stage of cluster growth:

(i) In order to connect the percolation parameter with the physical density of the condensing gas the percolation is carried out in a continuous three-dimensional space. The shape of all clusters is assumed to be given by spherical drops.

(ii) The clusters are randomly distributed within the three-dimensional space. New clusters are formed by a combined site-bond linkage criterion. The site probability is assumed to be one if two clusters have a non-vanishing overlap and to be zero else. The bond probability takes into account the mobility of particles of different masses in a gas at given temperature.

(iii) To include cluster-cluster reactions we propose a dynamical percolation. Starting with a gas of monomers a first percolation leads to a certain cluster distribution. Succeeding percolations are carried out always with the cluster distribution resulting from the preceeding one.

The results can be summarized as follow:

1) The size distribution develops as function of time from a pure exponentially falling one to a power law like distributions up to a peaked distribution at certain size. The theoretical evolution describes well that observed in experiment /3/.

2) A scaling law for the cluster density and cluster distributions as function of time and initial monomer density has been found. This scaling law is somewhat different to that known from coagulation theory /4/.

References

/1/ Knospe O., Schmidt R., Seifert G.; GSI-preprint and this report p. 33
/2/ Soler J.M. et al.; Phys. Rev. Lett. 49 (1982) 1857
/3/ Recknagel E.; Ber. Bunsengesellschaft Phys. Chem. 88 (1984) 201
/4/ Lai F.S. et al.; J. Colloid Int. Sc. 39 (1972) 395

PREFERENTIAL EMISSION OF FAST PARTICLES TO NEGATIVE ANGLES WITHIN THE TWO-STAGE MODEL

M. Biedermann and P. Mädler
TU Dresden, Sektion Physik, Wissenschaftsbereich Theoretische Physik

One of the most salient features of fast particles emitted in intermediate-energy heavy-ion reactions is the preferential emission to negative deflection angles /1,2/. Experimentally it can be investigated by either measuring in coincidence fast light particles and the circular polarisation of γ-rays perpendicular to the plane defined by the direction of the particle and the beam axis /1/, or projectile-like fragments and fast particle spectra both on the same and on the opposite side with respect to the beam /2/. VUU-calculations /1/ have shown, that the deflection to negative angles is an effect of the attractive mean-field of the target nucleus, while two-body collisions tend to equalize positive- and negative-angle emission. Consequently, investigations of the preferential emission to negative angles may yield direct informations about the interplay of mean-field effects and two-body collisions and, in particular, about the effective nucleon-nucleon cross section to be used for the collision term in VUU.

The present study is devoted to the question, whether the phenomenological two-stage model for fast particle emission /3/ is able to quantitatively describe such type of coincidence measurements. This question is quite delicate, since the relative weight of mean-field effects and two-body collisions within this model is essentially governed by ad hoc assumptions.

We have applied the TSM to the ^{14}N (49o MeV) + ^{165}Ho data of ref. /2/. In that experiment PLF (Z=5, 21o MeV $\leq E_{PLF} \leq$ 4oo MeV) have been detected at Θ_{PLF}= +1o^o, and neutron spectra to both sides of the beam $\Theta_n = \pm|\Theta|$ (in the plane defined by the PLF and the incident direction) have been taken in coincidence with those PLF at several angles Θ relative to the beam. Fig. 1 shows the data in comparison with the TSM calculations (for more details and discussions, see /4/). A reasonable agreement with the data is obtained on an absolute scale.

In summary, we have shown that the assumptions of the TSM concerning the relative weight of two-body collisions do not contradict experimental findings which are a sensitive measure of that property.

References: /1/ Tsan M.B. et al.; Preprint MSUCL-558 (1986)
/2/ Caskey G. et al.; Phys. Rev. C31 (1985) 1597
/3/ Biedermann M. and Mädler P.; Z. Phys. A323 (1986) 315
/4/ Mädler P.; Dissertation B, TU Dresden, 1988

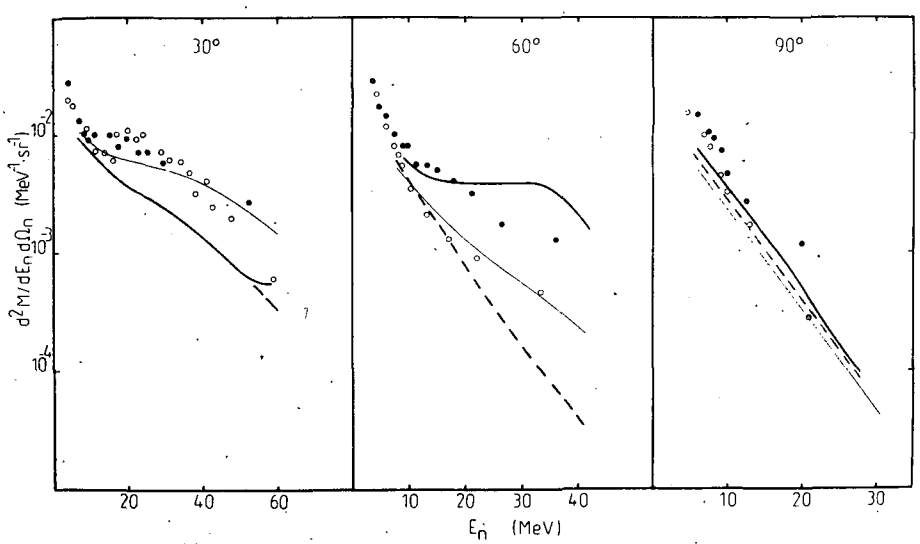

Fig. 1

Comparison of TSM calculations with neutron spectra in coincidence with PLF both to negative and positive angles $\Theta_n = \pm 3o^o$, 6o^o, 9o^o. Thin lines (TSM) and open circles (data /2/) correspond to positive, thick lines (dashed: HZ-contribution, full: PEP+HZ) and full circles (data /2/) to negative angles.
For details, see text.

PARTICLE ESCAPE FROM TIME-DEPENDENT MEAN FIELDS

B. Milek
Joint Institute for Nuclear Research, Dubna, USSR
R. Reif
TU Dresden, Sektion Physik, Wissenschaftsbereich Theoretische Physik

The particle emission during the collective motion of nuclei as in heavy-ion collisions and fission processes has been investigated within a semiclassical model which replaces the force centers by two one-term separable potentials /1,2/. This approach has been extended for the case of oscillating fields which simulate damped collective vibrations (frequency ω) of a dinuclear system with respect to the relative distance and the shape.

With the ansatz

$$V(t) = \sum_{n=1,2} e^{-i\vec{R}_n(t)\vec{p}} \; V_n(t) \; e^{i\vec{R}_n(t)\vec{p}} \tag{1}$$

$$V_n(t) = (V_0 + \delta_n(t) \; |\beta_{\ell m}\rangle\langle\beta_{\ell m}| \tag{2}$$

in which $\vec{R}_n$ and $|\beta_{lm}\rangle$ denotes the position of nucleus n and a harmonic oscillator state of angular momentum l, respectively, the time-dependent single-particle Schrödinger equation has been solved with a state of binding energy $E_B < 0$ as an initial state. From the single-particle wave function after 5 - 1o oscillations the differential emission probability $dP/d\varepsilon$ has been calculated. It turns out that the particle is preferrentially emitted with an energy

$$\varepsilon_{max} = \hbar\omega + \Delta E_B - |E_B| \; , \quad \Delta E_B = \frac{1}{2} \, |E_B^{min} - E_B^{max}| \tag{3}$$

where $E_B^{min,max}$ are defined in the adiabatic basis referring to the Hamiltonian $H(R,\delta)$.

The calculations demonstrate that pre-fusion particle emission in central heavy-ion collisions at the Coulomb barrier could serve as a signature for nuclear elastoplacticity leading to specific giant quadrupole oscillations in the collective variables before fusion /3/.

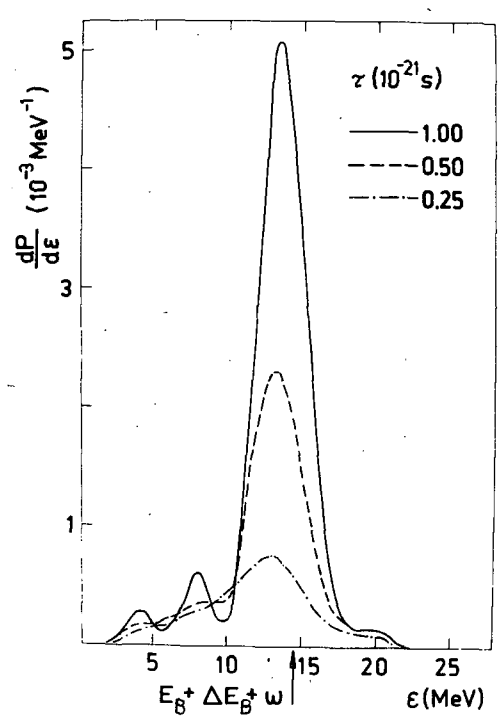

Fig. 1
Emission spectrum ($\hbar\omega$ = 2o.7 MeV) for various damping constants τ

References

/1/ Milek B., Reif R. and Revai J.; Phys. Lett. 15oB (1985) 65
/2/ Milek B., Reif R. and Revai J.; Phys. Rev. C (in press)
/3/ Lukasiak A. and Nörenberg W.; Z. Phys. A326 (1987) 79

GAMOW STATES IN AN EXPLICITLY TIME-DEPENDENT MODEL

B. Milek
Joint Institute for Nuclear Research Dubna, USSR
G. Mutschke and R. Reif
Technical University Dresden, GDR

The problem of non-statistical particle emission in heavy-ion collisions was considered in the past by performing an expansion of the single-particle wave function in a suitable chosen basis. In our previous work /1/, for example, we used an adiabatic two-center basis with finite depth potentials including Gamow states in order to take into account a part of the continuum. Cassing and Nörenberg /2/ have used a so-called diabatic basis of a two-center oscillator. In both cases the picture of a radioactive decay with time-dependent decay paramters has been applied for the calculation of the emission spectra. The angle-integrated emission probability from a single Gamow state with position E(t) and width $\Gamma(t)$ which depend on time via the classical trajectory of the ions is determined in such a picture by a simple time integration

$$dw/d\varepsilon = \lim_{t\to\infty} 1/\pi \int_0^t dt' \, (-\dot{n})\, \Gamma / ((E-\varepsilon)^2 + \Gamma^2). \qquad (1)$$

Here, $\dot{n}$ is the decay rate of the occupation n which is assumed to follow a generalised decay law $\dot{n}(t) = -2\Gamma(t)n(t)$. But there exists no rigorous justification for this procedure. The application of time-dependent separable potentials $V_0(t)|\beta_{\ell m}\rangle\langle\beta_{\ell m}|$ with angular momentum $l \geq 1$ allows a comparision of the approximated method (equ. (1)) with the exact one (equ. (2)) /3/

$$d^3w/d\vec{k} = \lim_{t\to\infty} |\langle\vec{k}(t)|\Psi(t)\rangle|^2. \qquad (2)$$

In order to quantify the non-adiabaticity of the change in the potential, we introduced the parameter $\alpha = |\Delta V_0/(TE_B^2)|$. The calculations have been performed for an initial binding energy $E_B = -4$ MeV, l=2 and an interaction time T from 1 to 5×10^{-22}s. As we can see from the figure (dashed lines: equ. (1), full: equ. (2)) for large α there is a high-energy component which can not be reproduced by the emission from Gamow states. But already at $\alpha = 0.4$ ($T=5\times10^{-22}$s) the shape of the exact spectrum and the exact position of the peak is well reproduced.

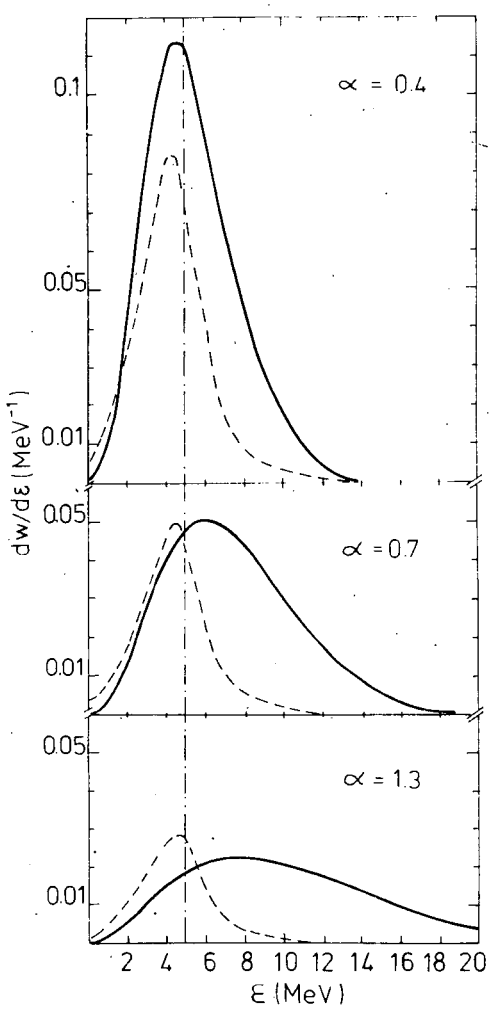

References

/1/ Milek B. and Reif R.;
Nucl. Phys. A458 (1986) 354
/2/ Cassing W. and Nörenberg W.;
Nucl. Phys. A431 (1984) 558
/3/ Milek B., Reif R. and Revai J.;
KFKI-report 19/A (1987), subm. to Phys.Rev.C

ORDER OUT OF CHAOS IN ATOMIC NUCLEI

I. Rotter
Zentralinstitut für Kernforschung Rossendorf, Bereich KF

The formation of order out of chaos is one of the most interesting problems in present time /1/. Although it is a general problem it should be discussed carefully in some special cases which are proved experimentally in detail. Such a case might be the atomic nucleus the properties of which are investigated for more than fifty years.

In standard nuclear reaction theory, the motion of the nucleons is assumed to be a chaotic one /2/. The nuclear states are proposed to be statistically independent although this assumption could not be proven experimentally and all the nuclear structure studies point to a regular motion of the nucleons.

In order to clarify this problem, microscopic calculations for an open nuclear system have been performed in dependence on the degree of coupling between the nucleus (subspace Q) and the surrounding continuum of reaction channels (subspace P). The method used is the Rossendorf continuum shell model /3/. The degree of coupling between the two subspaces has been varied by varying the distance ΔE_R^{SM} between the states (for details of the calculations see refs. /4,5/).

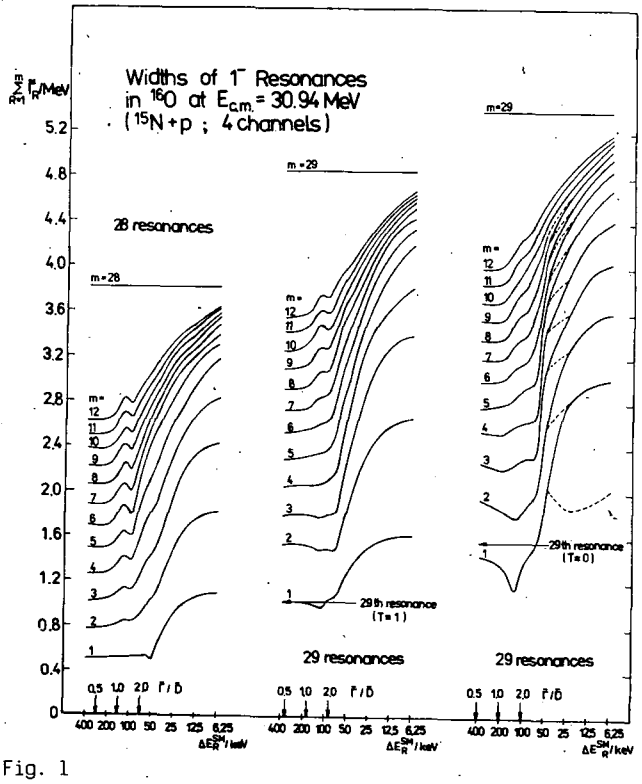

Fig. 1

In fig. 1, the dependence of $\sum_{R=1}^{m} \tilde{\Gamma}_R$ for the m largest widths ($\tilde{\Gamma}_1 \geqslant \tilde{\Gamma}_2 \geqslant \ldots \geqslant \tilde{\Gamma}_N$) on the distance ΔE_R^{SM} between the shell model states R corresponding to 1^- resonances in ^{16}O is shown. The calculations are performed with 28 and 29, respectively, resonances of 1p-1h and 2p-2h nuclear structure and with the four channels $^{15}N_{g.s.} + p$, $^{15}N_{3/2} + p$, $^{15}O_{g.s.} + n$ and $^{15}O_{3/2} + n$. The width of the 29th resonance, calculated without external mixing, is marked by an arrow. The results shown in fig. 1 illustrate the behaviour of the nuclear system in dependence on the degree of overlapping $\bar{\Gamma}/\bar{D}$ or on the degree of external mixing of the resonance states via the continuum.

It holds /4,5/

$$\sum_{R=1}^{N} \tilde{\Gamma}_R = \sum_{R=1}^{N} \Gamma_R, \qquad (1)$$

where $\tilde{\Gamma}_R$ are the widths of the resonance states R calculated by taking into account the external mixing, i.e. the eigenvalues of

$$H_{QQ}^{eff} = H_{QQ} + H_{QP} \cdot G_P^{(+)} H_{PQ}, \qquad (2)$$

and Γ_R are the widths calculated by neglecting the external mixing, i.e. the diagonal matrix elements of H_{QQ}^{eff}. The total number of resonance states with the same quantum numbers J and π is designated by N. Due to the condition (1) it follows

$$\sum_{R=m+1}^{N} \tilde{\Gamma}_R = \text{const} - \sum_{R=1}^{m} \tilde{\Gamma}_R \qquad (3)$$

at a certain excitation energy E.

The quantum chaos is defined by a strong mixing of the eigenfunctions of the A nucleon system in the basic wavefunctions as well as by an information loss on its spectroscopic properties. As long as spectroscopic information on the A nucleon system can be obtained from the experimental data, the motion of all A nucleons should be considered as a regular one. Otherwise, it is chaotic and the different nuclear states manifest themselves in the cross section not by isolated resonances but by fluctuations around an average value. The widths of the resonance states are, in such a case, small with small differences in absolute value.

In a closed system, a chaotic motion of the nucleons corresponds to the formation of an equilibrium state. The different basic states are excited with a probability which is about the same for all of them, and the lifetime of the equilibrium state is infinite by definition. In the open system, the basic states are also excited with a probability which is more or less the same for all of them, if the external mixing is strong enough. But in contrast to a closed system, the open system has to organize itself in such a manner that the lifetime of the states reached is long. Otherwise, they cannot be considered as equilibrium states. Due to the condition (3), the enlargement of the lifetimes of some levels must be compensated by a reduction of the lifetimes of other levels.

The numerical results (fig. 1) show that the compensation takes place by a reduction of the lifetimes of a small number of states. The stronger the external mixing, the larger is the difference between the widths of the many long-living states and those of the few short-living states. The redistribution of the widths starts rather suddenly at $\bar{\Gamma} \approx \bar{D}$.

The matrix elements of the operator H_{QP} between the wavefunctions of the Q space and the scattering wavefunctions of the P space are involved in both expressions the width $\tilde{\Gamma}_R$ as well as the excitation probability of the resonance state R via one of the reaction channels. A long lifetime is correlated therefore with a small excitation probability and vice versa.

It follows that in an open system, the equilibrium state with a chaotic motion of the nucleons can not be reached immediately. On the way to the equilibrium, another state far from equilibrium appears which becomes soon the overwhelming one due to its large and fast probability of excitation. This state can be represented by a regular (and not chaotic) motion of all but one nucleon.

The two extreme cases of reaction mechanism at low and high level density are very well known in nuclear reaction theory. While information on the nuclear structure of the resonances in the A nucleon system can be obtained at low level density, this information is lost at high level density. According to the chaotic motion of the nucleons, the resonance states can be seen at high level density as fluctuations around an average value only. The average value is determined by the fast direct process which contains the information on the reaction channels. In these channels, the motion of only A-1 nucleons is a regular one.

References

/1/ Prigogine, I. and I. Stengers, Order out of chaos (London 1984 and Moscow 1986)

/2/ Bohr, N., Nature 137 (1936) 344, H.A. Weidenmüller, Comments on Nuclear and Particle Physics 16 (1986) 199

/3/ Barz, H.W., I. Rotter and J. Höhn, Nucl. Phys. A 275 (1977) 111; I. Rotter, Fiz. Elem. Chastits At. Yadra 15 (1984) 762 (translation 15 (1984) 341 and ZfK-508 (1983))

/4/ Kleinwächter, P. and I. Rotter, Phys. Rev. C 32 (1985) 1742

/5/ Rotter, I., J. Phys. G (1988)

COMPUTER EXPERIMENTS OF THE LATERAL SOLID PHASE TRANSFORMATION OF Si-LAYERS FOR SOI

H.-J. Müller and K.-H. Heinig
Zentralinstitut für Kernforschung, Rossendorf, Bereich KF

The solid state conversion of thin amorphous Si-layers on insulating substrates (SOI) is of increasing interest for the production of high speed and ultra-large scale integrated circuits. Especially for the 3-dimensional integration, the solid state transformation is of special interest because of the low transformation temperature, which is as low as about 600°C. A promising technique for the production of monocrystalline Si layers is the so-called lateral solid-phase epitaxy (L-SPE), starting from a seed window within the underlying insulating SiO_2 layer. This L-SPE is limited by the nucleation and growth of randomly oriented crystallites (known as primary crystallization PC) within the amorphous layer ahead of the epitaxial frontier. If the epitaxial frontier does impinge with such a growing crystallite, the epitaxy is locally stopped. If the density of crystallites is large enough, a total blocking of the growing L-SPE frontier results.

The theoretical investigation of complex processes during the phase transformation by the method of computer simulation (CS) has been established to be a useful way for the foundation of the theoretical understanding as well as for practical use. Thus for example, a semi-empirical CS /1,2/ of the PC has allowed a comprehensive study of static and kinetic features of the polycrystalline structure formation. The principles of the CS has been extended to describe the more complex competition between PC and L-SPE in thin films /3,4/. In Fig. 1 a computer plot during the transformation together with a scheme for the structure of the films and the seed window for the L-SPE is given.

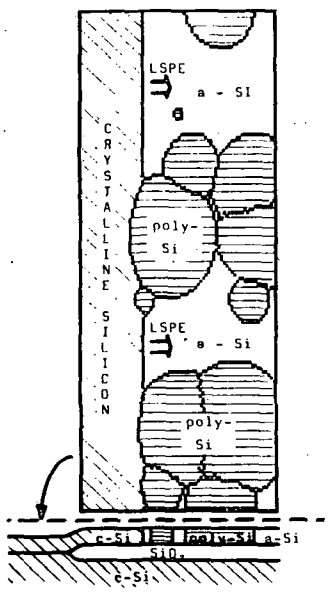

Fig. 1: computer plot of the transformation with a scheme of layers

A lot of different conditions have influence on the L-SPE. From theoretical point of view, their influence on the transformation process can be suitably approximated by the relations of three fundamental parameters, which are the rates for

(i) the nucleation of randomly oriented crystallites J_n
(ii) the lateral growth of the nucleated grains V_p and
(iii) the epitaxial growth of a monocrystalline Si layer V_e.

A variation of the relations between the rates can simulate qualitatively different external conditions.

The process of nucleation, which possesses a statistical character concerning space and time, is simulated by a grand canonical Monte-Carlo method. The growth of grains and the L-SPE are controlled by constant lateral growth velocities.

The computer experiments have been carried out in different modes, which are characterized by the qualitative behaviour of the three rates. The most interesting characteristics of the L-SPE is given by the epitaxial length, by its value after blocking as well as its kinetic behaviour.

One technique to fabricate SOI structures by L-SPE is the furnace anealing. Because of the thermal activation not only of the epitaxial growth but also of the growth of grains, there should be no difference in their rates ($V_e=V_p$). The main result of the investigation of thermally activated crystallization consists in the statement that the ratio between the epitaxial length and the appropriate radius of poly-Si, formed at an equal temperature is <u>independent of the transformation temperature</u>.

If the films are recrystallized after ion implantation by furnace annealing, $V_e=V_p$ can be also assumed but the dopants influence the growth and/or the nucleation rate with respect to the undoped samples. In the case of B-doping it is has been established experimentally that the growth rate is enlarged about 8 times, while the nucleation rate is nearly unchanged by the doping. Starting at an arbitrarily choosen ratio between nucleation and growth rate, the growth rate has been increased by a factor of 8 with respect to the starting value. The simulation yields an enlargement of R_p by a factor of 2 and a decrease of the transformation time to 0.25, which are in good agreement with experimental data of 2 and 0.2, respectively.

/1/ Müller, H.-J., Heinig, K.-H. and Hennig, K.; J. de Physique XII (1987) 137
/2/ Müller, H.-J. and Heinig, K.-H.; Nucl. Instr. & Methods 22 (1987) 526
/3/ Müller, H.-J. and Heinig, K.-H.; SOI-Layer production studied by computer experiments, Proceedings of the E-MRS Strasbourg, June 1986
/4/ Müller, H.-J. and Heinig, K.-H.; Thermally activated and ion beam induced lateral solid phase epitaxy, Proceedings of the EPM87, Dresden 1987

ELECTRONIC STOPPING CROSS-SECTIONS FOR THE MEV IMPLANTATION OF B^+ AND P^+ INTO SILICON

M. Posselt, W. Skorupa, Zentralinstitut für Kernforschung, Bereich KF

In the case of MeV implantation into silicon the electronic stopping of the ions is usually much larger than the nuclear stopping. In the given energy region the electronic stopping power acts similar to a continuous braking force whereas the nuclear stopping power shows considerable fluctuations. Therefore, the mean projected range of the ions is mainly determined by the electronic stopping, the range statistics is caused by the fluctuations of the nuclear stopping power.
Due to various promising applications in the semiconductor technology the interest in high energy implantation has increased rapidly. In the last three years many experimental material has been published. On the other hand, for practical applications a reliable theoretical prediction of MeV ranges and range profiles is necessary. This is complicated for the MeV implantation of B^+ and P^+ into silicon. Here, the energy of the implants is in the region near the maximum of the electronic stopping cross-section. In this energy range the formulae for the electronic stopping known from the implantation at lower energies are not very precise To get appropriate values for the electronic stopping cross-sections we have compared the available experimental data for the MeV implantation of B^+ and P^+ into silicon /1-8/ with theoretical calculations using different models for the electronic stopping with different parameters. The calculations have been performed using the TRIM Monte Carlo simulation program /9/. The results are shown in the table. Three models have been considered: (i) the combination of the Lindhard-Scharff and the Bethe-Bloch formulae (LSBB), (ii) the modified Brandt-Kitagawa model of Ziegler, Biersack and Littmark (ZBL) and (iii) the original Brandt-Kitagawa approach (BK). In /10/ these models are described in detail. In the LSBB and the ZBL model there are the empirical parameters C_k and C_Λ, respectively. With our results a more reliable prediction of the corresponding MeV ranges and range profiles in silicon becomes possible.

ion	energy range	model	parameter
B^+	0.1 - 1.0 MeV	LSBB	$C_k = 1.6$
	0.1 - 2.0 MeV	ZBL	$C_\Lambda = 1.0$
	1.0 - 4.0 MeV	LSBB	$C_k = 1.3$
P^+	0.1 - 7.0 MeV	LSBB	$C_k = 1.2$
	0.1 - 1.2 MeV	BK	--
	0.1 - 1.0 MeV	ZBL	$C_\Lambda = 1.0$
	1.0 - 2.5 MeV	ZBL	$C_\Lambda = 0.9$
	2.5 - 7.0 MeV	ZBL	$C_\Lambda = 0.8$

/1/ Ingram, D. C. , J. A. Baker and D. A. Walsh, Nucl. Instr. and Meth. B7/8 (1985) 361.
/2/ Ingram, D. C. , J. A. Baker, D. A. Walsh and E. M. Strathman, Nucl. Instr. and Meth. B21 (1987) 460.
/3/ Spinelli, P. , A. M. Cartier and M. Bruel, Nucl. Instr. and Meth. B21 (1987) 450.
/4/ Tamura, M. , N. Natsuaki, Y. Wada and E. Mitani, Nucl. Instr. and Meth. B21 (1987) 438.
/5/ Wang, L. K. , C. T. Chuang and G. P. Li, Solid State Electronics 29 (1986) 739.
/6/ Wilson, R. G. , J. Appl. Phys. 60 (1986) 2797.
/7/ Wong, H. , E. Deng, N. W. Cheung, P. K. Chu, E. M. Strathman and M. D. Strathman, Nucl. Instr. and Meth. B21 (1987) 447.
/8/ De Pontcharra, J. , P. Spinelli and M. Bruel, MRS Symp. Proc. 45 (1985) 115.
/9/ Ziegler, J. F. , J. P. Biersack and U. Littmark, The Stopping and Range of Ions in Solids, Pergamon, New York, 1985.
/10/Posselt, M. and W. Skorupa, Nucl. Instr. and Meth. B21 (1987) 8

DETERMINATION OF SPLITTING PARAMETER FUNCTIONS FOR NEUTRON SHIELDING CALCULATIONS BASED ON NON-ANALOGUE MONTE CARLO METHOD

G.-R. Jaenisch
TU Dresden, Sektion Physik, Wissenschaftsbereich Theoretische Physik
F. Seidel [1)]
VEB Kombinat Kraftwerksanlagenbau, Berlin

Neutron shielding calculation are performed for the (r-z)-geometry model of a pressurised water reactor (PWR) using the multigroup Monte Carlo program SMO /1/. In order to decrease the variance of the non-analogue Monte Carlo game an optimal parameter set is searched. As a quantity of main influence on the variance, particulary the weight function is considered, which is used in the geometrical splitting. The probabilistic determination of the weight function G(i,g) for splitting planes i= [1,N] and energy groups g= [1,M] is a more extensive problem than the original shielding problem. The weight function must be determined over the whole domain with high precision. An inaccurate determination of only one of the N.M parameters can imply that especially in deep penetration problems the particle flow could be interrupted or the calculation effort could be increased unacceptabely.

In /1/ the demand

$$G(i,g) = \frac{C}{\overline{w^{(+)}(i,g)}} \qquad (1)$$

is used for the determination of the weight function G(i,g). This means that for each of the N zones and M energy groups the mean contribution $w^{(+)}(i,g)$ of a particle at (i,g) to the result at the shield point (i',g') multiplied with the particle weight G(i,g) is constant, $w^{(+)}(i,g)$ can be calculated as

$$w^{(+)}(i,g) = \sum_{g' \geq g} P(i,g \to g')\, w^{(+)}(i,g') \qquad (2)$$

where P(i,g→g') is the collision probability in zone i including down scattering from group g to g'. $w^{(+)}$ is the mean contribution of the particle starting at (i,g') to the result at (i,g). $w^{(+)}$ (i,g') is calculated statistically by the SMOKE code /1/, a program version of SMO. The application of SMOKE shows that a great calculation effort is required for realistic shielding problems. A manual adjustment (especially the flatting of the statistical fluctuations) is recommended /1/.

$w^{(+)}$ can be interpreted as a influence function. For that reason the splitting parameter function is calculated to

$$G(i,g) = \frac{C}{\overline{\phi^{+}(i,g)}} \qquad (3)$$

using the solution $\phi^{+}(i,g)$ of an adjoint S_n-calculation which is using a P_3S_8-approximation. With respect of this approximation the effort of the S_n calculation is about three times smaller than those of a SMOKE calculation. As well, a manual adjustment is not required after a deterministic calculation. The results of both of the corresponding SMO shielding calculations using the weight function of eq.(1) and (3) are shown in the figure. The same number of source neutrones were played in the both SMO calculations, therefore the calculation effort is nearly the same. The statistical errors of the both SMO solutions are also shown in the figure. The comparision offers that the weight function of eq.(3) has led to a satifactory variance reduction. Moreover, the variances are smaller in some subdomains if the weights of eq.(3) will be used.

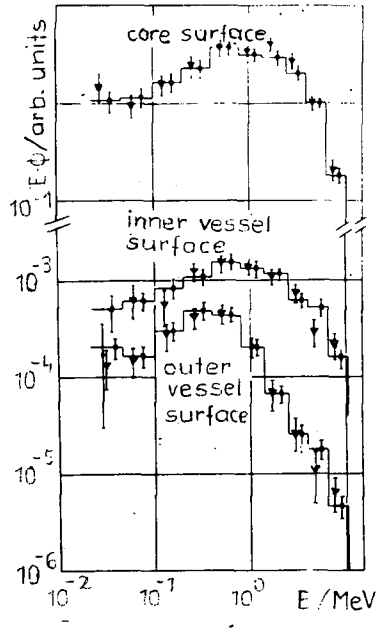

Energy flux distribution at the inner/outer vessel surface and the core surface calculated by SMO using statistically (↕) or deterministically (↕) splitting weights.

References:

/1/ H.-U. Barz, Kernenergie 7 (1987) 8

1) Aspirant at TU Dresden, Sektion Physik, WB Theoretische Physik

APPLIED METHODS

STANDARD FUNCTIONS IN THE CASE OF FIBRE TEXTURES

S. Matthies, K. Helming and T. Steinkopff
Zentralinstitut für Kernforschung Rossendorf, Bereich KF
K. Kunze
Zentralinstitut für Physik der Erde, Potsdam

In quantitative texture analysis standard functions are used in connection with the interpretation of the Orientation Distribution Function (ODF), the test of reproduction methods and the investigation of ghost phenomena /1/. Because of the analyticity of the most interesting functions it is possible to get them with any numerical accuracy (e.g. without series termination errors or approximations due to numerical integrations). Fitting the main components of an ODF by bell-shaped distributions the given texture can usually be interpreted by a small set of characteristic parameters /2/.

Up to now for the introduced standard functions a non-solvable integration remains in order to get the corresponding pole figure expression in the special case of fibre components. Two new model distributions (GAUSS-shaped and LORENTZ-shaped) can be defined for this case satisfying all the demands on standard functions:

All orientations g_0^F, which transform the given fibre axis $\vec{n}_0$ regarding to the sample coordinate system K_A into the fibre axis $\vec{h}_0$ regarding to the crystal coordinate system K_B ($\vec{h}_0 = g_0^F \cdot \vec{n}_0$), lie on the fibre thread $g_0^F = \{\vec{h}_0, \varphi\}^{-1} \cdot \{\vec{n}_0, 0\}$ ($0 \leq \varphi < 2\pi$). The "central" character of the model ODF means, that it only depends on the orientation distance $\tilde{\omega}^F$ between an arbitrary orientation g and the fibre thread g_0^F (with $\cos \tilde{\omega}^F = \vec{h}_0 \cdot g \cdot \vec{n}_0$) as well as on a width parameter.

In analogy to the case of spherical components the GAUSS-shaped fibre standard function is defined as follows:

$$f^F(S, \tilde{\omega}^F) = N^F(S)\, e^{S \cos \tilde{\omega}^F}, \quad N^F(S) = \frac{S}{\sinh S} . \tag{1}$$

The width parameter S leads to the halfwidth $b = 2 \cdot \arccos(1 - \ln 2/S)$ and enables to realize the full width spectrum from a random distribution ($S \to 0$) up to a delta-like distribution ($S \to \infty$). The coefficients of a series expansion of (1) in D-functions /1/ read

$$C_l(S) = N^F(S)(2l+1)\sqrt{\frac{\pi}{2S}}\, I_{l+1/2}(S) , \tag{2}$$

and the integration over the projection thread $(\vec{h}_i, \vec{y})$ leads to the pole figure expression

$$P^F(S, z_1, z_2) = N^F(S) I_0(S \cdot \sin \Theta_1 \cdot \sin \Theta_2) \exp(S \cdot \cos \Theta_1 \cdot \cos \Theta_2) \tag{3}$$

with $z_1 = \cos \Theta_1 = \vec{h}_i \cdot \vec{h}_0$, $z_2 = \cos \Theta_2 = \vec{y} \cdot \vec{n}_0$.

Using the pole figure expression for spherical components as the LORENTZ-shaped fibre standard function

$$f^F(T, \tilde{\omega}^F) = \frac{1 - T^2}{(1 + T^2 - 2T \cdot \cos \tilde{\omega}^F)^{3/2}} \tag{4}$$

the halfwidth, C-coefficients and pole figure can be represented by analytically closed expressions, too.

For $\vec{n}_0$ = (001) the given expressions describe the special case of so-called cyclic textures most frequently considered in practice.

References

/1/ Matthies, S. et al.: Standard Distributions in Texture Analysis. Berlin: Akademieverlag
/2/ Lücke, K. et al, Z. Metallkde. 77 (1986) 312

A NEARLY ISOMETRIC REPRESENTATION OF THE SPACE OF EULERIAN ANGLES (G-SPACE)

K. Helming and S. Matthies
Zentralinstitut für Kernforschung Rossendorf, Bereich KF
G.W. Vinel
Zentralinstitut für Kernforschung Rossendorf, Bereich G

Commonly the representation of the orientation distribution function f(g) is given by sets of G-space sections with isolines for f(g) values. For the description of an orientation g three Eulerian angles $\{\alpha, \beta, \gamma\}$ are used and e.g. a γ= const section is given in a rectangular frame for α and β. Fig. 1 shows such a representation of a model function $f^M(g)$ constructed by bell-shaped distributions /1/ $f(g_0,g) = f(\tilde{\omega})$ depending on the orientation distance $\tilde{\omega}$ between g and the position of the component g_0

$$\cos \tilde{\omega}/2 = \cos(\sigma - \sigma_0)\cos\beta' \cos\beta'_0 + \cos(\delta - \delta_0)\sin\beta' \sin\beta'_0 \qquad (1)$$

with $\sigma = (\alpha + \gamma)/2$, $\delta = (\alpha - \gamma)/2$ and $\beta' = \beta/2$.

Two components PI and PII with Gaussian form and a halfwidth 15° were mixed for the case of cubic-orthorhombic symmetry. It is easy to be seen that the rectangular representation in fig. 1 is not the best one to reflect the complex $\tilde{\omega}$-metric (1) of the G-space. For instance the (bell-shaped)component PI looks like a tube in the vincinity of $\beta = 0$.

If we interpret the angles $\beta' = \beta/2$ and $\delta = (\alpha - \gamma)/2$ for $\sigma = \sigma_0$ as spherical ones /2/ the half orientation distance $\tilde{\omega}/2$ will just correspond to the angle distance of the directions $\vec{r} = (\beta', \delta)$ and $\vec{r}_0 = (\beta'_0, \delta_0)$ (cf. (1)). Furthermore all isolines of a bell-shaped distribution (in regard with $\tilde{\omega}$) will be concentric circles on a sphere representing a σ-section. Therefore the representation by σ-sections (fig. 2) is more suitable than the first one for studies of forms of texture components and distances between them.

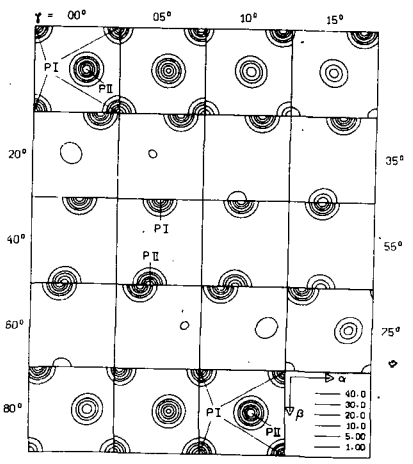

Fig. 1

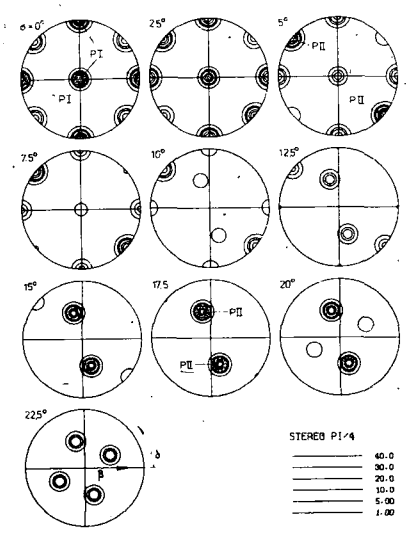

Fig. 2

A model ODF represented in form of
fig. 1) γ-sections using conventional rectangular coordinates
fig. 2) σ-sections using a special stereographic projection

References

/1/ Matthies, S. et al.: Standard Distributions in Texture Analysis. Berlin: Akademieverlag 1987

/2/ Helming, K. et al., Proc. of the 8th ICOTOM (Santa Fé, 1987), to be published

NUMERICAL ASPECTS OF THE NORMAL DISTRIBUTION IN THE ORIENTATION SPACE

S. Matthies
Zentralinstitut für Kernforschung Rossendorf, Bereich KF
G.W. Vinel
Zentralinstitut für Kernforschung Rossendorf, Bereich G

Interpreting orientation distributions in texture analysis by means of texture components certain model distributions are used in practice. On the other hand many problems of texture analysis can be mathematically modellized with the help of such distributions.

The model distributions should be of physically adequate form as well as be given by mathematical expressions permitting to calculate them with high numerical accuracy in order to avoid model induced errors in testing or fit procedures. Gaussian-shaped or Lorentzian-shaped curves are used for this reason /1/. The term "Gaussian" was chosen because the corresponding expressions are similar to the well-known normal distribution in the common one-dimensional space.

The form of the normal distribution follows as a result of the so-called central limit theorem of probability theory that can be formulated in more complex spaces also leading to the "truly" Gaussian distribution correspondingly. Recently this was performed for the orientation space by T.I. Savjolova /2/. However, the final result could be represented in form of a Fourier series only (ω - orientation distance, $0 \leq \omega \leq \pi$)

$$f(\varepsilon, \omega) = \sum_{l=0}^{\infty} (2l+1)\, e^{-\varepsilon l(l+1)} \sin((2l+1)\omega/2)/\sin\frac{\omega}{2}, \qquad (1)$$

possessing a bad convergence for typical in practice small halfwidths $b < \pi$ ($\hat{=} \varepsilon \ll 1$) of bell-shaped curves. Moreover, the form of the distribution (1) cannot be seen explicitly, and it is especially unfavourable that a direct connection is missing between the width parameter ε and b. But $f(\varepsilon, \omega)$ can be represented in an analytically closed form /3/ using Jacobi's Teta functions /4/:

$$f(\varepsilon, \omega) \cdot \sin\frac{\omega}{2} = -q^{-1/4}/(2\pi)\, \frac{\delta}{\delta v}\, \Theta_2(v,q), \quad v = \frac{\omega}{2\pi}, \qquad (2)$$
$$q = e^{-\varepsilon}.$$

Now a special transformation can be used leading to an expression of especially favourable form for the case of practical interest ($b < \pi$):

$$f(\varepsilon, \omega) = \sqrt{\pi}\, \varepsilon^{-3/2}\, e^{\varepsilon/4}\, e^{-(\omega/2)^2/\varepsilon} \left[1 + O(\varepsilon, \omega)\right] \omega/(2 \sin\frac{\omega}{2}); \qquad (3)$$
$$\varepsilon \approx b^2/\left\{16 \ln\left[b/(2 \sin(b/4))\right]\right\}.$$

The term $O(\varepsilon, \omega)$ is proportional to $e^{-\pi^2/\varepsilon}$ and can commonly be neglected. Already for a relatively large halfwidth $b = 60°$ it is of the order of 10^{-43} only. For $b = 15°$ typical in practice we have $O \approx 10^{-695}$.

R e f e r e n c e s

/1/ Matthies, S. et al.: Standard Distributions in Texture Analysis. Berlin: Akademieverlag

/2/ Savjolova, T.I.: Preface to Novye Metody Issledovanija Tekstury Polikristallicheskich Materialov. Moscow: Metallurgija 1985

/3/ Matthies, S. et al.: Submitted to Textures and Microstructures. (1988)

/4/ Erdélyi, A. (Ed.): Higher Transcendental Functions (Vol. II). New York: McGraw Hill Book Company 1953

DISCRETE STATISTICAL TREATMENT OF TEXTURE DEVELOPMENT

T. Steinkopff and S. Matthies
Zentralinstitut für Kernforschung Rossendorf, Bereich KF

Conventional "grain by grain" methods simulating processes of texture development /1,2/ are as a rule computer time expensive. Supposing that for well defined single orientations the possible orientation transitions connected with the concrete process (or with its substeps) are known (previously calculated and stored) the numerical expense for the determination of the final orientation distribution belonging to any initial distribution can be considerably reduced. At the same time the statistics of the results will be improved. Up to now this concept has been only used to simulate martensitic transformations. The method suggested should be especially useful for the simulation of deformation textures subdividing the deformation process into indentical elementary deformation steps.

The method:

The starting point is an assumed cell structure of the G-space containing N cells C_n (of volume V_n) and a constant value f_n^i of the ODF within the n-th cell:

$$\sum_{n=1}^{N} V_n = \sum_{n=1}^{N} V_n \cdot f_n^i = 1 \; . \qquad (1)$$

For sufficiently small cells the "centre" of C_n at g_n will well represent all orientations the n-th cell contains. Now for each g_n the set of all possible (M_n) final orientations $g_n^{m_n}$ ($m = 1,2,\ldots,M_n$) is calculated for the considered transformation process (e.g. martensitic transformation, $M_n = 24$ for the Kurdjumov-Sachs model) once only and the corresponding cell addresses $\nu = C_n^{m_n}$ ($g_n^{m_n} \in C_n^{m_n}$) are stored.

Then for any initial texture f^i the discrete final orientation distribution f^e can be calculated (the $\nu = C_n^{m_n}$, M_n, V_n are known) with a minimum of numerical expense by ($\nu,\nu' = 1,2,\ldots,N$)

$$f_{\nu'}^e = \sum_{n=1}^{N} f_n^i \cdot V_n \,/\, M_n \cdot \sum_{m_n=1}^{M_n} \delta_{\nu\nu'}/V_{\nu'} \; . \qquad (2)$$

If the M_n possible solutions are realized with different statistical weights w_{m_n} (determined by the physical parameters of the process) the corresponding expression reads:

$$f_{\nu'}^e = \sum_{n=1}^{N} f_n^i \cdot V_n \cdot \sum_{m_n=1}^{M_n} w_{m_n} \cdot \delta_{\nu\nu'}/V_{\nu'} \qquad (3)$$

with

$$\sum_{m_n=1}^{M_n} w_{m_n} = 1 \; . \qquad (4)$$

The case of martensitic transformation with classic variant selection is given by $w_{m_n} = 0$ for the $M_n - \overline{M}_n$ forbidden variants and $w_{m_n} = 1/\overline{M}_n$ for the $\overline{M}_n$ allowed ones, respectively.

A variation of the selection rules concerns the w_{m_n} only whereas the $C_n^{m_n}$ remain the same for a given transformation model.

In order to get a continuous final distribution the intensities $f_n^e \cdot V_n$ can be replaced by Gaussian distributions /3/ $\varphi(g_n,b,g)$ with the maximum at g_n and a halfwidth b of the order of cell size:

$$f^e(g) = \sum_{n=1}^{N} f_n^e \cdot V_n \cdot \varphi(g_n,b,g) \; . \qquad (5)$$

R e f e r e n c e s

/1/ van Houtte, P. et al.: Development of Textures by Slip and Twinning. In: Preferred Orientation in Deformed Metals and Rocks: An Introduction to Modern Texture Analysis, ed. Wenk, H.R., San Diego: Academic Press 1985
/2/ Furubayashi, E., Eisen und Stahl, Japan 71 (1985) 1155
/3/ Matthies, S. et al.: Standard Distributions in Texture Analysis. Berlin: Akademie-Verlag 1987

PARTIAL STRUCTURE FUNCTIONS FOR AMORPHOUS $Fe_{83}B_{17}$

W. Matz
Zentralinstitut für Kernforschung Rossendorf, Bereich KF
A.V. Serebryakov, Yu.A. Levin
Institute for Solid State Physics, Academy of Sciences of the USSR, Chernogolovka

For the determination of partial structure factors for the amorphous alloy $Fe_{83}B_{17}$ by neutron diffraction three samples with different isotopic composition were prepared: 1) with natural iron, 2) with the isotope ^{54}Fe, and 3) with a mixture of ^{nat}Fe and ^{54}Fe (50:50). The amorphous samples were prepared by the melt-spinning technique, resulting in ribbons of about 1 mm in width.

A detailed analysis of the experimental data and the system of linear equations for estimation of the partial structure factors showed, that the contrast variation by isotope substitution is not strong enough to allow a direct determination of partial structure factors of the Faber-Ziman-type /2,3/. On the other hand, the Bhatia-Thornton-formalism /2/ can be used to estimate all three partial structure functions of the number-concentration-type (N-C). For the structural investigation of amorphous $Fe_{83}B_{17}$ both types of partial structure functions were used. In the case of the Faber-Ziman-formalism the pair contribution B-B was neglected as it was done for a-$Fe_{75}B_{25}$ /1,3/ and only the partials for the pairs Fe-Fe and Fe-B were determined. In figs. 1 and 2 the partial atomic distribution functions of the Faber-Ziman and the Bhatia-Thornton-type are shown, respectively. From the functions $G_{FeFe}(r)$ and $G_{FeB}(r)$ of fig. 1 the typical interatomic distances r_k (in nm) and the coordination numbers N_k were estimated.

Fe-Fe: r_1=0.255 (N_1=11.0+0.3) / r_2=0.420 (N_2=20.2+1.3) / r_3=0.500 (N_3=22.3+1.5)

B-Fe: r_1=0.215 (N_1= 6.0+0.3) / r_2=0.335? (N_2=4.7+0.6) / r_3=0.385 (N_3= 9.8+1.0) / r_4=0.455 (N_4=21.3+1.8)

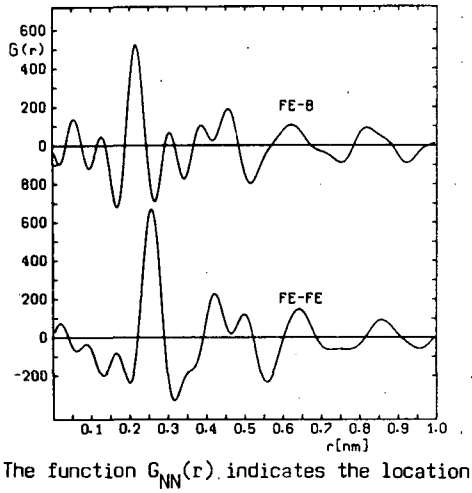

◀ Fig. 1
Partial atomic distribution functions of pairs Fe-Fe and Fe-B.

Fig. 2 ▶
Partial atomic distribution functions in the number-concentration formalism (Bhatia-Thornton).

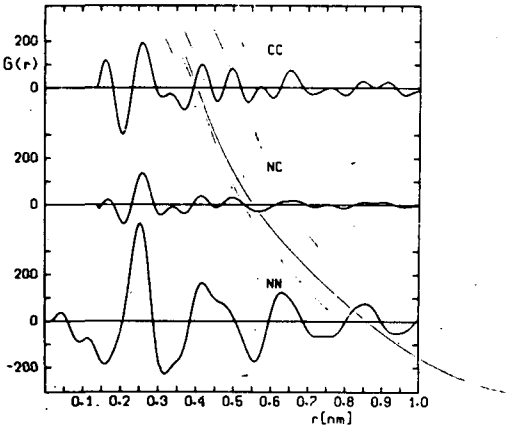

The function $G_{NN}(r)$ indicates the location of coordination shells by their maxima (number-number-correlation). So all listed distance values were found in $G_{NN}(r)$ of fig. 2 although the Fe-B distances give less pronounced maxima. In the concentration fluctuation function $G_{cc}(r)$ coordination shells of like atoms result in maxima while such of unlike atoms in minima. The behavior of $G_{cc}(r)$ corresponds with the data obtained from $G_{FeFe}(r)$ and $G_{FeB}(r)$ with exception of the maximum at r=0.335(5) nm. This maximum should be the first boron-boron distance because it correlates with a minimum in $G_{FeFe}(r)$. The deviation of $G_{NC}(r)$ from zero and the partials of fig. 1 indicate well developed chemical short range order (s.r.o.) in amorphous $Fe_{83}B_{17}$.

While the iron-iron correlations are quite similar to other amorphous Fe-B alloys /1,4/, the iron-boron correlations exhibit some differences. The small coordination number N^{B-Fe}=6 together with the "normal" behavior of $G_{FeFe}(r)$ may be explained by the microheterogenous structure model for amorphous alloys /5/. In this case the model structure should be composed of the phases α-iron (with crystalline like s.r.o.) and dense random packed Fe_3B. Model calculations are in progress.

References

/1/ Matz, W., H. Hermann, and N. Mattern, J.Non-cryst.Solids 93(1987)217
/2/ Waseda, Y. The Structure of Non-Crystalline Materials, McGraw-Hill, New York 1980, ch. 1
/3/ Matz, W., N. Mattern, and W. Löser, Gem. Jahresbericht 1983, ZfK-530(1984)64
/4/ Nold, E. et al., Z.Naturforsch. 36a(1981)1032
/5/ Hermann, H. and N. Mattern, J.Phys.F16(1986)131

A METHOD FOR THE VARIATION OF THE NEUTRON SCATTERING LENGTH DENSITY IN SOLVATING MATERIALS

F. Eichhorn
Zentralinstitut für Kernforschung, Rossendorf, Bereich KF
F. Häußler
Technische Hochschule Leipzig, Sektion Naturwissenschaften

Materials containing inhomogeneities (e.g. particles of different phases) of sizes in the order of 1 nm ... 10 µm cause small-angle scattering of neutrons (SANS), the intensity of which is determined by the difference of the coherent-scattering length density between neighbouring particles or particles and matrix /1/. For a multi-phase material SANS intensity consists of contributions of all of the constituents.

As known, the coherent scattering length b_c for neutrons is different for the isotopes of a chemical element; especially a great difference exists for hydrogen ($b_c^H = -0.37 \cdot 10^{-14}$ m) and deuterium ($b_c^D = 0.65 \cdot 10^{-14}$ m). This feature is used for labelling of polymer parts for a subsequent structure investigation by SANS. Also the Christiansen filter technique for measuring the neutron scattering length of a powder material is based on that: the material is immersed in a liquid, and its composition is varied up to that concentration that the SANS intensity vanishes.

The scattering length density of solvating (especially hydrating) materials can be controlled, if the solvatation process is carried out with a solvation medium of a definite isotope composition /2/. Then the scattering length density is given by

$$\varrho = (1 - c)\ \varrho_H + c\,\varrho_D,$$

here are ϱ_H and ϱ_D the scattering length density of the hydrate obtained by hydration with pure H_2O and pure D_2O, respectively, c is the concentration of D_2O in the hydration water. In this way ϱ can be varied in the range between ϱ_H and ϱ_D. As an example of application of this method the investigation of hydrated cement paste will be given. Pores in cement or concrete determine essential properties of these materials like strength, heat insulation, and penetration of water. Their sizes can be measured by SANS, but they exist within a matrix of mainly $C_3S_2 \cdot 2.5w$, $Ca(OH)_3$, and $C_3A \cdot CaSO_4 \cdot 12w$. Therefore SANS intensity contains information of all of them /3/.

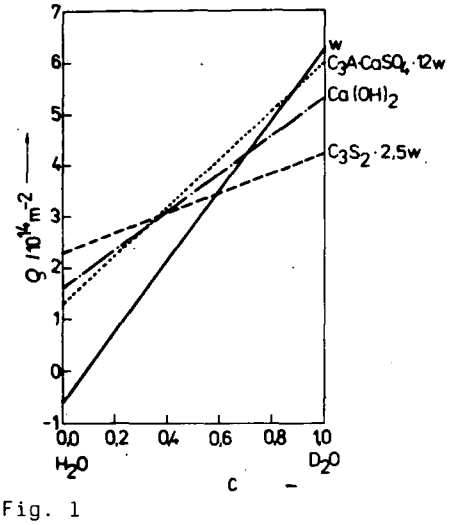

Fig. 1

Neutron scattering length density of water and hydrated cement phases in dependence on the concentration of D_2O in the hydration water
C—CaO, S—SiO_2, A—Al_2O_3, w—H_2O

Fig. 1 shows the dependence of the neutron scattering length density of water and of cement phases on the concentration of D_2O in the hydration water. As seen, it is possible with the proposed method to obtain equal scattering length density for two different phases (in the case of cement accidently for a third phase, too). If cement powder is hydrated with water of 38 % D_2O, then the product consists of pores and cement hydrate, which is chemically different but neutron-optically homogeneous. For the determination of size and size distribution of pores then the well-known two phase model may be used in a straightforward way and estimations or results of other methods are unnecessary.

References

/1/ Kostorz, G.: Treatise on Materials Science and Technology. Vol. 15 (ed. G. Kostorz) Academic Press 1979, p. 227

/2/ Eichhorn, F., F. Häußler, Patent DD 304 639

/3/ Allen, A.J. et al., J. Physics D15 (1982) 1817

SECONDARY EXTINCTION IN TEXTURE ANALYSIS BY NEUTRON DIFFRACTION

A. Mücklich
Zentralinstitut für Kernforschung Rossendorf, Bereich KF
P. Klimanek
Bergakademie Freiberg, Sektion Metallurgie und Werkstofftechnik

Neutron diffraction analysis of textures in single-phase polycrystalline materials is usually based on the assumption that

- the orientation distribution of the crystallites is independent of the locus within the scattering volume,
- absorption can be treated as a volume effect,
- the conditions of kinematic scattering theory are fulfilled by all crystallites (i.e. primary extinction can be neglected),
- secondary extinction between different crystallites is without importance and
- in each point of the pole figures the total integrated intensity (i.e. the total diffraction profile) is measured.

As shown in previous work, in texture measurements of real polycrystalline materials /1/ deviations from this propositions must be taken into account which can cause remarkable uncertainties of the registered data. In the present paper the influence of secondary extinction due to the grain structure of the scattering sample is analyzed. In materials with random orientation of the grains this effect is equal for all reflections /2,3/ and can therefore be neglected in measurements using relative intensities. However, in the case of texturized samples another behaviour must be expected. In order to conceive the problem which has not been treated hitherto we performed the following considerations:
The corrected (for volume and attenuation) intensity $I_h^{corr}(y)$ corresponding to a direction y of a pole figure $P_h(y)$ is usually given by

$$I_h^{corr}(y) = I_h^{exp}(y)\, C_h(\mu,y) \qquad (1)$$

where $I_h^{exp}(y)$ is the observed intensity and $C_h(\mu,y)$ the correction factor for the sample geometry used /4,5/. In a sample without texture the attenuation coefficient is isotropic and can be expressed by the sum $\mu = \tau + \sigma_i + \sigma_c$ (i - incoherent, c - coherent) but in texturized polycrystals it becomes direction-dependent and must formally be described by $\mu(y) = \tau + \sigma_i + \sigma_c E_h(y)$. $E_h(y)$ characterizes the orientation dependence of the extinction coefficient and can therefore be termed extinction pole figure. Accordingly the correction factor of equation (1) depends on the texture itself and must be replaced by $C_h'(\mu(y),y)$. Each value $E_h(y)$ is defined as the ratio of total intensities which are scattered in samples with and without texture by the crystallites along the pathes of the incident and the diffracted beam corresponding to y. Details concerning the calculation of $E_h(y)$ and $C_h'(\mu(y),y)$, resp., will be published elsewhere.

Using texture data of annealed Cu-sheets (2 mm in thickness, cube texture with ODF-orientation densities of about 50) calculations have shown that in pole figures errors of the magnitude of ± 10 % are possible. The influence of secondary extinction depends on the sample thickness and on the ratio $\sigma_c/(\sigma_i + \tau)$ and can give rise to errors up to ± 50 % in unfavourable cases (e.g. Fe-sheets with thickness 10 mm).

References

/1/ Klimanek, P., Annual Report 1986, ZfK-621, 109
/2/ Terminasov, Ju.S., A.V. Kuznecov, Freiberger Forschungshefte B80 (1963) 5
/3/ DeMarco, J.J., P. Suortti, Phys. Rev. B4 (1971) 1028
/4/ Decker, B.F. et al., J. Appl. Phys. 19 (1948) 388
/5/ Schulz, L.G., J. Appl. Phys. 20 (1949) 1030
/6/ Schulz, U., Ingenieurpraktikum, ZfK Rossendorf 1987

DETERMINATION OF DAMAGE PROFILES BY PIXE MEASUREMENTS

C. Ascheron, R. Flagmeyer, J. Vogt, G. Otto, A. Schindler[+]
Karl-Marx-Universität Leipzig, Sektion Physik
[+]Zentralinstitut für Isotopen- und Strahlenforschung der AdW, Leipzig

We tried to extend the application of proton-induced X-ray emission, which delivers integrated information on surface layers, to a differential depth -resolution method. For this purpose

(i) X-rays were excited under channeling conditions (PIXE-C), thus small-impact parameter processes like inner-shell ionization and direct backscattering were strongly reduced (see fig. 1);

(ii) damage profiles were revealed by bevelling the samples with 1 keV Ar^+ ions, thus shifting the exciting beam along the surface depth-dependent information is obtained;

(iii) optimization of excitation conditions was considered by testing the correlation between damage density and PIXE-C informations for the utilization of

a) different exciting particles and

b) different excited characteristic X-rays.

As an example the results of measurements on hydrogen-implantation damaged GaP single crystals are presented in figs. 1 - 3.

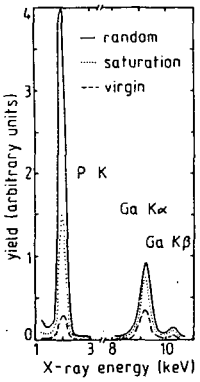

Fig. 1

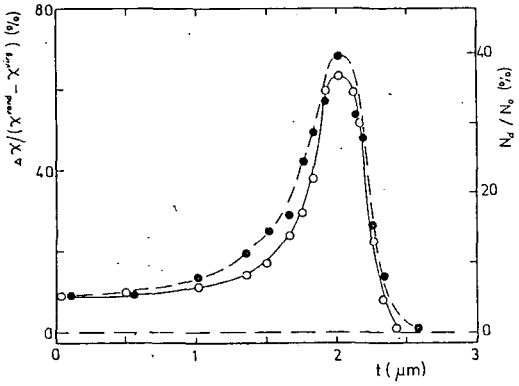

Fig. 2

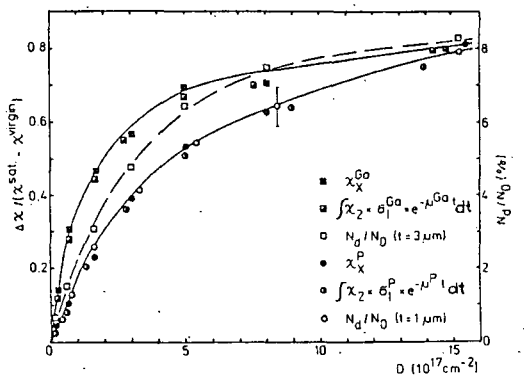

Fig. 3

Fig. 1: X-ray spectra of GaP excited by 1 MeV protons incident randomly and in (111) lattice direction.

Fig. 2: Depth profile of relative changes in the PIXE-C yields $\Delta\chi/(\chi^{rand} - \chi^{virg})$ (•) excited with 1 MeV He^+ ions, and profile of damage density N_d/N_0 (o) on H implanted GaP (T_{imp} = 300 K, E_p = 300 keV, D = 3 x 10^{17} cm^{-2}).

Fig. 3: Fluence dependence of the measured (filled symbols) and computed (half filled symbols) P-K and Ga-K PIXE-C yields in comparison to damage density.

The measurements indicate:

- PIXE-C measurements give information on radiation damage since they reflect backscattering yield in a modified form. The X-ray yield measured at the surface is proportional to $\int_0^R p \cdot \chi_2(t) \cdot \sigma_I(E(t)) \cdot e^{-\mu t}\, dt$ with χ_2 as the dechanneling flux, σ_I as cross section for X-ray production and $e^{-\mu t}$ as self absorption.
- The relation between changes in the PIXE-C yield and damage density is the closer the thinner the layer characterized by the radiation (for He^+ excitation in fig. 2 a proportionality factor of about 2). This layer is the thinner the lower the penetration depth of exciting ions and the stronger the absorption of exploited X-rays. This means for the example considered:
  - (i) The excitation with heavier He^+ ions is favoured against H^+ excitation in studies of depth profiles.
  - (ii) The less absorbed Ga-K radiation, which characterizes thicker surface layers, reacts strongly to weaker damage since the effect of dechanneling more contributes to excitation. Therefore, changes in X-ray yield are not simply proportional to damage density.
- The combination of PIXE-C with the ion beam etching technique offers the possibility of directly using PIXE-C for damage profiling /1/.

R e f e r e n c e

/1/ C. Ascheron et al., Cryst. Res. Tech. 22, 1493 (1987)

A COMPARATIVE POSITRON STUDY OF THE PRODUCTION OF VACANCY DEFECTS IN PARTICLE IRRADIATED GaP, InP AND Si SINGLE CRYSTALS

C. Ascheron, G. Dlubek[+], R. Krause[++], H. Erhard[++]
Karl-Marx-Universität Leipzig, Sektion Physik
[+] Pädagogische Hochschule Halle, Sektion Physik/Mathematik
[++] Martin-Luther-Universität Halle, Sektion Physik

Particle irradiation induced defects in semiconductor crystals are of interest in connection with device technologies. As two quite different cases concerning the type of irradiation-induced lattice defects high energetic proton bombardment and neutron irradiation are considered: high-energetic protons produce mainly point-like defects, and fast neutrons cause mainly larger displacement cascades. This difference in the predominating defect type is also expressed in the annealing behaviour /1/.
We tried to compare the production of vacancy type defects (i) by fast neutrons and fast protons and (ii) in elemental and in compound semiconductors.
As a measure for the concentration of negatively charged or neutral vacancy-type defects in figs. 1 and 2 the positron lifetime and the S-parameter are presented in dependence on the fluence.

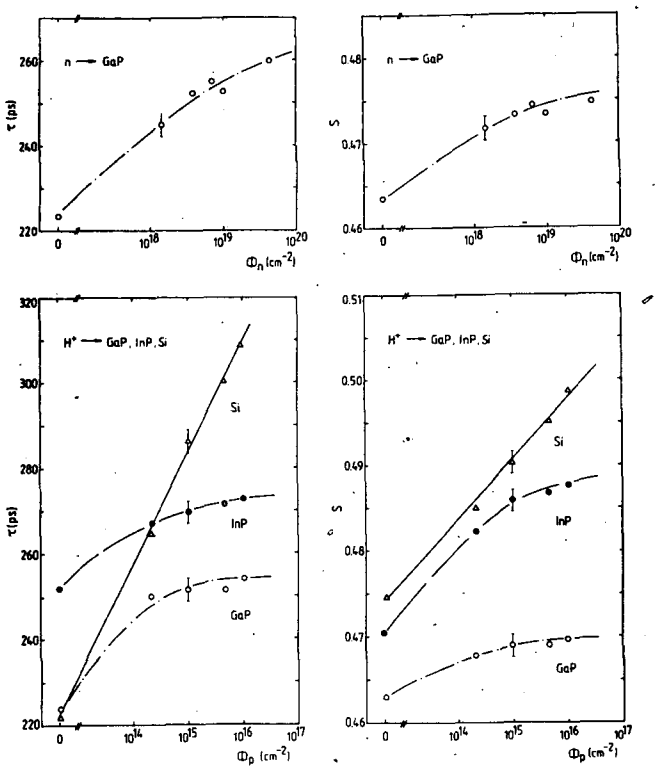

Fig. 1: Fluence dependence of the average lifetime $\bar{\tau}$ (a) and of the curve shape parameter S (b) in
(1) GaP irradiated with fast neutrons and in
(2) GaP, InP and Si irradiated with protons of nearly continuous energy distribution in the interval E_p = 0.3 - 1.7 MeV.

The measurements indicate that lifetime and S-parameter increase with fluence in a qualitative similar manner. This gives evidence that vacancy-type lattice defects, which are able to trap positrons, are produced by neutron and proton bombardment. The higher lifetime and S-parameters reached in neutron irradiated GaP may be attributed to small clusters of vacancies in both sublattices.
The comparison of the three materials shows that InP behaves analogously to GaP, but Si shows much stronger increases in $\bar{\tau}$ and S. This strong difference between compounds and elemental semiconductors holds also for neutron irradiated material /2/. It could be attributed
(i) to the high mobility of vacancies and to their tendency to agglomerate to vacancy complexes in elemental semiconductors /3/, and
(ii) to the fact that in compounds agglomerates of vacancies of the same sublattice such as $(V_{Ga})_n$, e.g., are expected to exhibit positron lifetimes not strongly exceeding the values typical of monovacancies since the vacancies are separated by the atoms of the P-sublattice.
Therefore, it seems reasonable that in radiation damaged compounds $\bar{\tau}$ and S saturate near or only slightly above the values of monovacancies.

References

/1/ C. Ascheron et al., Annual Report ZfK 1986, p. 76
/2/ G. Dlubek et al., Appl. Phys. A 42, 125 (1986)
/3/ S. Dannefear et al., Phys. Rev. B 22, 6135 (1980)

EXTENDED DEFECTS IN HYDROGEN IMPLANTED GaP SINGLE CRYSTALS

C. Ascheron, H. Bartsch[+]
Karl-Marx-Universität Leipzig, Sektion Physik
[+]Institut für Elektronenmikroskopie der AdW, Halle

We have performed cross-sectional TEM studies on proton bombarded and on in two steps post-annealed GaP /1/. The measurements indicate:

- Up to proton fluences $D \approx 3 \times 10^{16}$ cm^{-2} no differences are visible between implanted and unimplanted material.
- At fluences $D \approx 10^{17}$ cm^{-2} a narrow bright band, which points to a highly stressed layer, appears at the depth of the "buried" damaged hydrogen containing layer (fig. 1 a).
- Very high fluence implantation ($D \approx 8 \times 10^{17}$ cm^{-2}) or annealing at medium temperatures of samples exhibiting highly stressed layers, makes flat lenticular cavities and extrinsic dislocation loops appear within the hydrogen containing layer (fig. 1 b). These extended defects lie in {111} planes, and they are filled with hydrogen as the strong strain contrast images around the disc-shaped large defects suggest. Such contrasts are typical for gas filled microcavities. The structures observed are explained as hydrogen platelets being the prestate of blisters.
- Within the highly damaged zone, at a depth slightly smaller than that of the maximum of H concentration, electron beam enhanced annealing makes simpler defects coagulate to Frank loops (fig. 1 c). These results suggest:

(i) After high fluence proton implantation the stopping zone is supersaturated with smaller defects.

(ii) In proton bombarded GaP the formation of extended defects does not happen by a direct process immediately during implantation but by the mobilization and following agglomeration of point defects and of smaller defect complexes by thermal stimulation.

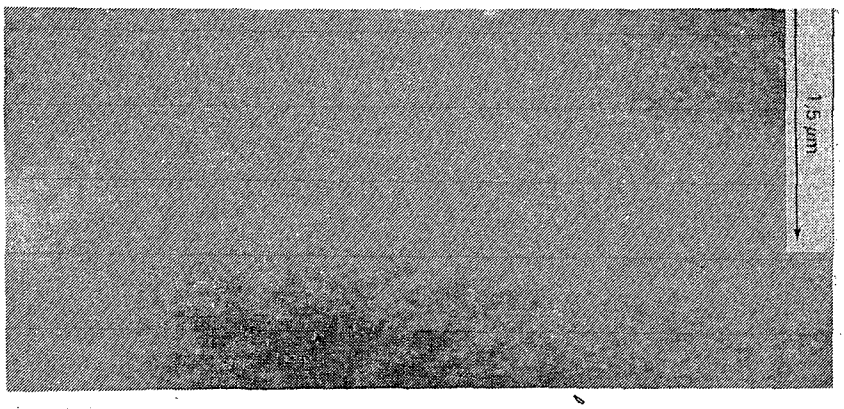

Fig. 1 a

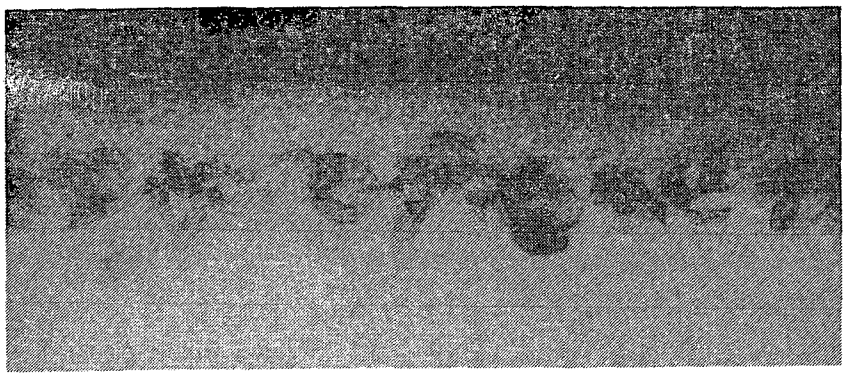

Fig. 1 b

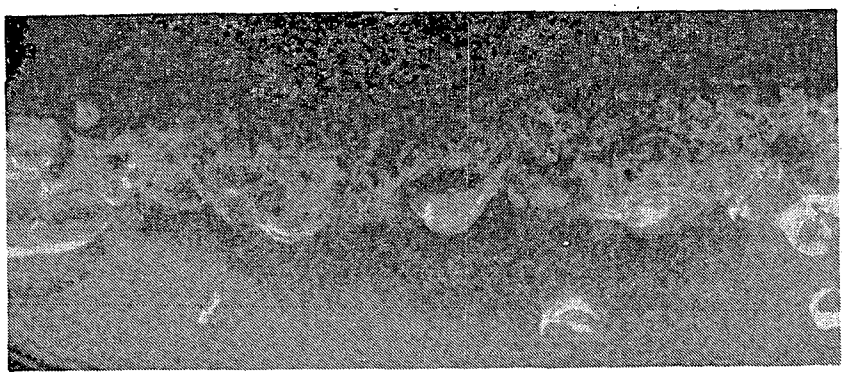

Fig. 1 c

R e f e r e n c e

1/ C. Ascheron et al., Nucl. Instr. and Meth. B 28, 350 (1987)

Figure 1:
Cross-sectional TEM micrographs of (100) GaP

(a) implanted with 2×10^{17} cm^{-2} 300 keV ($\alpha = 40^{\circ}$, $T_{imp} = 300K$)

(b) showing microcracks after annealing ($T_{an} = 720$ K, t = 30 min) and

(c) indicating additional extended defects within the stopping zone after electron beam enhanced annealing.

RELATION BETWEEN MICROHARDNESS AND DAMAGE DENSITY IN ION BOMBARDED GaP

C. Ascheron, H. Neumann, G. Otto, V. N. Bugrov[+], S. A. Karamyan[+]

Karl-Marx-Universität Leipzig, Sektion Physik
[+]Joint Institute of Nuclear Research, Dubna

We have studied the changes in microhardness of ion-bombarded GaP single crystals in relation to radiation-induced lattice disorder. Our former studies of the near-surface mechanical properties show

(i) point defect hardening within the near-surface region /1/,

(ii) a weaker effect of extended defects on the microhardness within the highly damaged "buried" layer /2/ and

/iii/ solid-solution hardening effects which depend upon the chemical nature of the ion species implanted /3/.

In order to investigate the effect of the implanted ion species on changes in the mechanical properties (111) GaP single crystals were bombarded with H^+, He^+, N^+, Ne^+, P^{2+} and Ar^{2+} ions, and microhardness and damage density were measured. Experimental conditions were choosen in such a manner that the measured microhardness was characteristic of the surface region of the implanted crystals and not essentially influenced by the strongly damaged "buried" layer which contains the implanted atoms. Fig. 1 shows the fluence dependence of changes H in microhardness.

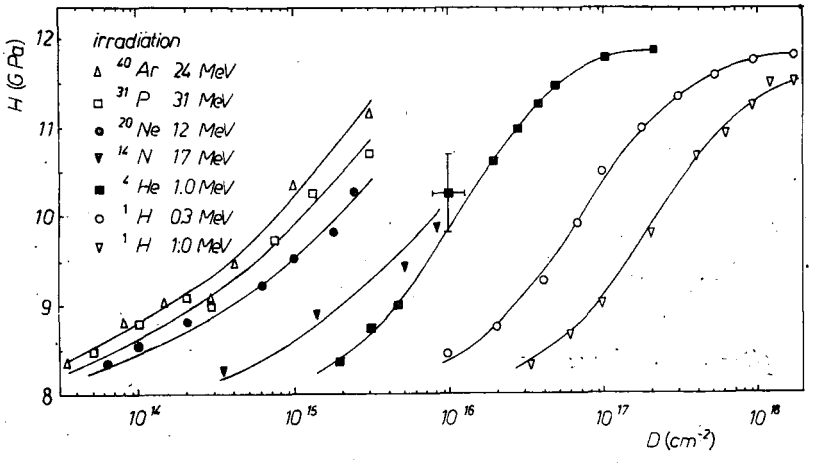

Fig. 1

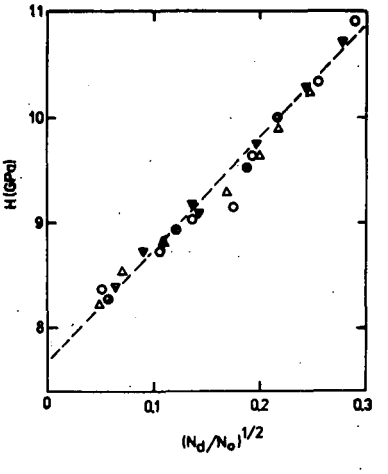

Fig. 2

Fig. 1: Microhardness H as a function of ion fluence.
Fig. 2: Dependence of microhardness H on damage density N_d/N_o in GaP /5/.

The measurements show a tendency of microhardness and of damage density to saturation with increasing ion fluence. The dependence of changes in microhardness upon damage density (fig. 2) indicates that at damage densities $N_d/N_o \lesssim 10$ % the microhardness follows the relation

$$H = H_o + B\,(N_d/N_o)^{1/2}$$

where H_o is the microhardness of unimplanted material ($H_o = 7.9 \pm 0.1$) GPa, and B is a constant having a value $B = (10.5 \pm 0.5)$ GPa. The found square-root dependence of microhardness on damage density is in accordance with models for the description of pinning sites on dislocations which deliver a critical stress for moving dislocations proportional to $(N_d/N_o)^{1/2}$. The qualitative accordance of the effect of the various ions confirms the supposition that in all cases considered the same types of defects, namely point-like defects /4/, give rise to the microhardness changes.

R e f e r e n c e s

/1/ C. Ascheron, H. Neumann, Nucl. Instr. and Meth. B 18,161 (1987)

/2/ C. Ascheron, H. Neumann, Cryst. Res. Tech. 22, 1493 (1987)

/3/ C. Ascheron, R. Schäfer, Annual Report ZfK 1986, p. 75

/4/ C. Ascheron et al., phys. stat. sol. (a) 97, K15 (1986)

/5/ C. Ascheron, H. Neumann, phys. stat. sol. (a) 103, K 81 (1987)

PROTON BOMBARDMENT INDUCED VOLUME CHANGES AND LATTICE DISORDER IN InP, GaAs, GaP, Ge AND Si

C. Ascheron, A. Schindler+, R. Flagmeyer, G. Otto

Sektion Physik, Karl-Marx-Universität Leipzig

+ Zentralinstitut für Isotopen- und Strahlenforschung der AdW Leipzig

On InP, GaAs, GaP, Ge and Si single crystals implanted with 0.3 and 1.2 MeV protons swelling, strain and radiation damage are studied as a function of fluence and of proton energy. Swelling was determined by step height measurements /1/, strain of GaP and InP by Kossel effect measurements /1/ and of GaAs, Ge and Si by Auleytner measurements /2/. Damage density was studied by use of RBS/C measurements with 1.7 MeV He^+ ions.

The investigations show that within the highly damaged region t_2 (for E_p = 0 - 0.3 MeV) all materials exhibit nearly coinciding and strong volume dilation whereas the near-surface region t_1 (for E_p = 0.3 - 1.2 MeV) is considerably expanded only in GaAs, GaP and Ge. InP even contracts as the measurements of relative swelling $\Delta h/t_1$ and of strain $\Delta d_{111}/d_{111}$ indicate (fig. 1 a).

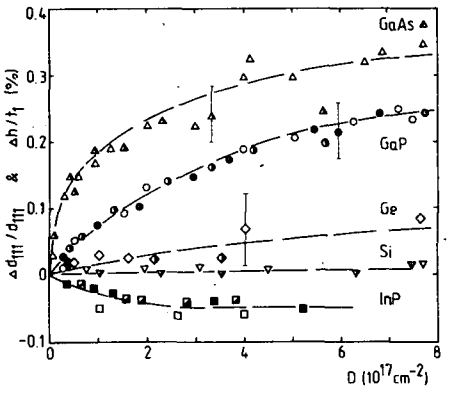

Fig. 1 a

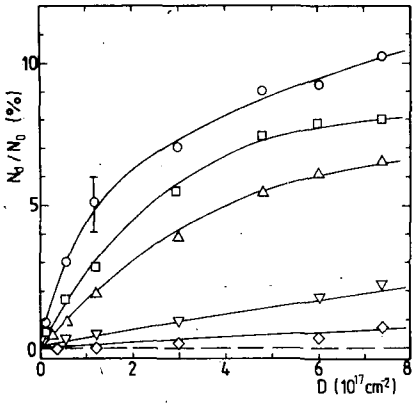

Fig. 1 b

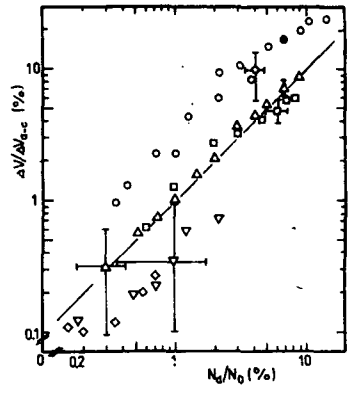

Fig. 2

Fig. 1: Fluence dependences of a) relative swelling $\Delta h/t_1$ and strain $\Delta d_{111}/d_{111}$ and of b) damage density N_d/N_o in the layer t_1 of proton bombarded InP (o), GaAs (□), GaP (Δ), Ge (▽) and Si (◇).

Fig. 2: Normalized swelling $\Delta V/V_{a-c}$ (with ΔV as actual swelling and ΔV_{a-c} as volume difference between amorphous and perfect crystalline material) as function of damage density for InP (o), GaAs (□), GaP (Δ), Ge (▽) and Si (◇).

From the results of the investigations presented it can be concluded:

- Volume changes of proton bombarded material result from defect induced lattice strain and from the additional volume need of the incorporated atoms.
- In the less damaged surface layer t_1 swelling is determined by defect induced lattice strain only. Accordingly, in this layer swelling coincides with integrated strain (fig. 1 a).
- The compound semiconductors show stronger damage by higher energetic protons than the elemental semiconductors, probably due to the formation of antisite defects. At room temperature the "susceptibility" to radiation damage increases in the succession Si, Ge, GaP, GaAs, InP (fig. 2).
- The degrees of densitometrically and ionometrically determined disorder agree within a factor of about 2 in the near-surface layer where point-like defects predominate (fig. 2). This means: The relative volume changes per defect nearly correspond to the relative volume difference between amorphous and crystalline material. This relation holds also for InP where a defect induced lattice contraction is observed.
- At higher fluences ($D > 10^{17}$ cm^{-2}) the swelling of the "buried" layer is -additional to defect swelling- strongly effected by the incorporated hydrogen. Hydrogen has two effects: (i) H expands the lattice due to the additional volume need of implanted atoms. (ii) H supports the formation of voids and consequently of plastic deformations of the implanted crystals.

R e f e r e n c e s: /1/ C. Ascheron et al., to be publ.; /2/ V. Geist, D. Stephan, to be published

LATTICE STRESS AND DETRIMENTAL EFFECTS OF HIGH-FLUENCE HYDROGEN IMPLANTATION

C. Ascheron, A. Schindler[+], A. Setzer[++]
Karl-Marx-Universität Leipzig, Sektion Physik
[++]Karl-Marx-Universität Leipzig, Sektion Chemie
[+]Zentralinstitut für Isotopen- und Strahlenforschung der AdW, Leipzig

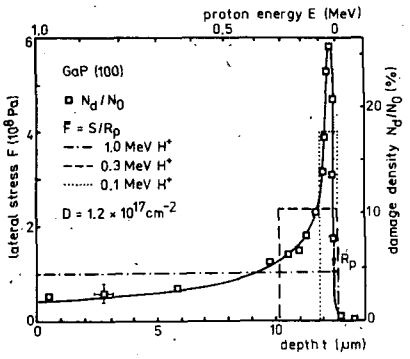

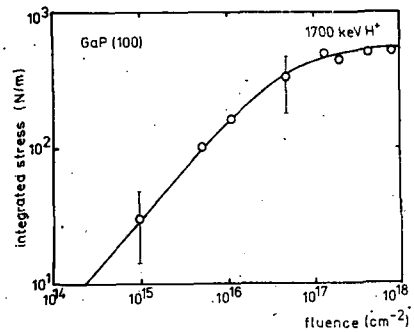

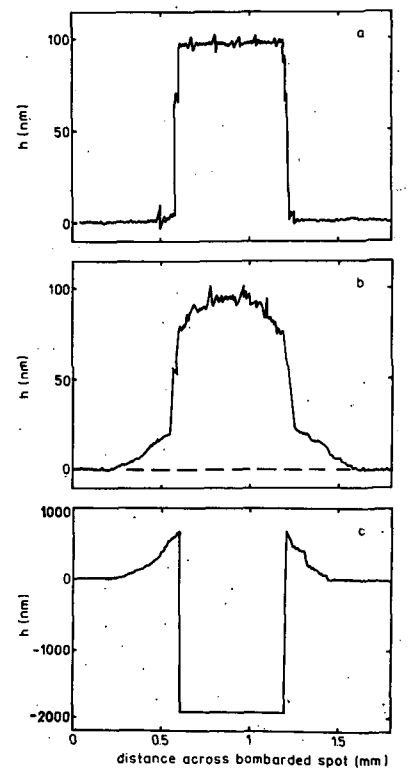

Ion implantation into materials leads to stresses within and around the bombarded region since the implanted layer tends to expand due to (i) the produced lattice disorder and due to (ii) the additional volume requirement of the implanted atoms while the implanted layer is constrained by the substrate. Stress can partly be released by expansion normal to the surface. Lateral stresses within and around the implanted spots are nearly uncompensated. Measurements on GaP, bombarded with protons of equal fluences but different energies and correspondingly different integrated damage, show that lateral compressive stress F qualitatively follows the defect profile (fig. 1). Accordingly, the integrated lateral stress S increases with rising fluence (fig. 2). S exhibits saturating behaviour for fluences $D > 10^{17}$ cm^{-2} due to the occurrence of stress releasing dislocations and plastic deformations. The formation of microcracks and voids is further stimulated by the volume need of implanted atoms. Profilometer studies on implanted samples make this process evident:

- The stress releasing expansion of the implanted area normal to the surface is expressed as formation of a step in height at the borderline between implanted and unimplanted areas (fig. 3 a).
- An increase in stress due to high dose implantation or annealing (increase of gas pressure) leads to a separation of the implanted layer off the underlying bulk material. This is expressed as bending of the implanted region (fig. 3 b).
- Further increase in stress makes the whole implanted layer flake off (fig. 3 c).

The uniformity in depth of the flaking process, which occurs at the depth where tensile stress reaches its maximum, i.e. at the interface between the "buried" heavily damaged, hydrogen containing layer and the undamaged bulk material, is confirmed by SEM measurements, which show plate-like fracture patterns /1/.

Figure Captions

Fig. 1: Depth profile of lateral compressive stress F and of damage density N_d/N_o derived from masurements on samples implanted with 0.1, 0.3 and 1.0 MeV protons.

Fig. 2: Fluence dependence of integrated stress S in proton bombarded (100) GaP.

Fig. 3: Talystep records of GaP surfaces
a) partly irradiated at 300 K,
b) subsequent annealed at 720 K and
c) irradiated at 650 K.

Reference

/1/ C. Ascheron et al., Nuclear Instr. and Meth. B 28, 350 (1987)

RBS/CHANNELING STUDY OF (In,Ga)As/GaAs SINGLE STRAINED-LAYER HETEROSTRUCTURES

R. Flagmeyer
Karl-Marx-Universität Leipzig, Sektion Physik
M. Höricke
Zentralinstitut für Elektronenphysik, Berlin

$In_xGa_{1-x}As$/GaAs(100) single heterostructures (x=0.02-0.13, film thickness 20-100 nm) were analysed by 1.7 MeV He^+ RBS and channeling concerning thickness, In content, crystalline quality, and commensurability of the strained films. Especially, we showed /1/ that the ⟨112⟩ channeling angular-scan method is a suitable technique for the direct determination of the lattice strain in this large-mismatched system ($f \approx 0.07\ x$).
Up to a critical thickness, the lattice mismatch of heteroepitaxial layers is accommodated by tetragonal distortion $\varepsilon_T=(a_\perp - a_\parallel)/a$, where $a_\perp$ and $a_\parallel$ are the vertical and the in-plane lattice constants, resp. It is related to the "kink" angle ψ_k between the offnormal ⟨hkl⟩ axes of the layer and the substrate.

$$\psi_k\langle hkl\rangle = {}^k\langle hkl\rangle \cdot \varepsilon_T.$$

Recording the angular scan profiles of the backscattering yields according to the layer and the substrate ψ_k is measurable as the angular shift $\Delta\psi$ between the two channeling dips (cf. Fig. 1). This method was first demonstrated for the Ge_xSi_{1-x}/Si system /2/ and has general applicability to pseudomorphic structures including strained layer superlattices /cf. 3/.

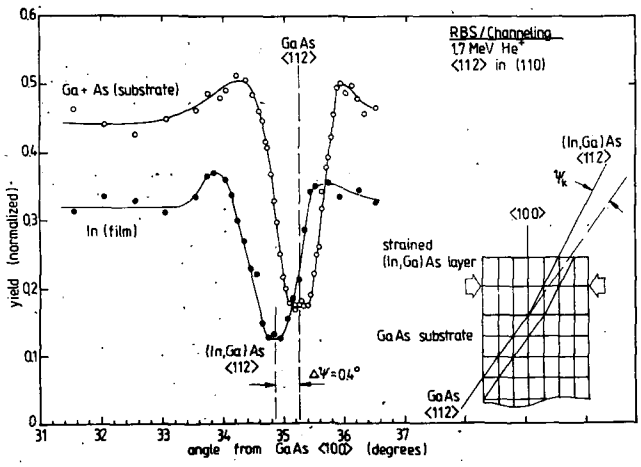

Figure 1
Channeling angular scans in (110) plane through ⟨112⟩ axis of the backscattering yield from a 20 nm $In_{0.13}Ga_{0.87}As$ film on GaAs(100). The schematic (inset) shows the accommodation of the lattice mismatch by compressive strain and the angular separation $\Delta\psi$ of the substrate and film ⟨112⟩ channeling directions.

On the suggestion of Hashimoto /4/ we used the higher indexed ⟨112⟩ axis ($k_{\langle 112\rangle}$=0.47) and the "open" (110) tilting plane to minimize the steering effect. We found full strained layers up to 50 nm thickness with dislocation densities below the detection limit of ion channeling and X-ray diffraction. The ε_T values were close to the expected ones for ideally coherent epitaxy, in good agreement with the results of XRD measurements which complete the RBS/channeling analysis /5/.

References

/1/ R. Flagmeyer and M. Höricke, Nucl. Instrum. Meth. Phys. Res. B, in the press
/2/ A.T. Fiory, et al., J. Appl. Phys. 56 (1984) 1227
/3/ R. Flagmeyer et al., this report, p. 57
/4/ S. Hashimoto, et al., Nucl. Instrum. Meth. Phys. Res. B 13 (1986) 45
/5/ R. Flagmeyer, M. Höricke, T.G. Andersson, H. Rhan, U. Pietsch, and H. Berger, to be published

DETERMINATION OF STRAIN IN (In,Ga)As/GaAs STRAINED-LAYER SUPERLATTICES BY ION CHANNELING

R. Flagmeyer, Karl-Marx-Universität Leipzig, Sektion Physik
K. Lenkeit, Humboldt-Universität Berlin, Sektion Physik
Yu. O. Kanter and A.A. Fjodorov, Institute of Semiconductor Physics, Novosibirsk

Various $In_xGa_{1-x}As$/GaAs SLS's grown on (100)GaAs substrates by MBE with and without alloy buffer layers were characterized by RBS/channeling and X-ray diffraction /1/. The samples are composed of 4 - 20 nm thick layers with 10 - 15 periods and x-values of 20 - 24 %.

In SLS's the lattice mismatch is accommodated by alternating compressive and tensile strain in the layers. The resulting tetragonal distortion /cf. 2/ is related to slight "kinks" in direction of Ψ_k at each interface (Fig. 1 b) along an inclined axis, e.g. for the $\langle 110 \rangle$ axes of (100) grown SLS's. This "kink angle" can be measured (i) by simultaneously recording the angular scans for layers 1 and 2 provided that the elements of both layers be selectively resolved in the RBS spectrum /3/.
However, if only the In signal of the ternary layer (2 nd in our case) can be resolved (ii) the angular shift $\Delta\Psi_2$ relative to the average $\langle 110 \rangle$ row direction is measured (Fig. 1 a), $\Delta\Psi_2 = (a_{\perp 2} - a_{\parallel})/2\, a_{\parallel}$, where $a_{\perp}$ and $a_{\parallel}$ are the vertical and the parrallel lattice constants, resp. For SLS 1 from $\Delta\Psi_2 = 0.65^o$ and the $d_1 : d_2$ ratio of 2.3 a kink angle of 0.93^o is obtained in agreement with the XRD result.

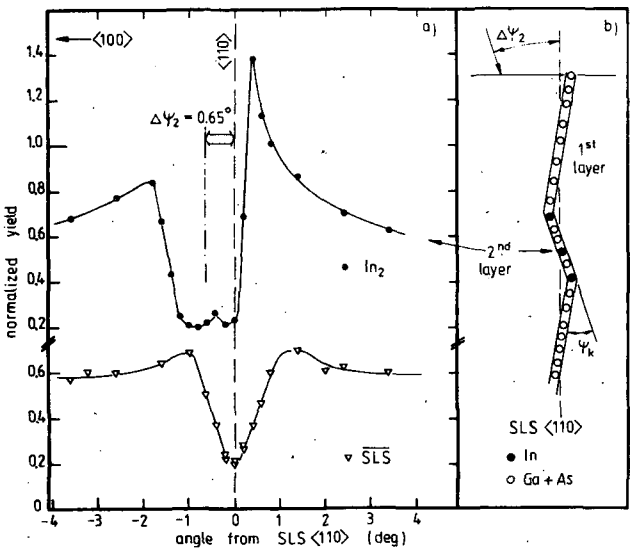

Figure 1
(a) Angular scans in (100) plane through $\langle 110 \rangle$ axis for the 2nd layer (In backscattering signal) and SLS 1 as whole ($In_{0.24}Ga_{0.76}As$/GaAs, 9.2/21.6 nm thick, 10 periods). (b) Schematic representation of $\langle 110 \rangle$ rows with $\Psi_k = 0.93^o$

For very thin layered SLS's and even if the two types of layers cannot be distinguished we proposed a new general method (iii) to determine Ψ_k. Taking the $\langle 110 \rangle$ angular scans for the SLS and a GaAs crystal (Fig. 2 b) under identical experimental conditions Ψ_k is obtained from the angular width of the GaAs dip at the yield level of χ_{min} of the SLS dip (Fig. 2 a). The kink angle of $\approx 0.8^o$ agrees closely with the predicted value of 0.78^o based on the x-value and the elastic theory.

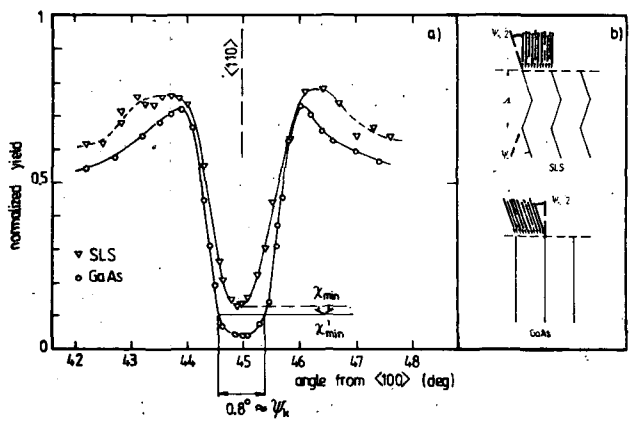

Figure 2
(a) Angular scans through $\langle 110 \rangle$ axis in (100) plane for the $In_{0.20}Ga_{0.80}As$/GaAs (20/20 ML, 13 periods) thin layered SLS 4 and for a GaAs crystal.)b) Schematic of ion beam incidence between kinked SLS' and straight GaAs rows

References

/1/ R. Flagmeyer, K. Lenkeit, T. Baumbach, Yu. O. Kanter, and A.A. Fjodorov, to be published
/2/ R. Flagmeyer, and M. Höricke, this report, p. 56
/3/ S.T. Picraux, et al., Appl. Phys. Lett. 43 (1983) 1020

METHOD FOR GETTERING OF FAST DIFFUSING IMPURITIES IN DEVICE STRUCTURES

C. Ascheron, H. Klose+, W. Frentrup+

Karl-Marx-Universität Leipzig, Sektion Physik
+ Humboldt-Universität zu Berlin, Sektion Physik

Damaged regions which were produced by back side implantation are able to act as a sink or getter for fast diffusing impurities /1/. We tried to develop a method to control the distribution of impurities by the defined creation of "buried" gettering layers located near by the active zone of optoelectronic devices by ion bombardment /2/. We studied the gettering behaviour of non-amorphized layers of different defect types produced by light ion bombardment. Crystals were doped by implantation of low energetic Cu^+ ions, tempered in order to homogeneously dope a surface layer, irradiated with higher energetic H^+ and He^+ ions and annealed in order to redistribute the Cu atoms within the damage profiles.

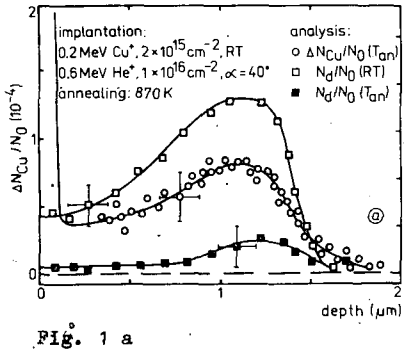

Fig. 1 a

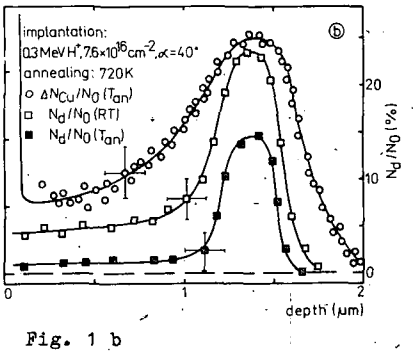

Fig. 1 b

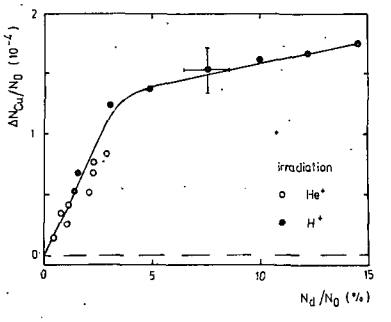

Fig. 2

Fig. 1: Depth profiles of damage density N_d/N_o (determined by RBS/C) on as implanted (□) and annealed GaP (■) and of the concentration N_{Cu}/N_o (measured by SIMS) of gettered Cu atoms (o) for the bombardment with 0.6 MeV He^+ ions (a) and 0.3 MeV protons (b).

Fig. 2: Copper gettering in GaP in dependence on the damage density, measured on H^+ (o) and He^+ (•) bombarded samples which were tempered at 720 K and 870 K, resp.

The results of these measurements, which are presented in figs. 1 and 2, indicate:

1. The relatively simple defects produced by H^+ and He^+ bombardment are already at the medium temperature of 720 K strongly decorated by the Cu atoms. Compared to Si in GaP remarkable gettering effects already occur at lower temperatures.
2. The broadening of the Cu profile against the damage profile towards the surface points out to a non-linear relation between damage density and gettering efficiency; and the broadening towards the undamaged bulk crystal observed on the stronger damaged H^+ bombarded sample makes us assume gettering at the interface between highly stressed damaged layer and undamaged bulk material. Within this layer stress releasing extended defect structures and microcracks occur.
3. Temperature treatment principally has two opposite effects on the gettering process:
   (i) diffusivity of impurity atoms increases with temperature, consequently the probability to reach sinks due to long-range migration increases,
   (ii) the number of trap centres and of impurity-defect complexes decreases due to defect annealing. The reduction depends upon the defect type /3/.

   The optimum temperature of gettering efficiency varies with the predominating defect type. Our measurements show that the smaller defect complexes produced by H^+ and He^+ bombardment have a higher gettering efficiency at 720 K than at 870 K.
4. A study of the correlation between gettering efficiency and damage density and type shows that extended defects have lower gettering ability per involved point defect than isolated point defects (fig. 2 and /4/). The critical damage density for the predominance of extended defects is $N_d/N_o \approx 5$ % in samples annealed at 720 K. This is also reflected in the gettering efficiency (fig. 2).

R e f e r e n c e s :
/1/ B. J. Masters et al., Proc. 1st Int. Conf. Ion Impl. Semicond., New York 1971, Gordon and Breach, p. 81
/2/ C. Ascheron, H. Klose, DDR-Patent DD 232138 A1
/3/ C. Ascheron et al., Ext. Abstracts, Int. Conf. Nucl. Anal. Meth., Dresden 1987, p. 17
/4/ C. Ascheron et al., Proc. 3. Int. Autumn Meeting Gettering Defect Eng. Semicond. Tech., Berlin 1987, Akademie-Verlag, p. 304

A SIMPLE DEVICE FOR ELEMENTAL ANALYSIS OF SAMPLES WITH AN EXTERNAL PROTON BEAM

D. Lehmann, B. Krause, U. Lehmann, and R. Wipper
Karl-Marx-Universität Leipzig, Sektion Physik, WB Angewandte Kernphysik

On the Leipzig van de Graaff accelerator an experimental apparatus has been installed which allows the proton beam to be extracted from the vacuum of the beam guide system and to hit a sample in the open air. The purpose of such a device is the quantitative analysis of the elemental content using the PIXE and/or PIGE methods in samples which are not stable or are otherwise extremely sensitive to ion irradiation in vacuum. The relatively low maximum available proton energy from our accelerator (≈ 1700 keV) strongly restricts design and construction. Thus we had to minimize the ion path outside the vacuum.

To realize this and to consider further conditions a modular construction was chosen. Fig. 1 shows details of the device. In a commercial cross piece (K65, HV Dresden), which was linked to the end of a beam guide line of the accelerator, an insulated construction carrying the beam diffuser (thin carbon target) /1/, a quartz beam viewer and the beam energy monitoring target (Al) is mounted. The next element of the device, a cube-shaped vacuum chamber, contains the fast-closing safety valve /2/. One side of it is connected to a vacuum station, consisting of a mechanical and a Roots-type pump and some control elements. In the beam direction follows the 'noselike' exit foil construction with a 7.5 µm thick Kapton window (DuPont). This flange also carries an insulated plate, on which the sample holder and a detector fitting especially designed for our Si(Li) detector are mounted. The target holder can also be modified for the measurement of liquid samples. The set-up allows to vary the distance between exit window and sample surface (10...30 mm), the detection angle (70°...110°), the angle between target normal and beam (15°...55°) and the beam spot diameter on the sample (1...6 mm).
Besides direct charge collection on the insulated sample holder for monitoring the number of projectiles, in the case of PIXE measurements it is also possible to take the yield in the argon peak produced through the interaction of the projectiles with the Ar contained in the air. Fig. 2 shows a PIXE spectrum of Wagras, a colloidal graphite, measured with the described device.

References

/1/ H.U. Frey et al., Ann. Report 1986, ZfK-621 (1987) 144
/2/ B. Krause and D. Lehmann, Ann. Report 1986, ZfK-621 (1987) 145

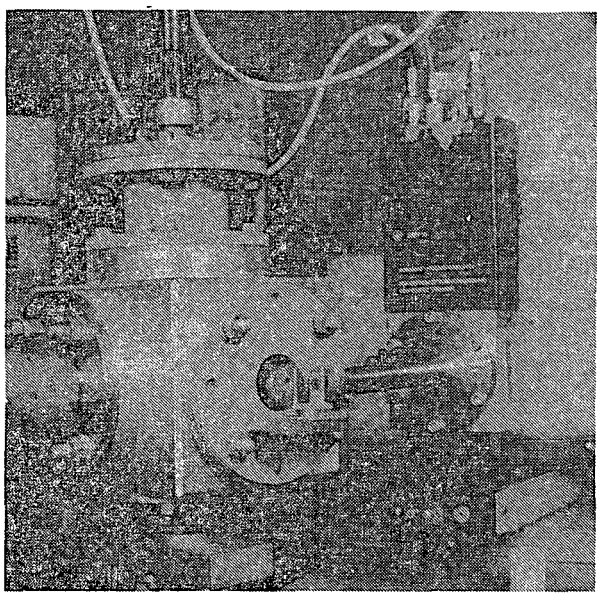

Fig. 1: View of the external beam device

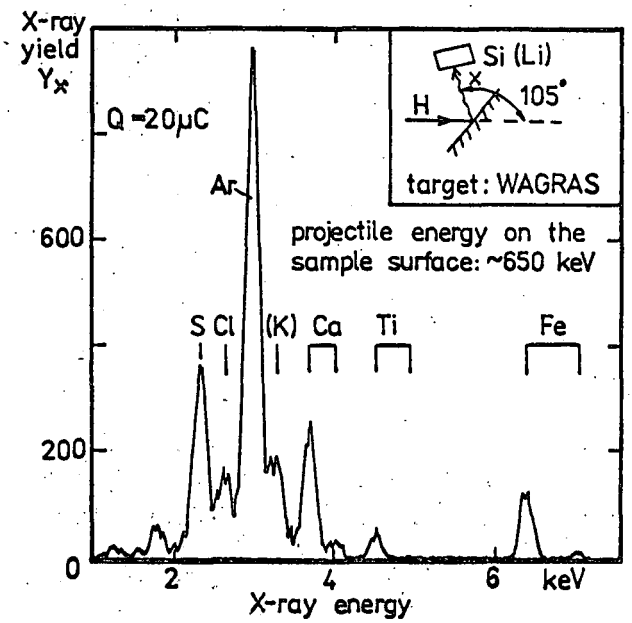

Fig. 2: PIXE spectrum of a Wagras sample

FLUORINE PROFILING APPLIED TO DENTAL PRACTICE

H.-E. Zschau, F. Plier and G. Otto
Karl-Marx-Universität Leipzig, Sektion Physik, WB Angewandte Kernphysik
C. Wyrwich, A. Treide
Karl-Marx-Universität Leipzig, Sektion Stomatologie
Poliklinik für Orthopädische und Kinderstomatologie

The success of caries prevention with fluorine containing varnishes depends on exact timing of the clinical application. In order to check this the fluorine concentration profile in the outermost enamel surface region gives helpful informations. Fluorine depth profiles can obtained using proton Induced Gamma-Ray emission spectrometry (PIGE) at resonance reactions /1,2/. The resonance of the reaction $^{19}F(p,\alpha\gamma)^{16}O$ at proton energy E_p = 340 keV (Γ_R = 2.5 keV) allows the profiling up to a depth of about 1 µm with a near surface resolution of 20 nm (angle of incidence 45 degrees), whereas fluorine profiles up to a depth of at least 3 µm can be measured by taking of the resonance at E_p = 935 keV ($^{19}F(p,p'\gamma)^{19}F$, Γ_R = 8.1 keV) with a near surface depth resolution of 100 nm in the same geometry. An exhaustic discussion of the experimental details is published in /2,3/.

After experiments with in vitro prepared bovine teeth /3/ now human enamel applicated local in vivo with Duraphat^R was investigated. Three teeth from the same person were prepared with the laquer and extracted after 1, 14 and 28 days (samples A1, A24 and A28 resp.). The control sample extracted before is denoted by A0. The results can be summarized as follows:

- The fluorine level of prepared enamel is distinctly higher than in the control within the whole investigated region.
- In the depth region from more than 400 nm up to at least 2.2 µm the fluorine profiles of the prepared samples are very similar.
- In the near surface region there is only a small lack of fluorine in the samples A14 and A28 showing stability of fluorine enrichment.
- Surprisingly in contrast to the in vitro preparation the starting value of the profiles (immediately after application) is significantly lower /4/.

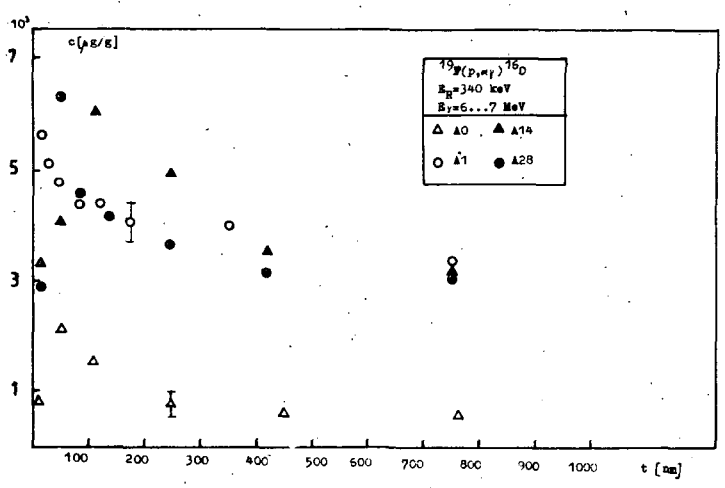

Figure 1
Fluorine concentration profiles measured with the reaction $^{19}F(p,\alpha\gamma)^{16}O$.

References

/1/ U. Wolf et al., Annual. report 1984, ZfK-559 (1985) 84
/2/ H.-E. Zschau et al., Annual report ZfK-584 (1986) 72
/3/ H.-E. Zschau et al., Annual report ZfK-621 (1987) 81
/4/ H.-E. Zschau et al., Proc. 4th Meeting on Nuclear analytical Methods, Dresden 1987, p. 395.

ELEMENTAL ANALYSIS OF LIGNITE SAMPLES BY MEANS OF PIXE

J. Vogt and G. Otto
Karl-Marx-Universität Leipzig, Sektion Physik, WB Angewandte Kernphysik
C. Wischnewski
Karl-Marx-Universität Leipzig, Sektion Chemie, WB Analytik

There is a great demand for quantitative trace element analyses of lignites. Therefore quick and accurate methods of analyses are necessary to collect more geochemical data. The advantage of PIXE (Proton Induced X-ray Emission Spectroscopy) over other methods in terms of simple sample preparation, multi-element capability, sensitivity, and speed are well documented [1].
The topic of our investigation was to test PIXE as an accurate analysis method for such heterogenous, fine grained, and compositionally complex samples, like lignites.
The collected material was air dried and ashed at 800 °C [2]. Thick targets were prepared by pressing the ash powder with a small amount of a binding agent (polystyrene) into pellets. The target surface was carbon coated to prevent charge build up.
The proton beam with an energy of 1700 keV was generated from the 2 MV Van de Graaff accelerator of the Karl Marx University Leipzig. To overcome inhomogenity problems a beam diameter of 7 mm was used. The target current was kept below 100 nA to avoid target destruction by the beam. Proton induced X-rays were detected with a Si(Li) detector (δE=190 eV) and the spectra were accumulated and evaluated using the computer controlled multichannel analyzer EDR 184 (ZWG Berlin). The concentrations were evaluated by means of a new computer program for thick target PIXE written in PASCAL running on the personal computer PC 1512. X-ray production cross sections were obtained using the fit by PAUL [3]. The stopping power was calculated according to the fit by ANDERSEN & ZIEGLER [4] and the X-ray attenuation was determined from the tables by LEROUX & THINH [5]. For calibration we used thick standards of pure elements or simple compounds. The analysis was made in two steps. At first the main and minor components were measured without any filter in front of the X-ray detector. In the second step the trace element contents were determined using a X-ray filter of high purity silicon (thickness 250 µm).
Table 1 lists the result of the analysis of a lignite ash sample. The comparison of this values with results of the analysis of the same material by means of AES (Atomic Emission Spectrometry) showed considerable differences especially for potassium [2]. This may be caused by the enhancement effect, because the sample contain a high amount of calcium.

Table 1: Result of PIXE analysis of the lignite sample

Element	Content[%]	Element	Content[ppm]	Element	Content[ppm]
Si	20.3	Ni	50	Rb	2.9
S	8.1	Cu	31	Sr	1081
K	0.15	Zn	15	Y	83
Ca	7.05	Ga	34	Zr	1190
Ti	1.67	Ge	3.5	Nb	52
Mn	0.002	As	15	Ba	352
Fe	1.87	Se	0.5	Pb	46
		Br	2.0	Th	0.6

The following conclusions could be drawn:
- For a lot of elements the PIXE method allowed the precise and accurate analysis of ashed lignite samples.
- The insertion of the enhancement effect correction in our computer program is necessary.
- For rapidity the possibility of direct analysis of coal samples by PIXE, but also by PIGE and RBS should be investigated.

References
[1] S.A.E. Johansson, Nucl.Instr.Methods, B22 (1987) 1.
[2] C.Wischnewski, Dissertation, KMU Leipzig 1987.
[3] H.Paul, Nucl.Instr.Methods, B3 (1984) 5.
[4] H.H.Andersen, J.F.Ziegler, The Stopping Power and Ranges of Ions in Matter, Vol.3, Pergamon Press, New York,1977.
[5] J.Leroux, T.P.Thinh, X-ray Spectrometry 8(1979)2, p.85

PIXE AND RBS ELEMENTAL ANALYSIS OF COAL LIQUIDS

W. Knolle, and G. Otto
Karl-Marx-Universität Leipzig, Sektion Physik, WB Angewandte Kernphysik

Impurities down to trace level play an important role in the process of coal liquefaction: e.g. for the reduction of catalyst activities (catalyst poisoning), as cause of corrosion processes and deposits on walls of containing vessels, for environmental pollution due to wastes and emission of toxic materials and for the characterization of the liquid coal conversion products.

Problems for the PIXE analysis of coal oils arise from the instability of the liquids in vacuum and from the unknown, strongly varying matrix composition.

Vacuum-resistant targets were prepared by thermal degradation at 150 - 200 °C. By adding conc. sulphuric acid (1 ml/g oil) possible losses of volatile trace elements were reduced due to the formation of stable sulphates /1/. The coked, carbonaceous residue was pelletized with the help of a glue (styrene, 20 % by weight).

The PIXE analysis was made with 1.7 MeV protons. The beam with a diameter of about 6 mm was homegenized by a carbon diffuser (120 nm thick). X-rays were detected with a Si(Li)-detectpr with 195 eV FWHM at 5.9 keV. The target stability for beam intensities <7 nA/mm^2 was tested by successive irradiations /2/.

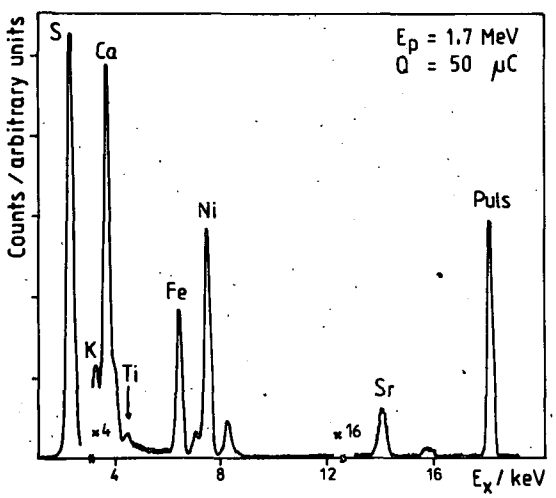

Figure 1: PIXE spectrum of an ashing residue (linearly scale)

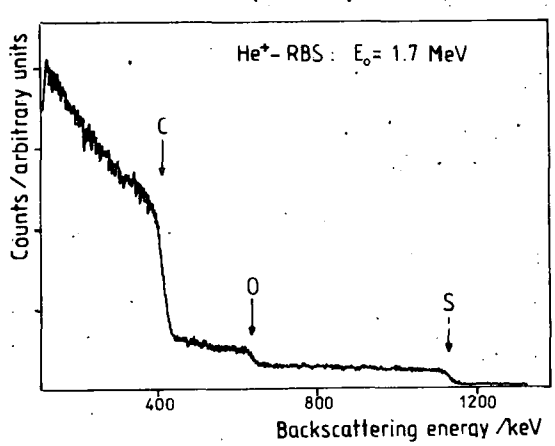

Figure 2: RBS spectrum of an ashing residue

Fig. 1 shows the spectrum of an ashing residue; Sr was added as an internal standard to reproduce all mass rations during the ashing procedure.

The matrix composition was determined with the help of He$^+$ RBS (E_0 = 1.7 MeV, backscattering angle = 160°). The concentration ratios of the main elements carbon, oxygen and sulphur were deduced from the step heights in the spectrum (fig. 2). These ratios were converted into absolute concentrations with the help of the absolute sulphur content due to PIXE analysis. Then the hydrogen content was estimated as difference from 100 %

The composition thus obtained serves as a new matrix for the PIXE evaluation. The iterative evaluation of the PIXE and RBS spectra results in 10 - 15 % accuracy for all (trace) element concentrations of the residues /2/.

References

/1/ J.J. Comford and S.M. Hsu
NBS spec. publ. 674 (1982) 139
/2/ W. Knolle, diploma work Karl-Marx-University Leipzig, 1987

HYDROGEN ANALYSIS BY MEANS OF THE NUCLEAR REACTION $^{1}H(^{15}N, \alpha_0)^{12}C$

D. Grambole, F. Herrmann and W. Rudolph
Zentralinstitut für Kernforschung Rossendorf, Bereich KF

Usually the resonant nuclear reactions $^{1}H(^{19}F, \alpha\gamma)^{16}O$ or $^{1}H(^{15}N, \alpha\gamma)^{12}C$ are used for quantitative hydrogen analysis in the near surface region of solid materials. To measure the hydrogen depth profiles with good resolution the 6.385 MeV ^{15}N resonance is often applied /1/. Depth profiles are obtained measuring the γ-ray yield in dependence upon the incidence energy EN. The γ-ray spectrum of the hydrogen interferes with a time dependent background which has to be separated. In most cases beam intensities of about 20 to 30 nA are employed.

Generally, three dimensional (3D) concentration profiles of elements can be measured by nuclear microprobes. In comparision to mm beams the ion current at microprobes is two orders of magnitude smaller, hence the hydrogen induced γ-ray spectrum is completely shadowed by the background. Therefore we tried to apply the α-particle channel of the reaction $^{1}H(^{15}N, \alpha_0)^{12}C$ at EN = 5.4 MeV for microbeam hydrogen detection. The energies of α-particles, recoiled atoms ^{1}H, ^{28}Si, ^{52}Cr and scattered ^{15}N atoms were calculated in dependence upon the emission angles (fig. 1). At $\vartheta > 90°$, used for measurements with the nuclear microprobe, only the α-particles and the ^{15}N atoms scattered at heavier matrix atoms are emitted. The ^{15}N atoms can be absorbed by 2 µm polyester foil in front of the silicon surface barrier detector. With this absorber only the α-particles reach the detector as shown in fig. 2, spectrum b. In contrary to the γ-ray spectrum the α-particle spectrum contains the hydrogen depth profile directly.
The reaction $^{1}H(^{15}N, \alpha_0)^{12}C$ seems to be suitable for measurements of 3D hydrogen profiles by nuclear microprobes.

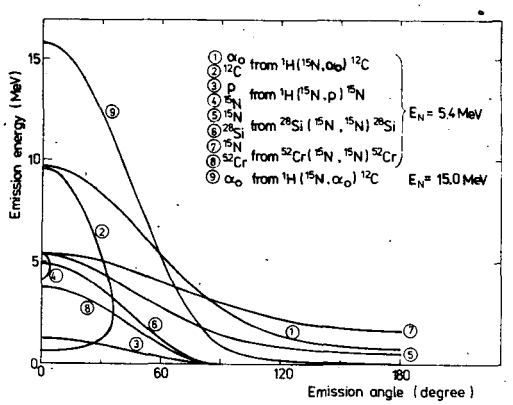

Fig. 1
Angular dependence of emitted particles at ^{15}N energies of 5.4 and 15.0 MeV

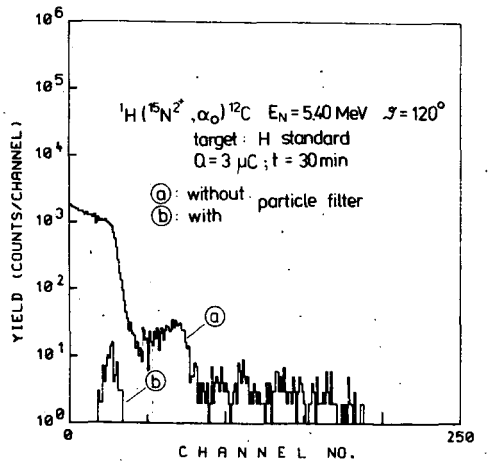

Fig. 2
Particle spectrum emitted from a 280 nm thick SiN layer (18.6 at.% H) on Si bombarded with 5.4 MeV ^{15}N

References

/1/ Rudolph, W. et al., J. Radioanal. Chem. 83 (1984) 99

INVESTIGATION OF PIECO CERAMICS WITH THE ROSSENDORF NUCLEAR MICROPROBE

F. Herrmann, D. Grambole and W. Rudolph
Zentralinstitut für Kernforschung Rossendorf, Bereich KF

Objects of investigation were pieco sinter ceramics used as ultrasonic sensors for diagnostic purposes in nuclear power plants. These ceramics consists of $(Pb_{0.6}Ba_{0.4})Nb_2O_6$. We were interested to know wheter the three elements Pb, Ba, and Nb are homogeneously distributed after the sintering process. The aim was to find out if there are inhomogeneities at lateral resolution of about 10 µm; therefore the measurments were performed at the microprobe /1,2/.

We measured the elements Pb, Ba, and Nb by means of proton induced X-ray emission (PIXE). The obtained spectrum (fig. 1) allowed a good separation of the three elements. The proton beam of Ep = 3 MeV was focused to a diameter of about 10 µm and was scanned over an area of 1 x 1 mm^2.

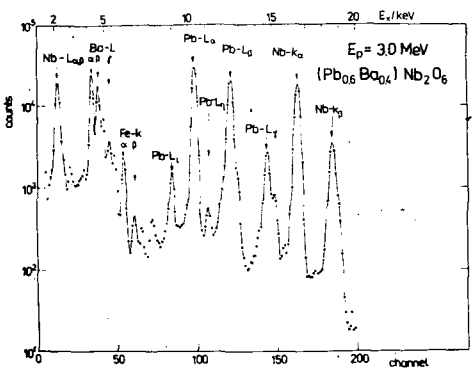

Fig. 1
PIXE spectrum of the investigated pieco ceramics

The events measured by means of a Si(Li) detector arranged at 120° in respect to the beam direction were gathered in the memory of the colour display and visualized simultaneously for the three elements. These elemental maps or the single events (energy and local information) were recorded on magnetic tape cassettes.

The first examinations of the ceramics showed a strong inhomogeneous distribution of the elements. But, concentration minima or maxima of all elements were found at the same positions. This was due to the very rough structure of the ceramics /3/. After improving the surface roughness good homogeneity was got.

Supposing a homogeneous distribution the number of events per pixel must fluctuate around the mean contents according to a Gaussian distribution. In case of a broader experimental distribution homogeneity will be worse. The elemental maps show where and in which size inhomogeneities exist (figs. 2,3).

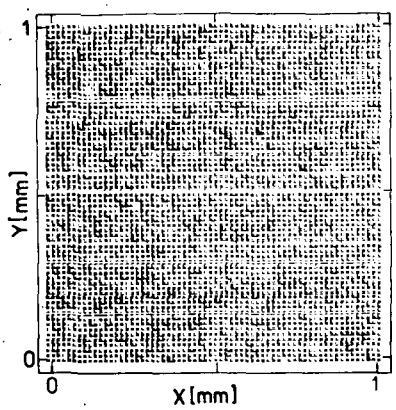

Fig. 2
Elemental map of lead (specimen no. 4)

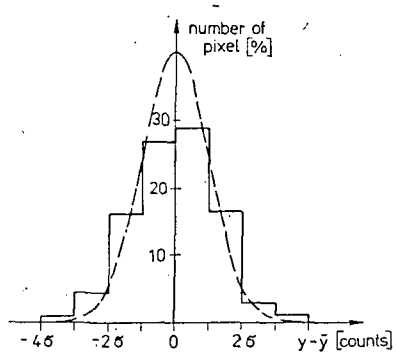

Fig. 3
Number of pixels in the lead window of specimen no. 4 with corrosponding deviations from the mean contents $\bar{y}$. $\sigma = \sqrt{\bar{y}}$ is the statistical error of $\bar{y}$. The dashed curve fits a Gaussian distribution with the width σ. The inhomogeneity is here smaller than the statistical error (~5.5 %)

R e f e r e n c e s

/1/ Grambole, D., F. Herrmann, Gemeinsamer Jahresbericht 1984, ZfK-559 (1985) 92
/2/ Fromm, W.-D. et al., Annual Report 1985, ZfK-584 (1986) 90
/3/ Grambole, D. et al., Annual Report 1986, ZfK-621 (1987) 73

HYDROGEN DEPTH PROFILING ON HF-SPUTTERED Cr-Si RESISTANCE LAYERS

C. Neelmeijer, D. Grambole, C. Heiser, F. Herrmann, R. Grötzschel and W. Rudolph
Zentralinstitut für Kernforschung Rossendorf, Bereich KF
G. Sobe, H. Schreiber, G. Weise, H. Grießmann and A. Heinrich
Zentralinstitut für Festkörperphysik und Werkstofforschung, Dresden

Thin films on the basis of CrSi are suitable to produce high resistance structures in microelectronic semiconductor devices /1/. In comparison to the reactive Plasmatron sputtering technique changed electrical properties (ρ, TK) have been observed when depositing the resistance layers by means of HF-diode sputtering /2/. For this reason an extensive analytical study of these layers had been initiated including hydrogen depth profiling making use of the $^{1}H(^{15}N,\alpha\gamma)^{12}C$ nuclear reaction in the vicinity of the 6.385 MeV resonance energy /3/.

Fig. 1 presents some results as obtained for both layer deposition at different HF-plasma powers and different post-annelaing (30Cr70Si melting target).
Obviously, low power (70 W) deposition without annealing generates resistance layers to be characterized by large amounts of incorporated hydrogen (tab. 1) which quickly diffuses out during the ^{15}N ion bombardment (H-plateau yield of the spectrum measured for the 70 W non-annealed sample). Subdivision of the accumulated ion charge, i.e. number of $^{15}N^{2+}$-projectiles, gives the hydrogen outdiffusion behaviour (insert of fig. 1), hence allows a zero-bombardment extrapolation of the ^{12}C γ-radiation (E_γ = 3...5 MeV) signal. As shown in fig. 1 and tab. 1 an increase of the HF power causes a decrease of the hydrogen content inside the CrSi layer material. An analogous behaviour is observed after post-annealing of low power (70 W in fig. 1) deposited films.
To deduce hydrogen concentrations (tab. 1) matrix compositions were determined by means of Rutherford backscattering spectrometry.

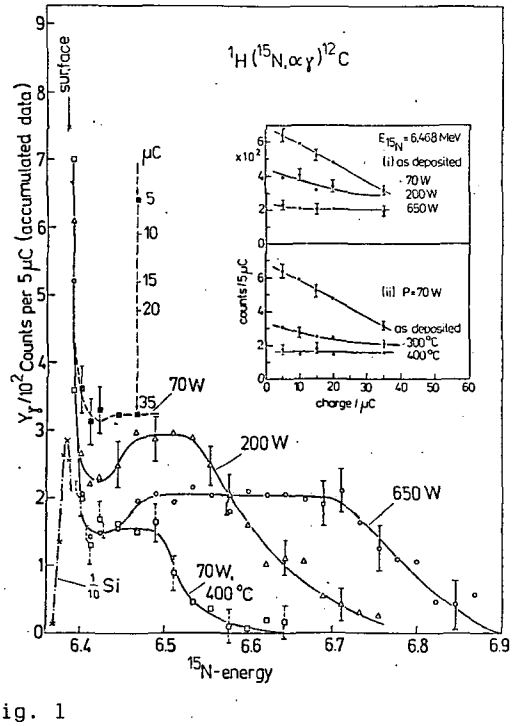

Fig. 1
H-depth profiles and H-outdiffusion during ^{15}N-bombardment for HF-sputtered CrSi layers

Table 1
Deposition parameters and hydrogen contents of Hf-sputtered CrSi films

HF-power /W/	annealing temperature /°C/	layer thickness /nm/	hydrogen content /at %/
650	-	171	4.7
200	-	112	10.7
70	-	69	13.0
70	300	69	8.4
70	400	69	3.5

References

/1/ G. Sobe et al., Thin solid films 128 (1985) 149
/2/ G. Sobe et al., ZFW K4/3/86 (1986)
/3/ W. Rudolph et al., J. Rad. Nucl. Chem. 83 (1984) 99

APPLICATION OF THE BRAGG IONIZATION CHAMBER FOR ERD

E. Hentschel, R. Kotte, H.-G. Ortlepp, F. Stary, D. Wohlfarth

Zentralinstitut für Kernforschung Rossendorf, Bereich KF

Stimulated by the development of the 4π-spectrometer PHOBOS /1/, Bragg ionization chambers (BIC) were found to improve substantially the known ERD method. The good energy as well as Z resolution /2/ of BICs offer the possibility to measure concentration profiles of different elements - independently on each other - up to a depth determined by the range of the incoming bombarding ions. Fig. 1 illustrates the principle of the method and the used symbols. The recoiled ion (Z_i, A_i) gets the initial energy

$$E_i(0) = \frac{4A_0A_iE_d}{(A_0+A_i)^2}\cos^2\Theta$$

The energy losses $\Delta E_0(d) = E_0 - E_d$ of the bombarding ion and $\Delta E_i(d) = E_i(o) - E_i(d)$ of the recoiled ion may be taken from the known stopping power of the bulk material in the case of low impurity concentration. High (e.g. stoichiometric) concentrations of foreign elements need an iterative procedure. The volume concentrations (in atoms/cm^2) follow from

$$c_i(d) = \frac{\sin\alpha}{I_0}\cdot\frac{\Delta I_i(d)}{\Delta d}\cdot\frac{1}{\Delta\Omega}\cdot\left(\frac{d\sigma_i(d)}{d\Omega}\right)^{-1},$$

with

$$\frac{d\sigma_i(d)}{d\Omega} = 0.5184\left(\frac{Z_0Z_i}{E_d\,(MeV)}\right)^2\left(\frac{A_0+A_i}{A_i}\right)^2\cdot\frac{1}{\cos^3\Theta}\ \frac{fm^2}{sterad}$$

This method has been used for investigating the concentration profiles of buried compound layers /3/ in Si (fig. 2) with 45 MeV $^{35}Cl^{8+}$ ions of our tandem accelerator. The ranges to be analysed amount to about d = 1 µm with a depth resolution of Δd = 15...20 nm. Fig. 3 shows the possibilities to analyse surface impurities with ERD or elastic scattering of the bombarding ions, the latter giving a very bad mass resolution.

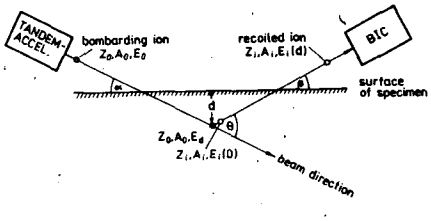

Fig. 1 Principle of the method

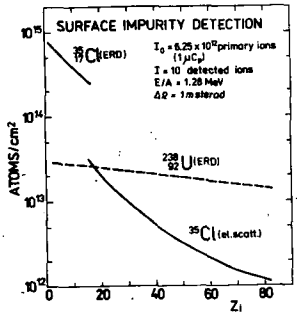

Fig. 3 Minimum surface contaminations to be analysed

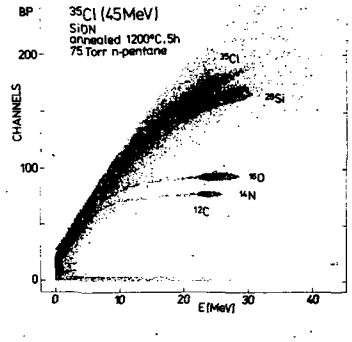

Fig. 2 Bragg peak height BP vs. energy E of an annealed SiON layer

References

/1/ Akhperdshanian, A.G. et al., Report JINR R 13-87-760

/2/ Kotte, R. et al., Report ZfK-591 (1986); Nucl. Instr. and Meth. in Phys. Res. A257 (1987) 197

/3/ Skorupa, W. et al., Proc. 4th Int. Conf. Radiation Effects in Insulators, Lyon, 6. - 10.7.1987, Nucl. Instr. and Meth. in Phys. Res. (in press); this report, p. 77

AN EXPERIMENTAL ARRANGEMENT FOR ^{35}Cl-INDUCED ERD-ANALYSIS AT THE 5 MV TANDEM ACCELERATOR

C. Neelmeijer, H. Böhme, K. Brankoff, L. Kumpf and W. Rudolph
Zentralinstitut für Kernforschung Rossendorf, Bereich KF

Elastic recoil detection (ERD) represents a complementary analytical tool to the well established Rutherford backscattering technique. ^{35}Cl-induced ERD allows the simultaneous detection of elements $Z \lesssim 9$ as well as depth profiling within the near surface region (50 nm...1 µm) of solids /1/. In comparison to nuclear reactions ERD holds the advantage to be characterized by a steady projectile energy dependence of the reaction cross section which varies with the square of the target atomic number according to the Rutherford law.

A new experimental arrangement has been installed at the 5 MV tandem accelerator to make use of the 30 MeV $^{35}Cl^{6+}$ beam for ERD analytical work /2/. The computer controlled mechanical-operating unit enables a quick selection of the angles of incidence α and detection ϑ, respectively, as well as of the horizontal sample position. For maximum information depth we use $\alpha = 20°$ but $\alpha = 4°$ if high depth resolution is required near the target surface ($d \lesssim 100$ nm). After penetrating a 9.2 µm thick Mylar foil, which stops elastically scattered Cl-projetiles completely, the target recoil atoms are collected within an implanted Si-detector (ZfK production) routinely at $\vartheta = 30°$. Projectile monitoring takes place by Rutherford backscattering of ^{35}Cl particles at a 150 nm thick gold layer deposited on a rotating propeller. Vertical slit diaphragms of different width (0.2...1 mm) are adjustable manually to ensure a proper angular divergency of the impinging beam. A vacuum lock guarantees a quick change of the complete target holder.

As an example fig. 1 presents the result of first test experiments. A sequence of 20 nm thick layers produced by plasma enhanced CVD of Si-nitride and amorphous silicon, respectively, was bombarded with 30 MeV Cl ions at $\alpha = 4°$. The ERD spectrum ($\vartheta = 30°$) of ^{14}N and ^{1}H recoil atoms resolves clearly the target sandwich structure indicating different hydrogen concentrations within the two types of PECVD layer materials. This result is in a good agreement with former studies using the $^{1}H(^{15}N,\alpha\gamma)^{12}C$ resonance reaction. However, the ERD data aquisition time was less than 10 % of those necessary for stepwise H-depth profiling by means of the $(^{15}N,\alpha\gamma)$ reaction.

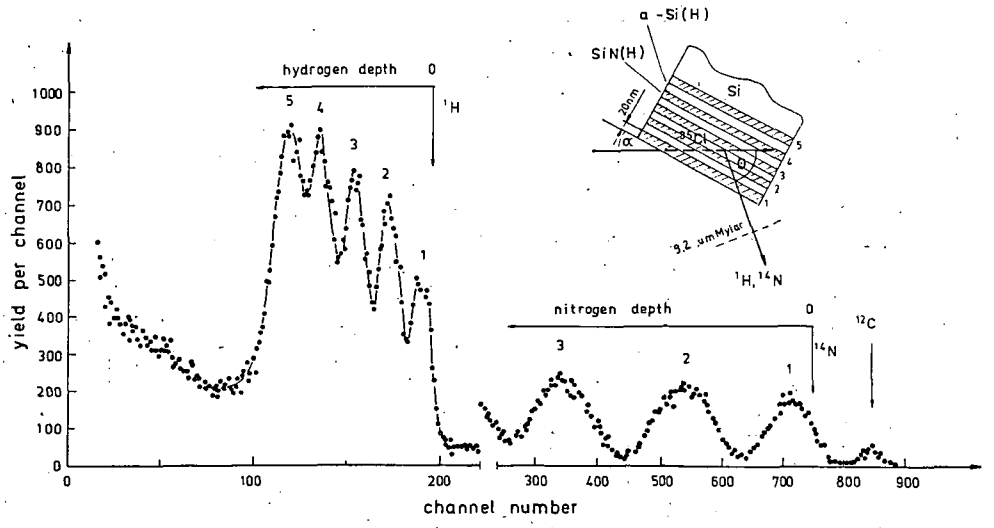

Fig. 1
ERD spectrum of a PECVD sandwich structure

R e f e r e n c e s

/1/ C. Nölschner et al., Nucl. Intrum. Methods 218 (1983) 116
/2/ C. Neelmeijer et al., KFC 2.87-ERD (1987)

NONDESTRUCTIVE ANALYSIS OF PAINTINGS BY A 4 MeV EXTERNAL PROTON BEAM

C. Neelmeijer, H. Matthes and W. Pfestorf
Zentralinstitut für Kernforschung Rossendorf, Bereich KF
H.-P. Schramm
Hochschule für Bildende Künste, Dresden

Besides of routine microscopic studies several methods of modern natural science have been applied to identify the complex layer structure of art paintings. Usually radiation induced diagnostics as UV-, IR- and X-ray fluorescence-spectroscopy image a nondestructive depth sensitive topography, whereas pigment analysis, e.g. by chemical methods, atomic absorption and laser spectrometry or neutron activation, requires a mechanical sample taking.

Proton induced X-ray emission (PIXE) in atmospheric air enables a nondestructive highly sensitive multielement ($Z \geqslant 14$) analysis of pigment components even at very small (1 mm^2) spots /1/.

The 4 MeV proton beam from the 5 MV Tandem accelerator of the ZfK Rossendorf was collimated and allowed to exit into the atmosphere through a 2 µm thick HAVAR foil (fig. 1). After penentrating about 2 cm of nitrogen or helium the protons hit the surface of the painting inducing both X-ray and γ-ray emission. An energy dispersive Si(Li) X-ray spectrometer (δE_x = 180 eV) arranged at 135° backward angle was shielded with a 150 µm thick Mylar absorber to avoid pulse pile-up due to intense low energy X-radiation, e.g. Ca K-radiation from the $CaCO_3$ ground of the painting.

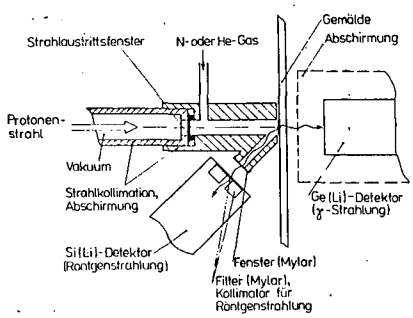

Fig. 1
PIXE/PIGE external beam arrangement

No visual damage had been caused even to the surface varnish when irradiating 30 s with 1 nA/mm^2 current density and operating with a cooling gas jet as demonstrated in fig. 1. Nitrogen was used as cooling gas which at the same time removes the X-radiation of atmospheric argon.

As an example fig. 2 compares X-ray spectra of different blue pigments as measured on an historic altar painting of the 15th century (Azurit blue) and a modern pigment specimen (Manganese blue), respectively /2/. The intense Pb X-ray lines originate in interactions of protons with white lead pigments.

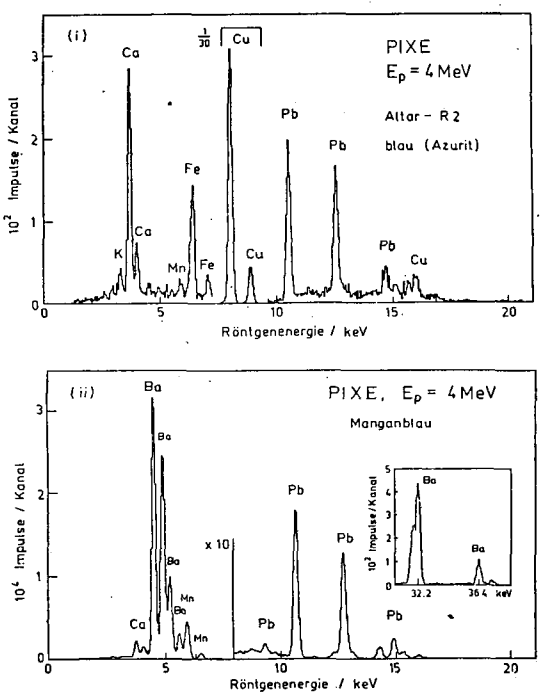

Fig. 2
X-ray spectrum of blue pigment
(i) Azurit $2CuCO_3 \cdot Cu(OH)$, Altar 1500
(ii) Manganese blue $BaMnO_4 \cdot BaSO_4$, 1986

References

/1/ T. Tuurnala et al., Nucl. Instrum. Methods B14 (1986) 70

/2/ H.-P. Schramm et al.: Wiener Berichte über Naturwissenschaft in der Kunst. Vol. 4/5 (1988), ed. by A. Vendl and B. Pichler, Hochschule für angewandte Kunst Wien, in press

DETERMINATION OF THE CONTENT OF NATURAL ACTIVITIES IN SHIELDING MATERIALS BY THE INTENSITY OF X-RAY FLUORESCENT PEAKS

S. Unterricker, Kim Jung Ho, W. Stolz
Bergakademie Freiberg, Sektion Physik

For the construction of low-level counters and spectrometers materials with a very low concentration of intrinsic activities are required. The direct γ-spectrometric determination of radioactive impurities in shielding and construction materials by Ge-detectors is only possible by an apparatus with an extremely low background /1/. The entire radioactivity of the sample is also reflected in the intensities of the X-ray fluorescent peaks. Radiation from the intrinsic radioactivity of the sample causes fluorescent radiation by filling the inner shells of ionized atoms. Thereby the K-series lines are most intensive. For the heavy elements Hg, Pb and Bi the K_α - and K_β -series have energies between 70 and 90 keV (Fig.). The K_α - and K_β -lines can be resolved in every case. Our spectrometer consists of a 45 cm^3 Ge(Li)-detector completely shielded by 9 cm of lead and 2 cm of mercury /2/.

X-rays are strongly attenuated by the measured substances which were filled into Marinelli-beakers. They can only be detected if they come from a layer of thickness $(\mu')^{-1} \sim 1\ gcm^{-2}$ or $\sim$ 1 mm of lead. X-rays from the detector and preamplifier have very low energies and these from the shield are of low intensity (see background spectrum). Therefore the fluorescent lines represent the X-ray fluorescent (Xf) intensity of the sample only and this is proportional to the intrinsic activity of the sample. The self absorption in the sample can simply be considered. If the sample is sufficiently thick the whole Xf radiation comes from a depth of $\sim (\mu')^{-1}$ but now without selfabsorption. Therefore the sample thickness x has only a week influence on the Xf intensity if $x \ll (\mu'\varrho)^{-1}$ is realized.

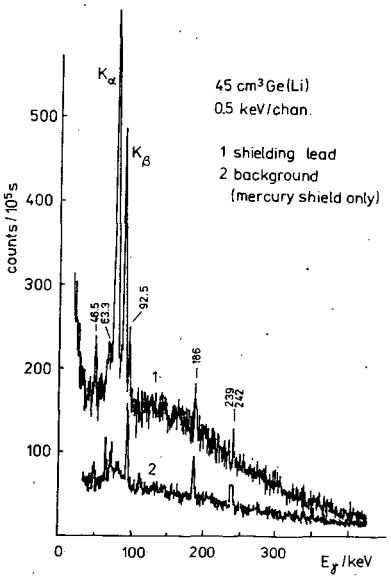

Fig.:Low energy γ-spectra of a lead sample and the corresponding background

Table: Integral and Xf-lines intensities for selected shielding materials (5N means 99.999 % purity)

	thickness in g cm^{-2}	counts/10^4s 0.1-1.0 MeV	counts/10^4s·kg Xf-lines
yellow lead bricks	8.9	12800(50)	15900
lead- 4N electrolytic Halsbrücke/Freiberg	12.2	2700(50)	5360
lead slabs 40 a old, Muldenhütten/Freiberg	13.0	800(30)	2590
bismuth- 3N, Halsbrücke/Freiberg	11.0	-260(30)	1520
lead - Korea	10.2	-910(20)	340
mercury - China	13.6	-1040(30)	90
lead- 5N, Hungary	4.1	-45(30)	390
bismuth- 5N, Bulgaria	3.9	-110(30)	370

In the table Xf pulse rates per mass are compared with the integral rates /3/. We can see a clear parallelism between the two values. Advantages of the Xf method are: not time-consuming, small sample weights, simple correction for self-absorption, low blank rate, and sufficient selectivity. A disadvantage is its applicability to materials with sufficiently high Z only.

References

/1/ S. Unterricker et al., submitted to 'Isotopenpraxis'
/2/ Kim Jung Ho; Dissertation A, Bergakademie Freiberg,1987
/3/ Kim Jung Ho, S. Unterricker, W. Stolz; Annual Report 1986, ZfK-621 (1987) 83

MOESSBAUER INVESTIGATIONS OF DIOCTAHEDRAL PEGMATITIC MICAS

C. Pietzsch, Bergakademie Freiberg, Sektion Physik
W. Schmidt, Bergakademie Freiberg, Sektion Geowissenschaften

Mössbauer investigations belong to the programme of mineralogical investigations of micas for many years /1,2/. While geochemical data of micas are discussed as indicators during search and exploration of deposits there are only little starting points to interprete Mössbauer data in this sense. With the considerations represented first Mössbauer investigations of completely geochemically characterized and genetically exactly classified dioctahedral micas are described. The set of samples included Muscovites and Lepidolithes from the pegmatitic destrict of Alto Ligonha (North Mocambique). The main part of these samples is from the Nb-Ta-deposit Muiane. They were taken along a profil reaching from the border to the centre of pegmatite with a length of nearly 250 m. All Muscovites investigated are crystallizations of the magmatic environment while the Lepidolithes originate from hydrothermal conditions by metasomatic processes. All these micas are member of the polytyp 2M1. The iron distribution derived from the Mössbauer data is shown in table 1. This table shows that three different types of spectra and, thus, patterns of iron distribution exist in the micas investigated.

1. In the Lepidolithes of the deposit Muiane only M1(cis)-positions are occupied by both Fe^{2+} and Fe^{3+} (A, B).
2. In two Muscovites of the centre part of the deposit, iron is present in all possible positions (C, D), with a predominance of Fe^{2+} on M1-positions.
3. In the Muscovites of the outer part of the deposit (G, F), only the M2(trans)-positions are occupied by Fe^{3+}, the M1-positions remaining empty. It is surprising that the three Muscovites (E, I, K) taken away from other regions of the deposit show the same mark.

A special place holds the sample H, belonging to an exposure northly Muiane. Owing to the shortage of geological data no classification of this deposit is possible. The Mössbauer data allow to discuss a genetical membership of the deposit Muiane.

It can be seen that by contemplating only the Fe^{2+}/Fe^{3+} proportion no well-defined statements can be drawn concerning the genetic classification and the geochemical properties of these micas. From the figure results that the content of Fe^{2+} both in M1- and M2-positions is not well defined genetically. The content of Fe^{3+} especially in the normally unoccupied M2-positions recognites a clear development which obeyed the genetic classification. Figure 1 shows the distribution of total iron content and its distribution on the lattice sites M1/M2.

Table 1: The iron content and its distribution on the octahedral coordinated M1- and M2-lattice positions

Sample	Fe^{2+}/Fe^{3+}	M1 % Fe^{3+}	M2 % Fe^{3+}	M1 % Fe^{2+}	M2 % Fe^{2+}
A	1.64	0.36	-	0.59	-
B	1.59	0.51	-	0.81	-
C	1.44	0.66	1.15	2.07	0.53
D	1.61	0.79	0.37	1.54	0.33
E	1.13	-	1.33	0.59	0.91
F	1.63	-	1.45	1.76	0.60
G	1.20	-	1.62	1.46	0.49
H	3.6	0.15	1.24	1.41	-
I	0.48	-	2.13	0.92	0.10
K	0.79	-	1.80	0.94	0.48

Fig. 1: The iron content and its distribution on the lattice sites M1 and M2

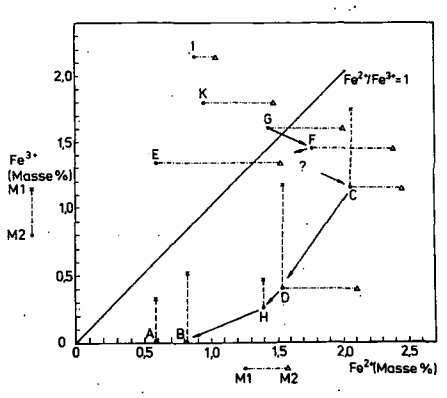

R e f e r e n c e s

/1/ Annersten, H., Am. Mineral. 59 (1974) 143 - 151

/2/ Rossman, I. R. in: F. W. Baily (Ed.) Mica: A rewiev in mineralogy Vol. 13 (1984) Min. Soc. America

STANDARDIZATION PROBLEMS OF CPAA MEASUREMENTS IN GEOLOGICAL SAMPLES

D. Degering, S. Unterricker and W. Stolz
Bergakademie Freiberg, Sektion Physik

The Charged Particle Activation Analysis (CPAA) has become a valuable complement to other activation possibilities for a large number of materials. In a previous paper /1/ we showed the fitness of this method for investigations in geological samples. To reduce systematic errors a careful choice of the standardization technique is necessary. We utilized the method of internal standard: Let us consider the activation of the nuclides X and St, belonging to the element X' and the internal standard St', respectively, in a certain matrix. The product nuclides are Y and St*. Then the following relation holds:

$$c_{X'}/c_{St'} = (N_{OY}/N_{OSt^*}) \cdot (h_{St}/h_X) \cdot (M_X/M_{St}) \cdot F_i \qquad (1)$$

$$\text{with} \quad F_i = \int_{E_{thr}}^{E_o} (\sigma_{xy}/\varepsilon_M)dE \Big/ \int_{E_{thr}}^{E_o} (\sigma_{StSt^*}/\varepsilon_M)dE \qquad (2)$$

(c_i - concentration of element i; N_{Oj} - number of produced nuclei j; h_i - isotopic abundance of nuclide i; M_i - molar mass of i; σ_{ij} - excitation function of the reaction from i to j; ε_M - atomic stopping power of the matrix; E_0 - energy of incident projectiles; E_{thr} - threshold energy of the activation reaction; E - projectile energy). F_i describes the effect of the matrix in consequence of the $\sigma(E)$ dependence and the energy-range-relation. According to /2/, the ratio $\varepsilon(Z_1, E)/\varepsilon(Z_2, E)$ for elements with the atomic number Z_i is nearly constant in the energy range where $\sigma(E)$ is substantial:

$$\varepsilon(Z_1,E)/\varepsilon(Z_2,E) = K(Z_1,Z_2) \qquad (3)$$

K varies the less the lower the difference $|Z_1 - Z_2|$ is. Since the range of the atomic numbers of the major elements in the earth crust is small (Z = 6...20) /3/ relation (3) is a good approximation in our case. Now we can establish a function $\varepsilon_0(E)$ so that

$$\varepsilon(Z,E) = K_0(Z) \cdot \varepsilon_0(E) \qquad (4)$$

Then (2) becames

$$F_i = \int_{E_{thr}}^{E_o} (\sigma_{xy}/\varepsilon_0)dE \Big/ \int_{E_{thr}}^{E_o} (\sigma_{StSt^*}/\varepsilon_o)dE \qquad (5)$$

which is matrix-independent. Using the γ-peak areas I_0 corrected by decay and measuring time, which are proportional to N_0 we get from

(1) $c_{X'}/c_{St'} = m(X',St') \cdot I_{OY}/I_{OSt^*}$. (6)

The calibration factor m may be derived from investigations in reference samples. As an example Fig.1 shows our calibration of the Sr-determination by the reaction $^{88}Sr(d,2n)^{88}Y$. Fe served as internal standard by means of its activation product ^{57}Co. The linear dependence holding for standard materials with different composition delivers a m-value m = 7.46±0.65. Thus, if e.g. the Fe-content of a sample is known, the Sr-concentration can be determined by equation (6).

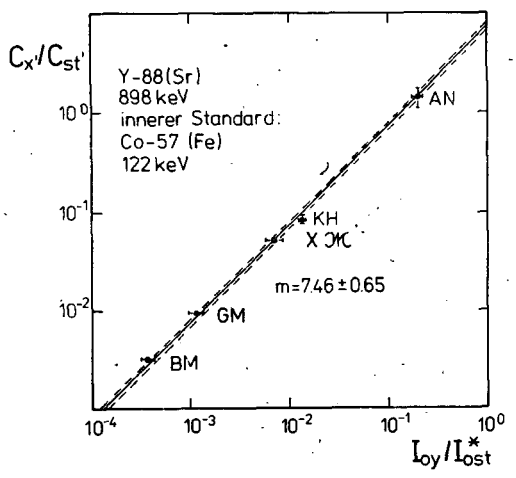

Fig.1.: Dependence $c_{X'}/c_{St'}$ on I_{OY}/I_{OSt^*} for the Sr-determination, using Fe as internal standard

References

/1/ Degering,D.,S.Unterricker,W.Stolz, Proc. of the 4th Meeting on Nucl. Anal. Meth., Dresden 1987, Vol. 1, 182
/2/ Vandecasteele,C., K.Strijckmans, J. Radioanal. Chem. 57 (1980) 121
/3/ Rösler,H.J., Lehrbuch der Mineralogie, Leipzig 1979

APPLICATION OF THIN LAYER ACTIVATION (TLA) ON INVESTIGATION OF CAVITATION PROCESSES

K. Eichhorn and E. Richter

Zentralinstitut für Kernforschung Rossendorf, Bereich G

The phenomenon of cavitation is characterized by two phases. In a first one a deformation of the surface appeares, in a second phase material losses occur. Accurate measurement is required to determine the begin of the second phase of cavitation, the gradient of material losses and the area of cavitation at the surface.

TLA succesfully has been used for wear measurements and it is a technique which meets the requirement. Beside it involves the advantage of in situ measurement.

Investigations were made at the test stand of the TU-Dresden /1/ in which cavitation is generated by means of a rotating disk in water. Specimens of white-metal were activated at the Rossendorf cyclotron by ^{4}He-Ions of 17.5 MeV resulting an activation depth of about 50 µm. For measurement of material losses the generated activity of ^{121}Te, ^{121m}Te and ^{123m}Te was used. For that reason irradiation parameters were find out by activating a stack of Sn-foils (fig. 1).

The measurement states, that TLA-technique is useful for investigation of cavitation. The begin of erosion as well as the gradient of material losses both depending on velocity of the streaming fluid and running time is discovered precisely. As expected, material losses do not appear over the whole surface of the sample. The autoradiograph (fig. 2) shows the affected area in a good manner.

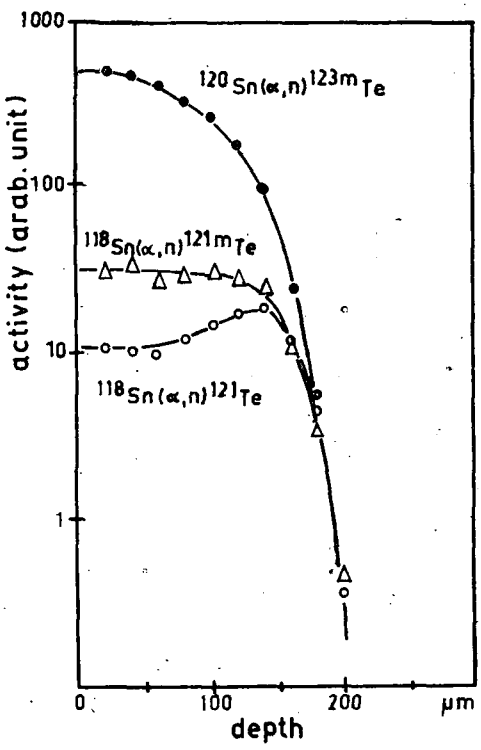

Fig. 1
Activity/depth curve produced in a stack of Sn-foils by 28 MeV - α - particles

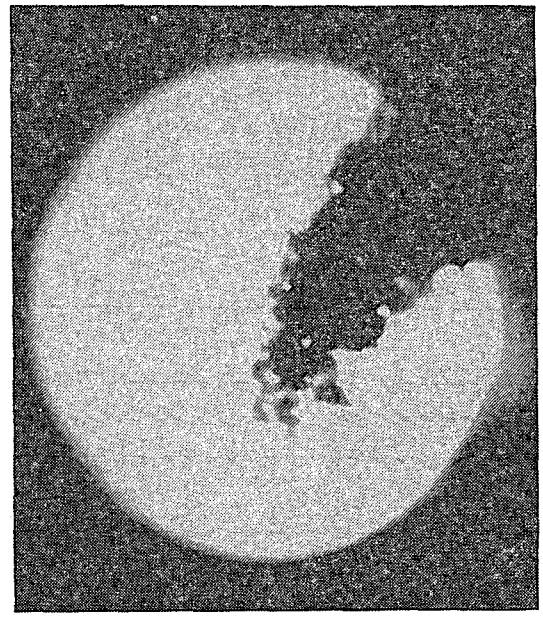

Fig. 2
Autoradiograph of a sample after a running-time of about 7 hours.
Black - area = affected part of the surface.

/1/ Bux, K. Vorbereitende Untersuchungen zur Werkstofferosion am Versuchsstand "Rotierende Scheibe", TU Dresden, Sektion 12, Wissenschaftsbereich Strömungstechnik, Bericht I 1279/1985.

SEMICONDUCTOR SECONDARY ELECTRON DETECTOR FOR IMAGING WITH ION MICROBEAM

L. Bischoff, F.K. Naehring, M. Deutscher
Zentralinstitut für Kernforschung Rossendorf, Bereich KF

The rapid development of microelectronic technology to introduce submicron structures for the VLSI level requires new tools to produce such devices. The Focused Ion Beam (FIB) is a very usefull tool for direct implantation with a writing beam, for direct patterning by sputtering, for ion beam lithography as well as for corrections on microelectronic circuits or photolithographic masks. For the application of a FIB it is necessary to get an image from the working region of the beam on the target. For this aim ion beam induced secondary electrons (SE) are used to produce an electrical signal of each scan position. The x and y coordinates are determined by the deflection parameters. The image processing in the FIB equipment is shown in Fig. 1 /1/. In order to restrict the sputter damage only a few scans should be taken to map the surface.

A semiconductor detector (SCD) working with a 10 kV acceleration potential was investigated for the SE evidence. The circularly shaped SCDs sensitive area of 2 cm^2 is located around the primary beam near the target.The calculated differential energy loss in the detector material depending on the acceleration voltage of the SE is shown in Fig. 2.

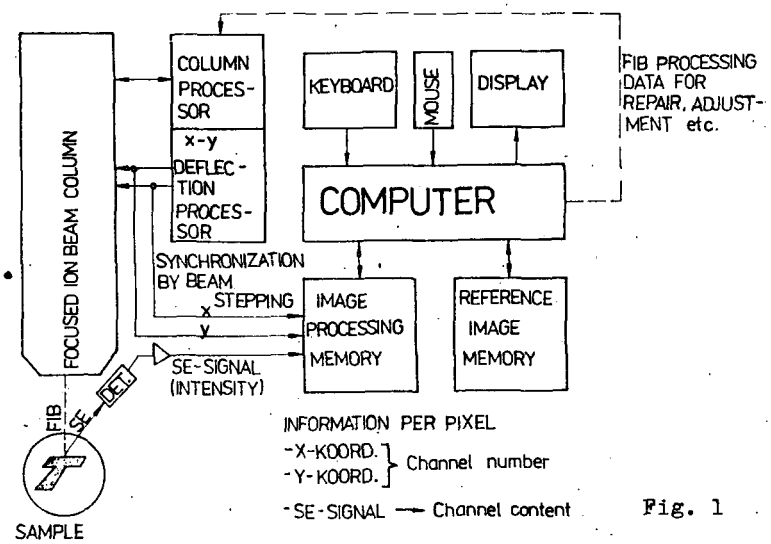

Fig. 1

A SE current of 1 nA to the detector working in a current mode leads to a voltage of about 0.3 V on the preamplifier output. The inner amplification of the detector amounts to 1500 at 8 kV SE energy. Fig. 3 shows the output signal depending on the acceleration voltage and the working frequency. The use of a coupling capacitor to bridge to the low voltage level leads to a 3 dB cutoff frequency of 500 Hz. The introduction of optocoupling devices as well as of ultra high resistivity silicon detectors allows to work at higher frequencies up to the MHz range.

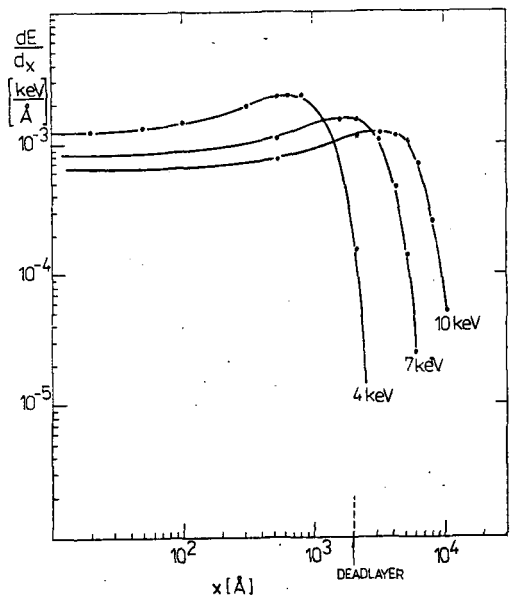

Fig. 2

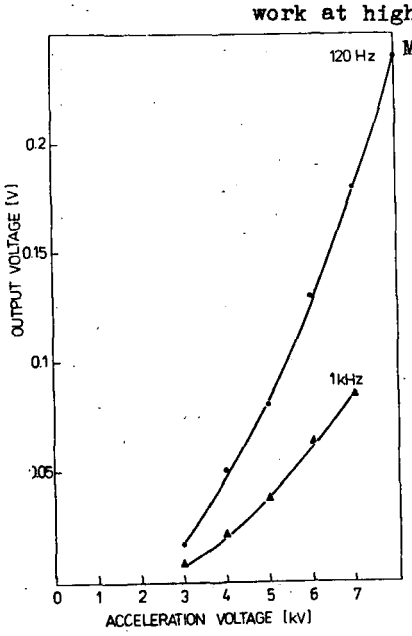

Fig.3

Reference /1/:
L. Bischoff, F.K. Naehring, M. Deutscher: Proc. 7. Tagung "Mikrosonde", Dresden 20.-22. 01. 1988

A MOSFET-BASED SENSOR FOR DETECTION OF LOW ENERGY ELECTRONS AND IONS

M. Teichfuß
Central Institute of Nuclear Research Rossendorf, GDR

The term "integrated sensor" suggests the joining of the primary measurement function of the sensor with conditioning of its output signal. The integrated circuit technology involves the MOS-structure providing a rich field for sensor application. Smallness and easy handling makes the MOSFET attractive for detection of primary beam induced electrons and ions. For instance in ion microbeam arrangments, the detection of secondary electrons (SE) emitted from the target surface during primary beam interaction, enables an on-line beam detection technique. A sensor for SE consisting of a N-channel MOSFET and the discharge circuit at the Gate was designed and first structures were tested with Se-currents in the range of 10^{-12} A up to 10^{-9} A. The SE are collected at the surface of the Gate, whereby the SE-current builds up a signal charge at the Gate controlling the Drain-Source-current of the FET (Fig. 1).

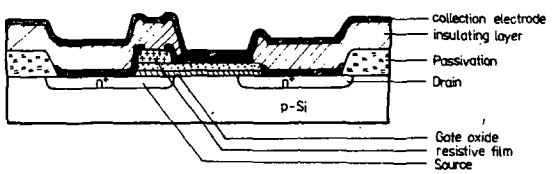

Fig. 1
Schematic structure of the Electron Sensitive Field Effect Transistor (ESFET) /1/

First tests with SE-currents below 10^{-9} A shows good agreement with calculated current-gain-characteristics (Fig. 2). The minimum detectable SE-current is in the range of $5 \cdot 10^{-12}$ A up to $3 \cdot 10^{-11}$ A. The bandwidth of the sensor was tested with amplitude modulated SE-currents up to a frequency of 1 Mc. The first experiments delivered gratifying current-gain-characteristics up to a frequency of 100 kc. With a optimized sensor variant we should reach a band-width of 1 Mc which is expecially required in ion microbeam arrangments.

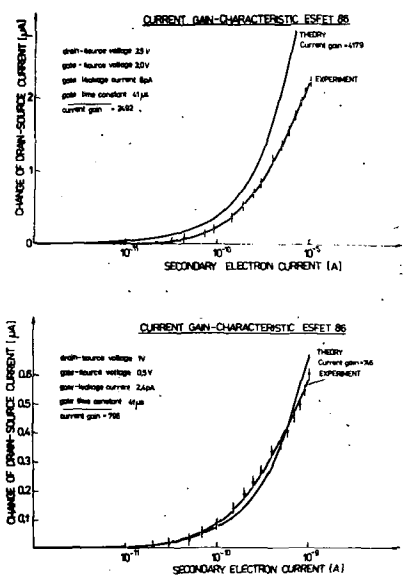

Fig. 2
Measured changes of the Drain-Source current versus the input Se-current

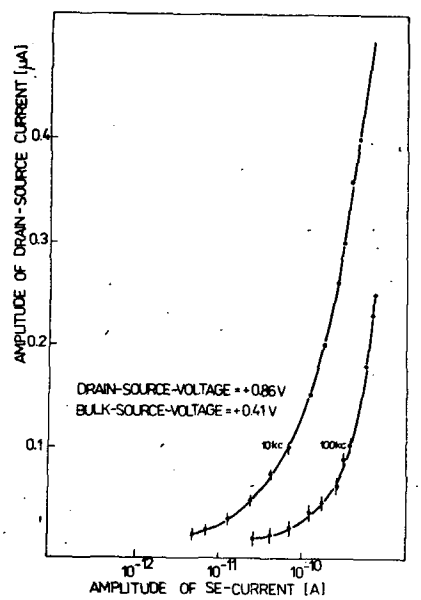

Fig. 3
Amplitude of the Drain-Source current versus the input amplitude of the Se-current

References

/1/ Deutscher, M., J. von Borany, M. Teichfuß, WP H01L 3071400

ANALYSIS OF Ar ION BEAM ETCHING INDUCED SURFACE DAMAGE OF GaAs BY MEANS OF ^{64}CU ADSORPTION / AUTORADIOGRAPHY AND RBS / CHANNELING - ANGULAR DEPENDENCE AND RAPID THERMAL ANNEALING -

A. Schindler, R.Fechner, R. Flagmeyer+, D. Panknin++, F.Bigl

Zentralinstitut für Isotopen- und Strahlenforschung Leipzig der AdW der DDR

+ Karl-Marx-Universität Leipzig, Sektion Physik

++ Zentralinstitut für Kernforschung Rossendorf der AdW der DDR

In previous studies /1,2/ we investigated the energy- and the dose-dependence as well as the depth profiles of the Ar+-ion bombardment damage of GaAs (100) surfaces by means of ^{64}Cu adsorption and autoradiographic detection and RBS/channeling. In this paper results on the angular dependence of the damage and on the rapid thermal annealing, measured by the mentioned methods, are presented.

The experimental conditions of the Ar ion beam etching, of the Cu adsorption, of the autoradiography and of the RBS analysis were the same as in /1,2/. The ion incident angle with respect to the surface normal was varied from 0° to 90°.

The angle of incidence is of practical importance in semiconductor manufacturing for planarizing steps or for tailoring etch structure profiles.

As an interesting feature shown in Fig.1, the maximum of crystal damage was found to be around 15°, both by the RBS/channeling and by the ^{64}Cu adsorption/autoradiography technique. A similar dependence was obtained for the N_2^+ reactive ion beam etching of InP.

The decrease of damage for normal incidence has not yet been fully understood. Considering that the incident angle of 0° is parallel to the <100> axis, it can be attributed to some anomalous phenomena such as ion channeling. After Lindhard /3/ the critical angle for Ar^+ ion channeling along <100> in GaAs for very low energies is about 10°, that is in the range of the divergence angle of the ion beam. On the other hand, with increasing damage density up to the saturation level the channeling effect becomes more and more insignificant. The damage at 90° polar angle results from the divergence of the ion beam.

A first attempt was made to recover the disordered surface layer by means of rapid thermal annealing - RTA. The interest in RTA of compound semiconductors has been generated by less stringent restrictions on the methods of surface protection.

The GaAs samples were placed in a quartz chamber with an N_2 atmosphere and heated by a light pulse using flash lamps or halogen lamps in the temperature range from 300 to 900 °C. The best results up to now have been achieved with 0.4 sec halogen lamp annealing at temperatures around 400 °C. As measured by RBS surface peak intensities (Fig.2) lattice defects caused by 1 keV Ar ion beam etching with doses up to $5*10^{14}$ cm^{-2} recovered completely. At the damage saturation level (>$3*10^{15}$ cm^{-2}) about 60 % of the disorder still remains in the surface region.

That means, successful annealing takes place at ion doses below the monolayer equivalent dose where damage saturation cannot be reached. There exist undamaged and damaged parts in the surface layer at such low ion doses /4/. We suppose that only under such conditions a complete annealing of the disordered layers is possible. ^{64}Cu/autoradiography experiments designed to investigate RTA of ion beam etched GaAs, and especially to measure possible low concentrations of residual disorder and depth profiles not measureable by RBS, are in preparation.

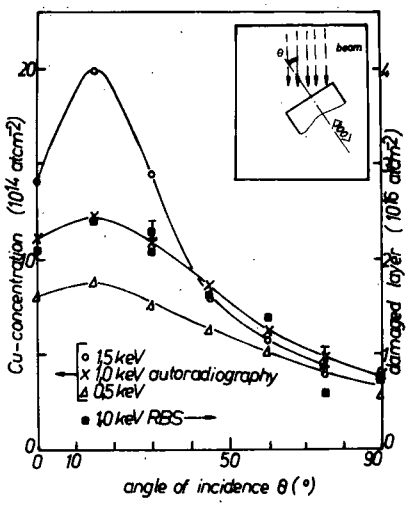

Fig. 1
Dependence of the saturation damage (Ar^+ dose > $10^{16}cm^{-2}$) on the polar angle of the ion beam incidence θ .

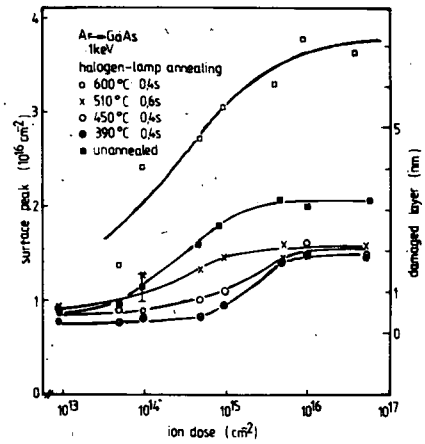

Fig. 2
Halogen lamp annealing of ion beam etched GaAs measured by RBS/channeling.

R e f e r e n c e s

/1/ R. Fechner, A. Schindler, R. Flagmeyer, F. Bigl, Gemeinsamer Jahresbericht ZfK-621, 86 (1987)

/2/ R. Fechner, A. Schindler, F. Bigl, J. Flachowsky, Gemeinsamer Jahresbericht ZfK-621, 87 (1987)

/3/ J. Lindhard, Kong. Danske Vid. Selsk., mat.-fys. Medd. 34, No. 14 (1965)

/4/ Y. Sekino, N. Owari, M. Kudo and Y. Nihei, Jap. J. Appl. Phys. 25, 538 (1986)

NITROGEN AND OXYGEN PROFILES OF ION BEAM SYNTHESIZED SILICON OXYNITRIDE LAYERS DETERMINED BY ELASTIC RECOIL DETECTION

W. Skorupa, E. Hentschel, R. Kotte, F. Stary and K. Wollschläger
Zentralinstitut für Kernforschung, Rossendorf, Bereich KF

Rutherford Backscattering Spectrometry and Channeling techniques are very efficient tools in investigating the properties of ion beam synthesized silicon on insulator(SOI)-structures. A disadvantage in studying the formation of silicon oxynitrides is the overlapping of the nitrogen and oxygen related peaks of the RBS spectra due to the low mass difference of these elements /1/.

For this end Elastic Recoil Detection (ERD) was performed using a 33.6 MeV $^{35}Cl^{+}$-beam of the Rossendorf tandem accelerator and Bragg-peak spectroscopy with a special ionisation chamber. Details of this method are given in Ref. 2. The samples were implanted and annealed in nearly the same manner as reported before /1/. The total implanted dose used in the experiment reported here was $6.2 \cdot 10^{17} cm^{-2}$.

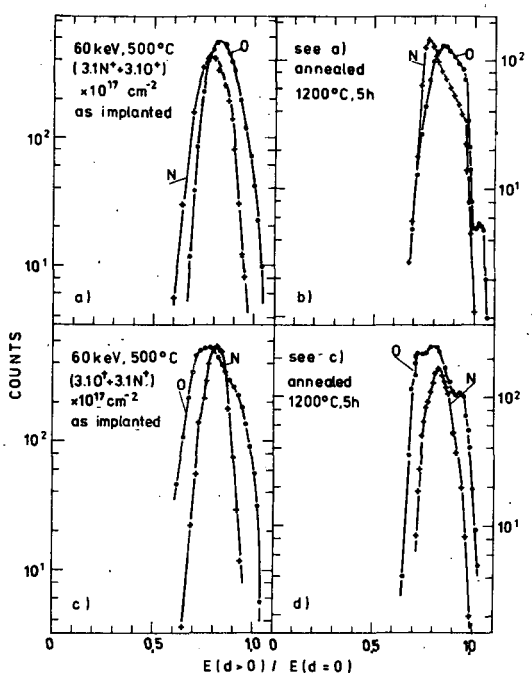

Fig. 1
Oxygen and nitrogen profiles evaluated by ERD. The surface is located at E(d > 0)/E(D=0) = 1.0, the depth increases going left from this value (E - energy of the particles recoiled from a depth d)

In Fig. 1 the profiles extracted from the Bragg-peak spectra are shown. Already after implantation a distinct difference is visible for the two investigated cases. For SiNO (Fig. 1a) the FWHM of the two profiles is comparabel and the nitrogen profile lies somewhat deeper. Taking into account the comparable range of oxygen and nitrogen in silicon this can be explained by an increase of the stopping power of nitrogen rich silicon due to the increased density leading to a range reduction for the secondly implanted oxygen. For SiON the oxygen profile lies deeper than for SiNO and its FWHM is nearly twice that of the nitrogen profile especially due to a shoulder on the surface side. The nitrogen profile is centered within this profile. The deeper position of the firstly implanted oxygen is due to the lower stopping power of pure silicon. The higher FWHM may be related to volume swelling as reported earlier for oxygen implanted silicon /3/ but it has to be proved whether such an effect can be mirrored by ERD. After annealing the profile tails are generally steeper suggesting smaller interregions between silicon and the buried layer (Fig. 1b,d). By RBS and XTEM it was found that the interfaces for the SiNO-system (Fig. 1b) are smaller.

Furthermore, for the latter system the oxygen profile is somewhat flat topped and contrary to the as-implanted case the tails of the two profiles coincide after annealing. The nitrogen distribution was strongly changed in piling up on the substrate side.

A further discussion of these results considering also those of other methods is given in Ref. 4.

References

/1/ Skorupa, W. et al., ZfK-621 (1987) 100; Proc. EMRS, Strasbourg 1987
/2/ Hentschel, E. et al., this report, p. 66
/3/ Kreissig, U. et al., Thin Solid Films 98 (1982) 229
/4/ Skorupa, W. et al., Proc. REI 4, Lyon 1987; Nucl. Instrum. Methods B (in press)

ELECTRICAL ACTIVATION OF BORON IMPLANTED SILICON DURING THE EARLY STAGE OF RAPID THERMAL ANNEALING

R. Kögler, E. Wieser
Zentralinstitut für Kernforschung Rossendorf, Bereich KF

A. Armigliato, E. Landi, S. Solmi
C.N.R. Istituto LAMEL, Bologna

Rapid thermal processing (RTP) has now become recognized technology for submicron device technology. For optimization of the temperature-time cycle numerical modelling of processes like electrical activation of implanted dopants and dopant redistribution becomes an important tool. With this respect boron implanted silicon is a very complex system because the damaged surface layer becomes not amorphous by room temperature implantation using fluences of technical interest. Therefore the electrical activation of boron proceeds relatively slowly compared to the recrystallization of an amorphous surface layer. Its time dependence should be taken into account if RTP is considered.

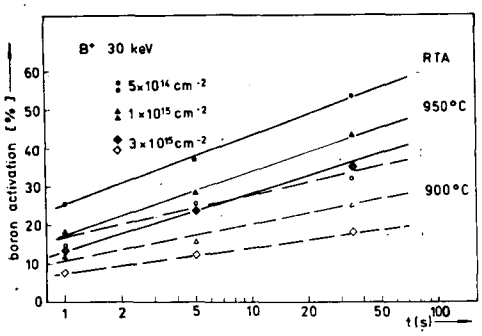

Fig. 1
Temperature and time dependence of the electrical activation

Fig. 1 shows the time dependence of the electrical activation at 900 and 950 °C, respectively, for three different doses. Up to a fluence of 1×10^{15} cm^{-2} solubility effects are neglegible. The maximum boron concentration is in this case still below the solubility limit (see below).

Fig. 1 shows that complete electrical activation can not be obtained in times characteristic for RTP using $T_{max} \leq 950$ °C. The low activation is due to the low velocity of the activation process at these temperature and not to solubility effects.

At T_{max} = 1000 °C for the dose of 1×10^{15} B/cm^2 (no solubility effect) nearly complete electrical activation is measured already for annealing with holding at T_{max} for 1 s. Taking into account the temperature rise time and the small effect of $T_{max} \leq 950$ °C we conclude that complete activation is obtained at 1000 °C in in $t < 5$ s.

In /1/ a model for the electrical activation of boron has been proposed on the base of low temperature furnace annealing. An activation energy of 5 eV has been found. The preexponential factor τ_0 of the time constant for activation ($\tau = \tau_0 \exp(E_a/kT)$) is assumed as increasing with increasing defect density. The linear dependence of activation on log(t) observed here for temperatures below 1000 °C is in agreement with the results in /1/. Therefore the dependence of τ not only on temperature but also on the damage concentration and in this way on the depth x within the profile proposed in /1/ should be valid also for the early stage of RTP. The results of Fig. 1 are in reasonable agreement with the activation energy of 5 eV assumed in /1/.

The maximum charge carrier concentration p_{max} obtained by RTP is significantly higher than the equilibrium solubility. For the dose of 1×10^{16} cm^{-2} annealing for 1 s at 900 °C and 1000 °C results in p_{max} equal 1.2×10^{20} cm^{-3} and 2.3×10^{20} cm^{-3}, respectively. The corresponding equilibrium solubilities are 7.2×10^{19} cm^{-3} and 1.2×10^{20} cm^{-3}.

This effect is much more pronounced for implantation into preamorphized silicon. Due to the epitaxial recrystallization of the amorphous layer electrical activation proceeds very fast already at 900 °C. Complete electrical activation has been obtained by RTP at 900 °C/1 s up to 3×10^{15} B/cm^2. In this case p_{max} exceeds the equilibrium solubility by a factor 4.

References

/1/ Seidel, T.E., A.U. MacRae, Proc. 1st. Int. Conf. on Ion Implantation in Semiconductors, Thousand Oaks, Gordon and Breach, New York 1970, p. 149

THE EFFECT OF OXYGEN ON ELECTRICAL ACTIVATION AND DIFFUSION OF ARSENIC IN SILICON BY RTA

R. Kögler and E. Wieser
Zentralinstitut für Kernforschung, Rossendorf, Bereich KF

In VLSI device processing As implantation often is carried out through an oxide cap. But in the case of an implantation of $1 \cdot 10^{16}$ As^+ cm^{-2} through a SiO_2 cap of only 30 nm the sheet carrier concentration after RTA (T_{max} = 1000 °C t_h = 1 s) is reduced by about 40 % in comparison to implantation in bare Si.

The cause of the effect is the high oxygen concentration near the SiO_2-Si interface due to recoil implantation. We have investigated this effect by implantation of arsenic and oxygen in bare silicon. Beside the electrical activation also the influence of oxygen on the diffusion behaviour of arsenic is considered.

Following the idea of Sadana et al. /1/ we assume that a formation of As-O or As-Si-O clusters takes place at high oxygen concentration in silicon (10^{20} cm^{-3}).

From our experimental results we were able to determine some important characteristics of these clusters /2/. We conclude:

- the formation of As-O clusters is proprtional to the oxygen concentration in silicon
- the clusters are electrically inactive and non or less mobil
- the clusters need high temperatures (above 1100 °C) to resolve
- the decay of the clusters is nearly independent on t_h in time scale of RTA.

Taking into account this, the results are interpreted qualitatively.

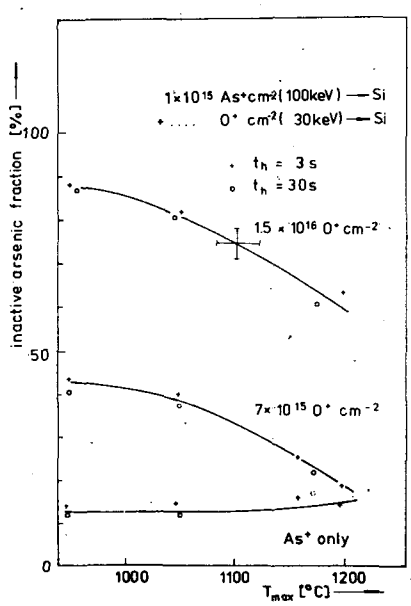

Fig. 1
Decay of As-O clusters in dependence on RTA-treatment

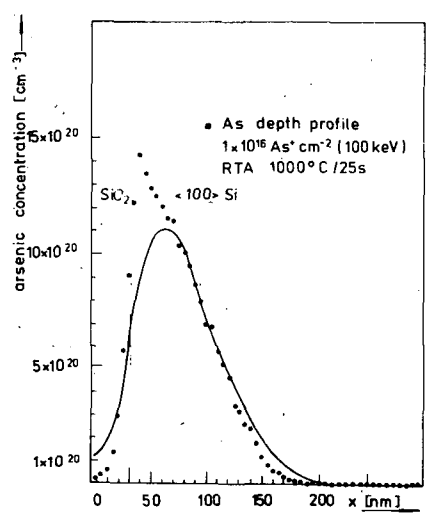

Fig. 2
Formation of As-O clusters near the SiO_2-Si interface where the recoiled oxygen concentration is very high
(The line shows a calculated As-profile without cluster formation)

R e f e r e n c e s

/1/ Sadana, D.K. et al., Nucl. Instrum. Methods 209/210 (1983) 743
/2/ Koegler, R. and W. Wieser, EPM 87, Dresden, Sept. 1987

ELECTRICAL ACTIVATION OF ARSENIC ATOMS IN ION BEAM RECRYSTALLIZED SILICON LAYERS

M. Voelskow, W. Skorupa and J. Matthäi
Zentralinstitut für Kernforschung, Rossendorf, Bereich KF

Ion beam induced epitaxial crystallization (IBIEC) is a method for recrystallization of amorphous silicon layers at very low temperatures. In a previous work it was shown that high dose arsenic implanted layers (100 keV, 10^{15} cm^{-2}) can be recrystallized under nitrogen irradiation already at a temperature of 400 °C well below those of conventional furnace annealing /1/. Using an energy of 165 keV of the N^+-annealing ions a dose of $7 \cdot 10^{16}$ cm^{-2} is sufficient for full recrystallization of the surface layer. But, as indicated by RBS and TEM investigations, further irradiation up to a dose of $1.2 \cdot 10^{17}$ cm^{-2} leads to the evolution of a second defect peak in the region of the regrown amorphous layer. The depth of this defect peak corresponds well to the projected range of the arsenic atoms used for amorphization.

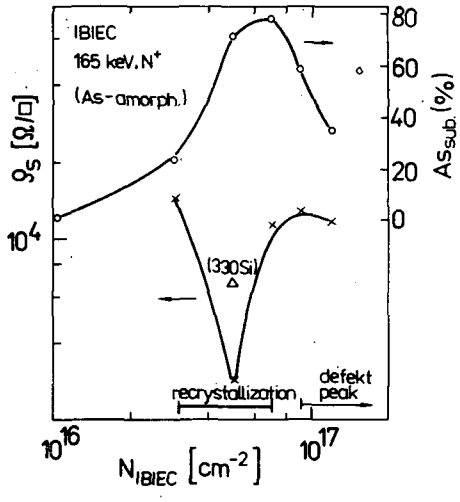

Fig. 1
Dependence of the concentration of substitional arsenic atoms (upper curve) and of the sheet resistivity (lower curve) on the IBIEC dose

Because of this defect behavior, which is unusual compared to conventional annealing, one can expect the dopant activation to be influenced by the IBIEC process too. In Fig. 1 (lower curve) the dependence of sheet resistivity obtained by Hall effect measurement on the IBIEC dose is shown. In the initial stage of the IBIEC process the resistivity decreases drastically which gives rise to the assumption that more and more arsenic atoms are built in on electrically active lattice sites in the recrystallized part of the layer. However, a further increase of the implantation dose leads to an increase of the sheet resistivity again, although the recrystallization front has not yet reached the surface. This behaviour is very surprising because the substitional part of the arsenic atoms calculated from the channeling spectra is still increasing reaching about 80 % in the case of full recrystallization (upper curve in Fig. 1). Only the appearance of the second defect peak leads to a reduction of the substitutional part of arsenic atoms. We propose that this reverse annealing effect in the sheet resistivity is related to the accumulation of point defects in the doped layer during the movement of the recrystallization front. This point defects will be created especially at the depth corresponding to the projected range of the nitrogen ions. A part of those moving to the surface may be trapped by arsenic atoms forming electrically inactive point defect clusters or secondary defects like loops. The question arises why the part of substitutional arsenic atoms is still increasing when the electrical activity decreases. We speculate that the formed defects are of coherent type as they can be obtained for example for the case of arsenic in silicon at concentrations exceeding the solubility limit in silicon. In this case defect clusters contain arsenic atoms in positions with small distance from their normal substitutional sites.

References

/1/ Voelskow, M., W. Skorupa and J. Matthäi, ZfK-621 (1987) 102

PATTERNING OF THE UNDERLAYING SiO_2 - LAYER AS A METHOD OF PRODUCING GRAIN BOUNDARY FREE SILICON STRIPES ON INSULATING SUBSTRATES

J. Matthäi, M. Voelskow and K.-H. Stegemann

Zentralinstitut für Kernforschung Rossendorf, Bereich KF

One of the favourable technique for producing SOI-structures is the zone-melting recrystallization of large area thin silicon layers on silicon dioxide. This process results in a (100)-oriented crystalline layer with the typical subgrain boundary pattern ("feather structure").

For circuits with high packing density, i.e. with small active areas of elemental devices, it is necessary and sufficient to obtain grain boundary free areas at desired positions. In a previous work we have presented two methods of producing such areas based on the transversal modulation of the temperature within the melted zone/1/. This was realized by an array of absorbing or reflecting stripes located on the top of or embedded in the encapsulating layer.

In this paper we present a third method for localisation of grain boundaries, firstly proposed by Hoand et al. /2/.

Silicon wafers, (100) oriented, were thermally oxidized up to 1 µm. Then a relief pattern was etched in the underlying oxide resulting in stripes extending from one side to the other of the wafer. Thin zones (0,5 µm) were 10 µm wide and thick ones were 30 µm wide. A 440 nm thick film of polysilicon was then deposited by LPCVD process. Finally, a 1,2 µm thick oxide film and a 30 nm thick silicon nitride films were desposited also by LPCVD as a cap preventing delamination of the film during the zone melting process. The scan speed used in our experiment was 1 mm/s.

Fig. 1 shows a micrograph of a Schimmel-etched SOI-wafer with grain-boundary confinement. As clearly shown, due to the reduced heat flow to the substrate grain boundaries are located in the areas corresponding to the thicker underlying oxide.

Fig. 1: Photomicrograph of a Schimmel-etched SOI-wafer with grain-boundary confinement

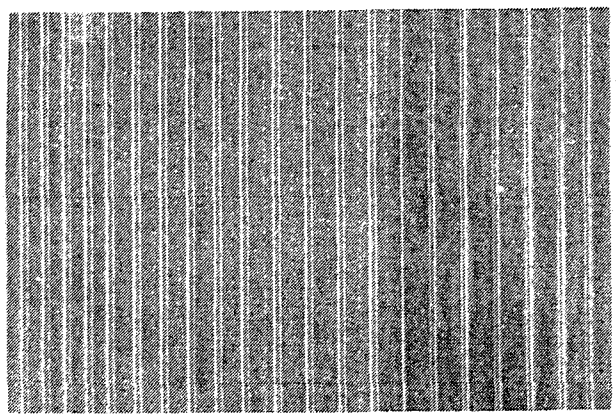

References

/1/ J. Matthäi et al., ZfK - 584, 59 (1986)
/2/ M. Haond et al., Mat. Lett. 4, 13 (1985)

SILICON AND CHROMIUM DISTRIBUTION IN IMPLANTED AND SHORT TIME ANNEALED GaAs

D. Panknin
Zentralinstitut für Kernforschung, Rossendorf, Bereich KF
Ya.B. Fattachov
Kazan Physico-Technical Institute, Kazan
C.E. Richter and M. Gericke
VEB WF Berlin

For a good electrical activation it is necessary to carry out the annealing at temperatures and times sligtly below the dissociation threshold of the GaAs surface. In this contribution the Cr distribution after the annealing treatment is discussed.

Si is implanted in the dose range up to 10^{16} cm^{-2} at an energy of 200 keV into SI, Cr-doped (100) GaAs at about 30 and 100 °C, respectively. Capless annealing was performed in N_2 atmosphere by flash lamp irradiation with dwell times between 50 and 500 ms or using halogen lamps with times $\geqslant$0.5 s.

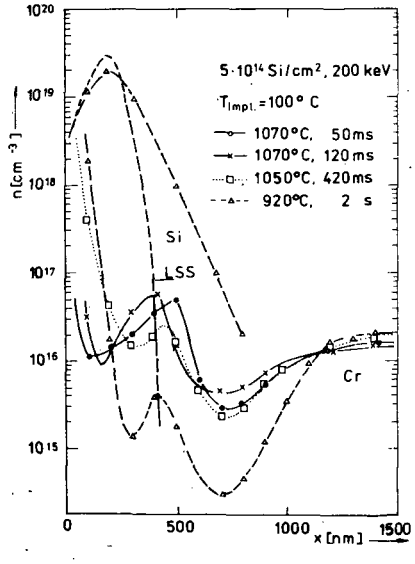

Fig. 1
Cr distribution for 100 °C implantation after capless annealing

The as-implanted Si profiles are remarkably broadened compared to a Gaussian distribution. This is due to radiation enhanced diffusion /1/. The depth distribution of Cr in the as-implanted state is characterized by a weakly increasing concentration in the surface region. Whereas after the annealing treatment a remarkable segregation of Cr at the surface is observed. Increasing annealing time causes an increase of the surface pile-up. Consequently the surface near region shows a Cr depletion. Within the depleted layer an enhanced Cr concentration is found in the depth between R_p and $R_p + \Delta R_p$ of the Si profile. For longer times ($\geqslant$400 ms) at adequate lower temperatures we observe a decrease of this Cr peak and the peak is also shifted to the surface up to a depth corresponding to the penetration depth of the LSS profile. Compared to the 100 °C implantation the room temperature implanted sample shows a very complicated Cr distribution with a second Cr peak in the depth of R_p of the Si profile.

Considering the residual defects after RTA we have found for all implantation and capless annealing conditions an one to one depth correlation between the position of the dislocation band an the Cr peak /2/.

From the one to one depth correlation of the Cr peak and the dislocation band for different implantation and annealing conditions we conclude that the main process of the formation of the Cr peaks is trapping of Cr on dislocations.

At capless annealing conditions, which are necessary for a good electrical activation, some lost of As from the surface can not be avoided. Thereby, As vacancies arise causing the Cr segregation at the surface. Consequently, near the surface region Cr depletion arises. In consequence of the concentration gradient Cr diffuses from the depth to the surface. Within the depletion region Cr will be trapped on dislocations formed during annealing. The weak shift of the Cr peak observed in the figure 1 is caused by a shift of the maximum defect density. Annealing at lower temperatures and adequate longer times (920 °C) leads to a lower density of larger loops. This defect state is obviously not so effective in trapping of Cr /2/.

References

/1/ Panknin, D. et al., Nucl. Instrum. Methods B19/20 (1987) 492
/2/ Panknin, D. et al., EPM 97 (in press)

SHORT TIME TRESHOLD FOR ELECTRICAL ACTIVATION OF IMPLANTED AND ANNEALED GaAs

D. Panknin and E. Wieser
Zentralinstitut für Kernforschung, Rossendorf, Bereich KF
Ya.B. Fattachov and I.B. Khaibullin
Kazan Physico-Technical Institute, Kazan

The maximum annealing temperature of GaAs is limited by its dissociation. This contribution presents results concerning the short time threshold for which electrical activation can still be achieved by capless annealing using temperatures > 1000 °C for amphoteric dopants Si, Ge, Sn and non-amphoteric dopants Se, S, Te. The temperature dependence of the electrical activation for annealing times between 50 ms and 2 s is also discussed.

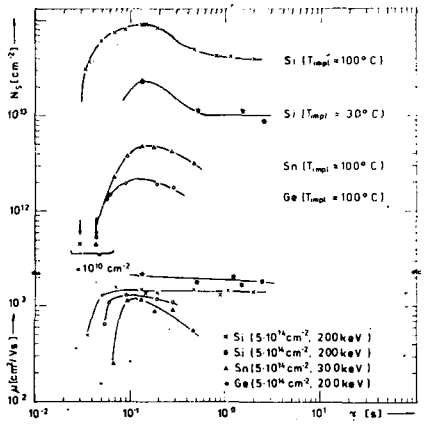

Fig. 1
Sheet carrier concentration (N_S) of the amphoteric dopants in dependence on the annealing time at the maximum temperature

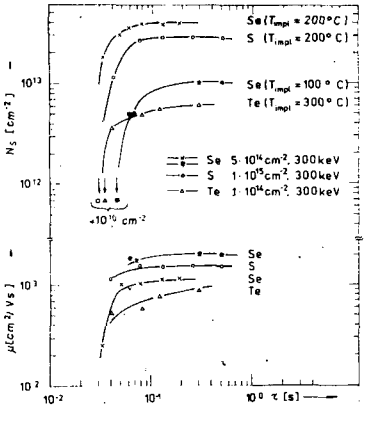

Fig. 2
Sheet carrier concentration and mobility of the non-amphoteric dopants in dependence on the annealing time at the maximum temperature

Cr-doped (100) GaAs was implanted at temperatures between 30 and 300 °C. Annealing was performed in N_2 atmosphere without a caplayer by flash lamp or halogen lamp irradiation. The temperature and time values used were slightly below the dissociation threshold of the GaAs surface.

In Fig. 1 sheet carrier concentration and mobility are shown in dependence on the dwell time at the maximum temperature for capless annealing of the amphoteric dopants. The implantation temperature ($T_{impl.}$) is also varied. Fig. 2 shows the same dependence for the non-amphoteric dopants.

A time threshold for activation is observed at about 30 and 45 ms for implantation at elevated and room temperature, respectively. The time dependence of the sheet carrier concentration N_S is characterized by a transition region at short times and a nearly constant value at longer times. For the amphoteric dopants the time dependence of N_S is moreover characterized by a maximum at about 150 ms. The time dependence of the mobility is very similar to that of N_S.

The time threshold for activation is independent on the kind of dopants but depends on the damage state caused by the implantation. From this we conclude that the time threshold is an attribute of the lattice structure /1/. The maximum of the carrier concentration at about 150 ms for amphoteric dopants can be explained by the assumption of a dopant concentration on Ga sites higher than the equilibrium values found for longer annealing times. Obviously, the Ga sites will be occupied at the beginning of the annealing with a higher probability /2/.

R e f e r e n c e s

/1/ Panknin, D. et al., EPM 87 (in press)
/2/ Panknin, D., Nucl. Instrum. Methods B19/20 (1987) 492

THE STRUCTURE OF PROBE ENVIRONMENTS IN IMPLANTED TETRAHEDRALLY COORDINATED SEMICONDUCTORS

S. Unterricker, Bergakademie Freiberg, Sektion Physik

The clear interpretation of the microscopic structure of the environments of implanted probes in semiconductors is still an open question. Probe methods, whereby implanted atoms act as probes for their own surroundings are very suitable to solve this problem. Mössbauer effect (ME) source measurements and time differential perturbed angular correlation (TDPAC) investigations in silicon give different pictures regarding to the nature of defect cascades.

ME studies in $^{119}In(^{119}Sn)$ implanted Si /1/ with ^{119}Sn as Mössbauer nucleus show that for the as-implanted samples the majority of probes is substituted in nearly undisturbed environments. By a thermal treatment the rest of probe environments anneals completely.

TDPAC-measurements in $^{111}In(^{111}Cd)$ implanted Si /2,3,4/ gave broad quadrupole frequency distributions for nearly all probes. The annealing behaviour as described in refs. /2/ and /3/ is quite different. This problem was solved by the investigations /4,5/ which showed that the character of doping influences in a decisive manner the annealing of probe environments. In the case of n-type Si nearly undisturbed cubic environments appear for all probes after suitable thermal treatments, whereas for p-type Si strong perturbations also in the thermally treated samples exist, the reason of which are defects in the electronic structure of the probe. The lack of electrons in the conduction band causes electronic after-effects following the decay of ^{111}In by K-capture.

In a recent paper Lindner et al. /6/ published channeling measurements with electrons and positrons emitted from implanted radioactive In atoms in Si. These investigations were utilized to find out the lattice location of In implanted in Si. The results are directly comparable with the ME and TDPAC investigations mentioned above. They show that a considerable part of probes is substituted in surroundings with only weak lattice disordering. A thermal treatment at 700 K increases the channeling effect indicating a defect annealing.

TDPAC measurements in the system $^{111}In(^{111}Cd)$ Si and also in different $A^{III}B^{V}$- and $A^{II}B^{IV}C_2^{V}$-compounds /7,8/ exhibit unambiguously that in the as-implanted cases practically all of the probes sit in disordered regions. Electronic defects can be excluded if, as it is possible by far in the most cases, a complete annealing is observed /3,7,8/. The ^{119}Sn ME is not very sensitive to the quadrupole interaction, therefore the line broadening is not significant to make clear predictions to this side of the problem.

In all tetrahedrally coordinated semiconductors a tetrahedral next neighbour coordination is prefered in such a manner that in the radiation damaged samples the bond angles are only weakly bent (random distribution of bond angle deviations $\sim 10^{o}$) and the bond lengths differ no more than 1 % from their ideal values (this is one of the most discussed models for the structure of amorphous semiconductors). With this model we get a broad quadrupole frequency distribution with a most probable frequency $\hat{\omega} = 0$ for the cubic substances and a distribution with $\hat{\omega} > 0$ for noncubic semiconductors as observed in the TDPAC investigations of implanted samples. Most of the probes are substituted and the lattice channels are not destroyed. Naturally, this holds only for low ion fluences as realised in the discussed cases. Small atomic displacements reduce only the channeling yield. That means TDPAC, ME and electron channeling results are all in agreement with this model.

R e f e r e n c e s

/1/ Weyer, G. et al., Hyp. Int. 7 (1980) 449
/2/ Kaufmann,E.N. et al., J. Appl. Phys. 48 (1977) 3332
/3/ Unterricker,S.,F.Schneider, phys.stat.sol.(a) 75 (1983) 155
/4/ Deicher,M. et al., Nucl. Instr. Meth. Phys.Res. B 13 (1986) 499
/5/ Pasquevich,A.F.,R. Vianden, Phys. Rev. B 35 (1987) 1560
/6/ Lindner,G. et al., Phys. Rev. Lett. 57 (1986) 2285
/7/ Schneider,F.,S.Unterricker, phys.stat.sol.(a) 85 (1984) 45
/8/ Unterricker,S., Dissertation B, Bergakademie Freiberg, 1986

THE ELECTROPHYSICAL PROPERTIES OF ANODIC SILICON OXIDE FILMS USING Ar^+ IMPLANTED STARTING MATERIAL

G. Mende
Zentralinstitut für Kernforschung Rossendorf, Bereich KF
F. Fenske and H. Flietner
Zentralinstitut für Elektronenphysik, Berlin

Local ion implantation into n-type Si is a prerequisite for local anodic oxidation of Si without masks /1,2/. In some special cases of electronic device production it can be also necessary to implant the starting material with ions before passivation avoiding high temperature oxidation and annealing processes.

In the present work is investigated the influence of radiation damage on anodically grown MOS structures /3/ using Ar^+ implanted n-type Si (5 Ohm cm). The anodic oxide films were annealed at 400 °C in a nitrogen stream for 20 min followed by an annealing treatment after Al evaporation and dot photolithography at 450 °C in a nitrogen stream for 30 min.

In Fig. 1 is shown the influence of Ar^+ implantation dose of the starting material on the electrophysical properties of the Si/anodic oxide interface. A part of the samples were annealed before anodization at 450 °C in a nitrogen stream for 30 min. The surface state density in midgap does not change practically after implantation up to a dose of 10^{12} Ar^+ ions cm^{-2}. After implantation of higher doses an increase of surface state density can be observed. However, the fixed oxide charge density is constant after implantation up to a dose of 10^{14} Ar^+ ions cm^{-2} After implantation of 10^{15} Ar^+ ions cm^{-2} the fixed oxide charge density is increased.

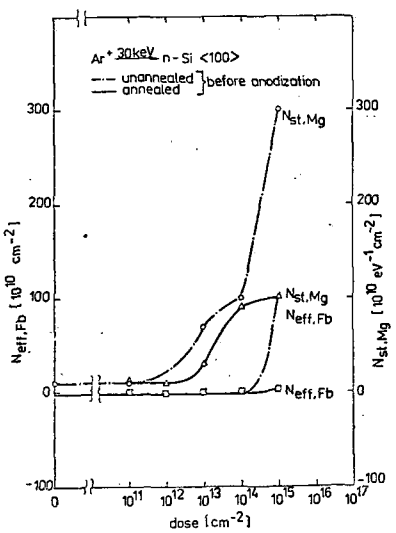

Fig. 1
The surface state density in midgap $N_{st,Mg}$ and the fixed oxide charge density $N_{eff,Fb}$ of anodically grown MOS structures as a function of Ar^+ implantation dose of the starting material with or without annealing as a parameter

Annealing before anodization diminishes the increase of surface state density and fixed oxide charge density.

The different influence of radiation damage on the surface state density and fixed oxide charge density can be explained by "annealing" of defects during anodic oxidation of implanted silicon.

It can be concluded that the oxide quality will be sufficient for passivation of electronic devices, if the starting material is implanted with 30-keV Ar^+ ions up to a dose of 10^{13} cm^{-2} (or of other ions under equivalent conditions causing the same radiation damage) and annealed before anodization. This may be also of interest for low temperature passivation of pn-junctions generated by ion implantation before anodization.

References

/1/ Mende, G., Thin Solid Films 46 (1977) L9
/2/ Mende, G., Thin Solid Films 55 (1978) 427
/3/ Mende, G. et al., Thin Solid Films 102 (1983) 65

MATHEMATICAL MODELLING OF THE CAPACITANCE CHARACTERISTICS AND THE THRESHOLD VOLTAGE OF A MOS STRUCTURE ON A THIN SILICON SUBSTRATE

N. Sieber, G. Otto
Central Institute for Nuclear Research Rossendorf, Dept. KF

A successfull application of SOI films in the microelectronic requires a knowledge of the electrical properties of the recrystallized silicon (r-Si) as well as of the interface r-Si/SiO_2. MOS structures fabricated in thin silicon layers on SiO_2 have electrical properties which are typically influenced by the charge coupling between front and back silicon interfaces /1,2/. Thus, a precise determination of electrical properties of these structures by CV measurements such as free carrier concentration, generation lifetime, threshold voltage etc. can be affected by the silicon thickness and the charge at the interface recrystallized silicon/underlying insulator.

In this work a general solution for the dependence of the space charge capacitance characteristic and the threshold voltage of a thin - based MOS structure on various properties of the back interface is given.

The semiconductor capacitance can be calculated using the approximate charge analysis /3/.

The calculation of the low and high frequency capacitance was performed for the case with accumulated back surface ($u_{S2} \geq 0$).

The decreasing base thickness results in an increasing minimum normalized capacitance C_{min} for both the low frequency and the high frequency characteristic. For the same thickness the increase of C_{min} is inversely proportional to the substrate doping. This is due to the fact that the reduced back side field is inversely proportional to the substrate thickness and the doping concentration. The back side field affects also the width of the low frequency capacitance characteristic at the voltage corresponding to the depletion and inversion range. Consequently, for the surface potential $u_{S1} = 2\ u_F$ the threshold voltage V_{th} differs from the conventional ones. Furthermore, the determination of V_{th} requires precise knowledge of the back side potential and of the thickness of the thin substrate.

References

/1/ Jerhot, J., Phys. stat. sol. (a) 96 (1986) K 95

/2/ Lim, H.-K. and J.G. Fossum, IEEE Trans. Electron. Dev. ED-30, 10 (1983) 1244

/3/ Nicollian, E.H. and A. Goetzberger, Appl. Phys. Lett. 7 (1965) 216

CONTROLLING THE WIDTH OF THE MELTING ZONE IN AN EQUIPMENT FOR LATERAL ZONE MELTING

K. Wollschläger, J. Matthäi, K. Butter and M. Voelskow
Zentralinstitut für Kernforschung, Rossendorf, Bereich KF

In an equipment for lateral zone melting a stripe of a thin polysilicon layer can be molten and recrystallized. Such layers are embedded between silicon dioxide on an usual silicon substrate. The melting front moves slowly over the whole surface /1/. The width of the molten stripe depends on the power which is irradiated at the sample by means of halogen lamps and on the conditions of heat emission. For the automation of the lateral zone melting process one has to obtain an electrical signal, which is proportional to the width of the molten zone. This can be realized by a suitable optical projection of the zone on a CCD-camera. Special precautions are nessesary against the strong heat radiation of the molten region and its vicinity. Of course it is convenient, to have a picture with a constant scale at a stationary camera working at room temperature

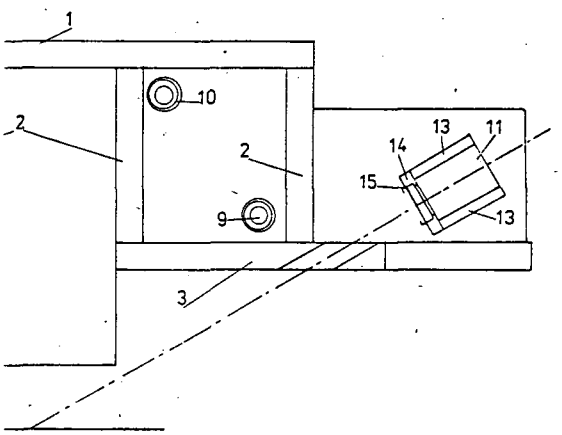

Fig. 1
Optical supplementary device
1,2,3 - cooled walls
9,10 - water in-, outlet respectively
11 - mirror for changing the optical axis
13,15 - support
14 - first lens

We have developt an optical device. It is directly mounted at the moving elliptical mirror above the sample. The entrance slit and the walls are cooled. The view angle is 30 degree over the horizontalline. Two achromatic lenses project the picture of the molten zone on one end of lighting mains. A CCD-camera with a photographic objective is situated at the other end of lighting mains. The picture contrast is caused by a different scattering behavior of polycristalline and molten silicon. No directly reflected light reaches the camera. Therefore the molten zone appears as a darker stripe. By means of a computer the electronic output of the camera is used to calculate a value, which is proportional to the width of the molten stripe. Furthermore a special programm written in machine code controlls the power of halogen lamps using triacs.

Instead of a CCD-camera it is possible to apply two photodiodes. The response of one of them is proportional to the brightness of the molten zone; the other one is proportional to the brightness of the vincinity of the molten region. By analogic division also a normalized value is receavable for controlling the process. Concluding results of our experiments show, that the automation of the process is possible.

References

/1/ Matthäi, J et al., ZfK-584 (1986) 59

DATA FILES FOR PHOTON MASS ATTENUATION COEFFICIENTS IN THE ENERGY RANGE UP TO 150 KEV

S.Fritzsche, G.Zschornack
Technical University Dresden, Department of Physics, Division of Applied Nuclear Physics, Mommsenstr.13, Dresden, 8027

For many practical purposes it is necessary to know photon mass attenuation coefficients in the photon energy range of the characteristic X-rays from all elements of the periodic table. For the user extensive tables of the mass attenuation coefficients at energies of intense characteristic X-ray transitions as well as parameter sets for calculating the desired values are of substantial interest.
To accomplish this demands, we have solved both problems on the basis of experimental and theoretical photon attenuation cross sections from Veigele /1/, who used at about 150 references to fit by a least-squares method the published data. By a logarithmic interpolation for all elements up to neptunium we have calculated the mass attenuation coefficients for the most intense X-ray transitions of all elements. This results are available as computer listings and as files on magnetic tape.
For a convenient handling of this data on small computers we have approximated the available values between the absorption edges of the considered atoms in the form

$$\ln \mu = x_0 + x_1 \ln E + x_2 (\ln E)^2 + x_3 (\ln E)^3$$

whereby μ describes the mass attenuation coefficient, E the photon energy and x_0, x_1, x_2, x_3 are free parameters for the approximation. The uncertainties in total attenuation cross sections after Veigele /1/ are considered by the actual fit as **weighting** factors. To get a criterion about the quality of results, we calculate a mean relative error quotient

$$RFQ = \frac{1}{M} \sum_{i=1}^{M} \frac{|\mu_{th}^{i} - \mu_{ex}^{i}|}{\Delta\mu_{ex}}$$

with $\mu_{th,ex}$ - calculated and original values of the mass attenuation coefficient and $\Delta\mu_{ex}$ - error of the original value of the mass attenuation coefficient. For instance, we give in the table the approximation result for krypton (Z=36). To satisfy always the condition RFQ < 0,1, we have sometimes the intervalls between absorption edges subdivided (indicated by "Z").

Table

Niveaus		Energie/keV	x_0	x_1	x_2	x_3	RFQ
	- L_3	1,000-1,675	8,1208	-2,7939	-0,0638	0,0750	0,0016
L_3	- L_2	1,675-1,727	8,9019	0,5459	-3,9760	1,1005	0,0038
L_2	- L_1	1,727-1,921	9,8969	-2,1654	-0,8819	0,4816	0,0004
L_1	- Z	1,921-4,000	10,2300	-2,8234	0,1054	-0,0272	0,0024
Z	- Z	4,000-8,000	11,3386	-4,7284	1,1704	-0,2200	0,0272
Z	- K	8,000-14,33	10,4267	-2,9754	0,0936	-0,0061	0,0024
K	- Z	14,33-30,00	11,7381	-2,5830	0,0577	-0,0179	0,0042
Z	- Z	30,00-60,00	12,9125	-3,1124	0,0629	-0,0035	0,0163
Z	- End	60,00-150,0	14,6896	-2,7964	-0,3989	0,0646	0,0400

All parameters of the fit are also available in form of computer listings and on magnetic tape. An extensive listing of all results will be published later.

REFERENCES:

/1/ W.M.J.Veigele: Atomic Data Tables, 5, 1973, p.51-111
/2/ S.Fritzsche: Research Report, TU Dresden, Department of Physics, Division of Applied Nuclear Physics, Dresden, 1987

DETECTION RATIO CALCULATIONS OF A JOHANSSON TYPE CRYSTAL SPECTROMETER WITH MOSAIC CRYSTALS

M. Schneider, A. Reichmann, G. Zschornack
Technical University Dresden, Department of Physics, Division of Applied Nuclear Physics, Mommsenstr. 13, Dresden, DDR-8027
M. Schiekel
Joint Institute for Nuclear Research, Dubna, USSR

Performing precise measurements of x-ray spectra with crystal diffraction spectrometers a detailed knowledge of lineshapes and detection efficiencies caused by geometrical abberations is necessary. Generally the possibility, that a photon of energy $h\nu = hc/\lambda$ can be registrated by a detector under a BRAGG angle ϑ_E is determined by the formula

$$p(\vartheta_E) = \int_{\vartheta_a} g(\vartheta_a, \vartheta_E) \int_{\lambda} \varepsilon(\lambda) e(\lambda) r(\lambda, \vartheta_a) d\lambda \, d\vartheta_a$$

with $\varepsilon(\lambda)$ as efficiency of the detector, $e(\lambda)$ the emission probability of the photon source and $r(\lambda, \vartheta_a)$ the reflectivity of analyzing crystal. The possibility $g(\vartheta_a, \vartheta_E)$ describes the geometrical influence of detecting arrangement thus, that a photon which arrives the crystal under an angle ϑ_a will strike onto the window of the detector.
In previous calculations this had been done using ideal crystals and neglecting attenuation inside the crystal /1-3/. Results showed, that there exist a strong dependence of line width and yield from the scattering angle, e.g. from energy of x-rays and crystal parameters. In reality do not exist ideal crystals, however. Thus it is necessary to take into account real topographic structure of the used crystals. Our calculations follow the program VERDI /2/. Real crystal topography was introduced using a number of mosaic blocks instead of ideal surface. Each block is assumed to be ideally. Normal vectors of neighboured blocks include finite angles ϑ_M. From the crystals manufactures date /4/ the maximum range of this angle can be estimated to be no more than 3'. Inside that range the angle is assumed to be normally distributed.
As a second fact absorption in the crystal depth had been taken into account. Calculations had been done presuming that the path of one photon do not leave the mosaic block on which it impinges originally. In this case no influence of depth distribution to line width and line centre shift is expected. The diffraction plane where the photon is reflected is choosen assuming the possibility of reflection to follow absorption rule. The calculated ratio of source emitted to detected photons is shown in fig. 1 as a function of maximum mosaic angle both for reflection at crystal surface and in the depth. Results show the strong influence of mosaic structure. As expected consideration of crystal absorption does not change curve shape, but only diminishes intensity.

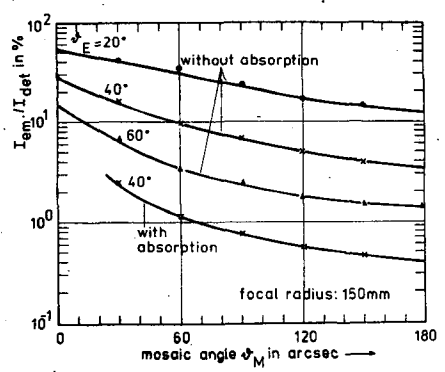

Fig. 1:
Dependence of the ratio source yield I_{em} to detection yield I_{det} on mosaic angle ϑ_M. Parameter is the Bragg angle ϑ_E.

References:
/1/ A. Reichmann, G. Zschornack, W. Wagner: 6. Arbeitsbericht "Energiereiche atomare Stöße", Gesamthochschule Kassel, 1985, S. 191
/2/ A. Reichmann: Work for Diploma, Technical University of Dresden, Department of Physics, Dresden, 1984
/3/ G. Zschornack, G. Müller, G. Musiol; Nucl. Instr. Methods 200 (1982) 481
/4/ ЛНРО BUREVESTNIK: Crystal data informations, Leningrad, 1987

Nd, Yb, Au and U L-SUBSHELL IONIZATION PROBABILITIES BY 92 MeV Ar IMPACT

H. Schmidt-Böcking, A. Skutlartz, W. Schadt, M. Wassermann
University of Frankfurt/Main, Institute of Nuclear Physics, D-6000 Frankfurt/Main
G. Nolte, N. Roller
Hahn-Meitner-Institut, D-1000 Berlin-Wannsee
G. Zschornack
Technical University Dresden, Department of Physics, Division of Applied Nuclear Physics, Mommsenstr. 13, Dresden, DDR-8027

Recent systematic studies /1-6/ of L-subshell ionization probabilities for very asymmetric collision systems established surprising and unexpected results. These new aspects made it neccessary to investigate more systematically the impact parameter dependence of the L-subshell ionization probabilities, especially for increasing ratios of projectile to target nuclear charge. For 92 MeV Ar impact the Nd, Yb, Au and U L-subshell X-ray emission probabilities have been measured over an impact parameter (b) range from far inside to about two times the L-shell radius. From the observed line shifts it could be derived that multiple outer shell ionization is important. However, this process is not varying with b in the investigated b-range, and is thus not influencing the relative b-dependence of the measured subshell probabilities.

From the experimental subshell probabilities it could be derived that the coupling between L-substates is very strong, therefore the two-state SCA /7,8/ calculations are in clear disagreement with these experimental data. Also the total L-shell ionization probability is not satisfactoryly well described by SCA /8/, even so for total probabilities the influence of the coupling between L-substates is strongly reduced. For the measurements the 92 MeV Ar beam from the VICKSI accelerator at the HMI was collimated to a beam size smaller than 0.5 mm^2 and impinged on thin solid targets of Nd, Yb, Au and U ($\leq 80\,\mu g/cm^2$) evaporated on carbon-backing. The scattered projectiles were detected in a position sensitive parallel plate avalanche detector /9/ with 16 concentric ring anodes having width Δr proportional to the ring mean radius r. Thus a scattering angle resolution $\Delta\vartheta/\vartheta = \pm 5\,\%$ was obtained. The detector was mounted at two different distances D away from the target region to cover the whole impact parameter region of interest. The impact parameter was derived from the measured scattering angle ϑ by using a pure unscreened Coulomb scattering potential. The L-X-rays were detected with two Si(Li) detectors, both mounted at 90° with respect to the beam axis. Both Si(Li) detectors were covered with thin Aluminium absorbers to reduce the characteristic target M- and projectile K-lines.

The coincidence between X-rays and scattered projectiles was achieved in fast-slow coincidence technique. The data were stored in 5-parameter event list mode on tape. The number of true coincidences per X-ray line and impact parameter was derived from the list mode data by setting windows on the relevant parameters and subtracting the random coincidences. The derived L-subshell ionization probabilities p(b,Li) show severe deviations from first order pertubation theory (SCA + corrections), because, as derived from the data analysis, L-substate coupling during the collision, which is neglegted in this approach, has a strong influence on the subshell ionization process. For instance we show at Fig. 1 $p(b,L_{tot})$ for Ar on Au. The data (solid points) are compared to the SCA calculation /8/ (also showing the different subshell contributions). The experimental $p(b,L_{tot})$ were obtained by dividing the X-ray emission probabilities p(b,Li) by the corresponding ω_1 and adding $p(b,Li)/\omega_1$ of all lines. Therefore the experimental $p(b,L_{tot})$ should not be affected by uncertainties in Coster-Kronig transitions or line width variations due to multiple outer shell ionization.

Very nice absolute agreement is obtained between SCA and experimental data for b between 1000 and 2000 fm, just inside the mean L-shell radius $_L$. Towards larger b the united atom wave function has to be replaced by the separated target wave function accounting for reduced perturbation, i.e. decreased binding energy. Thus the "separated atom" SCA would yield higher $p(b,L_{tot})$ in better agreement with the data.

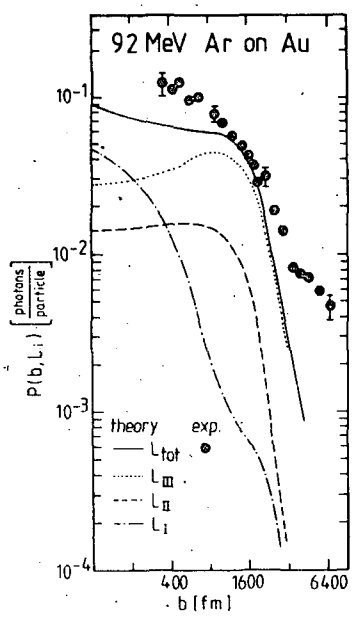

Fig. 1:
Total L-shell ionization probabilities in comparison with the SCA prediction (solid line). The dotted, dashed and dashed-dotted lines represent the corresponding L-subshell ionization probabilities. The data are not corrected for double collision effects in the solid target.

Therefore we can conclude that for Ar on Au the SCA predicts fairly well for $b \gtrsim \sqrt{2}/r_L$ the $p(b,L_{tot})$ even in the case of such a very strong perturbation. The experimental data show also a strong increase toward small b, whereas the SCA predicts a much weaker increase. Because we can exclude systematic deviations due to multiple outer shell ionization in the data, we believe therefore that the SCA model contains too crude approximations to describe the L-shell ionization in such collisions. It would be important to compare the data with a multichannel calculation /10/, in which coherently all multi-state processes are considered and the adiabatic rotation with the rotation of the internuclear axis R(t) is correctly taken into account. Interference effects between the multistate transition amplitudes could account for increased $p(b,L_{tot})$ towards small b.

References:

/1/ J. Ullrich et al.; Z. Phys. D2 (1986) 137
/2/ K. Dexheimer et al.; J. Phys. B19 (1986) 3083
/3/ S. Zehendner et al.; Z. Phys. D4 (1987) 243
/4/ H. Schmidt-Böcking et al.; Nucl. Instr. Methods B24/25 (1987) 64
/5/ L. Sarkadi, T. Mukoyama; J. Phys. B13 (1980) 2255
/6/ W. Jitschin et al.; J. Phys. B15 (1982) 763
/7/ D. Trautmann, F. Rosel; Nucl. Instr. Methods 169 (1980) 259
/8/ F. Rosel et al.; Nucl. Instr. Methods 192 (1982) 43
/9/ G. Gaukler et al.; Nucl. Instr. Methods 144 (1977) 115
/10/ R.S. Sokki, D. Crumpton; Nucl. Instr. Methods 192 (1982) 121; At.Data Nucl.Data Tables 30 (1984) 49

A METHOD FOR IONIZATION CROSS SECTION EVALUATION FROM X-RAY SPECTRA

P.Neumann, F.Stefan
Technische Universität Dresden, Sektion Mathematik, Mommsenstr.13, Dresden, DDR-8027
G.Zschornack
Technische Universität Dresden, Sektion Physik, Mommsenstr.13, Dresden, DDR-8027
M.Schiekel
Joint Institute for Nuclear Research Dubna, Head Post Office, P.O.Box 79, 101000 Moscow

In relativistic electron rings at the JINR heavy ion collective electron ring accelerator atoms or molecules are suczessive ionized by electron impact ionization. An effective diagnostics of the ionization process is possible by X-ray spectroscopy. From the measured X-ray spectra one can get informations about such ring parameters as the ion and electron numbers, the mean degree of ionization and the charge dispersion in the electron-ion ring. The analysis of ionization dynamics in the electron ring allows also an evaluation of ionization cross sections by electron impact. For this purpose we have developed a method for solution of the "reverse problem". The calculations are based on utilization of charge distribution spectra as a function of the ion ionizing time in the electron ring.

The ionization process in electron-ion rings can be described by the following set of equations

$$\frac{dN_o}{dt} = \pi d\bar{v}(n-N_o/S) - \sigma_o N_o v_e \rho_e - \sum_{k=1}^{z} \sigma_{o,k} v_{o,k} N_o N_k / S$$

$$\frac{dN_i}{dt} = (\sigma_{i-1} N_{i-1} - \sigma_i N_i) v_e \rho_e + \Big[\sum_{k=i}^{z} \sigma_{i-1,k} v_{i-1,k} N_{i-1} N_k + \sum_{k=0}^{i} \sigma_{k,i+1} v_{k,i+1} N_k N_{i+1} - \sum_{k=i+1}^{z} \sigma_{i,k} v_{i,k} N_i N_k - \sum_{k=0}^{i-1} \sigma_{k,i} v_{k,i} N_k N_i\Big] / S$$

$$\frac{dN_z}{dt} = \sigma_{z-1} N_{z-1} v_e \rho_e - \sum_{k=0}^{z-1} \sigma_{k,z} v_{k,z} N_k N_z / S \qquad (1 \leq i \leq z)$$

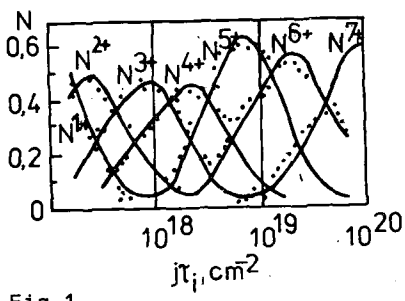

Fig.1
Charge distribution development for nitrogen ions in the electron ring

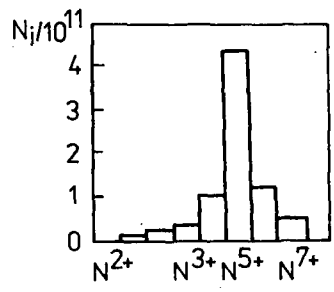

Fig.2
Calculated ion charge distribution at the end of the ring compression

with N_o and N_i - linear density of neutral atoms and ions of the charge i, respectively; $\bar{v}$ - mean velocity of neutral atoms perpendicularly to ring surface; n - density of neutral atoms outside of the ring; $v_{i,k}$ - mean relative velocity of ions with charges i and k; v_e, ρ_e - velocity and density of the electrons; $\sigma_{n,n+1}$ - ionization cross section for the process $A^{n+} + e^- \rightarrow A^{(n+i)+} + (i+1)e^-$; S - area of ring surface; V - ring volume. In the equations above only simple charge transfer is taken into account.

To solve the indicated set of differential equations, a weighted Runge-Kutta-algorithm in connection with optimization techniques is applicable. Because in this case it is difficult to get convergence in the solution, we used the method of least squares. Considering values from at different times measured X-ray spectra, one get a over-determined linear set of equations, whereby solutions are found by last squares techniques. For instance, in Fig.1 we give an example for the nitrogen ion charge dispersion in the electron ring, basing on calculated ionization cross sections, and in Fig.2 the calculated ion charge state distribution at the end of the ring compression /1/.

References:

/1/ F.Stefan; Research Report, TU Dresden, Department of Mathematics,Dresden, 1987

ACCELERATORS

OPERATION AND IMPROVEMENT OF THE CYCLOTRON U-120

B. Anders, R. Brückner, H. Büttig, H. Guratzsch, P. Hartmann, G. Kerber, H. Odrich, S. Preusche, H. Tyrroff and J. Weißig
Zentralinstitut für Kernforschung Rossendorf, Bereich G

As in previous years the cyclotron beam has been used mainly for basic nuclear research and isotope production. Table 1 shows the time distribution over the year 1987. In table 2 the accelerated particles are specified together with their percentages of the beam time.

Table 1
Beam time distribution for 1987

Cyclotron operational	5.269 h
Turning on and off; Maintenance	385 h
Scheduled revision	292 h
Total beam time:	4.592 h
Nuclear physics	1.488 h
Isotope production	1.544 h
Neutron therapy	196 h
Cyclotron improvement	978 h
Others	386 h

Table 2
Accelerated ions and their percentages of beam time

D^+	57 %
H_2^+	2 %
$^4He^{2+}$	33 %
$^{6;7}Li^{3+}$	8 %

For application in the positron emission tomography (PET) ^{11}C is mostly produced by the $^{14}N\ (p,\alpha)^{11}C$ reaction at proton energies of about 12 MeV. At present the cyclotron U-120 accelerates protons in the H_2^+-mode to 6.7 MeV per nucleon. With regard to PET the cyclotron will be modified into a variable-energy accelerator in order to accelerate protons up to the required energy in addition to the hitherto available particles. The construction of a new acceleration chamber is under way. The magnetic field will be shaped by concentric trim coils and specially formed Rose shims. The parameters of the coils and the Rose shims have been calculated using the computer code "POISCR" /1/ as well as special codes for a personal computer. The simulated magnetic-field distributions are in good agreement with the experimental values /2/.

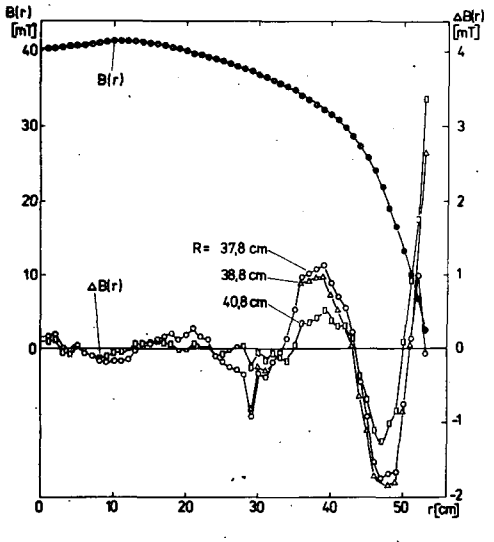

Fig. 1 shows the magnetic field distribution B (r) which is to be generated by the trim coils for the acceleration of protons at a central field of 1 T. The remaining misfit ΔB (r) after optimizing the currents of the trim coils is also displayed for three positions of the outer (most important) coil.

Fig. 1

Magnetic field distribution B (r) which is to be generated by the trim coils for particle acceleration at the central field of 1 T. The misfit ΔB (r) to the ideal field distribution is calculated as a function of three positions of the outer coil (R is the mean radius of the outer coil).

References

/1/ Iselin, Chr.; CERN Computer Centre Program Library, POISCR, T 604
/2/ Alenitskij, Yu. G. et al.; JINR 9-87-491, Dubna 1987

OPERATION OF THE ELECTROSTATIC ACCELERATORS IN 1987

W. Bürger and S. Turuc

Zentralinstitut für Kernforschung Rossendorf, Bereich G

Tandem-Accelerator

The accelerator has been used for experiments of nuclear physics, solid state physics, for thin layer activation, irradiation of polymer foils and for experiments in connection with the improving of accelerator components.

Characterizing parameters of accelerator employment are given in table 1 and 2.

	hours
Available time	5.954
Accelerator under voltage	4.200
Experiments with beam	3.801
Development	548
Maintenance and planned stand	896

table 1

species of ions	rel. op. time/%
p	10,0
d	24,1
d(pulsed)	9,1
^{14}N	11,5
^{15}N	17,4
^{35}Ce	22,3
Li,O,F Si,Cu,Br)	5,6

table 2

The accelerator had to be opened four times for maintenance. The life time of the charging belt (Greengate) is now more than 16.000 hours. But the outer view of the belt indicates that it will end its running time in the near future.

The power supply control of the analyzing magnet has been equiped with a new microcomputer aided proton resonance magnetometer. This device has been developed at the UJF Rez/CSSR. In particular it allowes the on-line control of the analyzing magnetic field by the experiment computer. The device works well, only a certain sensitivity against the influence of high voltage breakdowns inside the accelerator still must be eliminated.

At present we try to increase the transmission for heavy ions in the injection region. A wanted doublefocusing of the injection magnet assembly is produced by adding of two electrostatic quadrupol singlets before and behind the magnet thus allowing a better fit of the ion beam to the accelerator acceptance.

The equipment for foil irradiation for the production of nuclear track microfilters has been used to irradiate an area of 9.400 m^2 foil mainly by chlorine- and bromine-ions. The irradiation equipment has been completed. In order to increase the reproducibility of the hole density the monitoring of the beam current during the irradiation has to be improved. The investigations of art objects with an external beam have been continued.

Van de Graaff Accelerator

The 2 MV VdG accelerator has been used 3.275 hours mainly for nuclear analysis (protons, deuterons, helium ions).

We had to change our first Poly-c-belt after a running time of 4.300 hours. The belt showed local disruptions obviously caused by electrical stress and probably mechanically caused longitudinal tears. The rf ion source has run without maintenance, in particular the extraction system now has been stable operated for 6.700 hours.

AN IMPROVED EXTRACTION SYSTEM FOR A RF ION SOURCE

M. Friedrich and S. Turuc

Zentralinstitut für Kernforschung Rossendorf, Bereich G

In 1984 a new focusing and extraction system /1, 2/ was installed at the rf ion source of the 2 MV Van de Graaff accelerator. The original and the improved extraction system are shown in fig. 1 and 2.

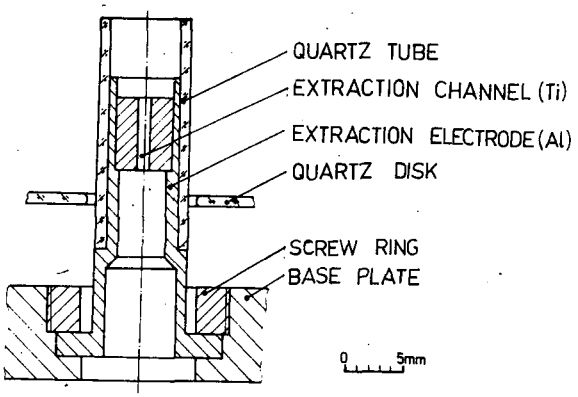

Fig. 1 Original extraction system

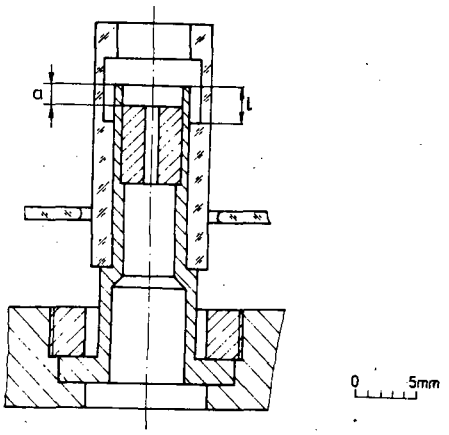

Fig. 2 Extraction system with shielded region l

The life time of an original ion source was about 300 hours in average and was limited by sputtering of the extraction channel. The present used modified ion source was installed in October 1985 and has operated up to the end of 1987 about 6700 hours without any maintenance. After this long period the source and beam parameters are still stable and, therefore, the final limit of operation time cannot be estimated. The mainly used beam parameters are 1-3 µA beam current (nonanalysed) for helium ions, 600 V extraction voltage and 1,0 - 1,7 MV terminal voltage.

From the extremely long source operation time some new aspects on the life time limitation of a rf ion source are abtained. The most important effect is the shielding of the quartz tube by the extraction electrode over the length l shown in fig. 2. This shielded length prevents electrical discharges between the electrode and the source plasma. From this follows that the geometry of the extraction system is already optimized and the ionoptical conditions for extraction must only be protected during source operation. A further important effect is the aligment of the highest plasma density on the axis of the extraction channel. This was obtained by a careful aligment of the rf coil and concentration of the source plasma by a permanent magnet. In the used low beam current mode the life time of the modified source is not limited by sputtering of the extraction channel but by erosion of the upper part of the extraction electrode shown by length a in fig. 2. A visual supervision of the ion sources has shown that the ever observed black deposit on the inner source wall of the modified source after 6.700 hours is less than in a source with original extraction system after 100 hours. This shows that the black deposit is not caused by the residual gas but mainly by sputtered material of the extraction electrode.

References

/1/ Dietrich J. and Friedrich M., Exp. Tech. Phys. 34 (1986)263

/2/ Friedrich M. and Turuc S., Annual report 1984 ZfK-559 (1985)139

NUCLEAR ELECTRONICS AND METHODS

INVESTIGATION OF LOW-PRESSURE GRID AVALANCHE COUNTERS

W. Seidel and H.-G. Ortlepp
Zentralinstitut für Kernforschung, Rossendorf, Bereich KF

The properties of low-pressure multiwire proportional chambers (MWPCs) have been investigated during the last few years with various gases, pressures, geometries and particles /1-4/. Breskin et al. have shown /1,2/ that MWPCs operated with pressures of about 2 Torr can be used for very fast timing. This is believed to be due to a double amplification process achieved at low gas pressures: (i) amplification in the "parallel plate avalanche counter" (PPAC) region far from the wires, where the electrical field is approximately constant (the reduced electric field strength E/p reaches values of several hundreds of V/cm.Torr); (ii) a second amplification step in the vicinity of thin (10 μm diameter) anode wires, where the reduced field strength is about two orders of magnitude higher. For the further improvement of the double grid avalanche counter (DGAC) /5/ we have investigated the double step amplification process for this detector type.

In order to test the detection efficiency and the time resolution in dependence of the diameter of the anode wires, we compared two small identical grid avalanche counters (GAC) with unequal electrodes (cathode foil and 20 or 50 μm anode wires, 1 mm spaced). The wire planes (30 mm in diameter) are located at 3 mm distance of the cathode foil. The electronics employed has been described elsewhere /6/. The detectors were operated in a common chamber filled with n-pentane in the pressure range of 1-5 Torr. The counting efficiency and the time resolution of both wire detectors were measured relative to a transmission PPAC (25 mm diameter, 2 mm gap width). Together with a ^{252}Cf source the PPAC was placed on a movable support for comparing both GAC's under the same conditions (gas pressure, bias, electronics) by shifting the ^{252}Cf source and the PPAC from one GAC to the other. No significant differences in efficiency and time resolution were found for 20 μm and 50 μm anode wires. The amplitudes of the output signals of both counters are shown in fig. 1. They turned out to be identical even for the highest reduced field strength. That means, we don't observe differences in the second amplification step although the electric field strengthes at the wire surface differ by a factor of 2.3 /7/. We determined the mean free path λ of the electrons in the avalanches from the experimental Townsend coefficient for n-pentane according to Brösicke /8/. The values of λ are in the same order of magnitude as the diameter of the inhomogeneous field region around the anode wires (≤ 0.3 mm). To our opinion this is the reason for the missing amplification differences between 20 μm and 50 μm wires in contrast to 10 μm wire diameter used in the investigations of Breskin /1,2/.

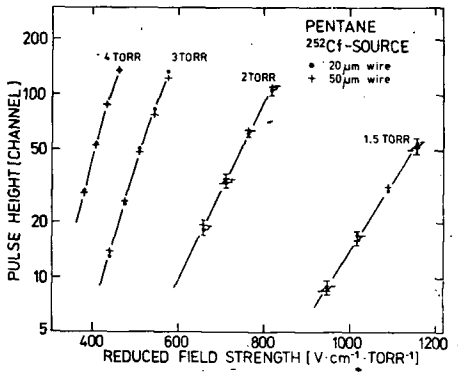

Fig. 1: Pulse height vs. reduced field strength at different gas pressures measured with fission fragments of a ^{252}Cf source

References

/1/ Breskin, A. et al., Nucl. Instr. and Meth. 165 (1979) 125
/2/ Breskin, A. et al., IEEE Trans. Nucl. Sci. NS-27 (1980) 133
/3/ Breskin, A. et al., Nucl. Instr. and Meth. 196 (1982) 11
/4/ Breskin, A. et al., Nucl. Instr. and Meth. 217 (1983) 107
/5/ Seidel, W. et al., annual report 1986, ZfK-621 (1987) 121; submitted to Nucl. Inst. Meth.
/6/ Ortlepp, H.-G., W. Seidel, annual report 1984, ZfK-559 (1985) 149
/7/ Charpak, G. et al., Nucl. Instr. and Meth. 80 (1970) 13
/8/ Brösicke, H., Diplomarbeit, Physikalisches Institut der Universität Heidelberg Heidelberg (1976), unpublished

REAL TIME DIGITAL PROCESSING OF BRAGG IONIZATION CHAMBER SIGNALS

A. Romaguera, W.D. Fromm and H.-G. Ortlepp
Zentralinstitut für Kernforschung, Rossendorf, Bereich KF

The development of a digital readout system for Bragg ionization chambers (BIC) /1/ has been continued /2/. This system consist of a charge sensitive preamplifier optimized for Bragg curve spectroscopy and two further modules (fig. 1). The Bragg curve digitizer (BCD) containes a shaping amplifier, an 8 bit flash ADC and a clock frequency generator. The Bragg digital processor recieves the digitized values of the Bragg curve signal. A digital comparator determines the threshold for pulse recognition. Two arithmetic units with fixed algorithms determine the integral (E) and the smoothed maximum (Z) of the signal as schematically shown in the lower part of fig. 1. Several questions concerning the analogue pulse shaping, the sampling frequency and the ADC resolution have been investigated by model calculations and with the help of a prototype of the system. At the CINR tandem accelerator test measurements were performed with a small BIC. Elastically scattered Si and several recoil ions were registered. Two-dimensional spectra obtained with the present system, but also with an analogue processing channel /3/ were stored in a 256 x 256 channel memory /4/ and analyzed generating different cuts. A comparison of both methods yielded the following results:

i) The energy resolution is comparable for ions heavier then carbon. For alpha particles the analogue system yielded better resolution due to its better signal to noise ratio.
ii) Under certain conditions the Z-resolution of the digital system is better ($Z/\Delta Z \approx 55$, fig. 2).
iii) The digital system is faster by one order of magnitude, easier to operate and cheeper.

Presently elaborated BCD and BDP CAMAC modules are under construction, dedicated to the PHOBOS spectrometer /5/.

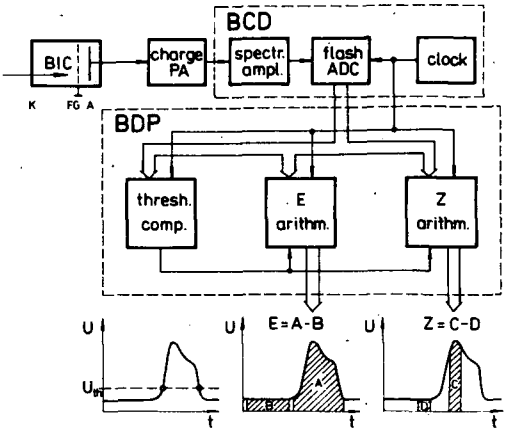

Fig. 1: Principle of the digital processing channel

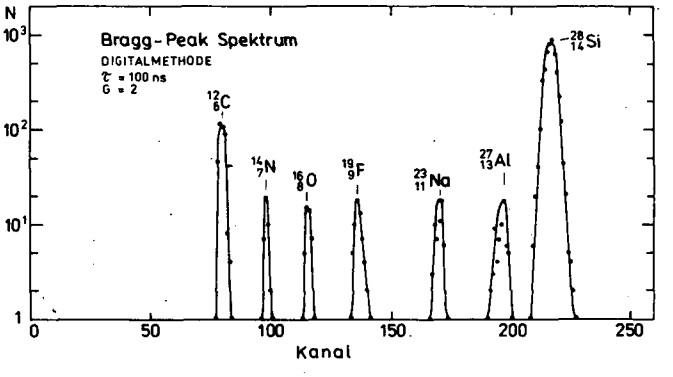

Fig. 2: Bragg peak soectrum of different elements (energy threshold - 25 MeV)

References

/1/ Romaguera, A., Ortlepp, H.-G., Annual report 1986, ZfK-621 (1987) 123
/2/ Romaguera, A., thesis, Akademie der Wissenschaften der DDR, Rossendorf 1987
/3/ Kotte, R. et al., Nucl. Instr. Meth. A 257 (1987) 244
/4/ Fromm, W.D., Kahlenbach, M., Annual report 1983, ZfK-530 (1984) 154
/5/ Sodan, H. et al., Annual report 1984, ZfK-559 (1985) 144

TEST EXPERIMENTS WITH A DETECTOR SYSTEM CONSISTING OF A DGAC AND A LARGE SOLID ANGLE BIC

A. Matthies, R. Kotte, H.-G. Ortlepp, W. Seidel
Zentralinstitut für Kernforschung, Rossendorf, Bereich KF

Test measurements have been performed with a prototype of a detector system designed for the 4π spectrometer PHOBOS /1/. The system consists of a position-sensitive double grid avalanche counter (DGAC) and a large solid angle (30 msr) Bragg ionisation chamber (BIC). Details of the DGAC and the BIC as well as test results have been published elsewhere /2,3,4/. In the following, optimisation results of the chamber working conditions are presented. The influence of the field shape, the field strength and the gas pressure has been investigated. The case of the BIC is a truncated hexagonal pyramid. Charged particles emanating from a point source on the axis of this detector travel along radial paths. In a homogeneous electrical field, a deviation of the ionisation path from the field lines results in a distortion of the ionisation current measured at the anode. In order to avoid this, a $1/r^2$ field is required in the detector volume. The latter geometry leads to an electron velocity varying along the drift path, and thus also to a distortion of the signal. We tested both field geometries.

The BIC was operated with P-10 (90%Ar-10%CH_4) gas, the DGAC - with n-pentane at a pressure of 4 Torr. During the measurements with a ^{241}Am-source four parameters are recorded: the position X and Y, the Bragg peak height Z and the energy E.

In figure 1 the dependence of the Z-signal on the energy is shown for the $1/r^2$ field. Only particles with small entrance angles ($\leq 2^o$) are taken into account. In the dynamical region of the BIC deviations up to 8% from the linear dependence are observed. A correlation between the Bragg peak height and the electron drift velocity along the chamber axis (fig. 2) is visible. The position dependent deviation in the case of a homogeneous field reaches only 3%. Moreover, a simple offline correction is possible, if the position of the particle is known (fig. 3). Therefore, further we used only a homogeneous field configuration.

The gas pressure (165 Torr) was adjusted such that the maximum range of the α-particles corresponds to the chamber length of 22 cm. The pressure dependence of the E-signal was negligible. The energy resolution of the chamber was found to be $\Delta E/E \leq 1.3\%$. An optimum Z-resolution ($\Delta Z/Z = 3\%$) was obtained at a reduced field strength (0.2 ... 0.3) V/cm Torr, corresponding to the maximum of the electron drift velocity in P-10 /5/.

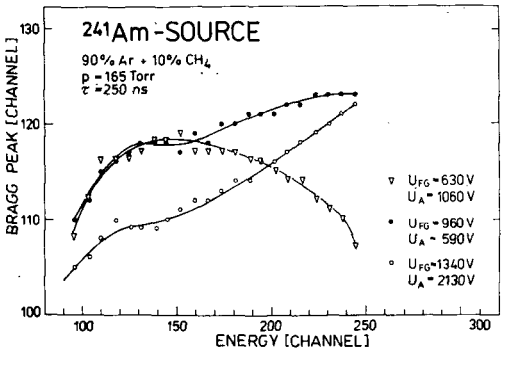

Fig. 1

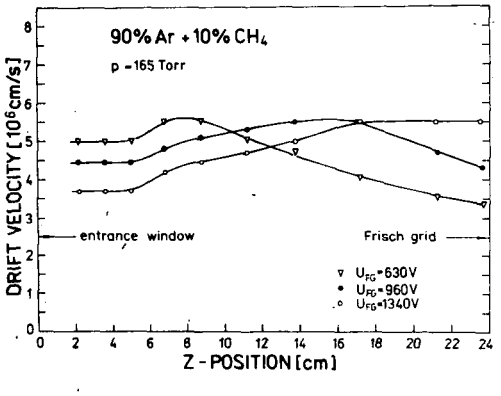

Fig. 2

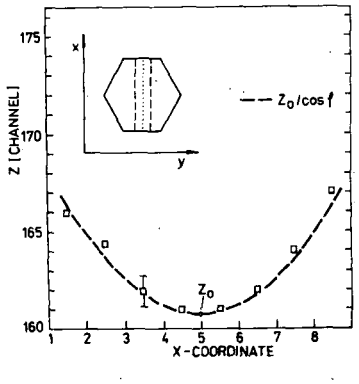

Fig.3

/1/ Sodan, H. et al, Jahresbericht 1984, ZfK-559(1985)144
/2/ Seidel, W. et al, Annual report 1986, ZfK-621(1987)121
/3/ Seidel, W. et al, Annual report 1986, ZfK-621(1987)122
/4/ Seidel, W. et al, this report, p. 96
/5/ Peisert, A., Sauli, F., CERN-report, CERN 84-08(1984)83

APPLICATION OF BRAGG CURVE SPECTROSCOPY TO CHARGE IDENTIFICATION IN NUCLEAR FRAGMENTATION

L.N. Andronenko, A.A. Kotov, V.I. Panichev and L.A. Vaishnene
Leningrad Nuclear Physics Institute, Gatchina, U.S.S.R.
W. Neubert
Zentralinstitut für Kernforschung, Rossendorf, Bereich KF

We constructed a new large-area axial ionization chamber which has an entrance window of 70 mm in diameter. After extensive tests with alpha-particles we have explored this ionization chamber for Bragg curve spectroscopy of products from nuclear fragmentation. For this purpose, this axial ionization chamber was tested at the external proton beam of the Gatchina synchrocyclotron. The ionization chamber was mounted at a distance of 50 cm from a thin nickel target located in the centre of an evacuated reaction chamber. Fragments were detected at 144 deg. with respect to the beam axis. The ionization chamber was filled with purified n-pentane of 55 Torr and it was operated at a reduced field strenght E/p = 2.2 V/Torr.cm in the cathode-anode volume. The anode signal was fed into a charge-sensitive preamplifier and the output signal was branched out to two CAMAC spectroscopy amplifiers which allow shaping times from 0.5 μs to 4 μs (for the Bragg peak amplitude-BP) and from 1 μs to 8 μs (for the energy signal). Both signals were digitized in 2K CAMAC ADCs which accepted subsequent signals to 8 μs delay. A double-grid avalanche counter was mounted near to the target and the appearance of a fragment delivered a trigger signal for the ADCs. The CAMAC data acquisition system was linked with the small computer SM-3.
The 2D-plot given in fig.1 shows well separated isotopic branches from Z=2 to Z=11. This plot is corrected for an ascent of about 5% of all branches. The dynamic range of the energy axis is determined by the minimum energy necessary for the formation of a Bragg peak (E/A ≃ 0.5 MeV/u) and the maximum particle energy which can be deposited in the active chamber volume. Fragments which punch through cause a "back bending" (observed up to N). The lower part of fig.2 shows the projection onto the BP-axis. The relationship between fragment charge Z_f and the BP amplitude is shown in the upper part. The resolution of adjacent nuclear charges amounts to be $Z/\Delta Z \approx 38...40$. The data analysis for a meassurement of Au + 1 GeV p is under way.

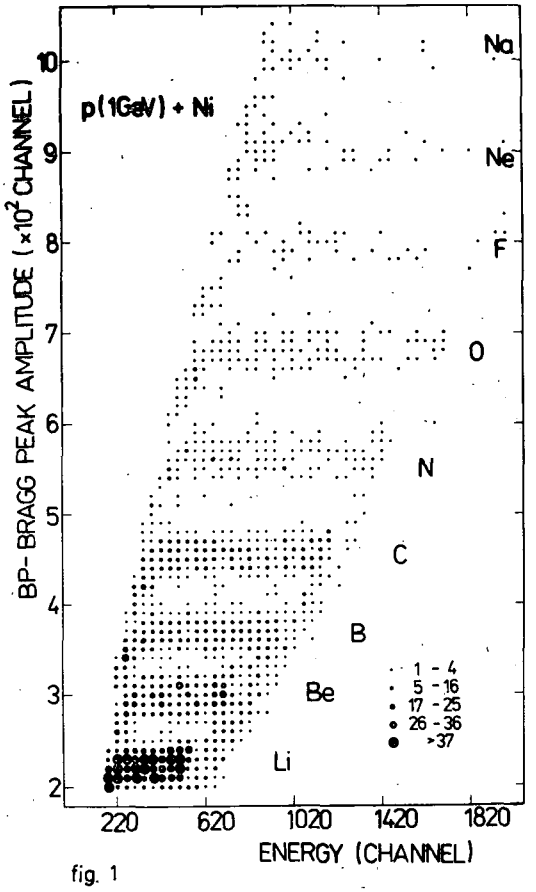

fig. 1

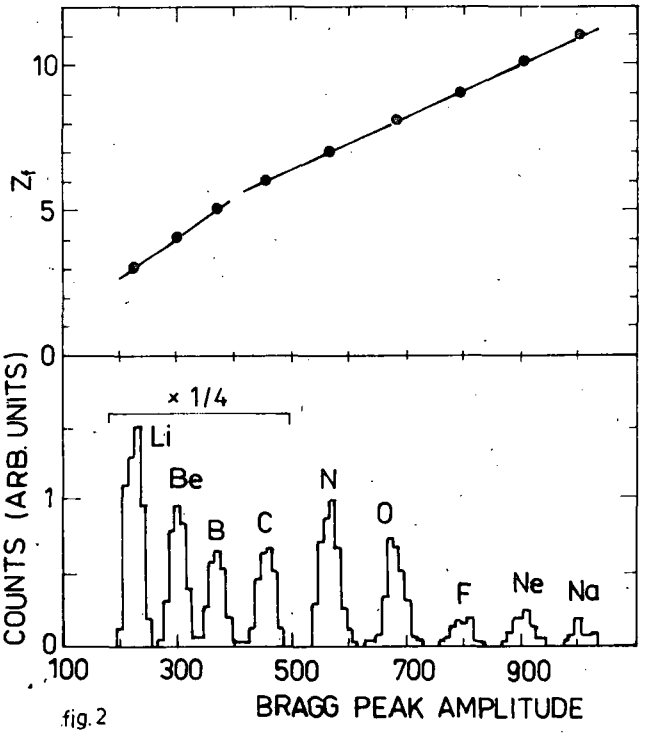

fig. 2

TEST OF READ-OUT METHODS WITH DELAY LINES

W. Neubert and J. Hutsch
Zentralinstitut für Kernforschung, Rossendorf, Bereich KF

Winded electromagnetic delay-lines have commonly impedances of some hundred ohms. A special fast preamplifier with adjustable input impedance was developed to match both circuits /1/. A delay-line capacitively coupled to strip electrodes of a PPAC delivered output signals with rise times of about 25 ns and 100 ns duration by using this preamplifier. In special cases there may occur limitations of the counting capability. Therefore, we tested a commercial dip delay-line (Belfuse 0446-0030-50) with 50 Ω impedance which makes it compatible with fast standard electronics. The conductive strips of a PPAC electrode were directly coupled to the taps of this passive delay-line chip via strip lines. Differences up to 45 mm of the strip-line lenghtes could not be avoided due to the ring-shaped electrode. The corresponding parasitic capacities are estimated to be in the range from 1.5 pF to 6 pF. In spite of these differences we observed only minor deviations of the delay time between the taps. The response and linearity of one strip-electrode is shown in fig.1. The linearity obtained with the dip delay line is nearly the same as found with a helical one. However, the dip delay line showed a lack of stability during continued operation in a low-pressure heptane athmosphere. The advantage of continous 50 Ω coupling can be also achieved with winded delay lines via pulse transformers /2/. In order to test this method, the evaporated conductive strips of the PPAC electrode were bonded to strip lines and from there short wires were soldered directly to the windings. We terminate this helical delay line by using a matching pulse transformer which consists of a small ferrite toroid (VEB Keramische Werke Hermsdorf, Mf 183, Mf 195) with 10 windings in the primary and 4 windings in the secondary. The square of the winding ratio is slightly overestimated to match the delay line to 50Ω and, therefore,gives a slight reflection of positive polarity (fig.2). We preferred this pulse shape in order to avoid false triggering. The corresponding current signal at the fast preamplifier output has a rise time of 8 ns and a duration of 20 ns. Fig.3 shows a part of a position spectrum obtained with this read-out.

R e f e r e n c e s

/1/ Ortlepp H.-G., Seidel W.; Jahresbericht ZfK 559 (1984), p.149.
/2/ Birk M., Breskin A. and Trautner N.; Nucl. Instr. Meth. 137 (1976) 393.

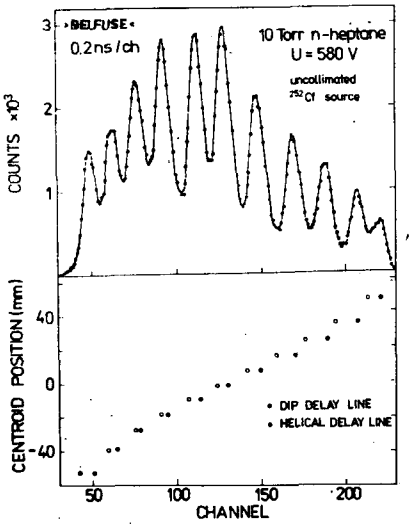

Fig.1

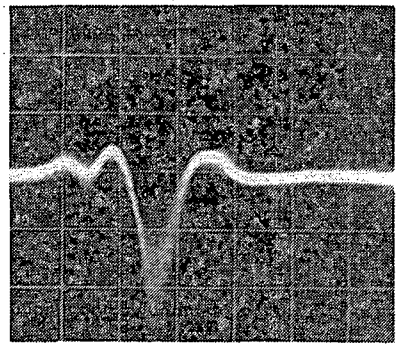

Fig.2
Pulses obtained with a ^{252}Cf source at the output of a current preamplifier. Vertical gain: 100 mV/div., time scale: 20 ns/div.

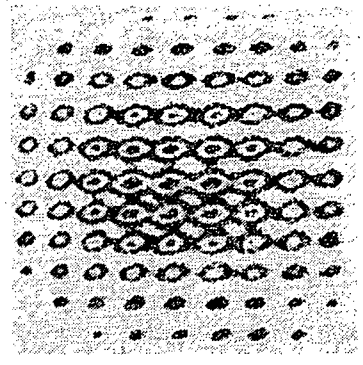

Fig.3
Detector response with an uncollimated source, Y-helical delay line, X-dip delay line

CsI(Tl) SCINTILLATION DETECTOR WITH PHOTODIODE READOUT

R. Schwengner, Th. Scholz, G. Winter, J. Rüdiger and U. Lorenz
Zentralinstitut für Kernforschung Rossendorf, Bereich KF

In recent years several detectors for charged particles of high energy have been designed that consist of a scintillator coupled to a photodiode /1,2/. CsI(Tl) has proved to be the most suitable scintillation material for photodiode readout since it has a relatively large photon yield and a light emission maximum at about 550 nm that is well matched to the spectral sensitivity of photodiodes /3/.

We have designed a CsI(Tl) scintillation detector with photodiode readout and made some first experiments with low-energy α particles. The cylindrical CsI(Tl) crystal had a diameter of 9.8 mm and a thickness of 8.3 mm. Within this thickness α particles with energies up to about 180 MeV can be stopped. The crystal was manufactured by Carl Zeiss Jena. The photodiode, produced by the detector group (KFA) of the ZfK Rossendorf, had an area of 10 x 10 mm^2 and a thickness of 0.25 mm. It was glued on a circuit board which held also the cylindrical crystal housing. This housing was made from Teflon and served also as light reflector. The CsI(Tl) crystal was coupled to the photodiode with silicone grease. The signals from the photodiode were amplified by a charge-sensitive preamplifier for silicon detectors /4/ and a spectroscopic amplifier ZFK-SPV 5024/100.

In the first experiment a ThC' source was placed directly onto the CsI(Tl) crystal. The photodiode was operated with a voltage of 60 V, where it had a dark current of 10 nA and a capacity of about 70 pF. The main amplifier had a shaping constant of 1 µs. The spectrum recorded during this experiment is shown in figure 1. In addition to the spectrum of the ThC' source it contains a pulser peak. This peak has a resolution of 5 %. The composite α-particle peaks with main components at 6.05 and 8.78 MeV have an energy resolution of 11 % and 10 %, respectively. It can be seen in the spectrum that the noise reaches up to about 4 MeV which is the low-energy threshold for the detection of α particles with this detector setup. The large energy equivalent of the noise may be caused by the inefficient light collection for the low-energy α particles which produce the light within a thin layer of about 0.06 mm at that surface of the crystal that is opposite to the photodiode. Contributions to the noise arise also from the internal noise of the photodiode and the preamplifier.

Further experiments are necessary to investigate the characteristics of the detector at different energies of charged particles and to improve the detector setup.

References
/1/ Glasow, R. et al., Nucl. Instr. Meth. 228 (1985) 354
/2/ Meijer, R.J. et al., Nucl. Instr. Meth. A256 (1987) 521
/3/ Grassmann, H. et al., Nucl. Instr. Meth. 228 (1985) 323
/4/ Ortlepp, G. and E. Schuster, Rossendorf annual report 1985, ZfK-584 (1986) 101

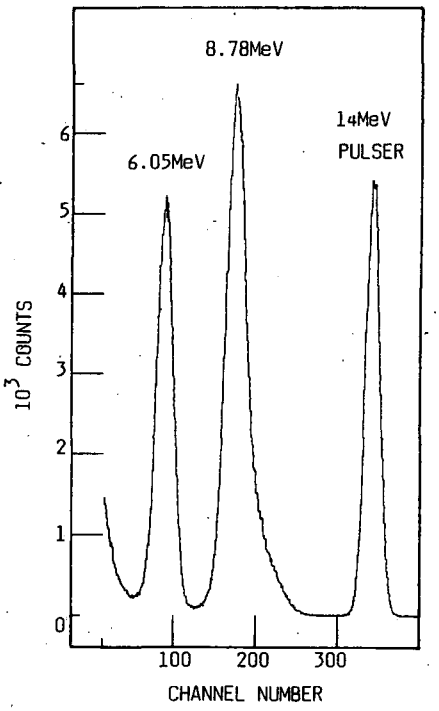

Figure 1.
Spectrum of a ThC' α-particle source recorded with a CsI(Tl) scintillator with photodiode readout.

ENERGY DEPENDENCE OF THE PROMPT REFERENCE IN γ - R.F. COINCIDENCE EXPERIMENTS

L.G. Kostova
Institute for Nuclear Research and Nuclear Energy, Sofia, Bulgaria

L. Käubler, H. Prade and G. Winter
Zentralinstitut für Kernforschung, Rossendorf, Bereich KF

If the lifetime of an excited nuclear state is smaller than the time resolution of the experimental set-up used in γ - r.f. coincidence experiments, the knowledge of a prompt reference appears to be a necessary condition for the determination of lifetime values. Applying the generalized centroid-shift method /1,2/ mean lifetimes in the region of 0.1 - 5 ns are deduced from centroid differences of time distributions of prompt and delayed γ-transitions. Therefore, a prompt reference line (zero-time line or "walk curve") has to be determined representing the centroid positions of prompt time distributions as function of the γ-ray energy. The shape of this prompt reference line depends on the properties of the timing set-up (Ge detector, preamplifier, fast amplifier, triggers etc.) and may be additionally affected by the particular time structure of the γ-rays in the spectrum under investigation. Thus, the zero-time line has to be determined for each experiment seperately using available prompt transitions in the γ-ray spectrum observed.

This work was intented to study the influence of the preamplifier, which is one of the most sensitive components of the timing set-up, on the energy dependence of the prompt reference line. Besides a standard experimental set-up as described in /3/ two different preamplifiers have been tested; an ORTEC preamplfier model 120-3F (PREAMP 1) and a ZfK preamplifier of the type LVV 5022-30 (ref. /4/).
Since the nucleus ^{155}Tb is known /5/ to have rotational states, which are deexcited by prompt γ-transitions, the test measurements have been performed by using the reaction ^{153}Eu(α,2n)^{155}Tb at the Rossendorf cyclotron. The γ-rays have been recorded with a 7.7 cm^3 planar Ge(Li) counter with an energy resolution of FWHM $\approx$ 2.4 keV at E_γ= 380 keV. The time resolution turned out to be nearly equal in both cases: $2\tau_0 \approx$ 13 ns at E_γ = 65 keV and $2\tau_0 \approx$ 7.5 ns at E_γ = 479 keV.
The results are displayed in fig. 1. The slope of the zero-time line obtained with the ZfK preamplifier is approximately a factor of three smaller than that for the ORTEC preamplifier. This smaller energy dependence might be more favourable, because the zero-time line is only defined at a few γ-ray energies and must be estimated by interpolation for the γ-ray energies of interest. It is, in particular, especially important for measurements of spectra of delayed γ-rays.

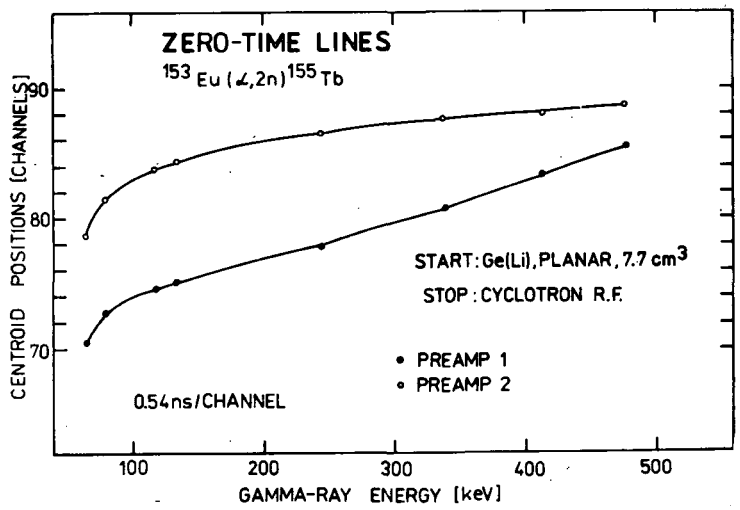

Fig. 1
Energy dependence of centroid positions of prompt γ-rays
PREAMP 1: ORTEC Model 120-3F; PREAMP 2: ZfK LVV 5022-30

R e f e r e n c e s

/1/ Schilling K.D. et al; Nucl. Phys. A265 (1976) 58
/2/ Andrejtscheff W. et al.: Nucl. Instr. Meth. 204 (1982) 123
/3/ Gabriel H.; PhD Thesis, ZfK-228 (1978)
/4/ Ortlepp H.G.; Annual report ZfK-408 (1980) 155
/5/ Winter G. et al.; Nucl. Phys. A176 (1971) 609

ELECTRONIC DEVELOPMENTS OF THE KFL GROUP

H.-G. Ortlepp and E. Schuster
Zentralinstitut für Kernforschung, Rossendorf, Bereich KF
A. Rink
Technische Universität Dresden, Sektion Elektrotechnik

Preamplifier for gaseous heavy ion detectors

The parameters of this charge sensitive preamplifier were matched to the Bragg ionization chambers of the spectrometer PHOBOS /1/. The sensitivity amounts to 2mV/MeV and the linear output range to 5 GeV (for an ionization chamber with typical gas). The input is protected against damage caused by gas discharges.

Three - channel CAMAC - controlled constant fraction trigger

This 1M CAMAC module was developed for the position sensitive avalanche counters of the PHOBOS spectrometer /1/, but may be used for other detector types, too. The threshold of each channel is set by a CAMAC command. The walk adjustment is performed automatically. The presence of input pulses exceeding the threshold is indicated by a LED in each channel and may be checked by a CAMAC function, too. The dynamic range reaches from -3 mV to -3 V. The shaping delay must be realized with an external cable.

Read- out electronics for 8-fold silicon particle detectors

The read- out system described in /2/ has been modified for detectors with the opposite bias sign. A new charge sensitive preamplifier and new individual channels providing the detector number information have been developed and fit again in the same read- out scheme without limitations of the dynamic range.

Linear gate

Two linear gates are housed in one 40 mm EGS module. The linear input range is 0 to +5 V. A positive TTL or a negative fast NIM signal at the gate input is delayed up to 1.2 μs and openes the linear gate for 0.5...5 μs. For the adjustment of the delay and the gate width a logical TTL output becomes active during the opening interval.

Sum amplifier

The sum amplifier is housed in a 40 mm EGS module. From two linear input signals (0...+5 V) four different weighted sums are derived. The weight coefficients are adjustable from 0.0 to 1.0 by potentiometers. An internal voltage source of +1.0 V may be switched to either of the two inputs for the determination of the weight coefficients by measuring the output voltage.

Single channel analyzer

Two single channel analyzers are housed in one 40 mm EGS module. They can work either individually or gated by a common strobe input signal. The lower and upper thresholds are adjustable independently in the range from 0 to +5 V. In the gated mode the delay of the output signal relative to the leading edge of the strobe signal is kept constant (40 ns) to preserve the timing information.

Universal pulse height selection system

This system includes modules of the three last above mentioned types and a logical combination module (overlap coincidence principle). It has been developed to select and analyze different regions of two- dimensional ΔE-E_r distributions, esspecially for absolute fission cross- section measurements using the time- correlated associated particle method. The possibilities of an earlier particle identification system /3/ have been extended in this way to provide more sophisticated background correction procedures.

References

/1/ Akhperdshanyan, A.G. et al., JINR Communication P13-87-760, Dubna 1987
/2/ Schmidt, B. et al., Annual Report 1984, ZfK-559 (1985) 152
/3/ Herbach, C. M. et al., Annual Report 1984, ZfK-559 (1985) 21

ELECTRONIC DEVELOPMENTS OF THE KFM-GROUP

W.D.Fromm and F.Schwarzenberg
Zentralinstitut für Kernforschung, Rossendorf, Bereich KF

The main activity was devoted to the development of the compact MCA /1/. Four functional units of the microprocessor system MPS 4944 were transferred into production: the ADC 4944-135, the DMA incrementer INC 4944-136, the V.24-IFSS-PIO interface VIP 4944-137 /2/ and the small TV monitor MON 4944-138 /3/. A party of five module sets was produced as laboratory samples. Three add-on boards for the homecomputers KC85.1 and KC87 were developed and three small auxiliary PC-boards were designed. Their parameters are summarized in the following short overview:

Serial Interface for KC85.1/KC87 ZfK 9907

The add-on module (95 * 110 mm²) uses 1 CTC and 1 SIO-circuit to provide 2 V.24 and 1 IFSS channel. The interface connectors conform to the robotron standard. The second V.24 channel uses the opposite row of the 26-pole connector. The module address is determined by a DIL-switch.

48kB DRAM for KC85.1/KC87 ZfK 9906

The 64kB dynamical RAM board (95 * 110 mm²) uses 8 U2164 chips. The first 16kB of the address space of the homecomputer are on the motherboard. Therefore the second 16kB region (4000-7FFF) is represented as two RAM-banks which are switched by an I/O-command. Furthermore the write-only regime can be activated by command.

Digital I/O for KC85.1/KC87 ZfK 9902

Two PIO-circuits are placed onto this add-on module (95 * 110 mm²). The address of the module is selectable with a DIL-switch. The card is highly configurable by wire bridges. At the input lines up to 16 limiting diodes can be connected. The outputs can be connected directly or via driver circuits (16 channels DL038) to the connector. 16 thick film resistors are foreseen for open collector lines. By this way a wide variety of applications can be realised.

Magnetic tape cassette adaptor ZfK 9916

This small board (75 * 30 mm²) is added to the VIP 4944-137 module and provides an adaptation to audio tape cassette drives. One bit of the PIO and one input of the CTC circuit are used to produce and recognise the usually employed two frequency coding. With the accompanying software programs and data can be recorded and retrieved from magnetic instead of paper tape.

Seven segment display block ZfK 7500.01

The color display 2D analyser /4/ is controlled by means of a small keyboard PBT 4944-20 which uses as output a byte display built from a row of 8 LED's. In order to improve the readability and in connection the functionality of the handsome unit a seven segment display board (48 * 48 mm²) containing 1 VQE24 and 2 D345 as hex-drivers was built. The display block is built into the keyboard box and allows an improved user interface. Combinations of this display block are used as test display for single board computers.

SIF1000-Centronics adaptor ZfK 7500.02

A number of high-speed graphical printers were supplied and could replace the old 1156 printer at MPS 4944 systems used in the laboratories. This could be achieved using a serial interface module and the corresponding driver software. On the other hand a direct adaptation of the SIF-1000 output to the Centronics port of the FX-1000 printer can be realised using two IC. The advantage results from the fact that neither the hard- nor the software of the MPS must be changed. The adaptor board fits into the butt of the normally used SIF-1000 connector.

References

/1/ Fromm,W.D. et al.; this report p. 105
/2/ Fromm,W.D. et al.; Annual report 1986, ZfK-621(1987)139
/3/ Angermann,H. et al.; Annual report 1985, ZfK-584(1986)104
/4/ Fromm,W.D.; Annual report 1985, ZfK-584(1986)138

COMPACT MULTI-CHANNEL ANALYSER ZfK 5193

W.D. Fromm, H. Angermann and H.G. Ortlepp
Zentralinstitut für Kernforschung, Rossendorf, Bereich KF

For many applications of the MCA technique as preparation and check of detector systems for experiments, control measurements in the nuclear laboratory practice, analysis of the contents of samples e.g. a portable and easy to handle MCA is needed. The earlier on the base of the microcomputer system MPS 4944 produced VKA 4995 /1/ is to bulky, heavy and expensive to fulfill this type of requirements. The development of an compact MCA announced 1980 by Robotron was ceased. Therefore possibilities were searched for to overcome the drawbacks of the VKA 4995 maintaining the MPS 4944 as technological basis of the development. The following measures allowed to compact the MCA into one EGS crate (Fig.1):

- the power supply is located behind the backplane of the MPS using switching regulators,
- the released space at the right hand side of the crate is occupied by the built-in small TV-monitor MON 4944-138,
- the new spectroscopic ADC 4944-135 was incorporated into the system eliminating the need of an additional EGS crate for the analog-to-digital converter,
- the spectra are constructed by means of a dedicated DMA incrementer INC 4944-136 /2/ replacing the dual-width and power consuming DMA-unit 4944-24,
- the today heavily used interfaces V.24, IFSS and Centronics are supported by the interface unit VIP 4944-137 allowing the usage of graphic peripherals (printer, plotter) and the connection to a personal computer,
- the spectra representation (512 channels * 256 intensities, linear autoscaling, logarithmic) is controlled by software using the intelligent graphics display driver GDD 4944-216 eliminating the need for a complex hardware-driven spectra display.

In this manner by maintaining and extending the necessary functionality of the MCA a more cost-effective solution could be achieved.

The ADC 4944-135 is of the Wilkinson-type (50 MHz) and has 3 conversion ranges of 256, 1024 and 4096 channels. The conversion ranges, coincidence mode and waiting time are controlled by the microcomputer. The converted address conforming to SI1.2 is presented at a front panel connector joined by a flat bus cable with the DMA unit INC 4944-136 which can handle addresses of up to 14 bit. Totally 16384 channels with 16 bit capacity are provided. If the capacity of 65535 counts is insufficient extensions to 20 or 24 bit capacity are foreseen by the software taking care of the overflow interrupt of the DMA-unit. The memory region dedicated to the construction of spectra is divided into pieces corresponding to the conversion range set for the ADC. Commands referencing to the spectra (start, clear, input, output) have therefore to be extended by the length (2,1,4) and number (0..N) of the spectrum. As mass storage unit a magnetic tape cassette drive /3/ can be connected. Spectra are written as binary files compatible to the EC 1055. The software for the MCA /4/ is modular structured and easily expandable. As a first application of the MCA time-differential measurements of uranium rods were performed /5/. 15 units of the MCA 5193 will be produced in 1988 by the device construction department.

References

/1/ Bergter,S. and Kühnert,S.; Proc.X.Int.Symp.Nucl.Electr. ZfK 433(1981)Vol.I, p.177

/2/ Kühnert,S.; Hardwarebeschr. 4944-112 Ba, Rossendorf 1986

/3/ Schwarzenberg,F.,Fromm,W.D.; radio,fernsehen,elektronik 35(1986)256

/4/ Fromm,W.D.; Programmbeschr. KVKA, Rossendorf 1987

/5/ Winter,G. et al.; this report p. 110

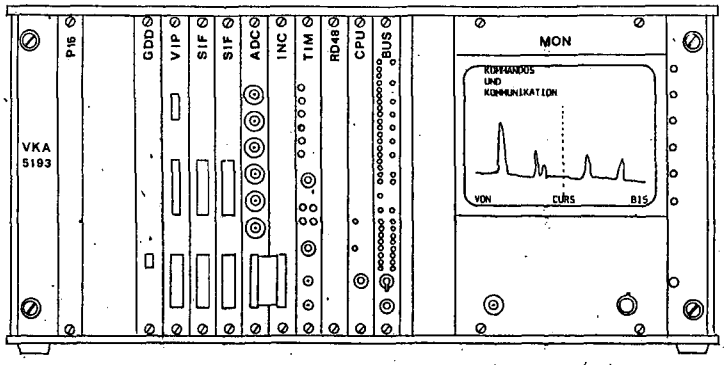

Fig.1 Front view of the MCA 5193 system

DYNAMIC STUDIES AT THE ROSSENDORF GAMMA-CAMERA

W.D. Fromm and R. Bergmann
Zentralinstitut für Kernforschung, Rossendorf, Bereiche KF und RI

The gamma-camera has been equipped with a microprocessor controlled data acquisition system/1/. Recently a major upgrade of the equipment was performed. The paper tape periphery was replaced by a dual magnetic tape cassette drive /2/ providing a reliable and compact storage medium for binary output of the recorded images. The recording format conforms to an international standard allowing the data transfer to the EC1055 computer for a more detailed analysis.
The quantitative evaluation of regions of interest (ROI) in a number of images was implemented using a joystick for the definition of up to 8 different ROI's. A light mark is positioned with the joystick into the two diametrical opposed corners of a rectangle. The number of the so determined ROI is indicated at the keyboard. The outline of the ROI corrected for the pixel size (4 * 4) is then shown overlaying the image. With a keystroke the contents of all ROI's set can be calculated and printed together with a time stamp. The background is estimated using the counts in pixels lying at the border of the rectangle and is corrected for the different numbers of pixels within the ROI and at the surrounding.
The study of the time-dependent distribution of radiopharmaceuticals in the living organism is an important problem. Usually minicomputers equipped with diskdrives are employed to store the events together with time tags in list mode. The inclusion of the 512 kB RAM-Floppy /3/ into the system allows the storage of 64 images (8 kB each). The transfer time for a picture amounts to 72 ms, the time for clearing the memory before starting the measurement of the next time-differential image is essentially the same (2.5 MHz Z80). Therefore a minimal time slice of 1 sec seems to be reasonable. Before starting the differential measurement the time step and the number of records have to be specified. The measurement can also be composed from two rows of expositions with different time bases (fast/slow phenomena). Single images can be called back into image memory. In addition a selectable 32 * 32 pixel area of four images can be shown simultaneously. A hardcopy of the images onto a graphics printer was also implemented. The intensity of every pixel is represented by the linear filling of an 8 * 8 field. Fig.1 shows the central region of a rat after injection of a lipophilic ^{99m}Tc complex. 30 pictures were taken at 10 sec intervals followed by 20 pictures at 1 min intervals.
The recorded data can be stored on magnetic tape cassette and afterwards read back to the RAM-floppy for presentation and evaluation purposes. The storage capacity of the RAM-floppy and one tape cassette are nearly the same (512 and 500 kB respectively).

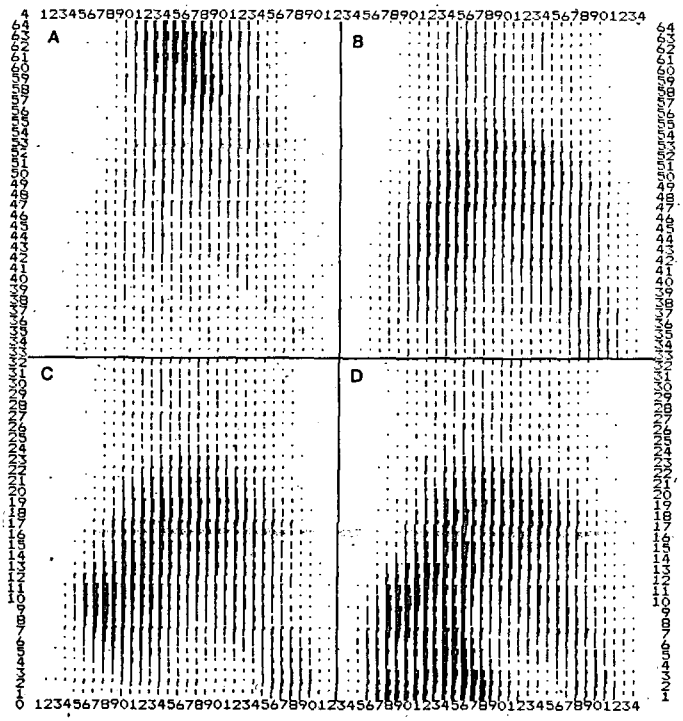

Fig.1 Radioactivity distribution of a rat after injection of ^{99m}Tc: the pictures are taken after 1(A), 3(B), 9(C) and 30(D) min and show activity in the heart, liver, spleen and intestine.

References

/1/ Fromm, W.D.; Gemeinsamer Jahresbericht 1983, ZfK-530(1984)130

/2/ Schwarzenberg, F. and Fromm, W.D.; radio,fernsehen,elektr.35(1986)256

/3/ Ihlenfeld, A. and Riedel, W.; radio,fernsehen,elektr.36(1987)268

A STATIONARY POSITRON CAMERA WITH HIGH-DENSITY AVALANCHE CHAMBERS

W. Enghardt, W.D. Fromm, P. Manfraß and M. Sobiella
Zentralinstitut für Kernforschung, Rossendorf, Bereich KF

In the course of constructing a positron emission tomograph that primarily will be applied to in-vivo tests of radiopharmaceuticals a stationary prototype camera for limited angle tomography was built up following the design of Jeavons et al. /1/. The device became operational in spring 1987. It consists of two detectors in a variable distance. Each detector is a 20 * 20 cm³ multi-wire proportional counter (MWPC) with delay line readout of the coordinates. The MWPC lies between two multi-hole converters that absorb the annihilation radiation and convert it to Compton or photoelectrons. The important MWPC parameters are: anode wire diameter 20 µm, spacing 2 mm; cathode wire diameter 70 µm, spacing 1 mm; cathode-anode distance 3 mm. The multi-hole converters have a sandwich structure: 16 foils of 0.2 mm thick lead-tin-antimony alloy insulated by 0.2 mm thick layers of glass fibre reinforced epoxy resin are glued together. The holes of 1.4 mm diameter were drilled on a 1.4 mm pitch. The converters are operated in the avalanche mode /2/ using a gas mixture of Ne + 6 % Hexan + 2 % i-propanol at normal pressure. The studies lead to these detector parameters are described elsewhere /3/.

Both detectors have an efficiency for 511 keV γ-radiation of about 7 %. The intrinsic spatial resolution amounts to 2.5 mm. The camera sensitivity for a point source in air is 325 cps/MBq at a detector distance of 36 cm. For a homogeneous activity distribution over a field-of-view (FOV) of 8 * 8 * 14 cm³ it decreases to 10 cps/MBq. In the latter case a signal-to-noise ratio of 2 has been measured for 20 MBq in the FOV at a camera time resolution of 40 ns. The spatial resolution of the system has been deduced from a measurement with three line sources of $[^{18}F]$-NaF solution with an integral activity of 10 MBq. The sources were placed in the midplane of the camera, the detector distance was 35 cm. In Fig. 1 the profile through the reconstructed image is displayed. From this a FWHM of 2.9 mm has been evaluated for the line spread function after reconstruction.

In order to study the capability of the camera for quantitation, images of two cylinders (diameters 22 and 20 mm, heights 53 and 32 mm) containing $[^{18}F]$-NaF solution in activity concentrations of 1.8 MBq/ml and 0.9 MBq/ml, respectively were taken. The sources were placed centrally between the two detectors mounted in a distance of 44 cm. Fig. 2 shows a section through a reconstructed plane containing one half of both cylinders. Obviously the concentration ratio of 2 : 1 is rather well reproduced within the statistical errors.

References

/1/ Jeavons A. et al.; Nucl. Instr. Meth. 176 (1980) 89
/2/ Jeavons A. et al.; IEEE Trans. Nucl. Sci. NS-30 (1983) 640
/3/ Manfraß P. et al.; Annual report 1986, ZfK-621 (1987) 128; Nucl. Instr. Meth. (in press)

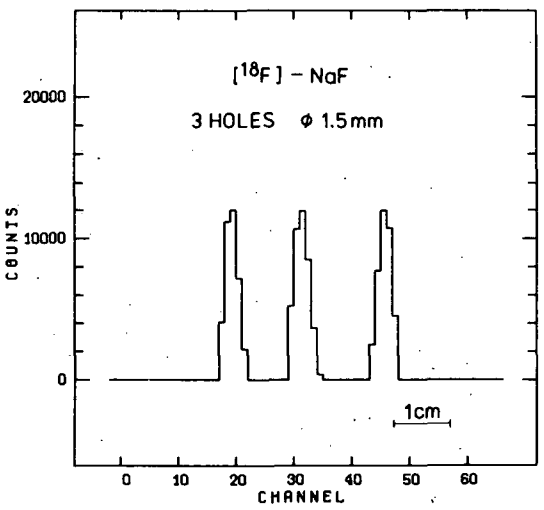

Fig. 1 Section through a plane of the reconstructed image of three line sources (voxel dimensions 1 * 1 * 13 mm³)

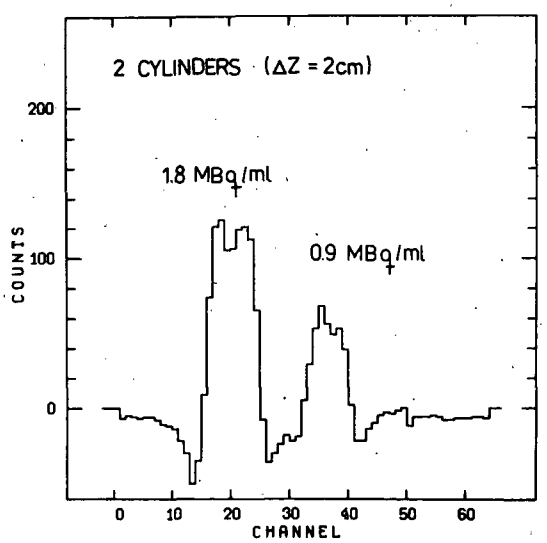

Fig. 2 Section through two uniform cylinders containing activity in a concentration ratio of 2 : 1 (voxel size 3 * 3 * 20 mm³)

THE PROCESSING OF THE STATIONARY POSITRON CAMERA DATA

W. Enghardt, W.D. Fromm and P. Manfraß
Zentralinstitut für Kernforschung, Rossendorf, Bereich KF

The processing scheme for the data delivered by the stationary positron camera /1/ is outlined in Fig. 1. If a coincidence of two γ-rays (γ_1 and γ_2) detected by the chambers D_1 and D_2, respectively is registered, the coordinates of the points where the γ-rays hit the detectors (x_1, y_1, x_2, y_2) are converted to 7-bit words and transferred to a microcomputer via direct memory access. The data are written in list mode to magnetic tape cassettes. Since the transfer rate to this storage device is limited to about 300 events per second, a data preselection is highly desirable. Therefore, events that fall outside the acceptance cone of the camera are rejected before recording. The constraint is deduced from the shift-invariance condition for the point response function, which has to be fulfilled, in order to make the limited angle techniques /2/ of tomographic reconstruction applicable. Depending on the activity distribution and the limits set up to 70 % of the measured events may be skipped. In order to provide a means for finding the correct object position, the data acquisition program simultaneously generates the midplane by backprojection and displays it. By inserting a 512 kByte RAM-floppy /3/ as circular buffer into the system the effective acquisition rate is increased, since 128 k valid events can be stored until the data-intake has to be reduced due to the limited transfer rate to the tape cassettes.

The further processing of the list mode data is performed off-line at the EC 1055 (mainframe) computer. Three-dimensional matrices with up to 16 slices (64 * 64 pixels) of adjustable thickness parallel to the chambers can be handled applying the event-by-event backprojection method and Fourier deconvolution for reconstruction. In order to reduce artifacts in the reconstructed tomograms, spatial nonuniformities of the detector efficiency are corrected for in the backprojection process by introducing weights. These are deduced from the experimentally determined blurring patterns in the detector planes caused by a centrally placed point-like source. The application of this method considerably improves the image quality, especially for objects with low activity gradients, e. g. in brain imaging.

The results of the reconstruction can be rewritten to magnetic tape cassettes for transferring to the FD 4971 colour display, where up to 16 tomographic planes can be simultaneously shown. For further processing, e. g. interactive image manipulation or application of medical software, the reconstructed data may be transferred via magnetic tapes to the EPR 1100/KANDI DS computers of the Clinic for Nuclear Medicine of the Medical Academy Dresden.

References

/1/ Enghardt W. et al.; this report p. 107
/2/ Tam K.C.; Report LBL-10039 (1979)
/3/ Ihlenfeld a. and Riedel W.; Radio, Fernsehen, Elektronik 36 (1987) 268

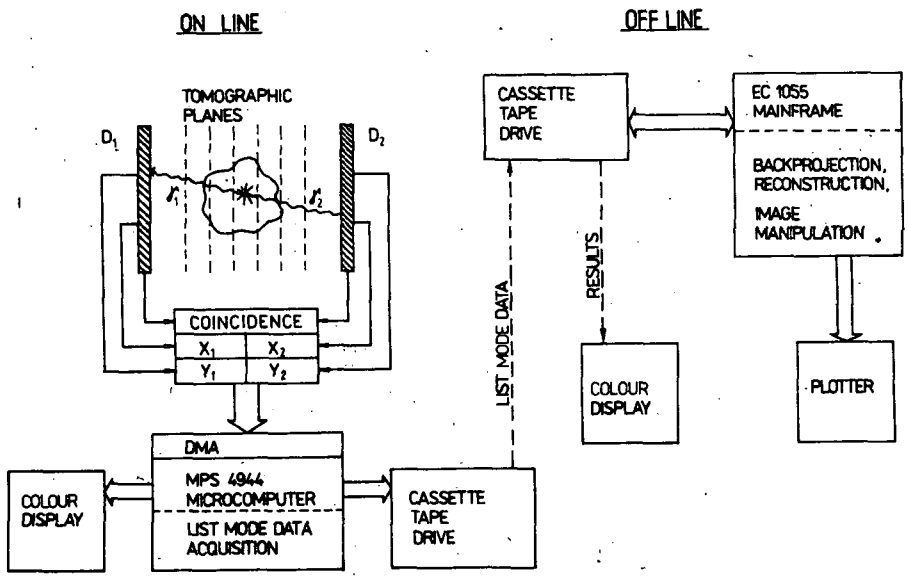

Fig. 1 The stationary positron camera data processing

IN-VIVO IMAGING WITH THE STATIONARY POSITRON CAMERA

W. Enghardt, P. Manfraß, D. Wohlfarth
Zentralinstitut für Kernforschung, Rossendorf, Bereich KF

R. Bergmann, G.J. Beyer, J. Steinbach
Zentralinstitut für Kernforschung, Rossendorf, Bereich RI

R. Bauer
Friedrich-Schiller-Universität, Jena

K. Günther
Karl-Marx-Universität, Leipzig

With the stationary positron camera /1/ first animal studies have been carried out. Skeletons of rats, mice and piglets have been imaged using $[^{18}F]$-NaF, furthermore brain metabolism studies for piglets with $[^{18}F]$-2-fluoro-2-deoxy-D-glucose (FDG) have been started. The positron emitter is produced at the Rossendorf cyclotron via the reaction $^{20}Ne(d,\alpha)^{18}F$ /2/.

In Fig. 1 skeleton images for a wistar rat are presented. About one hour after injection of 42.5 MBq $[^{18}F]$-NaF the rat was sacrificed, in order to allow static imaging. In the first study sagittal images (Fig. 1a) were taken. The activity in the field-of-view (FOV) at the beginning of the study was about 15 MBq. We registered 220 000 events in 90 min. Then the rat was rotated by 90° for transverse imaging. The image of Fig. 1b has been reconstructed from 200 000 events recorded in 120 min. After smoothing the backprojected images by means of Gauss' method and removing the blurring by Fourier deconvolution rather small details of the rat's skeleton can be clearly identified.

Fig. 2 shows sections through the head of a new-born piglet who was sacrificed one hour after administration of 190 MBq of $[^{18}F]$-FDG. Only about 4 % of the activity was found in the brain, i. e. at the beginning of the data acquisition about 5 MBq of activity were deposited in the FOV. Therefore, to reduce the background by scattered and accidental events, the parts of the body outside the FOV have to be carefully shielded or removed. The frontal (Fig. 2a) and sagittal (Fig. 2b) sections have been reconstructed from 450 000 and 400 000 events recorded in 90 and 250 min., respectively. The brain can be easily located in the upper parts of the tomograms.

References

/1/ Enghardt W. et al.; this report p. 107
/2/ Steinbach J. et al.; ZfK-570 (1985) 21

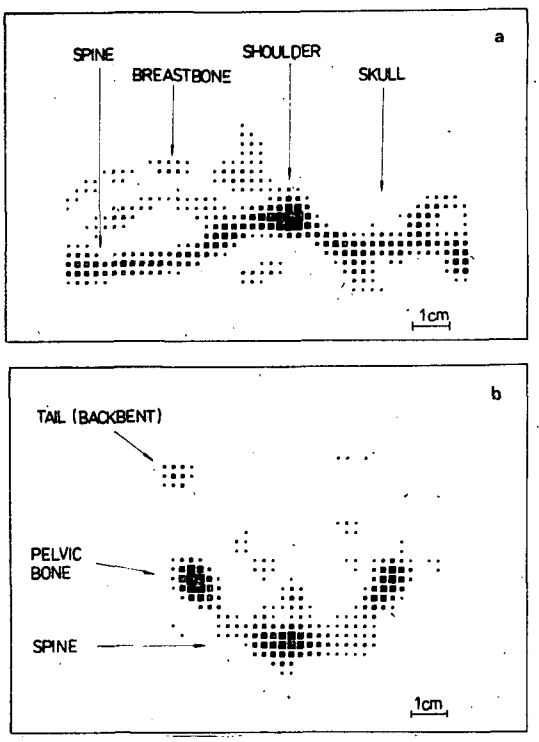

Fig. 1 Reconstructed sections through a rat after injection of [18-F]-NaF; (a) sagittal, (b) transverse

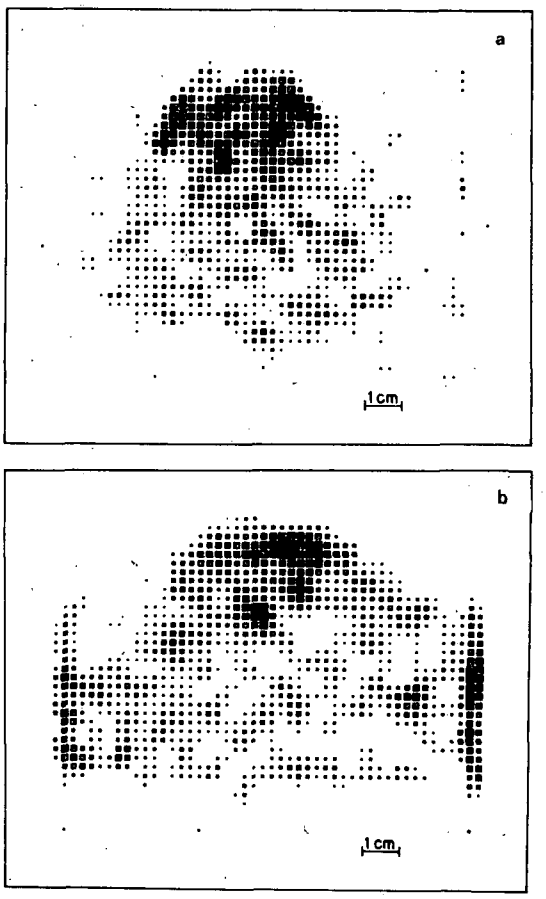

Fig. 2 Reconstructed sections through the head of a piglet after injection of [18-F]-FDG; (a) frontal, (b) sagittal

AN INVESTIGATION OF THE URANIUM DISTRIBUTION IN REACTOR FUEL ELEMENTS

G. Winter, W.D. Fromm, W. Schulze, Th. Scholz, M. Freitag and R. Schwengner
Zentralinstitut für Kernforschung, Rossendorf, Bereich KF

In continuing the investigation of reactor fuel elements /1/ a measurement of the uranium distribution along the axis of the element has been carried out. For this purpose the element was moved continuously with a constant velocity over a Ge(Li) detector and the γ-ray intensities were recorded during successive time periods corresponding to successive sections of the element. The detector was shielded with a lead cap of 1.5 cm thickness having an entrance slit of 1.1 cm width. In order to average over possible azimuthal irregularities of the distribution the element was in addition turned continuously around its axis (2 cycles s^{-1}). The measurements were performed by means of a microcomputer controlled compact multichannel analyser /2/ that was programmed to allow automatic data acquisition and handling. After starting the measurement the γ-ray spectrum was built up in the memory via an incrementing DMA module. Interrupt signals derived cyclically from a timer were used to initiate the transfer of the data within two selected intervals of the spectrum to a buffer and to calculate the differences between these data and those of the preceding transfer which are kept in an other buffer. The spectra of differences are then cyclically written on magnetic cassette tape. After executing the programmed number of time periods the timer and the DMA module were stopped and an EOF mark was written on the tape. Finally, the total spectrum that characterizes the total fuel element was written on tape. The first of the selected intervals of the spectrum contained the energies between 140 and 210 keV belonging to ^{235}U and the second interval contained the 1001 keV line that was indicative for the amount of ^{238}U in the element. Using an average velocity of the longitudinal motion of 0.0672 mm s^{-1} and time periods of 120 s width each the γ-ray intensities were measured for every section of 0.807 cm length. Totally a series of 90 data points corresponding to a total length of 72.6 cm was gathered. The maximum deviation of the velocity from the average value was 0.5 % in a series of 12 measurements. Two elements have been measured twice for checking the geometrical precision of the mechanical equipment. The two distributions obtained agreed within 1 % (see table 1). Due to the large acceptance angle of the collimator not only the section in front of the collimator slit but also neighbouring sections of the element contributed to the measured intensities. Therefore, the sequence of experimental data points was defolded with an experimentally determined response function of the collimator.

For an easy use of the results in further calculations we characterize the distribution along the axis by a mathematical model V(L) containing 5 free parameters: The beginning of the uranium layer relative to the geometrical beginning of the element (BL), the width of the step to the plateau of the distribution (WB), the length of the plateau (PL), the width of the step at the end of the uranium layer (WE) and the relative uranium content in the plateau (MR). The distribution V(L) is described as a product of two step functions $V(L) = S((BL - L)/WB) \cdot S((L - BL - PL)/WE) \cdot MR$, where the step function S(X) reads $S(X) = 1/(\exp(2.257 X + 1.16 X^2 + 0.202 X^3) + 1)$. The values of these parameters characterizing the distribution after defolding are compiled in table 1. The errors are given in parentheses in units of the last decimal. In the cases considered the function V(L) describes the distribution at each point with an accuracy of better than 3 %.

Table 1. Values of the parameters (in units of 0.807 cm) characterizing the uranium distribution in reactor fuel elements (see text).

Nr	BL	WB	PL	WE	MR
38	9.06(2)	0.99(7)	70.51(3)	1.62(6)	32830(90)
39	8.83(2)	1.32(4)	70.48(3)	1.64(4)	32720(60)
43	9.14(2)	1.44(4)	71.39(3)	1.78(4)	32410(60)
43	9.18(2)	1.53(3)	71.32(3)	1.80(4)	32430(60)
44	8.93(2)	1.15(4)	71.14(3)	1.77(4)	32160(60)
45	8.71(2)	1.44(4)	71.09(3)	1.66(4)	32620(60)
49	8.56(2)	1.13(4)	71.32(3)	1.77(4)	32310(60)
50	8.79(2)	1.61(4)	70.91(3)	1.62(4)	32690(60)
50	8.82(2)	1.58(4)	70.86(3)	1.60(5)	32550(60)
51	9.25(2)	0.86(5)	70.43(3)	1.36(5)	32540(60)
55	9.01(2)	1.15(5)	71.24(4)	1.62(5)	32100(70)

References:

/1/ Winter, G. et al.; Annual report 1984, ZfK-559 (1985) 89
/2/ Fromm, W. D.; this report p. 105

NEUTRON LEAKAGE FROM AN URANIUM SPHERE FED WITH 14 MEV NEUTRONS

T. Elfruth, T. Hehl, M. Töpfer, D. Seeliger, K. Seidel, and S. Unholzer
Technische Universität Dresden, Sektion Physik, WB Kernphysik
G. Streubel
WB Strahlenschutzphysik
D. Albert, W. Hansen, C. Reiche, and W. Vogel
Zentralinstitut für Kernforschung Rossendorf, Bereich Reaktorphysik
D.V. Markovskij and G.E. Shatalov
Institut Atomnoi Energii "I.V. Kurchatova", Moskva

In projects of fusion-hybrid-reactors uranium is used for neutron multiplication and energy enhancement. It is placed directly behind the wall of the D-T-plasma torus. At an incidence energy of 14 MeV the neutron number is enlarged in (n,2n), (n,3n) and fission processes. By measuring the neutron leakage from an uranium assembly fed with 14 MeV neutrons and comparing it with neutron transport calculations the data of all neutron interaction and multiplication processes and the transport code are tested.
Such a benchmark was carried out with an one-dimensional assembly, a spherical shell of 6 cm thickness consisting of depleted (to 0.4 % ^{235}U) metallic uranium. The geometrical arrangement is shown in Fig. 1. As neutron source positioned in the sphere centre, the pulsed neutron generator of the Technical University was used. Neutron leakage spectra were measured at detector position D with time-of-flight technique (TOF) and with proton recoil spectrometry (PRS). Eight activation and fission rates were determined at the shell surface. The experimental data could be normalized to one source neutron by means of the α-particle monitor of the generator. Calculations were carried out with the Monte Carlo codes BLANK and MORSE and with the S_n-code ANISN using data from the libraries ENDF/B-IV and ENDL-75. A more detailed description of the experimental and calculation methods are to find in Ref. /1/.
Some results are shown in Fig. 2. Remarkable deviations of the calculated leakage spectra from the measured distributions are observed in the high-energy range, 6 MeV < E < 12 MeV, and for E < 0.4 MeV. In both cases the calculations predict less neutrons. Probably, neutrons emitted from ^{238}U in the preequilibrium stage and in direct reactions are not adequately represented in the library data. The neutron leakage in E = 0.1 - 14 MeV per one source neutron found in the measurement is 2.34 (Neutrons with E < 0.1 MeV contribute to the total leakage with 5 % only). This value is close to the BLANK-ENDL-75 calculation, but different from the calculation with ENDF/B-IV data by 9 % (MORSE) and 17 % (ANISN), respectively.

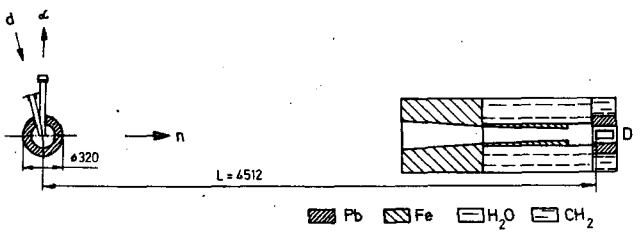

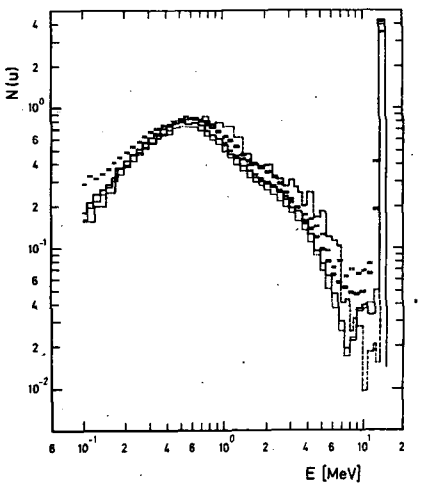

Fig. 1: Geometrical relations of the benchmark.

Fig. 2: Neutron leakage spectra per unit of lethargy and source neutron measured with TOF (ooo) and PRS (xxx) and calculated with BLANK-ENDL-75 (---), ANISN-ENDF/B-IV (...) and MORSE-ENDF/B-IV (——).

Reference

/1/ Elfruth, T. et al.; Atomkernenergie 49 (1987) 121

OPTIMAL NEUTRON SHIELDING BY AN IRON-WATER ASSEMBLY

E. Rodriguez and K. Seidel
Technische Universität Dresden, Sektion Physik, WB Kernphysik
K. Noack
Zentralinstitut für Kernforschung, Rossendorf, Bereich Reaktorphysik

Structural materials of a fusion reactor must sufficiently be shielded from neutron radiation. The superconducting coils of the magnets belong to the most sensitive elements. Radiation damage (displacement of atoms, gas production) and activation are mainly caused by fast neutrons. The fluence of neutrons penetrating the shield with energies $E \geq 0.1$ MeV, normalized to one incident neutron is usually used as measure for the quality of a shield. Neutrons bombarding the inboard shield of a D-T tokamak fusion reactor have 14 MeV energy. A promising arrangement consists of Fe for high-energy neutron moderating by non-elastic interactions followed by H_2O for further neutron moderation by elastic scattering and for absorption. There is limited place between plasma chamber and magnet so that the Fe to H_2O composition must be optimized at fixed total thickness of the shield.
With this aim, the slab assembly shown in Fig. 1 as insertion has been investigated. The total thickness is d = 60 cm, the slabs have sizes of 100 cm x 100 cm. With a point source of 14 MeV neutrons at Q, the neutron fluence at detector position D was calculated with the three-dimensional Monte Carlo code MORSE and group data from the library DLC-37 for several Fe-thicknesses (d_{Fe}). Fig. 1 shows some results.

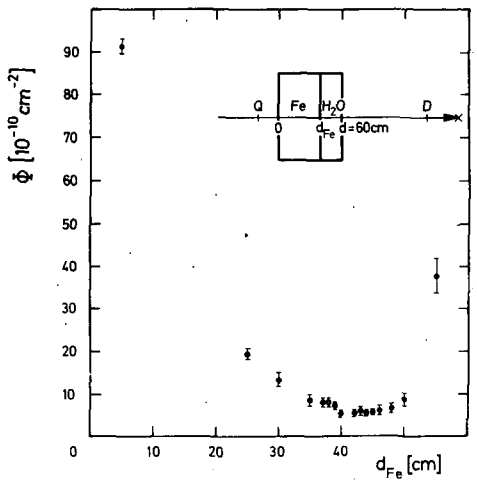

Fig. 1:
Fluence of neutrons arriving at detector position D = 426 cm with $E \geq 0.1$ MeV per one 14 MeV source neutron starting at Q = -5 cm as function of the Fe-slab thickness at fixed total thickness. A schematic representation of the geometrical arrangement is inserted. The x - axis goes through the centres of the slabs.

The fluence minimum obtained from these calculated points by a polynomial fit is at $d_{Fe} = (38.30 \pm 0.05)$ cm.
In addition, energy and time-of-arrival spectra as well as time-energy correlations were calculated. More details are to find in Ref. /1/.

Reference

/1/ Rodriguez, E., Diplomarbeit, TU Dresden, 1987

TEST OF A TRITIUM ADSORPTION SYSTEM FOR A HIGH FLUX NEUTRON GENERATOR

U. Gohs
Technische Universität Dresden, Sektion Physik, WB Kernphysik

A detritiation system /1/ has been elaborated for the high flux neutron generator INGE-1. One component of this system is the tritium adsorption system (TAS-1) for cleaning the generator exhaust gas. TAS-1 was constructed on the base of experiments to the catalytic oxidation of hydrogen isotopes in inert gas atmosphere and in an atmosphere involving oxygen /2/.
TAS-1 is based on the catalytic oxidation and adsorption method. The oxidation of hydrogen isotopes takes place in a reaction tube filled with palladium catalyst (Leuna-Kontakt-7748) and copper oxide catalyst (Leuna-Kontakt-4493). The hydrogen isotopes captured by this system will be adsorbed on the adsorbent (Wolfen-Zeosorb-5A) as oxide.

The tritium adsorption system was tested at the neutron generator INGE-1 (table 1). In using precious metal catalyst the decontamination factor at ambient temperature increase to a value greater than 10^3. In order to meet the requirements concerning the allowed maximum tritium concentration in the generator exhaust gas on different conditions TAS-1 was also tested in inert gas atmosphere.

Table 1

Experimental conditions on the neutron generator INGE-1

Hydrogen isotopes in exhaust gas	H_2, D_2
Hydrogen isotopes concentration	1.0 - 2.6 vol %
Oxygen concentration	8 - 11 vol %
Generator exhaust stream	0.08 - 0.18 $l \cdot h^{-1}$

From these results the conclusion can be drawn that the tritium adsorption system guarantees on neutron generator conditions a decontamination factor greater than 10^6 for 600 h if the reaction tube is heated up to 170°C.

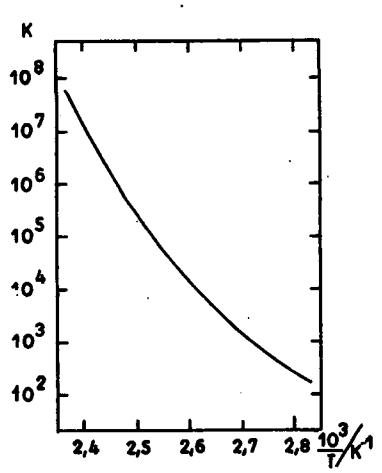

Fig. 1
Decontamination factor in inert gas atmosphere

REFERENCES

/1/ Gohs, U., ZfK-621 (1986) 142
/2/ Bittner, M., ZfK-621 (1986) 143

MYLAR FOIL AS AN EXIT WINDOW FOR AN EXTERNAL BEAM

D. Lehmann
Karl-Marx-Universität Leipzig, Sektion Physik, WB Angewandte Kernphysik

The essential element of an external beam device is an appropriate window for the exit of the ion beam from the accelerator vacuum. In this study we investigated the possibility to take Mylar foil, several years ago available under the trade name of Hostaphan (Kalle AG), which was not developed especially for such a purpose.
We checked two foil thicknesses, 3.8 µm (R3.8) and about 6 µm (R6). For these tests a vacuum chamber was assembled from commercially available components. The foil was glued vacuum tight on a special frame with EGK 19 epoxy resin. Then the whole device was mounted on the beam pipe. With this set-up we were able to adjust the gas pressure on either side of the foil window separately. The following results were obtained:
- the two foils were vacuum tight against atmospheric pressure. A final vacuum near 1 mPa was reached, which is comparable to the case without the test cell.
- The foil windows withstood slow and fast one-sided pressure changes.

For penetration experiments we only took R3.8 foils and protons with energies between 1550 and 1700 keV. In the windows used the projectiles lost about 100 keV energy. Ion currents of 0.5 to 5 nA and a pressure difference of 10 kPa between the front ant rear sides of the window did not rupture the foil or change its vacuum tightness for some hours (about one day), but the foil was stretched across the diaphragm hole and changed its colour to dark brown inside the beam spot. The change of experimental conditions to atmospheric pressure on one side of the window and an increase of the ion current to about 20 nA ruptured the foil already a few minutes later.
For both foils backscattering experiments with 1600 keV protons in vacuum showed a continuous decrease of their thickness to 60 % after irradiation with a charge of 50 µC (spot area about 0.5 mm^2) and also an oxygen loss near the surface in the same order (cf. fig. 1 a). Elastic recoil detection with He projectiles showed a similar behaviour in the case of hydrogen (fig. 1 b), which is known from the literature, too /1/.
To sum up, Hostaphan foils are appropriate for external beam facilities which work with a gas pressure near 10 kPa and with projectile beams in the order of 1 nA.

R e f e r e n c e s

/1/ L. Calcagno and G. Foti, Appl. Phys. Lett. 47 (1985) 363

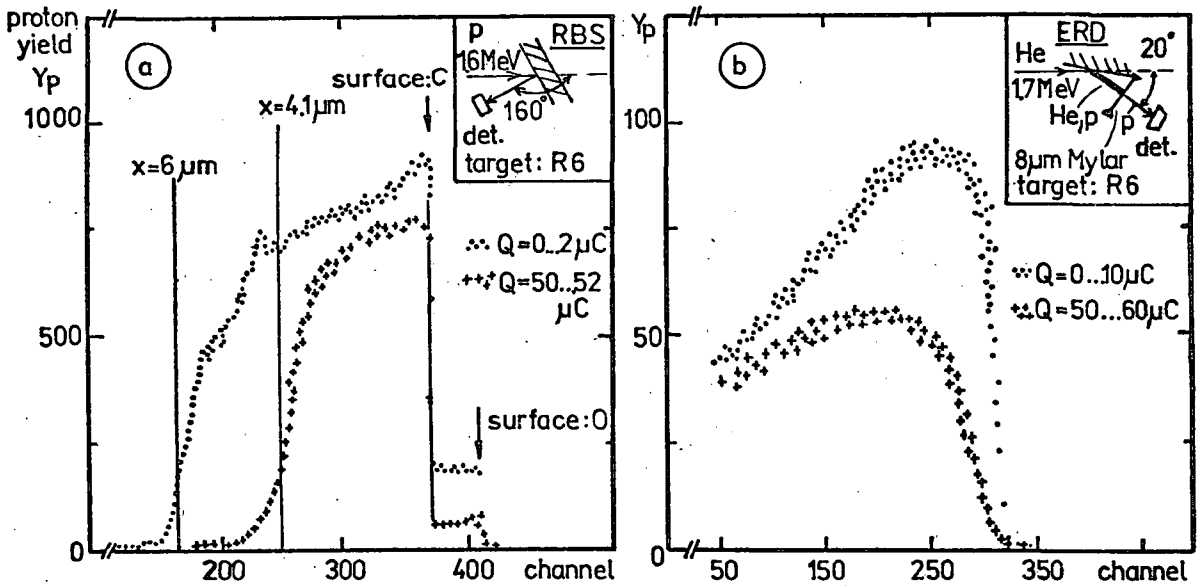

Fig. 1: Ion beam analysis of Hostaphan R6: (a) RBS spectra; (b) He induced ERD spectra

COMPUTATIONAL METHODS AND CODES

OS/8 FORTRAN IV ROUTINES FOR USE WITH CAMAC

U. Katesscenka

Staatliches Amt für Atomsicherheit und Strahlenschutz, Berlin

G. Pausch

Technische Universität Dresden, Sektion Physik, WB Angewandte Kernphysik

For the purpose of general capability of communicating with CAMAC-interfaced devices, user-controlled synchronizing program execution due to events associated with such CAMAC facilities, and Boolean bit manipulating of CAMAC data in the high-level programming language FORTRAN IV under the OS/8 operating system in a TPA-i computer environment /1,2/ equipped with a CAM 1.02 CAMAC crate controller, this report presents an implemented set of software subroutines recommended in /3,4,5,6/ for use with the CAMAC modular instrumentation and interface system of EUR 4100 /7/:

- Initiate CAMAC crate by CALL CINI (c)
- Perform CAMAC control by CALL CONT (n,a,f) or xq = CONT (n,a,f)
- Execute CAMAC read or write 24 bits in length by CALL CDAT (n,a,f,d) or xq = CDAT (n,a,f,d)
- Decode scalar variables assigned to the COMMON block named CMC reflecting the crate controller register state and the status of the preceding CAMAC action by CALL CSTA
- Link CAMAC-graded LAMs to statement labels in the main program suitable for switching to user-defined processes in response to the recognition of a LAM interrupt by K = 0; CALL LINK (gl1# i, gl2#j, ...,gln#l,K); GOTO (lab1,lab2,...,labn), K
- Return from user's LAM service by CALL LAMR
- Loose CAMAC-graded LAMs from the link to user processes by CALL LOOS
- Rotate 24-bit data left or right by d = ISHI (d1,K)
- Evaluate logical AND - 24-bit parallel - by d = IAND (d1,d2)

All presented parameters express data values in the FORTRAN IV language and may be of INTEGER or REAL type internally taken as truncated integers:

c,n,a - components of a CAMAC address: crate number, station number, subaddress

f - function code for a CAMAC action

d - CAMAC data stored in a storage entity capable of containing 24 bits. CAMAC bit 1 occupies the low-order bit position and bit 24 occupies the twenty-fourth position to the left (sign bit)

xq - status information concerning the initiated CAMAC cycle: The lowest-order bit contains the complement of the Q response; the next bit to the left contains the complement of X

gln#l - assigned graded LAM number l in the n-th position of the parameter list covering the n-th statement label in the label list of the GOTO statement

labn - executable statement label in the main program calling the LINK routine

The present software approach is accomplished by coding in statement syntax of the OS/8 SLANG4 assembler, part of the OS/8 FORTRAN IV system. The implemented routines make use of the error traceback feature extensively offered by the run-time system. In order to receive information on the effect of the requested CAMAC action at once, any subroutines mentioned above can also be used as INTEGER or REAL function returning the value of X and Q response as the function value. To a result of the LINK procedure the OS/8 FORTRAN Run Time System, FRTS, will be strongly overlaid in some parts, effecting its ability to handle CAMAC interrupts for real-time applications. By means of K=0 the computed GOTO statement will be caused to work as CONTINUE statement bypassing the bounds of strict standard FORTRAN according to which no type can be assigned to the label to identify a service routine which is intended to be executed out of sequence with respect to the calling program. It is the responsibility of the user to reset the LAM request and also to locate the LAM source at multiple source LOOK-AT-ME logic.

References:

/1/ OS/8 handbook, Digital Equipment Corp. Maynard, Mass., 1974

/2/ TPA-i computer manual, KFKI Budapest, 1975

/3/ From W.D, Tietze B.; ZfK - 385 (1979) 260

/4/ Fromm W.D; ZfK -385 (1979) 258

/5/ Fromm W.D; ZfK -408 (1980) 184

/6/ Fromm W.D; ZfK -443 (1981) 220

/7/ CAMAC - A modular instrumentation system for data handling EUR 4100e, ECSC-EEC-EAEC, Brussels-Luxembourg, 1980

PERSONAL COMPUTER PROGRAM PACKAGE FOR ION-OPTICAL PROBLEMS

J. Teichert and D. Janssen
Zentralinstitut für Kernforschung, Rossendorf, Bereich KF
M.A. Tiunov
Institute of Nuclear Research, Novosibirsk, USSR

In 1987 activities were started to develope a program package for the solution of ion-optical problems at personal computers (PC). Thereby much care has been taken making the programs easily to use by means of interactive working and many compter graphics. Although the program package is used mainly to design and optimize the optical column of an ion micro beam system it may be applied in many other fields like particle transport in electrostatic accelerators, electron-optical devices, ion-source development or particle detector design. At present the package contains two programs: the codes SAM-P and TRANS-P.

The program SAM-P solves the electrostatic or magnetostatic boundary problem for system with cylindrical symmetry using the charge-density method /1/. It is the improved PC version of the Novosibirsk's SAM code /2/ and allows the calculation of field or potential distributions and of particle trajectories (ray tracing). The Figure 1 shows the equipotentials in an electrostatic asymmetric einzel lens calculated with SAM-P. Furthermore the code computes the cardinal elements and aberration coefficients up to third order for electrostatic and magnetic lenses.

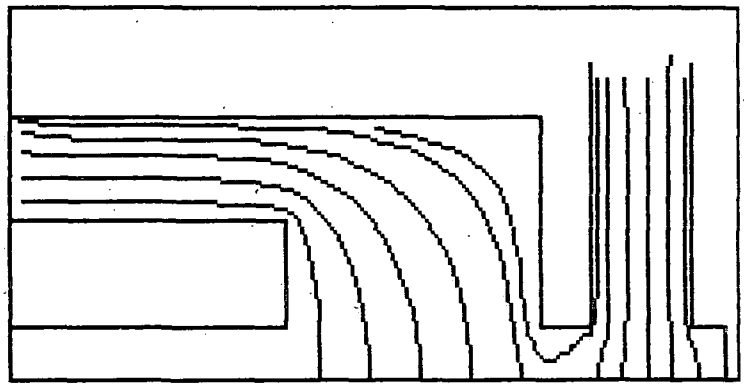

Fig. 1
Equipotential map of an asymmetric three electrode einzel lens.

The third-order particle transport program TRANS-P is the modified and extended version of the TRANS-86 code /3/ which based on the matrix method. It allows to synthesize interactively particle-optical systems consisting of round lenses, electrostatic and magnetic deflection systems, quadrupoles, Wien-filters, or magnetic sector fields. The code calculates optical properties like distortion or resolution, emittance plots or intensity distributions. In a special part of TRANS-P the effects disaligned optical elements may be investigated.

References

/1/ Renau, A. et al., J. Phys. E 15 (1982) 347

/2/ Tiunov, M.A., Fomel, B.M. and Jakovlev, B.P.; preprint 87-35, INR Novosibirsk 1987

/3/ Teichert, J., ZfK-Report, in press

BASIC PROGRAM TO MODELLING OF RBS SPECTRA ON THE MICROCOMPUTER OF THE EDR 184

F. Plier and H.-E. Zschau
Karl Marx Universität Leipzig, Sektion Physik, WB Angewandte Kernphysik

A BASIC program was developed for the multichannel analyser EDR 184 (ZWG Berlin) to the effective preparation and planning of RBS measurements with He^+ions on thick or thin, amorphous targets. It allows the simulating of backscattering spectra on targets consisted of maximal 8 elements for different experimental conditions. The depth dependence of concentrations of these elements can vary in 5 steps. Figure 1 shows schematically the basis idea used in program [1]. A minimal microlayer thickness of Δt=10 nm and a table of stopping power produced for the composition of target are applied to the calculations of the energies ${}_nE_1$ and ${}_nE_3$.

The program realizes the following tasks :

a) the table of stopping power is produced for the composition of the target with help of [2]
b) calculation of the files ${}_nE_1$ and ${}_nE_3$
c) element- and microlayerwise computation of the scattering yields and sorting and summing of these in a "multichannel analyser" with 400 channels
d) consideration of the detector resolution with help of a Gauß-filter (the energy straggling is not taken into account)
e) representation of the backscattering spectrum or of a spectrum component for a targetelement on a tv-screen

Figure 2 shows a backscattering spectrum modelled with the introduced programm for a five layer $Al_xGa_{1-x}As/GaAs$ structur [3].

REFERENCES

[1] Wei-Kan Chu, J.W. Mayer,M.-A. Nicolet, Backscattering Spectrometry, Academic Press, New York, 1978
[2] H.H. Andersen, J.F. Ziegler, The Stopping Power and Ranges of Ions in Matter, Vol.4, Pergamon Press, New York, 1977
[3] R. Flagmeyer, H.-E. Zschau, A. Koch, Annual report, ZfK 621,71,1986

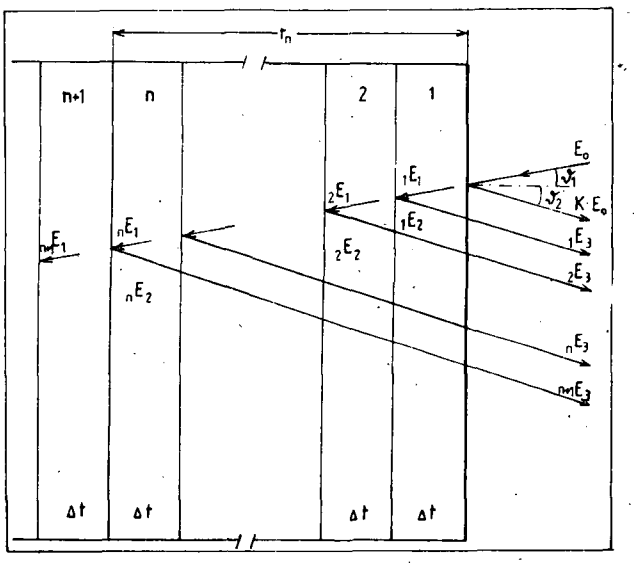

Fig.1: Concept and symbols used in the numerical method of calculating the energies ${}_nE_1$ befor and ${}_nE_2$ after the scattering at depth t_n and the corresponding detected energy ${}_nE_3$.The sample is divided in equidistant microlayers of the thickness Δt.

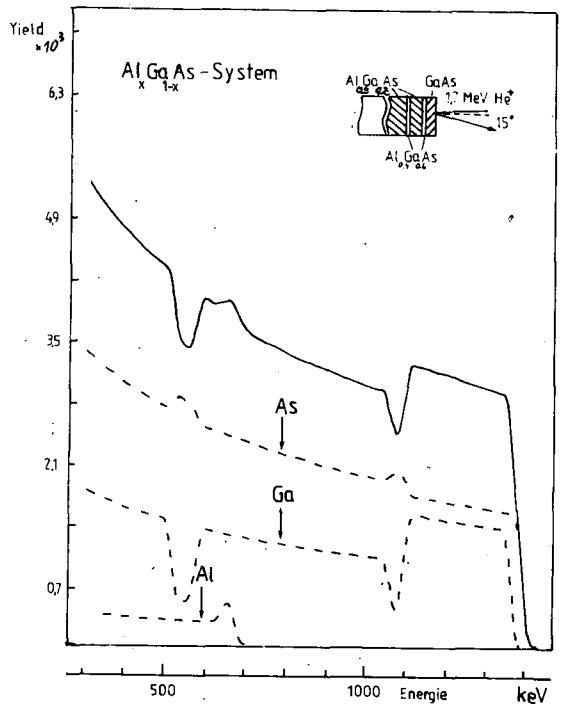

Fig.2: Backscattering spectrum for 1.7 MeV He^+ions incident random on 5-layer $Al_xGa_{1-x}As/GaAs$ structur. The scattering angle is θ =160°. Thickness and x values of the different layers are given in [3]. The dashed linies are the components of the spectrum.

LIST OF PUBLICATIONS, ACADEMIC PROMOTIONS, LECTURES AND CONFERENCE CONTRIBUTIONS, SCIENTIFIC MEETINGS, PATENTS AND AWARDS OF HONOUR

ZENTRALINSTITUT FÜR KERNFORSCHUNG, ROSSENDORF, BEREICH KF

VERÖFFENTLICHUNGEN

Ableev, V.G., G.G. Vorobev, Ch. Dimitrov, V.F. Dimitriev, S.M. Elisejev, S.A. Saporoshets, V.I. Inosemtsev, A.P. Kobushkin, A.G. Malinin, B. Naumann, L. Naumann, W. Neubert, A.A. Nomofilov, L. Penchev, N.M. Piskunov, I.M. Sitnik, E.A. Strokovsky, L.N. Strunov, V.I. Sharov
Peresaryadka p(^{3}He,t) pri impulsakh 4,4-18,3 GeV/c s roshdenijem delta-isobar
Preprint JINR Dubna P1-86-435, Submitted to Jad. Fiz

Ableev, V.G., G.G. Vorobev, S. Dshemuchadse, Ch. Dimitrov, A.P. Kobushkin, B. Kühn, P.K. Manyakov, L. Naumann, W. Neubert, A.A. Nomofilov, N.M. Piskunov, I.M. Sitnik, E.A. Strokovsky, L.N. Strunov, S. Tesch, E.A. Tshernykh, V.I. Sharov, S.A. Saporoshets
Search for Exotic Longlived Dibaryons
JINR Dubna Rapid Communications No. 13-85

Ableev, V.G., S.M. Elisejev, V.I. Inosemtsew, B. Naumann, L. Naumann, A.A. Nomofilov, N.M. Piskunov, I.M. Sitnik, E.A. Strokovsky, L.N. Strunov, V.I. Sharov, S.A. Saporoshets, Ch. Dimitrov, L. Penchev, A.P. Kobushkin, W. Neubert
Observation of the dominance of the target Δ-excitation and their collective nature in the (^{3}He,t) charge exchange at high energies
JINR Dubna E1-87-246
Contribution to XI. Int. Conf. an Particles and Nuclei (PANIC-87), Kyoto, Japan 1987

Ableev, V.G., Ch. Dimitrov, S.M. Elisejev, S.A. Saporoshets, V.I. Inosemtsev, A.G. Malinin, B. Naumann, L. Naumann, N.M. Piskunov, I.M. Sitnik, E.A. Strokovsky, L.N. Strunov, V.I. Sharov
Peresaryadka relativistkich yader Helia-3 v tritoni na uglorode s vosbushdeniem isobar v yadre-misheni
JINR Dubna PI-87-374

Ableev, V.G., B. Naumann, A.A. Nomofilov, N.M. Piskunov, V.I. Sharov, I.M. Sitnik, E.A. Strokovsky, L.N. Strunov, G.G. Vorobev, S.A. Saporoshets, S. Dshemuchadse, S. Tesch, A. Filipowski
Diffraction scattering of alpha particles on C, Al, Cu and Pb at 17.9 GeV/c
ZfK-607 (1986)

Andrae, H., H.-D. Geiler, E. Glaser, G. Goetz, M. Wagner, K.-H. Heinig
Explosive Crystallization of Ion-Implanted Si-Layers
Nucl. Instrum. Methods 19/20 (1987) 571

Andrae, G., E. Glaser, M. Wagner, H.-D. Geiler, G. Goetz, H. Bartsch, K.-H. Heinig, K. Hennig
Explosive Crystallization in Amorphous Si-Layers
J. de Physique E-MRS XII (1987) 157

Andronenko, L.N., L.A. Vaishnene, A.A. Kotov, M.N. Nesterov, N.A. Tarasov, W. Neubert
Oelenije vysokovozbushdjonnikh yader
Particles and Nuclei 18 (1987) 685

Andronenko, L.N., A.A. Kotov, L.A. Vaishnene, W. Neubert
Mass loss and linear momentum transfer in 1 GeV proton induced reactions on U, Bi and Sm
Proceedings XI. Int. Conf. PANIC'87, Kyoto, April 1987

Armigliato, A., S. Guimaraes, S. Solmi, R. Kögler, E. Wieser
Comparison of Boron Diffusivity During Rapid Thermal Annealing in Predamaged, Preamorphized and Crystalline Silicon
Nucl. Instr. Methods B 19/20 (1987) 512

Baither, D., D. Panknin, E. Wieser
Residual defects after light pulse annealing of implanted silicon
phys. stat. sol. (a) 102 (1987) 679

Balagurov, A.M., F. Prokert, B.N. Savenko
Phase Transition Effects in the Inkommensurate Modulated Single Crystal of $Sr_{0.7}Ba_{0.3}Nb_2O_6$
phys. stat. sol. (a) 103 (1987) 131

Barz, H.W., J. Bondorf, R. Donangelo, J. Lopez, H. Schulz
Ternary versus Binary Fragmentation Prozesses
Phys. Lett. B 194 (1987) 459

Barz, H.W., J. Bondorf, R. Donangelo, H. Schulz, K. Sneppen
Isotope Distribution in Nuclear Multifragmentation
Phys. Lett. B 191 (1987) 232

Barz, H.W., J. Bondorf, H. Schulz
On the Limiting Excitation Energy of Nuclei
Phys. Lett. B 184 (1987) 125

Barz, H.W., J. Bondorf, H. Schulz
Energy Spectra of Fragments Calculated with the Model of the Statistical Multifragmentation of Nuclei
Nucl. Phys. A 462 (1987) 742

Barz, H.W., J.P. Bondorf, H. Schulz, L.N. Andronenko, L.A. Vaishnene, W. Neubert
Onset of multifragmentation dominance at 1 GeV proton-induced nuclear reaction for target nuclei with A ≤ 160
Nucl. Phys. A 460 (1986) 714

Barz, H.W., B. Kämpfer, B. Lukacs, K. Martinas, Gy. Wolf
Deconfinement transition in anisotropic matter
Phys. Lett. B 194 (1987) 15

Barz, H.W., B. Kämpfer, L.P. Csernai, B. Lukacs
Two-fluid hydrodynamics applied to the deconfinement transition in the fragmentation region in ultra-relativistic nuclear collisions
Nucl. Phys. A 465 (1987) 743

Barz, H.W., H. Müller, H. Schulz
A Statistical Model for Multiparticle Production in Hadron-Hadron Interaction
Preprint NBI-87-34 (1987)

Bergmann, R., R. Bauer, D. Hoyer, M. Kretzschmar, G. Kampf, H. Schubert, W. Enghardt, P. Manfraß, J. Steinbach, K. Günther, G.J. Beyer, U. Zwiener, W.G. Franke
Erste tierexperimentelle Ergebnisse mit PET
Jubiläumskongreß für pathologische und klinische Physiologie der DDR
Jena, September 1987

Betzl, M.
Bericht über Internationale Winterschule Neutronenstreuung 1987
Kernenergie 30 (1987) 472; VfK-Mitteilungen 22 (1987) H. 2, 29

Betzl, M., K. Feldmann
Progress in Neutron Time-of-Flight Texture Studies at Pulsed Reactors
Proc. of XII. Conference on Physical Metallurgy,
Katowice-Kozubnik, Vol. 1, 223 (1987)

Bischoff, L., D. Mademann, K. Trützschler, G. Zschornack
Der Einsatz von Mikrostreifendetektoren in der winkeldispersiven Röntgenspektrometrie
Exp. Techn. Physik 35 (1987) 153

Dienel, G., U. Kreißig, E. Richter
Wear behaviour of ion implanted steel surfaces
Vacuum 36 (1986) 813

Enghardt, W., K.H. Kaun, H. Prade, J. Blümlein, K. Lanius
Limits on Heavy Axion Production from the reaction n(p,a)d
ZfK- 617 (1987)
Z. Phys. C, Particles and Fields, 35 (1987) 511
Contributions Int. Europhys. Conf. on High Energy Physics
Uppsala, 25 June - 1 July 1987
1987 Int. Symp. on Electron and Photon Interactions
Hamburg, July 1987

Enghardt, W., H. Prade, H.U. Jäger, I. Käubler, H.J. Keller, L.K. Kostov, F. Stary
Microscopic Structure of Semi-Magic Nuclei with 82 Neutrons or 50 Protons
Proc. 7th Int. Summer School on Nuclear Physics, Neutron Physics and Nuclear Energy,
Varna, 22. - 29. 9. 1985
Bulg. Academy of Sciences, Nuclear Energy 25 (1987) 227

Ertel, A., M. Betzl, P. Paufler, W. Voitus
Application of Neutron Diffraction Methods to Texture Studies on Natural Rock Salts
Cryst. Res. and Techn. 22 (1987) 209

Ertel, A., H. Kämpf, M. Betzl
Texture investigation of natural rock salt using neutron diffraction
Geologicky Zbornik-Geologica Carpathica, 38, 1, Bratislava (1987) 3

Fuentes, L., K. Feldmann, K. Walther, L.P. Drechsler, I. Dörfel, E.N. Vlassova, V.I. Matorin, M. Betzl
Texture Investigations of MnAl-Magnets by Neutron Time-of-Flight Diffraction
Cryst. Res. and Techn. 22 (1987) 449

Gersch, H.U.
Coulomb Final State Interaction in Identical Boson Interferometry
Z. Phys. A - Atomic Nuclei 326 (1987) 115

Gersch, H.U., W.G. Antonenko, M.A. Wasiljev, Ju.I. Grigorian, V.I. Manko
Physikalische Grundlagen und Methoden der Interferometrie von K-Mesonen aus der Wechselwirkung hochenergetischer Kerne (in russisch)
IAE-4318/2 Moskau 1986

Gippner, P., K.D. Schilling, W. Seidel, F. Stary, E. Will, H. Sodan, S.M. Lukyanov, G.G. Chubarian, Yu.E. Penionzhkevich, V.S. Salamatin, R. Schmidt, A. Popp
Energy-mass distributions observed in heavy-ion collisions leading to composite systems with Z = 100
Proc. 16th Int. Symp. on Nuclear Physics-Dynamics of Heavy-Ion Collisions, Gaußig, 10.-14.11.1986
ZfK-610 (1986) 42

Goncharova, N.G., A.N. Golzov, H.R. Kissener
Particle photodisintegration channels of ^{14}C
Nucl. Phys. A 462 (1987) 367

Golzov, A.N., N.G. Goncharova, H.R. Kissener
Stretched M 4 configurations in ^{14}C and ^{14}N
Nucl. Phys. A 462 (1987) 376

Gudima, K.K., G. Röpke, V.D. Toneev, H. Schulz
Entropy of a System Formed in Heavy Ion Collisions
Yad. Fiz. 45 (1987) 80

Haubold, H.J., B. Kämpfer
The LMC Inpernova as a probe for the outcome of stellar core collapse
Astron. Nachr. (1987) 308

Heera, V., B. Rauschenbach
On the calculation of multiplicities of quasicrystal diffraction spots
phys. stat. sol. (a) 143 (1987) K1

Heera, V., B. Rauschenbach
Some remarks on indexing of quasicrystal diffraction spots
phys. stat. sol. (b) 142 (1987) K97

Heera, V., B. Rauschenbach
On the calculations of the multiplicities of quasicrystal diffraction spots
phys. stat. sol. (b) 143 (1987) K1

Heidel, K., H.-G. Ortlepp
Zeitnahme an Subnanosekunden-Impulsen (in russisch)
Report JINR R13-87-184 (1987)

Helming, K., B. Rauschenbach
Determination of implantation-induced textures by electron diffraction
phys. stat. sol. (b) 138 (1986) K1

Hennig, K., K. Feldmann
Teksturnaja nejtronografija
Proc. of the V. Intern. Neutron School VIK Dubna, (1987) 452

Hermann, H., N. Mattern, W. Matz
Magnetic and structural properties of rapidly quenched ivouboron metallic glasses
phys. stat. sol. (6) 140 (1987) 581

Jäger, H.U.
Improved modeling of oxygen depth profiles in high dose oxygen-implanted silicon
phys. stat. sol. (a) 103 (1987) K75

Just, G., W.D. Fromm, H. Zwanziger
Computer assisted INAA measurements and statistical feature extraction in raw material exploration
Proceedings of the 4th Meeting on Nuclear Analytical Methods, Dresden, May 4-8. 1987, Vol. I, p. 231

Just, G., E.J. Langrock, W.D. Fromm, V.H. Chanto Arguedas
Computer aided INAA measurements and geochemical classification of various basaltic rocks from Costa Rica
Proceedings of the 4th Meeting on Nuclear Analytical Methods, Dresden, May 4-8, 1987, Vol. I. p. 269

Kachurin, G.A., I.E. Tyshenko, L.I. Fedina, E. Wieser, Ch. Weise
High Temperature Implantation of Silicon by B^+ and BF_2^+ Ions
phys. stat. sol. (a) 102 (1987) 265

Kachurin, G.A., I.E. Tyshenko, M. Voelskow
Legirovanie kremnia ionami bora pri temperaturach oblutschenia 600 - 1100 °C
Fiz. tekn. poluprov. 21 (1987) 1193

Kämpf, H., A. Ertel, P. Bankwitz, M. Betzl, G. Zänker
Texturuntersuchungen an Salinargesteinen mittels winkeldispersiver Neutronentexturanalyse - erste Ergebnisse
Zeitschr. f. angew. Geologie 33 (1987) 104

Kämpfer, B.
Phenomenology of cosmic phase transitions
Astron. Nachr. (1987) 303

Kämpfer, B., H.W. Barz, B. Lukacs
Relativistic Hydrodynamics in Curvilinear Coordinates
Experimentelle Technik der Physik 35 (1987) I, 13; II, 135

Kämpfer, B., H.W. Barz, B. Lukacs
Quark-gluon plasma formation in relativistic heavy ion collisions within the hydrodynamic description
Acta Phys. Slov. 37 (1987) 137

Kämpfer, B., B. Lukacs, G. Paal
Entropy production in tepid inflation
Phys. Lett. B 198 (1987) 17

Käubler, L., W. Enghardt, H. Prade, F. Stary, P. Carle, L.O. Norlin, K.-G. Rensfelt, U. Rosengard
The g-factor of the 10^+ isomer in ^{140}Ce and the temperature dependence of the parumagnetism of Ce in BaO
Proc. 7th Int. Conf. on Hyperfine Interactions, Bangalore, India, 8.-12.9.1986, Abstracts of Invited and Contributed Papers, DG:
Hyperfine Interactions 34 (1987) 381

Käubler, L., W. Enghardt, H. Prade, F. Stary, P. Carl/e, L.O. Norlin, K.-G. Rensfelt, U. Rosengard
The magnetic moment of the 10^+ isomer in ^{140}Ce and temperature dependence of the paramagnetism for Ce ions in BaO
Hyperfine Interactions 34 (1987) 381

Kirchbach, M.
Meson-exchange effects on 0^+ - 0^- beta-decay transitions in A=206 nuclei
Nucl. Phys. A 465 (1987) 705

Kirchbach, M.
Constraints on parity mixing matrix elements from hard-pion exchange corrections to first-forbidden beta decays
J. Phys. G: Nucl. Phys. 13 (1987) 135

Kirchbach, M.; H. Reinhardt
On the A-dependence of the meson-exchange corrections to the axial-charge density for n $s_{1/2}$ - n'$p_{1/2}$ β-transitions
NBI-Preprint 87-79 (1987)

Kissener, H.R., I. Rotter, N.G. Goncharova
Microscopic studies of electric dipole resonances in 1p shell nuclei
Fortschritte der Physik 35 (1987) 277

Klimanek, P., A. Mücklich
Sample-induced errors in quantitative diffraction analyses of textures Annual Report 1986, ZfK-621 (1987) 110

Kluge, G., R. Klabes, A. Thomas, R. Grötzschel, P. Süptitz
High energy ion beam induced Ag diffusion within amorphous Ag: GeSe2
phys. stat. sol. (a) 110 (1987) K9

Knospe, O., R. Schmidt, H. Schulz
Site-Percolation Approach for Mass and Isotopic Distributions in Fragmentation Reactions
Phys. Lett. B 182 (1986) 293

Kögler, R., E. Wieser, M. Voelskow, G. Otto
Transient Enhanced Diffusion and Electrical Activation of As in Si During Rapid Thermal Annealing
Nucl. Instrum. Methods B 19/20 (1987) 516

Kotte, R., H.-J. Keller, H.-G. Ortlepp, F. Stary
Bragg-peak spectroscopy of low-energy heavy ions
Nucl. Instrum. Methods A 257 (1987) 244

Kovacs, Zs. H. Müller
Hadron and fragment emission in cluster-excitation processes at medium energies
J. Phys. G: Nucl. Phys. 12 (1986) 1355

Kunze, D., D. Janssen
On the field calculation of an electrostatic multipole device
OPTIK 76 (1987) 61

Lück, H.B.
Kernspurmembranen und ihre Einsatzmöglichkeiten in der Lebensmittel- und Biotechnologie
Lebensmittelindustrie 34 (1987) 252

Lukas, P., P. Mikula, J. Kulda, F. Eichhorn
Neutron Interferometer at NPI Rez
Czech. J. Phys. B 37 (1987) 993

Mädler, P., L. Münchow, A. Pfitzner
Randomization of single-particle motion by collective fluctuations
Phys. Lett. B 198 (1987) 25

Manfraß, P., W. Enghardt, W.D. Fromm, D. Wohlfarth, K. Hennig
Positron Camera with High-Density Avalanche Chambers
European Meeting on Positron Studies of Defects, Wernigerode, March 1987
Crystal Research and Technology, 3/1988

Manfraß, P., W. Enghardt, W.D. Fromm, D. Wohlfarth
Positronenkamera mit Gasdetektoren
Jubiläumskongreß für pathologische und klinische Physiologie der DDR, Jena, September 1987

Manfraß, P., W. Enghardt, W.D. Fromm, D. Wohlfarth, K. Hohmuth
Positron emission tomograph with high-density avalanche chambers
Conference on Position Sensitive Detectors, London, September 1987

Matthies, S., G.W. Vinel, K. Helming
Standard Distributions in Texture Analysis. Vol. 1
Berlin: Akademie-Verlag 1987

Matz, W., H. Hermann, N. Mattern
On the Structure of Amorphous $Fe_{75}B_{25}$
J. non-cryst. Solids 93 (1987) 217

Matz, W., J. Kulda, P. Mikula
Determination of partial structure factors for amorphous $Fe_{75}B_{25}$ by polarized neutron diffraction
Proc. Int. Conf. "Advanced Methods of X-ray and Neutron Structure Analysis of Materials", Karlovy Vary 1987

Mücklich, A., P. Klimanek
Texture development during cold-rolling of (+β)-brass
Proc. of XII. Conference on Physical Metallurgy, Vol. 1, (1987) 219

Müller, H.-J., W.D. Fromm, K.-H. Heinig, F. Schwarzenberg
Pseudografik auf dem PC 1715 und dem A 7100
Mikroprozessortechnik, 1 (1987) 322

Müller, H.-J., K.-H. Heinig
Amorphous-to-polycrystalline transformation of Si by rapid thermal annealing studied by computer simulation
Nucl. Instrum. Methods B22 (1987) 524

Müller, H.-J., K.-H. Heinig
Computer simulation of primary crystallization amorphous to crystalline
J. de Physique XII (1987) 137

Naumann, B., L. Naumann, A.A. Nomofilov, N.M. Piskunov, V.I. Sharov, I.M. Sitnik, E.A. Strokovsky, L.N. Strunov, S.A. Saporoshets, V.G. Ableev, D.V. Anchishkin, A.P. Kobushkin, L. visireva, Ch. Dimitrov, L. Penchev, B. Kühn, W. Neubert
Study of the structure of light nuclei at small distances in experiments on fragmentation of polarized and nonpolarized deuterons
Proc. Spin-86 VII. Int. Symposium on high energy spin physics, Protvino (USSR), 22.-27. September 1986, Vol. II, p. 111

Panknin, D., E. Wieser, R. Grötzschel, C.E. Richter, M. Gericke, Ya.V. Fattachov, I.B. Khaibullin
Dopant distribution and electrical activation of Si implanted GaAs by short time annealing
Nucl. Instrum. Methods B19 (1987) 492

Portius, R., D. Dietrich, A. Hässner, Th. Raschke, E. Wieser, W. Wolke
Formation of Stable $MoSi_2$/Poly-Si Films by Rapid Thermal Annealing
phys. stat. sol. (a) 100 (1987) 199

Podurets, K.M., S.Sh. Shilshtejn, F. Eichhorn
Refraksionnoe smeshchenie otrazhenija nejtronov
Preprint IAE-4429/9 Moskva 1987

Posselt, M., W. Skorupa
The electronic stopping and range profile calculations for high energy implantation of phosphorous into silicon
Nucl. Instrum. Methods B21 (1987) 8

Prade, H., W. Enghardt, I. Dioszegi, L. Käubler, H.-J. Keller, F. Stary, G. Winter
In-beam investigations and structure studies of multiparticle excitations in the N = 82, 83 nuclei $^{138,139}Ba$
Nucl. Phys. A 472 (1987) 381

Prokert, F., A.M. Balagurov, B.N. Savenko
Phasenübergangseffekte an einem inkommensurabel modulierten Strontium-Barium-Niobat Einkristall $Sr_{0.7}$, $Ba_{0.3}Nb_{2.6}$
Preprint JINR Dubna P 14-87-38

Rauschenbach, B.
The characteristic temperature of ion beam mixing
phys. stat. sol. (a) 102 (1987) 645

Rauschenbach, B.
Microstructural investigations of iron implanted with nitrogen ions at the temperature of liquid nitrogen
II. Implantation in the dose range 1×10^{17} to 1×10^{18} N^+-ions/cm^2
Nucl. Instrum. Methods B 18 (1986) 34

Rauschenbach, B., V. Heera
Icosahedral quasicrystals of Al-Fe phase formed by ion beam mixing
J. Mater. Sci. Lett. 6 (1987) 401

Rauschenbach, B., V. Heera
Ion irradiation induced reamorphization of boron preimplantes iron
phys. stat. sol. (a) 100 (1987) 423

Rauschenbach, B., K. Hohmuth
Ion beam mixing in Al/Fe multilayered thin films
Nucl. Instrum. Methods B 23 (1987) 323

Rauschenbach, B., K. Hohmuth, K. Hennig
Phase transformation by ion beam mixing
E-MRS-Strassbourg, (1986) 199

Rauschenbach, B., K. Hohmuth, G. Kaestner
Microstructural investigations of iron implantes with nitrogen ions at the temperature of liquid nitrogen
I. Implantation in the dose range 1×10^{16} to 1×10^{17} N^+-ions/cm^2
Nucl. Instrum. Methods B 23 (1987) 316

Reinhardt, H.
Quantum hadrodynamics from low-energy QCD
Phys. Lett. B 188 (1987) 263

Reinhardt, H.
Scaling behaviour of the effective chiral action of QCD and stability of the chiral soliton
Phys. Lett. B 188 (1987) 482

Reinhardt, H., B.V. Dang
Restoration of chiral-symmetry breaking at Limite temperature and baryon density
J. Phys. G. 13 (1987) 1179

Rotter, I.
The interplay between regular and chaotic motion in nuclei
Mod. Phys. Letters A 2 (1987) 233

Rotter, I.
Coopèrative effects in nuclei and selforganization
Revue Rom. de Physique 32 (1987) 233

Röpke, G., D. Blaschke, H. Schulz
Pauli Quenching Effects in a Simple Model of Quark / Nuclear Matter
Phys. Rev. D 34 (1986) 3499

Rudolph, W., C. Bauer
Detection of surface contamination by resonance nuclear reactions
Particles and Nuclei 18 (1987) 820

Rumyantsev, A.Y., N.L. Mitrofanov, A.S. Ivanov, A.S. Ivanov, N.A. Chernoplekov, L. Weiss, H. Eschrig, R. Richter
Anomalies in the Phonon Spectra and the Fermi Surface of the random substitutional Alloy $Cu_{0.9}Ni_{0.1}$
phys. stat. sol. (b) 143 (1987) 625

Saupe, G., O.I. Serdink, G.D. Adeev, V.V. Pashkevich
Description of the mass and kinetic energy distributions of fission fragments using an adiabatic potential
Report JINR Dubna E4-87-409 (1987)

Schilling, K.D., P. Gippner, W. Seidel, F. Stary, E. Will, K. Heidel, S.M. Lukyanov, Yu.E. Penionzhkevich, V.S. Salamatin, H. Sodan, G.G. Chubarian
The Dubna double-arm time-of-flight spectrometer for heavy-ion reaction products
Nucl. Instrum. Methods A 257 (1987) 197

Schmalz, K., F.G. Kirscht, S. Niese, H. Richter, M. Kitter, W. Seifert, I. Babanskaya, H. Klose, K. Tittelbach-Helmrich, J. Schöneich
On the intrinsic gettering in Fe-contaminated Cz-Si
Phys. Status Solidi (a) 100 (1987) 69

Schubert, D., W. Jenschke, T. Uhlig, F.M. Schmidt
Piezoresistive Properties of polycrystalline and crystalline Silicon Films
Sensors and Actuators, 11 (1987) 145

Schulz, H., G. Röpke, K.K. Gudima, V.D. Toneev
Impact Parameter Dependence of the Specific Entropy and the Light Particle Yield in Relativitic Heavy Ion Collisions
Phys. Rev. C 34 (1986) 1294

Schulz, H., G. Röpke
A Note on Massive Quark-Matter Phase
Z. Phys. C 35 (1987) 379

Schwarzenberg, F.
Standard-Interfaces über den User-Port des KC 85/1
Mikroprozessortechnik 1 (1987) 311

Schwarzenberg, F., R. Wobst
Anschluß der Schreibmaschine S 6005 an KC 85/1
Mikroprozessortechnik 1 (1987) 315

Sieber, N., H. Oertel, M. Voelskow
Elektrische Eigenschaften von MOS-Strukturen, hergestellt in rekristallisiertem Silicium (r-Si)
17. Arbeitstagung "Physik der Halbleiteroberfläche", 17 (1986) 101

Skorupa, W., E. Wieser, R. Grötzschel, M. Posselt, H. Buecke, A. Armigliato, A. Garulli, A. Beyer, W. Markgraf
High Energy Implantation and Annealing of Phosphorus in Si
Nucl. Instrum. Methods B 19/20 (1987) 335

Skorupa, W., M. Voelskow, J. Matthäi
A pecularity of ion beam induced epitaxial crystallization with low implantation energies applied to doped amorphous silicon layers
phys. stat. sol. (a) 101 (1987) K 101

Skorupa, W., K. Wollschläger, U. Kreißig, R. Grötzschel, H. Bartsch
Properties of ion beam synthesized buried silicon nitride layers with rectangular nitrogen profiles
Nucl. Instrum. Methods B 19/20 (1987) 285

Sieber, N., D. Proskurovskij
Einfluß einer Wärmebehandlung mittels Elektronenstrahls oder Halogenlampen im Sekundenregime auf die elektrischen Eigenschaften von implantierten und nichtimplantierten MOS-Strukturen
18. Arbeitstagung "Physik der Halbleiteroberfläche", 18 (1987) 195

Sieber, N., D. Proskurovskij
Einfluß einer Wärmebehandlung mittels Elektronenstrahls oder Halogenlampen im Sekundenregime auf die elektrischen Eigenschaften von MOS-Strukturen
32. Intern. Wiss. Koll. TH Ilmenau, Vortragsreihen B1/B2, 4 (1987) 117

Sodan, H., S.M. Lukyanov, Yu.E. Penionzhkevich, V.S. Salamatin, G.G. Chubarian, K. Heidel, A. Popp, K.D. Schilling, E. Will, P. Gippner, C. Borcea
Wirkung der Schalenstruktur auf die Produktcharakteristik der Reaktion Zn + Sn (in russisch)
Report JINR Dubna R7-87-621 (1987)

Sodan, H., S.M. Lukyanov, Yu.E. Penionzhkevich, K. Heidel, V.S. Salamatin, G.G. Chubarian, P. Gippner, E. Will, K.D. Schilling, A. Popp
Untersuchung der Zerfallscharakteristik von Compound-Systemen mit Z = 100 (in russisch)
Proc. Int. School-Seminar on Heavy Ion Physics, Dubna, 23. - 30.9.1986, JINR D7-87-68 (1987) 479

Toneev, V.D., H. Schulz, K.K. Gudima, G. Röpke
Towards Nuclear Matter Equation of State
Particles and Nuclei 17 (1986) 1093

Wünsch, R., J. Zofka
Resonant and quasi-free mechanisms of sigma-production on nuclei
Phys. Lett. B 193 (1987) 7

VORTRÄGE

Ableev, V.G. et al. (presented by S. Tesch)
Structure of Light Nuclei from Scattering and Fragmentation at Relativistic Energies [a)]

Adeev, G.D., V.V. Pashkevich, G. Saupe
Description of the mass and kinetic-energy distributions of fission fragments in heavy-ion systems with Z = 108 [aa)]

Alexandrov, Y.A., F. Eichhorn, J. Kulda, P. Lukas, T.A. Macheklina, R. Michalec, P. Mikula, L.N. Sedlakova
Neutron-Optical Experiments at the IBR-2 Pulsed Reactor [b)]

Armigliato, A., R. Kögler, E. Landi, S. Solmi, E. Wieser
Electrical Activation of Boron Implanted in Silicon During the Early Stage of Rapid Thermal Annealing [c)]

Ascheron, C., H. Sobotta, V. Riede, C. Neelmeijer, R. Grötzschel, W. Rudolph, A. Schindler
Investigations of the annealing behaviour of hydrogen implanted GaP single crystals by means of particle induced gamma spectroscopy, infrared spectr. and RBC technique [k)]

Barz, H.W.
Nuclear Stopping power within the two-fluid model [a)]

Barz, H.W.
Two-fluid model for ultra-relativistic heavy ion reactions; GSI Darmstadt, 4. 3. 1987

Barz, H.W.
Two-fluid model with energy leak-out applied to asymmetric ultra-relativistic heavy ion collisions; VIK Dubna, 1. 10. 1987

Barz, H.W., H. Müller, H. Schulz
A Statistical Model for Multiparticle Production in Hadron-Hadron Interaction [a)]

Baither, D., H. Bartsch, D. Panknin
Residual defects in implanted GaAs after rapid thermal annealing with incoherent light [c)]

Baither, D., R. Kögler, E. Wieser
Effect of Oxygen Recoils on the Defect Annealing in Si During RTA [c)]

Betzl, M.
Möglichkeiten der Neutronenstreuung [g)]

Betzl, M., K. Feldmann
Progress in neutron-time-of-flight texture studies at pulsed reactors [h)]

Bischoff, L.
Neutronenkompensiertes Silizium für Detektoren
Wiss. Kolloqu. Inbetriebnahme Si-Technikum, ZfK, 12.11.1987

Bischoff, L.
Application of focused ion beams in VLSI technology [f)].

Bittrich, H.-J., F. Eichhorn, S. Möring, G. Möbius, S. Schlenker
Synthesis and structural characterization of diblock copolymers of deuterated and hydrogenated polystyrene [d)]

Bittrich, H.-J., F. Eichhorn, S. Höring, G. Möbius, S. Schlenker
Structural characterization of polymeric core-shell particles by small-angle neutron scattering [d)]

Bittrich, H.-J., S. Schlenker, F. Eichhorn
Neutronenkleinwinkelstreuung an Polymersystemen [e)]

Bittrich, H.-J., H. Tanneberger, S. Schlenker, F. Eichhorn
Strukturuntersuchungen an heterogenen Polymersystemen mit Neutronenkleinwinkelstreuung
10. Mikrosymposium "Physik der Polymere" TH Leuna-Merseburg, März 1987

Damm, V., A. Mücklich, K. Helming
Möglichkeiten der quantitativen Interpretation von Ergebnissen magnetischer Anisotropieuntersuchungen unter Anwendung der Neutronentexturanalyse

Dienel, G., A. Kolitsch, E. Richter, U. Scholz
Wear behaviour of ion implanted steels and hard metals c)

Dittes, F.M.
Skyrmionen, Seminar in KMU Leipzig, Juni 1987

Dittes, F.M.
Nonlocal expansion of the effective chiral action; Int. Symposium zur Elementarteilchentheorie, Sellin 12. - 16. 10. 1987

Eichhorn, F.
Rerfect Crystal Neutron Optics b)

Eichhorn, F.
Möglichkeiten der Neutronenkleinwinkelstreuung g)

Eichhorn, F., H.-J. Bittrich, S. Schlenker
SANS Investigations on Core-Shell Latexes v)

Eichhorn, F., F. Häussler
Mikrostrukturuntersuchungen am Beton mittels Neutronenkleinwinkelstreuung
10. ibausil (Int. Baustoff- und Silikattagung), Weimar, Mai 1987

Eichhorn, F., P. Mikula, P. Lukas
Aufbau und Erprobung einer NKWS-Anordnung e)

Eichhorn, F., S. Schlenker, H.-J. Bittrich
Strukturuntersuchungen an heterogenen Polymersystemen mit Neutronenkleinwinkelstreuung m)

Ertel, A., M. Betzl, H. Kämpf
Texture investigation of natural rock salt by neutron diffraction w)

Feldmann, K.
Experimentelle Ergebnisse der Texturuntersuchungen an den Stengelgneisproben SG 2 und SG 3 e)

Franzke, H.J., M. Betzl, K. Helming, W. Voitus
Texturen an Fluoriten aus Ganglagerstätten der DDR e)

Frischbutter, A., K. Feldmann, L.P. Drechsler
Quarzteilgefüge eines B-Tektonits (Stengelgneis) e)

Fromm, W.D.
Zur Weiterentwicklung des PC 1715
Methodisches Institutsseminar, Rossendorf, 30.4.1987

Fromm, W.D.
Einsatz von KRS 4201 in der Experimentautomatisierung, Methodisches Institutsseminar, Rossendorf, 4.6.1987

Fromm, W.D.
Vorstellung Kompakt-VKA, 7. Kolloquium Dünnschichtaktivierung, Dresden, 27.10.1987

Fujinami, M., Y. Ujihira, E. Richter, H. Reuther
^{57}Fe CEMS study of boron and carbon implanted iron; Int. Conf. Appl. Mößbauer Effect, Melbourne 16. - 21.8.1987

Gersch, H.U.
Results of the Department of Nuclear Physics and Applications i)

Gersch, H.U.
Identical boson interferometry i)

Gersch, H.U.
Kaon-interferometry j)

Gippner, P.
Energy-mass distributions observed in heavy-ion collisions leading to composite systems with Z 100 y)

Grambole, D., C. Heiser, F. Herrmann, C. Neelmeijer, W. Rudolph
The influence of the surface roughness on the measured hydrogen content of specimens k)

Grötzschel, R., B. Selle
RBS analysis applied to multilayer structures of thin dielectric films x)

Grötzschel, R., W. Rudolph
Ion beam analysis for layer and substrate analysis c)

Grötzschel, R., F. Herrmann, B. Selle
Analyse von seltenen Erden in dünnen Elektrolumineszenz-ZnS-Schichten mittels RBS m)

Häussler, F., U. Miehe, F. Eichhorn
Untersuchungen zur Mikrostrukturentwicklung des Zementsteins mittels NKWS e)

Häussler, F., H. Baumbach, F. Eichhorn
Neutronenkleinwinkelstreuung an zementgebundenen Betonen; 6. wiss. Konferenz 1986 der TH Leipzig "Zerstörungsfreie Prüfung mit Meßmethoden im Bauwesen", Leipzig, Dezember 1986

Hanicke, U.
Development-tendency in production of silicon detectors f)

Heera, V., B. Rauschenbach
Zur Theorie und Herstellung der Quasikristalle e)
Institutsseminar IFE Halle, 2.3.1987
Seminar WB Metallphysik, BA Freiberg, 11.3.1987
Seminar WB Kristallographie, HU Berlin, 19.3.1987
Sektorseminar LTF, VIK Dubna, 23.6.1987

Heinig, K.-H.
Zelluläre Automaten, Selbstorganisation und Schmelzinstabilität bei Lichtheizung, Seminar an der FSU Jena, 18.12.1986

Heinig, K.-H., H.-J. Müller
Computer Simulation of the Order-Disorder Transition in the Melt Morphology of Si Heated by Light s)

Heinig, K.-H., H.-J. Müller
Fundamental Aspects of Thermally Induced SOI Layer Formation c)

Heinig, K.-H., H.-J. Müller
Computer Simulation of Grain Boundary Confinement at Zone Melting Recrystallization c)

Heinig, K.-H., H.-J. Müller
Study of Structure Formation by the Melt Instability of Silicon at Light Heating c)

Heinig, K.-H., H.-J. Müller
Monte-Carlo-Simulationen von Schmelzinstabilitäten; 6. Fischlandkolloquium, Wustrow, 29.9.-1.10.1987

Heinig, K.-H., H.-J. Müller
Fundamentals of SOI Layer Formation; Seminar an der Staatsuniversität Mons (Belgien), 24.11.1987

Helming, K., B. Rauschenbach
Methodische Untersuchungen zur Bestimmung von Texturen dünner Schichten mittels Elektronenstreuung e)

Helming, K., S. Matthies, G.W. Vinel
ODF representation by means of -sections r)

Henke, D., R. Hentschel
Die Energiebreiten von Teilchenstrahlen o)

Hensel, E., R. Grötzschel, E. Richter
Ion beam mixing - a promising method to influence the surface properties of tool steels k)

Hensel, E., R. Grötzschel, E. Richter
Beeinflussung der Oberflächeneigenschaften von Werkzeugstahl mittels ion beam mixing m)

Hensel, E., R. Grötzschel, U. Scholz, E. Richter
Modification of surface properties of tool steel by ion beam mixing c)

Hermann, H., N. Mattern, W. Matz
Magnetische und strukturelle Eigenschaften amorpher Fe-B-Legierungen e)

Hildebrandt, Jüttner, Puosch, Jakubka, Stochul, Zacek, R. Grötzschel
Study of impurity transport by collector probe measurements in the CASTOR-tokamak, Int. Symp. on Phys. and Techn., Liberec, März 1987

Hoffmann, W., J. Hüller, M.T. Pham
Theorie und Anwendung von chemischen Sensoren auf Basis von elektronischen Halbleiterelementen, Institutsseminar, TH Leuna-Merseburg, Juli 1987

Hoffmann, W., J. Hüller, M.T. Pham, J. Schöneich
Ionenstrahltechnologie für chemische Sensoren n)

Hohmuth, K., R. Grötzschel, B. Rauschenbach
Ion beam mixing ib Cu/Au multilayered thin films c)

Jäger, H.U.
Improved modeling of oxygen depth profiles in high dose oxygen-implanted silicon c)

Jäger, H.U., J.A. Kilner, R.J. Chater, P.L.F. Hemment, R.F. Peart, K.J. Reeson
Modeling of ^{18}O tracer studies of the oxygen redistribution during formation of SiO_2 layers by high dose implantation [c)]

Kaun, L., A. Güth, A. Köthe, A. Mücklich, M. Betzl
Texturentwicklung in kontrolliert gewalztem HSB; 16. Metalltagung der DDR, TMB von Stahl, Dresden, Mai 1987

Kirchbach, M.
Mesonenaustausch; ZTF, Dubna, Laborseminar, Dezember 1986
Seminar, Inst. f. Kernphysik u. Kernenergetik der AdW, Sofia, VRB, März 1987

Kirchbach, M.
Mesonenaustauschströme
Seminar, IPH Zeuthen, Mai 1987

Kirchbach, M.
Importance of heavy-meson exchanges for ^{18}F parity-mixing [u)]

Kirchbach, M.
Meson-exchange Effects on the Nuclear Chiral Charge Density [p)]

Kögler, R., E. Wieser
The Effect of Oxygen on Electrical Activation and Diffusion of As Implanted Si During RTA [c)]

Kotte, R.
Ternary fission of ^{238}U induced by 13.5 MeV deuterons [q)]

Kovacs, Zs., H. Müller
Hadrons and fragments from excited clusters; PANIC, Kyoto, Japan, 20.4.-24.4.1987

Kreißig, U., A. Kahn, F.G. Rüdenauer, W. Steiger
Mass and energy distribution measurements at AuSi liquid metal alloy ion source [c)]

Küchler, R.
Die Anwendung von Ultraschalloberflächenwellen zur Untersuchung ionenimplantierter Oberflächenschichten [cc)]

Küchler, R., E. Richter
Heat production during ion implantation into metals and alloys [c)]

Küchler, R., E. Richter
The application of ultrasonic surface waves to the study of the production of surface layers after ion implantation [bb)]

Lehmann, D., C. Ascheron, C. Neelmeijer
Hydrogen depth profiling in H implanted semiconductors using elastic recoil detection [k)]

Lück, H.B., B. Gemende
Eigenschaften und Einsatzmöglichkeiten von Kernspurmembranen; 8. Diskussionstagung "Verfahrenstechnik", Köthen, 15.10.1987

Matthies, M.
Standardfunktionen und ihre Eigenschaften [e)]

Matthies, S.
Geisteratlas - Aufbau und einige methodische Weiterentwicklungen [e)]

Matthies, S.
Über die Normalverteilung im G-Raum; Seminar, Universität Metz, 10.7.1987

Matthies, S.
Das Paket universeller Standardprogramme; Seminar, Universität Metz, 10.7.1987

Matthies, S.
On the difference between the WIMV- and the Imhof algorithm [r)]

Matthies, S.
On the loss of Information about the ODF in pole figure measurements [r)]

Matthies, S.
Demands to ODF-represenation by G-space sections [r)]

Matthies, S.
On the basic elements and practical experiences with the WIMV-algorithm - an ODF-reproduction method with conditional ghost correction [r)]

Matthies, S.
Texturanalyse - Objekt, Anwendungsgebiet, Probleme; Seminar der HA Theorie des Bereiches KF, Rossendorf, 9.11.1987

Matz, W.
Struktur von Metaphosphatgläsern e)

Matz, W.
Instrumentierung der Neutronenstreuexperimente an der Spallationsneutronenquelle ISIS e)

Matz, W.
Neutronendiffraktion an Metaphosphatgläsern; Seminar der Abt. ONF des UJF Rez, März 1987

Matz, W., E.A. Goremychkin, D. Stachel
Neutronendiffraktionsuntersuchungen zur Struktur von Metaphosphatgläsern z)

Matz, W.
Möglichkeiten der Neutronendiffraktion bei der Strukturaufklärung an Gläsern; Seminar des Otto-Schott-Institutes der FSU Jena, 30.6.1987

Mátz, W., A.V. Serebrjakov
Estimation of partial structural factors for amorphous $Fe_{83}F_{17}$; 6. Arbeitsseminar DDR-UdSSR zum Thema "Herstellung, Struktur und Eigenschaften metallischer Werkstoffe nach extremer Vorbehandlung", Ahrenshoop, Oktober 1987

Matz, W.
Issledovanije struktury metafosfatnych stekol metodom nejtronnoj difrakciji; IX. Nationale wissenschaftlich-technische Konferenz mit internationaler Beteiligung "Glas und Feinkeramik", Varna, VR Bulgarien, Oktober 1987

Mende, G., R. Grötzschel, C. Heiser, C. Neelmeijer, W. Rudolph, A. Hofmann, J. Finster
Investigations on the mechanism of anodic Si oxidation by means of indicator neutron activation analysis, RBS, nuclear reactions and ESCA k)

Mende, G., M. Deutscher, H.-J. Döring, H. Flietner, K.-H. Heinig
Electron irradiation effects in MOS-structures using thin anodically grown SiO_2 films s)

Mende, G., M. Deutscher, H.-J. Döring, H. Flietner, B. Schmidt
Anodic oxydation of silicon as a low temperature oxidation method for passivation of semiconductor devices c)

Mende, G., M. Deutscher, H.-J. Döring, H. Flietner
The influence of 20-keV electron irradiation on thin anodic oxide films; Seminar Petrosavodsk UdSSR, 22.-24.9.1987

Mende, G.
Anwendungsmöglichkeiten der Silicium-Anodisation in der Mikroelektronik; 9. Herbstschule Isolatorphysik, Güstrow, 30.11.-5.12.1987

Michel, P., K. Möller, J. Mösner, G. Schmidt
A measurement of the forward differential cross section of the reaction $^1H(n,d)\gamma$ at E_n = 25 MeV t) u) und p) q)

Mikula, P., F. Eichhorn, P. Lukas, R. Michalec
A Medium Resolution Double-Crystal Diffractometer for SANS Studies v)

Mücklich, A., K. Hennig
Magnetische und kristallographische Textur metamorpher Magnetiterze e)

Mücklich, A., P. Klimanek
Texture development during cold rolling of (+β)-brass h)

Mücklich, A., P. Klimanek
Probenbedingte Fehlerquellen bei der quantitativen Texturanalyse; Rundtischgespräch der AG Texturen der Vfk der DDR, Dresden, Mai 1987

Mücklich, A., P. Klimanek
Sample-induced errors in the quantitative diffraction nanlysis of texture w)

Müller, H.-J., K.-H. Heinig
Theoretische Untersuchungen der SOI-Schichtherstellung durch laterale Festphasenepitaxie o)

Müller, H.-J., K.-H. Heinig
Computer simulation of solid phase crystallization in thin a-Si films x)

Müller, H.-J., K.-H. Heinig
SOI-Layer fabrication by lateral solid phase epitaxy of a-Si studied by computer experiments s)

Müller, H.-J., K.-H. Heinig
L-SPE studied by computer experiments c)

Müller, H.-J., K.-H. Heinig
Theoretical investigation of thermally activated and ion beam induced lateral solid phase epitaxy c)

Müller, H.-J., K.-H. Hennig
Grundlegende Aspekte der Festphasentransformation studiert mittels Computersimulation
6. Fischlandkolloquium, Wustrow, 29.9.-1.10.1987

Müller, H.-J., K.-H. Heinig
Computersimulation der lateralen Festphasenepitaxie amorph-kristallin in SOI-Strukturen [l)]

Münchow, L.
Halbklassische Methoden in der Theorie von Schwerionenreaktionen; Vorlesungsreihe an der Universität Catania (Italien), April 1987

Neelmeijer, C.
Nukleare Analytik und daraus abgeleitete Anforderungen an die Beschleuniger; Frühjahrsschule Bereich G, Hörnitz, März 1987

Neelmeijer, C., H.-P. Schramm, H. Matthes, W. Pfestorf
Möglichkeiten der Materialanalyse auf Kunstwerken mittels Protonenstrahlen (PIXE); Tagung der Restauratoren der DDR, Reinhardsbrunn, März 1987

Neelmeijer, C., H. Münzer, B. Schmidt, W. Rudolph, C. Heiser, D. Grambole, F. Herrmann
Etching of Si-nitride and Si-oxide layers after ion implantation [c)]

Neubert, W., W. Pilz, H. Märten, D. Richter (presented by W. Neubert)
Measurements of correlations between fragments and neutrons / or γ-rays in the s.f. of ^{252}Cf [i)]

Neubert, W., W. Pilz, K. Arnold, D. Lucas, H. Märten (presented by W. Neubert)
Angular distributions of prompt γ-rays in the binary fission of ^{252}Cf [j)]

Neubert, W.
Application of BCS to multifragmentation processes [q)]

Neumann, H., W. Matz, W. Hoyer
Zur experimentellen Technik und Auswertemethodik bei Neutronenbeugung an Schmelzen [z)]

Panknin, D.
Kurzzeitausheilung von GaAs-Vergleich verschiedener Ausheilmethoden [o)]

Panknin, D., E. Wieser, Ya.V. Fattachov, I.B. Khaibullin
Short Time Threshold for electrical Activation of Implanted and Annealed GaAs [c)]

Panknin, D., C.E. Richter, M. Gericke, Ya.V. Fattachov
Silicon and chromium distribution in implanted and short time annealed GaAs [c)]

Petukhov, V.Yu., I.B. Khaibullin, N.V. Kurbatova, E. Wieser
Electrical Resistivity of Silicon Implanted by High Dose Cr^+-Ions after Laser Annealing [c)]

Petukhov, V.Yu., I.B. Khaibullin, M.M. Zaripov, E. Wieser, R. Grötzschel
Formation of Epitaxial Layer $NiSi_2$ by High Dose Ion Implantation and Rapid Thermal Annealing [c)]

Petukhov, V.Yu., I.Z. Ilaldinov, I.B. Khaibullin, K. Wollschläger
Study of electrical and optical properties of fused quartz implanted by high dose Cr^+ and Fe^+-ions

Pilz, W., J. Mösner, G. Schmidt, K. Möller, P. Michel, B. Kühn (presented by W. Neubert)
Measurements of total cross sections in the $p(n,\gamma)d$ and $d(n,t)\gamma$ reactions at E_n = 25 MeV [i)]

Pilz, W., W. Neubert, H. Märten (presented by H. Märten)
Ismerenije uglovikh raspredelenij gamma-kvantov v spontannom delenii ^{252}Cf [aa)]

Pilz, W.
Angular distributions of prompt γ-rays in the binary and ternary fission of ^{252}Cf [q)]

Posselt, M., W. Skorupa
Zur Anwendbarkeit verschiedener Modelle für den elektronischen Bremsquerschnitt auf Reichweiteprofilberechnungen bei der Hochenergieimplantation von P in Si [o)]

Posselt, M., G. Otto
Computeruntersuchungen zur statistischen Verteilungsfunktion der Teilchen in ionenstrahlinduzierten Stoßkaskaden [o)]

Posselt, M., W. Skorupa
Range profile calculations for the high energy implantation of phosphorous into silicon [c)]

Posselt, M., G. Otto
Computer studies of the statistical distribution functions of particles moving in collision cascades [c)] und [bb)]

Posselt, M., W. Skorupa
Range and range profile calculations for the MeV implantation of phosphorous into silicon [bb)]

Posselt, M., W. Skorupa
Zur Berechnung von Reichweiteprofilen für die Hochenergieimplantation in Si [l)]

Posselt, M.
Modellierung der Implantationsprozesse mittels Monte-Carlo-Simulation; Problemseminar Bauelemente- und Prozeßsimulation, Karl-Marx-Stadt, 11.-13.11.1987

Prokert, F., A.M. Balagurov, B.N. Savenko
Phasenübergangseffekte an einem inkommensurabel modulierten Strontium-Barium-Niobat-Einkristall $Sr_{0.7}Ba_{0.3}Nb_2O_6$ e)

Prokert, F., K.S. Aleksandrov
Soft mode transition in hexagonal ABX_3 compounds; 15. Intern. Frühjahrsschule "Ferroelektrizität 87", Finken, April 1987

Rauschenbach, B.
Experimentelle Untersuchungen zu quasikristallinen Strukturen; Instituts-Seminar, IFE Halle, 2.3.1987

Rauschenbach, B., V. Heera
Formation and structure of implantation induced amorphous alloys x) c)

Rauschenbach, B.
Comperative investigation of phase transformation in Fe, Al and Ti after nitrogen ion implantation c)

Rauschenbach, B.
Ion beam mixing in Al/Fe multilayered thin films bb)

Reinhardt, H.
Die Funktionalintegrationsmethode in der Vielteilchentheorie; Vorlesungsreihe an der TU Dresden, Herbstseminar 1987

Reuther, H.
Conversion electron Mößbauer spectroscopic studies of ion implanted iron layers k)

Reuther, H.
Conversion electron Mößbauer spectroscopic study on phosphorus implanted iron y)

Reuther, H.
Konversionselektronen-Mößbauerspektroskopie- eine Methode zur Untersuchung ionenimplantierter Eisenschichten m)

Reuther, H., E. Richter, M. Fujinami, Y. Ujihira
CEMS studies of iron implanted with boron, carbon and phosphorus c)

Reuther, H., B. Rauschenbach, E. Richter
Ion implantation in metals - structure investigations and applications bb)

Richter, E.
Verschleißverhalten ionenimplantierter Werkzeugoberflächen cc)

Richter, E.
Verschleißschutz durch Ionenimplantation; 5. Fachtagung Anorganische Schutzschichten, Karl-Marx-Stadt, 30.9.-2.10.1987

Roß, R.
Determination of Lithium in Silicon by Neutron Activation Analysis k)

Roß, R., A. Zetzsche
Neutronendotiertes Silicium - ein Basismaterial für die Leistungselektronik; XXXII. Int. Wiss. Koll. der TH Ilmenau 26.-30.10.1987

Rotter, I.
Interplay between regular and chaotic motion in nuclei; Seminar, Inst. f. Kernforschung Swierk, 22.4.1987

Rotter, I.
Selbstorganisation und Atomkerne; Theorieseminar der KMU Leipzig, 10.6.1987

Rotter, I.
Selforganization and Atomic Nuclei p)

Rotter, I.
Regular and chaotic motion in nuclei; Separable Wechselwirkungen in verschiedenen dynamischen Problemen, Budapest, 7.-11.9.1987

Rotter, I.
Selbstorganisation im Atomkern; Ganztagskolloquium der TU Dresden "Nichtlineare Phänomene", 15.9.1987

Rotter, I.
Anwendungen von selbstkonjugierten Erweiterungen in der Quantenphysik; Selforganization and Atomic Nuclei workshop, Dubna, 29.9.-1.10.1987

Rotter, I.
Chaos and Order in Atomic Nuclei [q)]

Rudolph, W.
Ion beam methods in Rossendorf [i)]

Rudolph, W., K. Brankoff, D. Grambole, R. Grötzschel, C. Heiser, F. Herrmann, C. Neelmeijer
Veränderung von Polymerschichten durch Ionenbeschuß; 8. Arbeitstagung, Oberstdorf, April 1987

Rudolph, W., D. Grambole, R. Grötzschel, C. Heiser, F. Herrmann, C. Neelmeijer
Analysis of boron doped silicon oxide layers by means of He backscattering and prompt nuclear reactions [k)]

Rudolph, W., D. Grambole, C. Heiser, F. Herrmann, C. Neelmeijer
Hydrogen detection by means of the $^{1}H(^{15}N,\alpha\gamma)^{12}C$ resonance reaction [k)]

Rudolph, W., K. Brankoff, D. Grambole, R. Grötzschel, C. Heiser, F. Herrmann, C. Neelmeijer
Plastic foils as primary hydrogen standards for nuclear reaction analysis [k)]

Rudolph, W., R. Grötzschel, C. Heiser, C. Neelmeijer
Analysis of buried layers in semiconducting material by RBS and nuclear reactions [k)]

Rudolph, W., D. Grambole, R. Grötzschel, C. Heiser, F. Herrmann, P. Knothe, C. Neelmeijer
Hydrogen, oxygen and carbon losses during ^{15}N bombardment of PMMA layers; 12. Int. Conf. Atomic Collisions in Solids, Japan, Okayama, Oktober 1987

Saupe, G.
Description of the evolution of the mass asymmetry in heavy-ion reactions [y)]

Schindler, A., R. Fechner, R. Flagmeyer, D. Panknin, F. Bigl
Analysis of Ar ion beam etching induced surface damage of GaAs by means of ^{64}Cu adsorption/autoradiography and RBS/channeling [c)]

Schmidt, B.
Sensoren - Technologische Voraussetzungen und Entwicklungen im ZfK; Mikromechanik; 3. Beratung der Arbeitsgruppe Technologie der AdW der DDR, Berlin, 5.5.1987

Schmidt, B., U. Kreißig, H. Münzer, E. Rost
A Noval etch stop system based on high dose nitrogen implantation for thin crystalline silicon layer formation [c)]

Schmidt, B., D. Schubert
Present Status and Future of silicon sensors; 5th Int. School on Physical Problems in Microelectronics Varna, VR Bulgarien, May 18.-23.1987

Schott, H., B. Schmidt
Anwendung eines integrierten Positioniersensors in der Automatisierungstechnik; 5. Problemseminar "Sensortechnik", 27.4.-30.4.1987, Karl-Marx-Stadt

Schramm, H.-P., C. Neelmeijer, H. Matthes, W. Pfestorf
Untersuchung von Kunstwerken mittels ausgeführtem Protonenstrahl (PIXE); Wissenschaftsmesse der TU Wien, Österreich, Wien, März 1987

Schubert, D., T. Uhlig
Probleme der SOI-Technolgie für Drucksensoren [dd)]

Schubert, D., W. Jenschke
Elektrische dehnungsresistive Übertragungseigenschaften dünner polykristalliner und kristallisierter Siliciumschichten [dd)]

Schubert, D., T. Uhlig
Drucksensor mit dielektrisch isolierten Piezo-Widerständen [n)]

Schulz, H.
Nuclear Fragmentation and Liquid-Gas Phase Transition; Europhysics conference 1987, Albena, Bulgarien

Schulz, H.
Nuclear Fragmentation; Seminar NBI Kopenhagen Nov. 1986, Seminar GSI Darmstadt Februar 1987, Quark-Gluon Plasma; Seminar Dubna September 1987

Schulz, H.
Quark-Gluon Plasma; Universität Rostock, Oktober 1987

Schwarzenberg, F.
Der Commodore-Amiga; CAD-Anwendungen; Vorstellung RAM-Floppy RAF512; Methodisches Institutsseminar, Rossendorf, 30.4.1987

Seidel, W., H.-G. Ortlepp, F. Stary, H. Sodan
Double-grid avalanche counter with large dynamic range; London Conference on Position-sensitive Detectors, University College London, 7.-11.9.1987, Poster

Seidel, W.
Development and application of gas-filled detectors for heavy-ion reactions (in russ.); VIII. International Summer School on Nuclear Physics, Neutron Physics and Nuclear Energy, Varna, 19.-28.10.1987

Seidel, W., M. Andrassy, H.-G. Ortlepp, D. Walzog, F. Stary, H. Sodan
Untersuchungsergebnisse der Bragg-Kammer des Modell-Moduls für die Anlage "PHOBOS" (in russ.); Wissenschaftlich-methodisches Seminar im Laboratorium für Kernreaktionen des VIK Dubna, 17.2.1987

Seidel, W.
4π-Spektrometer PHOBOS (in russ.) [i)]

Seifarth, H.
Abscheidung von Si_3N_4-Schichten durch reaktives HF-Plasmatron-Sputtern [ee)]

Seifarth, H.
Abscheidung von Si_3N_4-Schichten durch reaktives HF-Plasmatron-Sputtern [l)]

Sieber, N., G. Otto
Mathematical Modelling of Threshold Voltage and Capacitance Characteristics at a MOS Structure on a Thin Silicon Substrate [c)]

Sieber, N., D. Proskurovskij
Annealing of Ion Implantation Damage at the Si/SiO_2 Interface by Electron Beam and Halogen Lamp Irradiation [c)]

Sieber, N., H. Oertel, M. Voelskow
Elektrische Eigenschaften von MOS-Strukturen, hergestellt in rekristallisiertem Silicium (r-Si) [ee)]

Sieber, N., D. Proskurovskij
Einfluß einer Wärmebehandlung mittels Elektronenstrahls oder Halogenlampen im Sekundenregime auf die elektrischen Eigenschaften von implantierten und nichtimplantierten MOS-Strukturen [ee)]

Sieber, N., D. Proskurovskij
Einfluß einer Wärmebehandlung mittels Elektronenstrahls oder Halogenlampen im Sekundenregime auf die elektrischen Eigenschaften von MOS-Strukturen; 32. Intern. Wiss. Koll., TH Ilmenau, 1987

Skorupa, W., K. Wollschläger, M. Voelskow, H. Bartsch, J. Albrecht, J. Götz
Formation of buried silicon nitride and silicon oxynitride layers in silicon by ion beam synthesis [c)]

Skorupa, W., M. Voelskow, J. Matthäi, K. Wollschläger, R. Grötzschel, H. Bartsch
Erzeugung von SOI-Strukturen durch Ionenstrahlverfahren; 32. Int. Wiss. Koll., Ilmenau, 26.-30.10.1987

Skorupa, W.
Hochenergieimplantation von Phosphor in Silicium [o)]

Skorupa, W., K. Wollschläger, U. Kreißig, R. Grötzschel, H. Bartsch
Properties of ion beam synthesized buried silicon nitride layers [m)]

Skorupa, W., K. Wollschläger, R. Grötzschel, J. Schöneich, E. Hentschel, R. Kotte, F. Stary, H. Bartsch, G. Götz
Properties of buried insulating layers in silicon formed by high dose implantation at 60 keV; 4. Int. Conf. Rad. Effects in Insulators, Lyon (France), 6.-10.7.1987

Skorupa, W.
Erzeugung von SOI-Strukturen durch Ionenstrahlverfahren; Problemseminar ZfK/ZMD, Rossendorf, 4.12.1986

Skorupa, W., K. Wollschläger, M. Voelskow, H. Bartsch, K.-H. Heinig
Formation of SOI-structures by ion beam synthesis at 60 keV [s)]

Skorupa, W.
Erzeugung von SOI-Strukturen durch Ionenstrahlverfahren [o)]

Skorupa, W.
Gettering in SOI-structures with ion beam synthesized buried silicon nitride layers; 2. Int. Autumn Meeting "GADEST", Garzau, 11.-17.10.1987

Skorupa, W., E. Wieser, R. Grötzschel, M. Posselt, A. Armigliato, A. Garulli, A. Beyer, W. Markgraf
High Energy Implantation and Annealing of Phosphorus in Silicon [c)]

Sobeslavsky, E., H.U. Jäger, W. Skorupa, K. Wollschläger
A model for nitrogen redistribution processes in high dose nitrogen implantation into silicon c)

Sobeslavsky, E.
Theoretische Aspekte der Stickstoffimplantation in Silicium; Seminar in: Physikalisch-Technisches Institut "A.I. Ioffe", Leningrad, 22.10.1987

Stary, F.
Activities of the Nuclear Physics Department of the Central Institute for Nuclear Research, Rossendorf (RDA); Instituts-Seminar in GANIL, Caen, 27.8.1987

Steinkopff, T., S. Matthies
Discrete statistical treatment of texture development r)

Strokovsky, E.A., V.G. Ableev, S.A. Saporoshets, B. Naumann, L. Naumann, A.A. Nomofilov, N.M. Piskunov, I.M. Sitnik, L.N. Strunov, V.I. Sharov, A.P. Kobuschkin, Ch. Dimitrov, L. Penchev, L. Visireva, B. Kühn, W. Neubert
Impulsnije spectry fragmentov v reakziyax fragmentazii relativistskikh yader d, ^{3}He, ^{4}He pod nulevym uglom n)

Teichfuß, M.
Zum Nachweis niederenergetischer geladener Teilchen l)

Teichfuß, M.
Development and Application of MOSFET-based Sensors f)

Tesch, S.
Nuclear Reaction Studies with Relativistic Beams of Light Nuclei at Dubna j)

Voelskow, M., W. Skorupa, J. Matthäi, H. Bartsch
Ion beam induced epitaxial crystallization of doped amorphous silicon layers c)

Voelskow, M., W. Skorupa, J. Matthäi, H. Bartsch, K.-H. Heinig
Ion beam induced epitaxial recrystallization of doped amorphous silicon layers s)

Voitus, W.
Wälzen von Polfiguren e)

Wagner, S., F. Neubert, Th. Otto, U. Kreißig, J. Schöneich
Physical model, properties and optoelectronical application of hydrogen implanted SOI MOSFET's c)

Weiss, L.
Untersuchungen der Struktur und der Dynamik der kondensierten Materie mit der Methode der Neutronenstreuung am Rossendorfer 10-MW-Reaktor; Seminar der HA Kern- und Festkörpertheorie des ZfK, Rossendorf, 14.9.1987

Wenk, H.R., T. Takeshita, C. Tome, H. Kern, S. Hofler, G. Will, S. Matthies
Texture development and plastic anisotropy in monomineralic rocks r)

Wieser, E., Ch. Weise, E. Vetter, Th. Gessner
Dotantenumverteilung in $MoSi_2$/Poly-Si-Schichtsystemen bei Kurzzeittemperung o)

Wieser, E.
Actual trends in doping and compound formation by implantation and subsequent annealing; V. International School on Physical Problems in Microelectronics, Varna, May 18-23, 1987

Wieser, E.
Silicierung durch Kurzzeittemperung n)

Wieser, E., Ch. Weise, E. Vetter, Th. Gessner, H. Lippmann
Redistribution of Implanted Dopants in $MoSi_2$/Poly-Si Structures During Silicidation Tempering c)

Wieser, E.
Rapid Thermal Processing for VLSI Application c)

Wünsch, R.
Sigma-Hyperons in nuclei u)

Wünsch, R.
An Alternative Interpretation of the Excitation Spectra of Sigma-Hypernuclei; LTF, VIK Dubna, Dezember 1986

Wünsch, R.
Hypernuclei; Inst. f. Kernphysik, Novosibirsk, Juni 1987

a) VIII. Int. Balaton Topical Conf. on Intermediate Energy in Nuclear Physics, Balatonfüred, 8.6.-13.6.1987

b) Int. Schrödinger Workshop "Matter wave interferometry", Wien, Sept. 1987

c) Intern. Conference on Energy Pulse and Particle Beam Modification of Materials, Dresden, 7.-11.9.1987

d) 31st IUPAC Macromolecular Symposium, Merseburg, 30.6.-4.7.1987

e) Int. Winterschule Neutronenstreuung, Stadt Wehlen, 26.-30.1.1987

f) IV. Vedecho-odborna Konf. mlad. prac., Rez, 2.-6.11.1987

g) 20. Fortschrittsberatung zur Endlagerung radioaktiver Abfälle, Stralsund, Nov. 1987

h) 12. Conf. on Physical Metallurgy, Katowice-Kozubnik, April 1987

i) 17. Kracow-Rossendorf-Rez-Kiev-Seminar, Kracow, März 1987

j) 19. Masurian Summer School on Nucl. Phys., Mikolajki, Sept. 1987

k) 4. Meeting on Nuclear Analytical Methods, Dresden, Mai 1987

l) 10. Tagung Physik und Elektronik, Berlin, 27.-29.10.1987

m) 5. Tagung "Festkörperanalytik", Karl-Marx-Stadt, 30.6.-3.7.1987

n) 3. Fachtagung Mikroelektronik-Technologie-Applikation, Karl-Marx-Stadt, 20.-22.10.1987

o) 12. Arbeitstagung "Ionenimplantation", Reinhardsbrunn, 30.3.-3.4.1987

p) Int. Symp. on Modern Developments in Nuclear Physics, Novosibirsk, 27.6.-1.7.1987

q) 17th International Symposium on Nuclear Physics, Gaußig, 9.-13.11.1987

r) ICOTOM 8, Santa Fe, September 1987

s) International Meeting of the European Materials Research Society (E-MRS), Strasbourg, 2.-5.6.1987

t) Frühjahrsschule der Kernphysik, Holzhau, 4.-8.5.1987

u) Int. Conf. on Theorie of Few Body-Systems and Quark-Hadron Interaction, Dubna, 16.-21.6.1987

v) 10th Discussion Conference "Small-Angle Scattering and Related Methods", Prag, Juli 1987

w) Int. Conf. "Advanced Methods in X-Ray and Neutron Structure Analysis of Materials", Karlovy Vary, Okt. 1987

x) 1. Int. Konf. über Schnellerstarrung metallischer Legierungen, Varna, 11.-17.5.1987

y) XXII School on Physics, Zakopane, 8.-15.5.1987

z) X. Arbeitstagung "Strukturuntersuchungen an nichtkristallinen und partiell kristallinen Stoffen" der VfK, Vietgest, April 1987

aa) Allunions-Symposium zur Physik der Kernspaltung, Obninsk, Juni 1987

bb) 5. International School on Vacuum, Electron and Ion Technologies, Varna, Okt. 1987

cc) INTERTRIBO 87, Strbske Pleso, 27.-29.4.1987

dd) 20. Fachkolloquium Informationstechnik, Dresden, 17.-19.2.1987

ee) Tagung Physik der Halbleiteroberfläche, Binz, 30.3.-4.4.1987

VERANSTALTUNGEN

Internationale Winterschule "Neutronenstreuung 1987", Stadt Wehlen, 26.-30.1.1987

Frühjahrsschule "Kernphysik", Holzhau, 3.-8.5.1987

International Conference "EPM-87 - Energy Pulse and Particle Beam Modification of Materials", Dresden, September 7-11, 1987

PATENTE

Hensel, E., W. Skorupa, K. Wollschläger, U. Kreißig
Verfahren zur Herstellung von Isolatorschichten in bzw. auf Halbleitersubstraten
DD 249 997 (23.9.1987)

Kögler, R., L. Zollfrank, M. Voelskow, Uhlig (ZMD), Hofmann (ZMD)
Strahlungsbeheizungsanlage für scheibenförmige Substrate
DD 249 569 A1 (9.9.1987)
DD 249 568 A1 (9.9.1987)

Lück, H.B.
Filterkassette mit tangentialer Überströmung
WP DD 249 413

Skorupa, W., K. Wollschläger, E. Hensel, U. Kreißig, H. Bartsch
Verfahren zur Herstellung vergrabener Isolatorschichten durch Ionenimplantation
DD 249 996 (23.9.1987)

WISSENSCHAFTLICHE PREISE

Institutspreise

1. Preis Kategorie I

Rotter, I.
Selbstorganisation in Atomkernen

2. Preis Kategorie I

Kirchbach, M., H.-U. Jäger
Einfluß von Mesonenaustauschströmen auf einfach verbotene β-Übergänge

3. Preis Kategorie I

Barz, H.W., Kämpfer, B.
Phasenübergang in Hadronenmaterie und Quarkfreiheitsgrade

Institutspreis Kategorie II, 1. Preis 1986/87

Lück, H.B., H. Matthes, G. Andrassy, W. Becher, M. Friedrich, B. Heinrich, W. Pfestorf, E. Schmidt
Kernspurmikrofilter

Sonderpreis für internationale Zusammenarbeit

Kotov, A.A., L.N. Andronenko, L.A. Vaishnene, I.P. Bondorf, R. Donangelo, G. Röpke, W. Neubert H. Schulz, H.W. Barz, E.N. Volnin (+)
Beiträge zur Multifragmentation

PROMOTIONEN A (Dr. rer. nat.)

Voelskow, M., J. Matthäi
Beeinflussung elektrischer und struktureller Parameter von implantierten polykristallinen Siliziumschichten durch Lichtimpulserwärmung
AdW der DDR, 10.7.1987

Lorenz, U., H. Ulrich
Si(Li)-Detektoren zur energiedispersiven Röntgenspektrometrie
AdW der DDR, 25.9.1987

Romaguera Fernandes, A.
Digitale Filtermethode zur Verarbeitung der Signale von Bragg-Ionisationskammern
AdW der DDR, 30.10.1987

Dang Viet Bac
Deconfinement-Phasenübergang und Quarkmaterie im nichttopologischen Soliton-Bag-Modell
AdW der DDR, 18.11.1987

PROMOTIONEN B (Dr. sc. nat.)

Iwe, H.
Relativistische Kern-Kern-Reaktionen im Rahmen des intranuklearen Kaskadenmodells
TU Dresden, 30.10.1987

DIPLOMARBEITEN

Hanicke, U.
Methodische Untersuchungen zur Ionenimplantation und Kurzzeittemperung bei der Präparation von Si(Li)-Detektoren
TU Dresden und ZfK Rossendorf, 1987

Miehe, U.
Neutronenkleinwinkelstreuung an Zementstein
TH Leipzig, 1987

BERUFUNG

Dr. sc. nat. Wieser, E.
Ernennung zum Professor für Festkörperphysik an der AdW der DDR, 3.9.1987

ZENTRALINSTITUT FÜR KERNFORSCHUNG ROSSENDORF, BEREICH G

VERÖFFENTLICHUNGEN

Alenitskij Yu. G., H. Guratzsch, N.L. Saplatin, S. Preusche, H. Tyrroff, S.I. Chesnova
The Choice of U-120 Cyclotron Trim Elements in the (1-1.45) T Induction Range,
Preprint 9-87-491, VIK Dubna (1987)

Dietrich, J.
A Linear Ion Optics Model for Extraction from a Plasma Ion Source
Nucl. Instrum. Methods A 262 (1987) 163

Eichhorn K., K. Bux
Verfahren zur Bestimmung der erosiven Wirkung kavitierender Strömungen auf Werkstoffe
WP G0 1 N/301 876.7

Eifrig Ch., K. Eichhorn, P. Hammer
Zweinuklidverfahren für kontinuierliche Abtragsmessungen
WP G0 1 N/308 521.3 2.11.1987

Eifrig Ch., K. Eichhorn, P. Hammer
Thin Layer Activation for Wear Studies in Compressors
Nucl. Instrum. Methods B 27 (1987) 45

Eichhorn K, S. Turuc, P. Hammer, Ch. Eifrig
Precise Activation for Wear Studies at the Rossendorf Tandem Accelerator
Procceedings of the Third Working Meeting Radioisotope Application and Radiation
Processing in Industry. Vol. 4, ZfI Leipzig

Hammer P., K. Eichhorn, Ch. Eifrig
A Study of Wear in Refrigerating Machines Using thin Layer Activation
Procceedings of the Third Working Meeting Radioisotope Application and Radiation
Processing in Industry. Vol. 4, ZfI Leipzig

Langrock E. J., K. Eichhorn, K. Gloe, P. Mühl
Erste Ergebnisse zur On-Line-Schnellextraktion mit Kronethern bei kernchemischen Experimenten
Isotopenpraxis 23 (1987) 8, 308

Schmidt D., H. Büttig, U. Jahn
Theoretische und experimentelle Untersuchungen zur Wärmeausbreitung in Targets für die
Anwendung der Thermographie in der Strahldiagnostik,
ZfK-619 (1987)

Werner T, K. Eichhorn
Anwendung der Dünnschichtaktivierung zur Verschleißmessung an Keilwellenverbindungen
Maschinenbautechnik 36 (1987) 9, 410

VORTRÄGE, die außerhalb des eigenen Kollektivs gehalten wurden

E. Richter
Stand und Perspektiven der Anwendung von Teilchenbeschleunigern
SAAS Berlin, 22.10.1987

K. Eichhorn
Zur Optimierung der Parameter bei Verschleißuntersuchungen mittels DSA
7. Kolloquium "Dünnschichtaktivierung", Dresden, 27.10.1987

VERANSTALTUNGEN

7. Kolloquium "Dünnschichtaktivierung", Dresden, 27.10.1987

XIV. Frühjahrsschule für Beschleunigungstechnik, Hörnitz, 23.-27.3.1987

TECHNISCHE UNIVERSITÄT DRESDEN, SEKTION PHYSIK, WB THEORETISCHE PHYSIK

VERÖFFENTLICHUNGEN

Münchow, L., R. Reif: Recent Developments in the Nuclear Many-Body Problem Vol. 2 Nuclear Reactions and Dynamics. Teubner-Texte zur Physik, Band 15, BSB B.G. Teubner Verlagsgesellschaft, Leipzig 1987

Kozulin, E.M., P. Mädler, M.B. Blinov, A.N. Moshaev, Yu.E. Penionshkevich: Investigation of neutron preequilibrium emission in reactions of ^{12}C (1o5 MeV) with ^{12}C, ^{27}Al, ^{56}Fe, ^{114}, ^{124}Sn, ^{181}Ta (in russisch). VIK Dubna Report P7-86-589, Dubna 1986

Ziesche, P., K. Kunze, B. Milek: Generalization of the Hellmann-Feynman theorem to Gamow states. J. Phys. A2o (1987) 2859

Mädler, P., L. Münchow, A. Pfitzner: Randomization of single-particle motion by collective fluctuations. Phys. Lett. 198B (1987) 25

Kartavenko, V.G., P. Mädler: Description of nuclear potentials and densities within the inverse problem. (in russisch) VIK Dubna Report P4-87-156, Dubna 1987 and Izwestia Akademii Nauk SSSR, Ser. Fiz., Vol. 51 (1987) 1973

Reif, R.: Semiclassical one-body dynamics of heavy-ion collisions. Proceedings of the Int. School-Seminar on Heavy-Ion Physics, Dubna, Sept. 1986, p. 54o

Mädler, P.: Description of fast nucleon emission within a phenomenological two-stage model. Proceedings of the Int. School-Seminar on Heavy-Ion Physics, Dubna, Sept. 1986, p. 554

Knospe, O., R. Schmidt, G. Seifert: Percolation approach for atomic and molecular cluster formation. GSI-Preprint, GSI-87-8o

Reif, R., R. Schmidt: Proceedings of the XVIth International Symposium on Nuclear Physics - Dynamics of Heavy-Ion Collisions - November 1o-14, 1986, Gaussig, p. 1 - 228 (Editors), ZfK - 61O

Gippner, P., K.D. Schilling, W. Seidel, F. Stary, E. Will, H. Sodan, S.M. Lukyanov, G.G. Chubarian, Yu. E. Penionzhkevich, V.S. Salamatin, R. Schmidt, A. Popp: Energy mass distributions observed in heavy-ion collisions leading to composite systems with $Z > 1oo$. ZfK-61o (1986) 42

Milek, B., R. Reif: Semiclassical treatment of a realistic nuclear two-state problem. ZfK-61o (1986) 59

Knospe, O., R. Schmidt, H. Schulz: Site-percolation approach for mass and isotopic distributions in fragmentation reactions. ZfK-61o (1986) 1o4

Biedermann, M., P. Mädler: A two-stage model for fast particle emission in heavy-ion collisions. ZfK-61o (1986) 114

DIPLOMARBEITEN

Knospe, O.: Ein Percolationsmodell für Multifragmentationsreaktionen

Jagdhold, U.: Untersuchung zur Rotationskopplung in einem semiklassischen Modell für periphere Schwerionenreaktionen

PROMOTION B (Dr. sc. nat.)

Schmidt, R.: Klassische und semiklassische Theorie dissipativer Schwerionenreaktionen

VORTRÄGE, DIE AUSSERHALB DES EIGENEN KOLLEKTIVS GEHALTEN WURDEN

Reif, R.: Semiclassical description of heavy-ion reactions.
Institut für Kernforschung Swierk, September 1987

Mädler, P.: Randomization of single-particle motion by collective fluctuations.
EPS Conference "From Cold to Hot Nuclei", Varna, September 1987

Reif, R.: Semiclassical description of heavy-ion collisions.
VIII. Internationale Sommerschule über Kernphysik, Neutronenphysik und Kernenergie, Varna, September 1987

Milek, B.: Gamow states in one-term separable potentials and particle emission in time-dependent problems. International Workshop "Separable potentials in various dynamical problems", Budapest, September 1987

Schmidt, R.: Evolution of the mass-asymmetry in dissipative heavy-ion collisions. Seminarvortrag GSI Darmstadt, Oktober 1987

Schmidt, R.: Evolution der Massenasymmetrie in dissipativen Schwerionenreaktionen. Seminarvortrag Institut für Theoretische Physik, Goethe-Universität, Frankfurt /Main, Oktober 1987

Schmidt, R.: Äquilibrierung der Massenasymmetrie in Schwerionenreaktionen. Seminarvortrag, Institut für Theoretische Physik, Justus-Liebig Universität, Giessen, Oktober 1987

Milek, B.: Gamow states in a two-center shell model and its applications. IV. Int. Conference of young scientists, Session C, Nuclear Physics and its applications, Rež, November 1987

TECHNISCHE UNIVERSITÄT DRESDEN, SEKTION PHYSIK, WB KERNPHYSIK

VERÖFFENTLICHUNGEN

Eckstein, P., U. Jahn, E. Paffrath, D. Schmidt, D. Seeliger: Intense Neutron Generator Development at the TU Dresden, IAEA Advisory Group Meeting on Neutron Source Properties, Leningrad, 9.-13.6.1986, IAEA-TECDOC-410, Vienna (1987) 369

Elfruth, T., D. Seeliger, K. Seidel, G. Streubel, S. Unholzer, D. Albert, et al., D.V. Markovskij, et al.: The Neutron Multiplication of Lead at 14 MeV Neutron Incidence Energy, Kerntechnik 49 (1987) 121

Märten, H., D. Richter, D. Seeliger, W.D. Fromm, R. Böttger, H. Klein: The ^{252}Cf(sf) Neutron Spectrum in the 5 - 20 MeV Energy Range, INDC(NDS)-134/L, Vienna (1987)

Märten, H., D. Seeliger: Description of the ^{252}Cf(sf) Neutron Spectrum in the Framework of a Generalized Madland-Nix Model, Nuclear Energy 25, Bulgarian Ac. Sci., Sofia (1987) 213

Märten, H.: Theoretical Description of the Cf-252 Fission Neutron Spectrum, IAEA Advisory Group Meeting on Neutron Source Properties, Leningrad, 9.-13.6.1986, IAEA-TECDOC-410, Vienna (1987) 144

Märten, H., A. Ruben, D. Seeliger: Calculation of Prompt Fission Neutron Spectra for Applied Purposes, ibid., 153

Märten, H., D. Richter, D. Seeliger, W.D. Fromm, W. Neubert: New Experimental and Theoretical Results of Cf Neutron Emission, ibid., 183

Märten, H., D. Richter, D. Seeliger, W. Neubert, A. Lajtai: Energy and Angular Distribution of ^{252}Cf Fission Neutrons in the Low Energy Range, ibid., 213

Schmidt, D., D. Seeliger, G.N. Lovchikova, A.M. Trufanov: Measurement and Systematics of Neutron Scattering on 6-Li and 7-Li Between 6 and 14 MeV, Nucl. Sci. Eng. 96 (1987) 159

Seeliger, D.: Techniques for 14 MeV Source Utilization, IAEA Advisory Group Meeting on Neutron Source Properties, Leningrad, 9.-13.6.1986, IAEA-TECDOC-410, Vienna (1987) 335

Seidel, K., D. Hermsdorf, H. Märten, S. Unholzer, H. Kalka, T. Elfruth, T. Hehl, M. Toepfer, S. Eckstein: Kerndatengewinnung und -einschätzungen für die Kernenergie, G4-Abschlußbericht, TU Dresden, Sektion Physik, WB Kernphysik (Mai 1987)

DIPLOMARBEITEN

Al Obiesi, Haitham: Differentielle Neutronenemissionsquerschnitte von Tantal bei 14 MeV Neutroneneinschußenergie

Bittner, Michael: Berechnung, Aufbau und Test eines Analysiermagneten für das Strahlführungssystem von INGE-1

Boneß, Gunnar: Konzeption und Aufbau einer Instrumentierung für Standardneutronenfelder

Claveria, J. Arias: Analyse experimenteller und theoretischer Daten zur Spaltneutronenemission aus der Spontanspaltung von 252-Californium

Jank, Klaus: Beschreibung der Neutronenemission aus U-238 bei 14 MeV Neutroneneinschußenergie

Neidel, Peter: Aufbau und Erprobung eines Tritium-Sicherheitssystems für den Neutronengenerator INGE-1

Rodriguez, Gonzales: Untersuchung des Neutronentransports durch eine Eisen-Wasser-Schichtanordnung bei einer Neutroneneinschußenergie von 14 MeV

Ruben, Andreas: Theoretische Analyse von Spaltneutronenspektren im Zusammenhang mit dem Studium der Energiebalance der Kernspaltung

Torjman, Maha: Einfache Methoden zur Parametrisierung doppelt-differentieller Neutronenemissionsspektren abgeleitet am Beispiel ^{93}Nb+n

PROMOTIONEN A (Dr.rer.nat.)

Elfruth, Tilo: Untersuchung der Neutronenemission von Blei bei 14 MeV Neutroneneinschußenergie, TU Dresden, 13. 5. 1987

Kalka, Harald: Excitonenmodell - mikroskopische Herleitung und Anwendung, TU Dresden, 14. 4. 1987

Paffratz, Elief: Entwicklung des Vakuumsystems eine Hochgradient-Beschleunigers und Untersuchung der Sekundäreffekte bei intensivem Strahlbetrieb, TU Dresden, 27. 2. 1987

VORTRÄGE, DIE AUSSERHALB DES EIGENEN KOLLEKTIVS GEHALTEN WURDEN

Elfruth, T., T. Hehl, H. Kalka, H. Märten, A. Ruben, D. Seeliger, K. Seidel, S. Unholzer: Double-Differential Neutron Emission Cross Sections for 238-U [a])

Kalka, H.: SMD/SMC-Model for Practical Applications [a])

Kalka, H., D. Seeliger, F.A. Shivopistsev: Statistical Multistep Direct and Compound Processes Below 30 MeV for 93-Niobium [b])

Märten, H., A. Ruben, D. Seeliger: Theory of Fission Neutron Emission [b])

Märten, H., D. Richter, D. Seeliger, W. Neubert, A. Lajtai: Energy and Angular Distribution of Neutron Emission in the Spontaneous Fission of 252-Cf [b])

Märten, H.: Kernenergie - Nutzen oder Verderben der Menschheit?, VP-Bereitschaft, Dresden, 22. 9. 1987

Märten, H.: Prompte Spaltneutronen in Experiment und Theorie, ZfK Rossendorf, Bereich KF, 30. 11. 1987

Märten, H., A. Ruben, D. Seeliger: Fission Energetics and Prompt Fission Neutron Emission [a])

Märten, H., D. Richter, A. Ruben, D. Seeliger: Experimental Study of Fission Neutron Spectrum of 232-Th [a])

Märten, H., A. Ruben, D. Seeliger: Consistent Theoretical Description of Energy and Angular Distributions of Prompt Fission Neutrons [a])

Märten, H.: Theoretical Models and Computer Codes for the Description of Prompt Fission Neutron Spectra, IAEA Advisory Group Meeting on Nuclear Theory for Fast Neutron Nuclear Data Evaluation, Beijing (VR China), 12.-16.10.1987

Pilz, W., W. Neubert, K. Arnold, D. Lucas, H. Märten: Angular Distributions of Prompt γ-rays in the Spontaneous Fission of 252-Cf [a])

Pilz, W., W. Neubert, K. Arnold, D. Lucas, H. Märten: Angular Distributions of Prompt γ-rays in the Spontaneous Fission of 252-Cf, Masurian Summer School on Nuclear Physics, Mikolaiki (Polen) 1987

Seeliger, D., K. Seidel, G. Streubel, S. Unholzer, T. Elfruth, D. Albert, K. Noack, K. Reiche, W. Vogel, W. Hansen, D.V. Markowskij, G.E. Shatalov: Messung der Neutronenausflußspektren aus einer Uraniumkugel (in russ.), RGW-Seminar Kernfusion, Varna, (VR Bulgarien) 5.-8.5.1987

Seeliger, D., K. Seidel, G. Streubel, S. Unholzer, T. Elfruth, D. Albert, K. Noack, K. Reiche, W. Vogel, W. Hansen, D.V. Markowskij, G.E. Shatalov: Differentielle Neutronenemissionsquerschnitte von Blei und integrale Messungen an Bleikugeln bei 14 MeV Neutroneneinschußenergie (in russ.), RGW-Seminar Kernfusion, Varna,(VR Bulgarien) 5.-8.5.1987

Seeliger, D.: Kerndaten für die Fusionsreaktortechnologie (in russ.), RGW-Seminar Kernfusion, Varna, (VR Bulgarien) 5.-8.5.1987

Seeliger, D.: Double-Differential Neutron Emission Cross Sections, Proc. d. IAEA AGM Neutron Data for Fusion Reactor Technology, Wien, 1987

Seidel, K., D. Seeliger, G. Streubel, S. Unholzer, T. Elfruth, D. Albert, K. Noack, K. Reiche, W. Vogel, W. Hansen, V.D. Markovskij, G.E. Shatalov: Differentielle Neutronenemissionsquerschnitte für Blei bei einer Neutroneninzidenzenergie von 14 MeV (in russ.) [b])

Seidel, K., D. Seeliger, V.K. Ignatovich, A. Meister, S. Mittag, W. Pilz: Temperaturverschiebung von Neutronenresonanzen (in russ.) [b])

Torjman, M., H. Kalka, D. Hermsdorf, D. Seeliger: A Semiempirical Description of Double-Differential Neutron Emission Spectra for 93-Niobium [a])

[a]) XVIIth Intern. Symp. on Nuclear Physics -Nuclear Reaction- Gaussig, Nov. 9-13, 1987

[b]) Intern. Conf. Neutron Physics, Kiev, 21-25.9.1987

VERANSTALTUNGEN

XVIIth International Symposium on Nuclear Physics -Nuclear Reactions- Gaussig, November 9 - 13, 1987

BERUFUNGEN

Dr.sc.nat. Andreas Meister wurde mit Wirkung vom 1.2.1987 zum Dozenten für Experimentalphysik an der TU Dresden - Sektion Physik - berufen.

TECHNISCHE UNIVERSITÄT DRESDEN, SEKTION PHYSIK, WB ANGEWANDTE KERNPHYSIK

VERÖFFENTLICHUNGEN

Bischoff, L., D. Mademann, K. Trützschler, G. Zschornack
Der Einsatz von Mikrostreifendetektoren in der winkeldispersiven Röntgenspektroskopie
Exp. Technik der Physik, 35 (1987) No. 3, 153

Hartmann, Fr.-W., K. Irmer
Radiometrische Steinortung auf Braunkohlen-Förderbändern
Wissenschaftl. Zeitschrift der TU Dresden, 36 (1987) 103

Heckel, J., W. Scholz
Description of Low-Energy Peak Distortion Observed in X-Ray Spectrometry with Si(Li) Detectors
X-Ray-Spectrometry, 16 (1987) 181

Heckel, J., P. Jügelt
Die Nutzung extremer Linien - zu Untergrundverhältnisse in der quantitativen energiedispersiven Elektronenstrahl-Mikroanalyse
X-Ray-Spectrometry, 16 (1987) 67

Herbach, G.-M., K. Merla, G. Musiol, G. Pausch
I.D. Alchasov, L.V. Drapchinsky, E.A. Ganza, S.S. Kostochkin, V.J. Kovalenko, P.S. Shpakov, S.M. Soloshenkov, S.M. Solovjev
Absolute measurements of the U-238 fission cross-section at 4.8 MeV and 18.8 MeV neutron energies
TU-Preprint 05-02-87

Irmer, K., G. Musiol
Radiometrische Qualitätsbestimmung von Braunkohle
Wissenschaftl. Zeitschrift der TU Dresden, 36 (1987) 97

Irmer, K.
A4-Bericht , Entwicklung eines Verfahrens zur Bestimmung des Füllstandes bei CO_2-TFB-Löschern
VEB Feuerlöschgerätewerk Apolda, Aug. 87

Kreiseler, D., G. Zschornack
Temperaturregelung am Analysatorkristall eines Kristalldiffraktionsspektrometers mit einem diskreten parameteroptimierten Regler
Exp. Technik der Physik, 35 (1987) No. 2, 111

Musiol, G., G. Pausch
Absolut- und Präzisionsbestimmung von Spaltquerschnitten wichtiger Nuklide der Reaktortechnik und deren Bedeutung für die Kernenergetik
Wissenschaftl. Zeitschrift der TU Dresden, 36 (1987) 87

Pausch, G., C.-M. Herbach, K. Merla, G. Musiol, R. Perez
Determination of fission fragment counting losses from the fission chamber spectrum
Part I: Idealized plane targets, TU-Preprint 05-08-87

Pausch, G., C.-M. Herbach, K. Merla, G. Musiol
Determination of fission fragment counting losses from the fission chamber spectrum
Part II: Scratched targets, TU-Preprint 05-09-87

Pausch, G., C.-M. Herbach, K. Merla, G. Musiol
Determination of fission fragment counting losses from the fission chamber spectrum
Part III: Appendix, TU-Preprint 05-10-87

Reichmann, A., G. Musiol, W. Wagner, G. Zschornack
Statistical Simulation of Geometrical Abberations in Curved Crystal Bragg-Spectrometers
TU-Preprint 05-01-87

Schmidt-Böcking, H., V. Dangendorf, I. Euler, I. Ullrich, S. Schmidt, G. Zschornack, S. Hagmann
Eine Apparatur zum Nachweis hochgeladener metastabiler Rückstoßionen
8. Arbeitsbericht "Energiereiche atomare Stöße", Gesamthochschule Kassel, GSI Darmstadt
EAS-8 p. 126

Zeuner, A.
A4-Bericht , Materialtransportuntersuchungen an einem Modell - Drehrohrofen
TU Magdeburg, März 1987

Zeuner, A.
A4-Bericht, Verweilzeituntersuchung an der Rohrschwingmühle einer Rohrtrogschwingmühle
VEB Kombinat Keramische Werke Hermsdorf, Dez. 1987

Zeuner, A.
A4-Bericht , Radiometrische Verweilzeituntersuchungen an einer Laboranlage zum Intensivconchieren von Schokoladenmassen
VEB Maschinenfabrik Heidenau, Dez. 1987

Zschornack, G., I. Reiche
Ein neues Programm zur Berechnung relativistischer Röntgenemissionsraten
8. Arbeitsbericht "Energiereiche atomare Stöße", Gesamthochschule Kassel, GSI Darmstadt
EAS-8 p. 111

Zschornack, G.
A Systemation of X-Ray Energies and Electron Binding Energies in Free Highly Charged Ions
Nucl. Instr. Methods, B23 (1987) p. 278

DIPLOMARBEITEN

Brumme, M.
Theoretische Untersuchungen zur Reduzierung der minimalen Nachweisgrenzen und des Analysenfehlers in der energiedispersiven Röntgenfluoreszenzanalyse geologischer Proben

Hanicke, U.
Methodische Untersuchungen zur Ionenimplantation und Kurzzeittemperung bei der Herstellung von Si(Li)-Detektoren

Jara Colom Luis Emilio
Beiträge zur Entfaltung winkeldispersiv gemessener Röntgenspektren mittels BAYES-Theorem

John, D.
I. Erarbeitung einer Konzeption für die Entwicklung eines energie- und ortsauflösenden Detektionssystemes auf der Basis von Si-Mikrostreifendetektoren
II. Zusammenstellung der Methoden zur Bestimmung der Nachweiseffektivität von Halbleiterdetektoren

Perez, R.
Untersuchung von U-235-Spalttargets bezüglich der Absorption von Spaltfragmenten

VORTRÄGE, DIE AUSSERHALB DES EIGENEN KOLLEKTIV GEHALTEN WURDEN

Herbach, C.-M., K. Merla, G. Musiol, H.-G. Ortlepp, G. Pausch, U. Todt, I.D. Alkhazov, L.V. Drapchinsky, E.A. Ganza, O.I. Kostochkin, S.S. Kovalenko, V.I. Shpakov, P.S. Soloshenko, S.M. Solovjev
Absolute measurements of the U-238 fission cross-section at 4.8 MeV, 8.4 MeV and 18.8 MeV neutron energies using the TCAPM
Proc. of the Internat. Conf. of Neutron Physics, Kiev, 21.-25. Sept. 87

Herbach, C.-M., K. Merla, G. Musiol, H.-G. Ortlepp, G. Pausch, U. Todt, I.D. Alkhazov, L.V. Drapchinsky, E.A. Ganza, O.I. Kostochkin, S.S. Kovalenko, V.I. Shpakov, P.S. Soloshenko, S.M. Solovjev
Absolute measurements of the U-238 fission cross-section at 4.8 MeV, 8.4 MeV and 18.8 MeV neutron energies using the TCAPM
XVII. Int. Symposium on Nuclear Physic - Nuclear Reactions- Gaußig, Nov. 9-13. 1987

Herbach, C.-M., K. Merla, G. Musiol, H.-G. Ortlepp, G. Pausch, W. Wagner, I.D. Alkhazov, L.V. Drapchinsky, E.A. Ganza, S.S. Kovalenko, O.I. Kostochkin, S.M. Solovjev, V.I. Shpakov
Revised Results of absolute fission cross-section measurements on Pu-239 at 4.9 MeV, 8.65 MeV, 14.7 MeV and 18.8 MeV neutron energy
Proc. of the Intern. Conf. of Neutron Physics, Kiev, 21.-25. Sept. 1987

Musiol, G., G. Pausch, C.-M. Herbach, K. Merla, R. Perez
Determination of fission fragment counting losses from the fission chamber spectrum
Proc. of the Intern. Conf. of Neutron Physics, Kiev, 21.-25. Sept. 1987

Musiol, G.
Kernenergie und Umwelt
Vortrag vor Professoren der TU Dresden, 26.3.87

Musiol, G.
Kernenergie und Menschheit
Forum an der TU Dresden, 4.5.87

Musiol, G.
Kern- und Elementarteilchenphysik am VIK Dubna
Museum für Geschichte der Stadt Dresden, 6.5.87

Musiol, G.
Kernenergie und Umwelt
Kolloqium der Sektion Physik des BAF, 27.5.87

Musiol, G.
Die Forschungskooperation der DDR mit dem VIK Dubna
Beirat für Physik des MHF, Berlin, 21.11.87

Reichmann, A., G. Musiol, G. Zschornack
Hochauflösende wellenlängendispersive Röntgenspektroskopie an Quellen hochionisierter Atome
Jahreshaupttagung der Phys. Gesellschaft der DDR, 24.-27.2.87, Berlin

Zeuner, A.
Anwendung radioaktiver Indikatoren in der Keramik
IV. Hermsdorfer Symposium, Nov. 87

Zeuner, A.
Einsatz von Radiotracern zur Prozeßanalyse durch die TU Dresden
Forschungszentrum der Mechanisierung der Landwirtschaft, Potsdam, Febr. 87

Zeuner, A., K.-E. Militzer, Th. Jentzsch
Materialtransportuntersuchungen an einem Drehrohrtrockner der Kaliumindustrie
Köthen, Okt. 87

Zschornack, G.
Quellen hochgeladener Schwerionen als Basisanlagen der atomaren Schwerionenphysik
Vortrag auf dem Kolloqium des Institutes für Kernphysik, Universität Frankfurt/Main, Juni 1987

Zschornack, G.
Möglichkeiten der Nutzung des Beschleunigers KUTI-20 als Ionisator für Schwerionen und der Durchführung von Experimenten zur Untersuchung von hochionisierten Atomen
Vortrag auf der 30. Tagung des Komitees für Schwerionenphysik und auf der Tagung des Kernstrukturkomitees des VIK Dubna, 13.-15. Okt. 1987

Zschornack, G.
Der Dubnaer Schwerionenbeschleuniger als Quelle hochionisierter Atome
Vortrag am ATOMKI, Debrecen/VR Ungarn, 9. Dez. 1987

Zschornack, G., G. Musiol, A. Reichmann
Der Einfluß der Meßgeometrie auf die Form und Position von Diffraktionsreflexen
Vortrag auf der 8. Tagung "Energiereiche atomare Stöße" Oberstdorf, 26.-30.1.1987

Zschornack, G.
Der Einsatz von Mikrostreifendetektoren zur positionsempfindlichen Spektroskopie charakteristischer Röntgenstrahlung
Vortrag am Zentralinstitut für Kosmosforschung der AdW der DDR, Berlin, Mai 1987

Zschornack, G.
Kernphysik im 20. Jahrhundert - Bedrohung und Hoffnung
Vortrag im Kulturbund der DDR, Pirna, April 1987

KARL-MARX-UNIVERSITÄT LEIPZIG, SEKTION PHYSIK, WB ANGEWANDTE KERNPHYSIK

VERÖFFENTLICHUNGEN

Ascheron, C., H. Neumann: Microhardness - damage density relationship in proton and helium implanted GaP single crystals. Nucl. Instrum. Meth. Phys. Res. B 18 (1987) 161

Ascheron, C., G. Otto, R. Flagmeyer, H.-E. Zschau, V.N. Bugrow, S.A. Karamyan: Damage profiling on high energy ion implanted GaP. Proc. 16th All-Union Conf. on Interactions of Charged Particles with Crystals, Ed Moscow State Univ., 1987

Ascheron, C., H. Bartsch, A. Setzer, A. Schindler, P. Paufler: The effect of hydrogen implantation induced stress on GaP single crystals. Nucl. Instrum. Meth. Phys. Res. B 28 (1987) 350

Ascheron, C., R. Flagmeyer, G. Otto, J. Vogt, H.-U. Frey: A study of radiation damage on proton bombarded GaP by PIXE. Cryst. Res. Technol. 22 (1987) 1497

Ascheron, C., H. Neumann, V.N. Bugrow, S.A. Karamyan: Microhardness of Ion Implanted GaP. phys. stat. sol. (a) 103 (1987) K 81

Ascheron, C., und H. Neumann: Depth profile of the microhardness in He^+ implanted GaP. Cryst. Res. Technol. 22 (1987) 1493

Flagmeyer, R., und B. Schumann: Characterization of epitaxial group II flueride films on (100)-oriented GaAs substrates by ion backscattering and channeling. Cryst. Res. Technol. 22 (1987) 893

Frey, H.-U., G. Otto, J. Vogt: Thick target PIXE analyses of elemental distributions across the surface and inside human fingernails. Nucl. Instrum. Meth. Phys. Res. B (1987)

Riede, V., H. Neumann, H. Sobotta, C. Ascheron, B.V. Novikov: Hydrogen-Induced Localized Vibrational Mode in Proton Implanted ZnSe Single Crystals. Sol. State Comm. 61 (1987) 113

Schumann, B., G. Kühn, W. Gasch, G. Wagner, R. Flagmeyer, O. Müller, W. Hauffe: Epitaxial $Ca_{0.43}Sr_{0.57}F_2$/GaAs(100) Heterostructures Grown by Flash Evaporation Technique. J. Cryst. Growth 82 (1987) 405

DIPLOMARBEITEN

Knolle, Wolfgang: Ionenstrahl-Stoffanalyse an Kohleprodukten, KMU Leipzig, Juli 1987

Plier, Frank: Ionenstrahlanalyse an Zähnen, KMU Leipzig, Juli 1987

VORTRÄGE

Ascheron, C., G. Dlubek, R. Krause, H. Erhard, D. Klimm: Positron study of vacancy defects in proton and neutron irradiated GaP, InP and Si. European Meeting on Positron studies of Defects, Wernigerode, März 1987

Ascheron, C., G. Otto, H. Neumann, G. Dlubek, R. Krause, S.A. Karamjan, V.N. Bugrov: Ion bombardment induced changes in microhardness of GaP, ebenda

Ascheron, C., M. Sobotta, V. Riede, C. Neelmeijer, R. Grötschel, W. Rudolph, A. Schindler: Investigations of the annealing behaviour of hydrogen implanted GaP-single crystals by means of PIGE, IRS and RBS/C technique. 4th Meeting on Nuclear Analytical Methods, Dresden, Mai 1987

Ascheron, C., G. Otto, R. Flagmeyer, H.-E. Zschau, V.N. Bugrov, S.A. Karamjan: Damage profiling on high energy ion implanted GaP. 17th All-Union Conf. on Interactions of Charged Particles with Crystals, Moskau, Mai 1987

Ascheron, C., H. Klose, D. Frentrup: Gettering of Cu in GaP due to defects generated by H^+ and He^+ bombardment. Int. Antuum School Gettering and Defect Engineering in Semiconductor Technol., Garzau, Oktober 1987

Baumbach, T., H. Rhan, R. Flagmeyer, H.G. Brühl, U. Pietsch: Charakterisierung von Heterobergängen mittels Rutherford-Rückstreuung (RBS) und Röntgenbeugung (RB) zur Optimierung von Bauelementestrukturen. Jahreshaupttagung der Physik. Ges. der DDR, Berlin, Februar 1987

Flagmeyer, R., M. Höricke: RBS/Channeling analysis of thin strained layers of $In_xGa_{1-x}As$ on GaAs(100) substrates grown by MBE. Symp. Molecular Beam Epitaxy, Frankfurt/Oder, März 1987

Flagmeyer, R., G. Otto, R. Fechner, A. Schindler, F. Bigl: Study of damage produced by low energy Ar ion beam etching of GaAs by means of RBS/Channeling technique and ^{64}Cu adsorption and autoradiographic detection. 4th Meeting on Nuclear Analytical Methods, Dresden, Mai 1987

Flagmeyer, R.: Analyse dünner Schichten und oberflächennaher Bereiche von Festkörpern mittels Rückstreuspektrometrie. Bereichsseminar ZfI Leipzig, Mai 1987

Flagmeyer, R., M. Höricke: RBS/Channeling analysis of strained $In_xGa_{1-x}As$ films on GaAs(100). 17th All-Union Conf. on Interactions of Charged Particles in Crystals, Moskau, Mai 1987

Flagmeyer, R., K. Lenkeit, Yu.O. Kanter: Rutherford Rückstreu- und Channelinguntersuchungen an verspannten $In_{0.2}Ga_{0.8}As$/GaAs-Supergitterschichten. 10. Tagung Physik und Elektronik, Berlin, Oktober 1987

Flagmeyer, R., H. Rhan, U. Pietsch, M. Höricke, H. Berger: siehe unten!+)

Flagmeyer, R., G. Oelgart, K. Kreher, R. Schwabe, F. Dugge, K. Jacobs, L. Lehmann: Charakterisierung von MOCVD-gezüchteten (Al,Ga)As-QW-Strukturen mittels Rückstreuspektrometrie und Fotolumineszenz. XIV. Herbstschule Physik und Chemie der AIIIBV-Halbleiter, Breitenstein, November 1987

Flagmeyer, R., K. Gärtner: Nachweis innerer Verzerrungen mittels RBS/channeling. ebenda

Frey, H.-U., G. Otto: PIGE- and PIXE-analyses of zeolites. 4th Meeting on Nuclear Analytical Methods, Dresden, Mai 1987

Hörig, W., V.F. Orlenko, H. Neumann, C. Ascheron: Near-edge optical properties of proton and helium implanted InP single crystals. European Meeting on Positron Studies of Defects, Wernigerode, März 1987

Knolle, W., G. Otto: Ionenstrahl-Stoffanalyse im Prozeß der Kohleveredelung. Wiss. Studentenkonferenz Karl-Marx-Stadt, Februar 1987

Lehmann, D., C. Ascheron, C. Neelmeijer: Hydrogen depth profiling in H implanted semiconductors using elastic recoil detection. 4th Meeting on Nuclear Analytical Methods, Dresden, Mai 1987

Lehmann, D.: Der gespaltene Atomkern - Fluch oder Segen. Urania-Vortragszentrum Leipzig, Juni 1987

Otto, G.: Proton-induced Kossel-Effect; fast Ion Interactions with Single Crystals. Institutskolloquium, Florida State University, Dep. of Physics, Tallahassee, USA, März 1987

Otto, G.: Proton-induced Kossel-Effect and Ion Beam Elemental Analysis at the Karl-Marx-University. Bereichskolloquium, Brootehaven National Laboratory Devision of Applied Science Upton, USA, April 1987

Otto, G.: Ion Beam Investigations at the van de Graaff of the Karl-Marx-University, Leipzig. Bereichskolloquium, Brooklyn College Dep. of Chemistry N.Y., USA, Mai 1987

Rentsch, H., K. Merta, H.-E. Zschau, J. Vogt and G. Otto: Chemical changes in the outermost bovine enamel layer during white spot lesion formation.14th ORCA Congress, Budapest, Juli 1987

Schindler, A., R. Fechner, R. Flagmeyer, D. Panknin, F. Bigl, G. Otto: Analysis of Ar ion beam etching induced surface damage of GaAs by means of ^{64}Cu adsorption autoradiography and RBS/Channeling. EPM 87, Dresden, September 1987

Schindler, A., R. Fechner, K. Kraft, R. Flagmeyer, F. Bigl: Untersuchungen zum Ionenstrahlätzen von A3B5-Halbleitern. 32. Int. Wiss. Kolloquium, TH Ilmenau, Oktober 1987

Vogt, J., H.-E. Zschau, G. Otto: Elemental analysis of geological samples by spectrometry of proton induced gamma- and X-ray radiation. 4th Meeting on Nuclear Analytical Methods, Dresden, Mai 1987

Vogt, J.: Quantitative Multielementanalyse geologischer Proben mittels PIXE, PIGE und RBS. Lehrgang Kernphysik, Analysenverfahren in den geologischen Wissenschaften der KMU, Leipzig, November 1987

Weinert, H., B. Schumann, R. Flagmeyer: Eigenschaften von MQW-Strukturen hergestellt mittels Flash-Verdampfung. 10. Tagung Physik und Elektronik, Berlin, Oktober 1987

+)Charakterisierung verspannter (In,Ga)As-MBE-Schichten auf GaAs-Substrat mittels RBS/channeling und Röntgenbeugung. 10. Tagung Physik und Elektronik, Berlin, Oktober 1987

Zschau, H.-E.: Elementanalytik am Ionenstrahl. Seminar, KKW Rheinsberg, Januar 1987

Zschau, H.-E.: Sicherheit von Kernkraftwerken. Urania-Forum, Interflug Leipzig, Mai 1987

Zschau, H.-E., J. Vogt, G. Otto, F. Plier, M. Schneider, A. Treide: Depth behaviour of fluorine, calcium, phosphorus and oxygen in tooth enamel after application of a fluoride varnish. 4th Meeting on Nuclear Analytical Methods, Dresden, Mai 1987

HUMBOLDT-UNIVERSITÄT ZU BERLIN, SEKTION PHYSIK, BEREICH 06 - ATOMSTOSSPROZESSE DER FESTKÖRPERPHYSIK

VERÖFFENTLICHUNGEN

J. Bollmann, H. Klose und K. Maass: Zur Auswertung von DLT-Spektren bei hohen Konzentrationen tiefer Zentren in oberflächennahen Bereichen, Proc. der 18. Tagung "Physik der Halbleiteroberfläche" des ZIE der AdW (eingereicht 05/87)

C. Ascheron, H. Klose, and W. Frentrup: Gettering of Cu in GaP due to defects generated by H^+ and He^+ bombardement, Proc. Int. Autuumn School GADEST 2, 304 (1987)

C. Ascheron, H. Klose, W. Frentrup, M. Griepentrog: Gettering of Copper in Proton- and Helium-Bombarded Regions of Gallium Phosphide, phys.stat.sol. (a) (erscheint in Vo. 106 Heft 1)

K. Holldack, H. Kerkow, and M. Reiche: Point defect migration and impurity diffusion in Si due to ion irradiation, Proc. Int. Autumn School GADEST 2, 185-189 (1987)

J. Bollmann, A. Mertens, and H. Klose: "Channeling effects at low-energy ion implantation, Proc. IPM, Dresden 1987

U. Schade, O. Maly, K. Vogel, W. Frentrup, P. Thiele: Untersuchungen zur thermischen Stabilität von Cr-Au-Kontakten auf p-GaAs, Experimentelle Technik der Physik 35, 297 (1987)

H. Günther, D. Menz: Die Anwendung von mit Pyrokohlenstoff-beschichteten Graphitformteilen in der Hochtemperaturtechnik, Zeitschrift Silikattechnik (eingereicht 12/86)

M. Riedel and H. Düsterhöft: Energy Distribution of Secondary Ions Emitted from Pure Elements and Alloys, Vacuum 37, 157 (1987)

G. Ferenczi, C. A. Londos, F. Pavelka, M. Somogyi, and A. Mertens: Identification of the carbon associated radiation damage levels in silicon, Defects in Semiconductors, ed. H. J. von Barleben; in Materials Science Forum Volumes 10-12, 947 (1986)

K. Holldack, H. Kerkow, W. Frentrup: Diffusionsanomalien in Silizium infolge Ionenbeschusses, Wiss. Zs. Techn. Universität Dresden 36, 64 (1987)

A. V. Dvurechenskii, V. P. Popov, B. P. Dashnikov, and M. Griepentrog: Disordering and amorphization of strongly doped Silicon at heavy-ion Bombardment, Poverchnost 9, 77 (1986) (in russ.)

M. Fried, T. Lohner, H. Kerkow et al.: Optical Properties of Thermally Stabilized Ion Implantation Amorphized Silicon, Nucl. Instr. Meth. Phys. Res. B 20, 577 (1987)

H. Kerkow, K. Holldack: Defect flux effect during ion implantation, Proc. EPM, Dresden 1987

K. Holldack, H. Kerkow: Impurity Redistribution in Silicon due to Ion Bombardment, Proc. EPM, Dresden 1987

K. Holldack, H. Kerkow: Radiation-enhanced Diffusion in Silicon due to Ion Bombardment, Proc. 4th. Working Meeting on Radiation Interaction, Leipzig 1987

K. Holldack, H. Kerkow, M. Gericke: Rate effects during radiation-enhanced Diffusion of Boron in Silicon, phys.stat.sol. (a) 102, 633 (1987)

K. Holldack, H. Kerkow: Flux dependence of damage accumulation in Si, phys.stat.sol. (a) 98, 527 (1987)

K. Kneipp: High-sensitive SERS on colloidal silver particles in aqueous solution, Exp. Techn. Phys. (eingereicht Sept. 1987)

K. Kneipp and J. Flemming: Surface-enhanced raman scattering (SERS) of nucleic acids adsorbed on colloidal silver particles: Adsorption behaviour and enhancement mechanism, Laser Scatt. Spectroscopy Bio. Objects 45, 115 (1987)

H. Kneipp and K. Kneipp: Surface-enhanced excited state raman spectroscopy (SEERS) using pulsed copper vapour laser excitation, Laser Scatt. Spectroscopy Bio. Objects 45, 115 (1987)

K. Kneipp, H. Kneipp and M. Rentsch: SERS on A 1,1'-Diethyl-2,2' Cyanine Dye Adsorbed on Colloidal Silver, Journ. of Molecular Structure, 156, 331-340 (1987)

A. F. Burenkov, U. Krause: Veränderung von Tiefenprofilen durch Sputtering, eingereicht bei Poverchnost (UdSSR), 07/87 (in russ.)

R. Köchert: Einige neue Aspekte über G. L. Lichtenbergs Arbeiten auf dem Gebiet elektrischer Erscheinungen der Atmosphäre, Zeitschrift der Lichtenberg-Gesellschaft "Photorin", BRD (eingereicht Sept. 87)

DIPLOMARBEITEN

S. Grossman: DLTS-Studien zur Kanalleitung niederenergetischer Magnesiumionen in Silizium.

U. Keiderling: Getastete Xenon-Hochdruckentladung.

J. P. Kuska: Elektronenaustausch bei Ionen-Oberflächen-Stößen.

U. Benner: Untersuchungen zur Parameterabhängigkeit der Strahlenschadensentstehung bei der Ionenimplantation von einkristallinem Silizium in Kanalrichtung im Vergleich zum Randomeinschuß.

DISSERTATIONEN A

K. Holldack: Ionenstrahlinduzierte Diffusion von Bor und Phosphor in Silizium.

VORTRÄGE

H. Klose und A. Mertens: Stand und Perspektiven der niederenergetischen Ionenimplantation, 10. Tagung "Physik und Elektronik", Berlin, 10/87

J. Bollmann, A. Mertens und H. Klose: Kanalleitungseffekte bei niederenergetischer Mg-Implantation in Silizium, 10. Tagung "Physik und Elektronik", Berlin, 10/87

R. Flagmeyer, K. Lenkeit, Yu. O. Kanter: Rutherford-Rückstreu- und Channelinguntersuchungen an verspannten $In_{0.2}Ga_{0.8}As/GaAs$ Supergitterschichten, 10. Tagung "Physik und Elektronik", Berlin, 10/87

W. Frentrup, B. Lukasch, U. Müller-Jahreis: Analyse dünner Platinsilizidschichten mittels Sekundärionenmassenspektrometrie, 10. Tagung "Physik und Elektronik", Berlin, 10/87

U. Schade, D. Maly, K. Vogel, W. Frentrup, P. Thiele: Investigation on the thermal stability of Cr-Au-contacts, Int. Conf. on Semiconductor Injection Laser "SELKO 1987", Holzhau 10/87

J. Bollmann, A. Mertens, and H. Klose: Channeling effects at low-energy ion implantation, EPM Dresden, 09/87

K. Lenkeit, P. Gehrmann, R. Stolle: Bestimmung von Durchbruchswinkeln beim Axial-Flächenübergang in Silizium, XVII. Allunionskonferenz über Wechselwirkung geladener Teilchen mit Einkristallen, Moskau, Mai 1987 (Russisch)

P. Gehrmann, K. Lenkeit, V. I. Shulga: Der Einfluß der Energieverluste und der Vielfachstreuung auf die Bewegung der Ionen unter den Bedingungen des Axial-Flächenüberganges, XVII. Allunionskonferenz über Wechselwirkung geladener Teilchen mit Einkristallen, Moskau, Mai 1987 (russ.)

J. Bollmann, S. Grossman, A. Mertens, H. Klose und R. Wedell: Erforschung der Kanalleitung im Gebiet niedriger Energien ($\lesssim$ 10 keV) mit Hilfe der SIMS und der DLTS, XVII. Allunionskonferenz über Wechselwirkung geladener Teilchen, Moskau, Mai 1987 (russ.)

K. Holldack, H. Kerkow, and M. Reiche: Point defect migration and impurity diffusion in Si due to ion irradiation, 2nd Int. Autumn Meeting, GADEST, Garzau, 10/87

C. Ascheron, H. Klose, and W. Frentrup: Gettering of Cu in GaP due to defects generated by H^+ and He^+ bombardement, 2nd Int. Autumn Meeting, GADEST, Garzau, 10/87

M. Riedel, E. G. Rüdenauer, H. Düsterhöft et al.: Quantification of alloys and semiconductors by cross-calibrated SIMS-instruments, SIMS-VI-Conference, Versailles, 09/87

A. Vorisov, N. Goryaga, N. Kabachnik, V. Petukhov, E. Romanowski, E. Sirotinin, R. Wedell: Die Polarisation protoneninduzierter Röntgenstrahlung bei Kanalleitung; als Vortrag für die XIIth Int. Conference on Atomic Collisions in Solids/Japan, Oktober 1987

U. Krause, R. Wedell: Kritische Analyse der Berechnung von Tiefenprofilen bei Kanalleitungsimplantationen, XVII. Allunionskonferenz über Wechselwirkung geladener Teilchen mit Einkristallen, Moskau, Mai 1987 (russ.)

M. Abbas, H. Kerkow, R. Wedell: Untersuchungen von Tiefenprofilen bei Kanalleitungsimplantationen, XVII. Allunionskonferenz über Wechselwirkung geladener Teilchen mit Einkristallen, Moskau, Mai 1987 (russ.)

M. Abbas, U. Benner, W. Frentrup, H. Kerkow: Schwerionenimplantation in Si unter Kanalleitungsbedingungen, 10. Tagung "Physik und Elektronik", Berlin, 10/87

K. Holldack, H. Kerkow, M. Gericke, M. Reiche: Hochtemperaturimplantation in Si, 10. Tagung "Physik und Elektronik", Berlin, 10/87

H. Kerkow, K. Holldack: Defect flux effects during ion implantation, EPM Dresden, 1987

K. Holldack, H. Kerkow: Impurity Redistribution in Silicon due to Ion Bombardment, EPM Dresden, 1987

K. Holldack, H. Kerkow: Radiation-enhanced diffusion in silicon due to ion bombardment, 4th Working Meeting on Radiation Interaction, Leipzig, 1987

M. Griepentrog, H. Düsterhöft, W. Schneider: Untersuchung und Charakterisierung von Katodenmaterialien mit Ionen- und Elektronenstrahlen, 1. Int. Fachtagung "Lichttechnik", Berlin, Januar 1987

E. Zena, M. Griepentrog, W. D. Müller: SIMS-Untersuchungen an edelmetallmodifizierten Nickel-Kobalt-spinellbeschichteten Titanelektroden, 5. Tagung Festkörperphysik, Karl-Marx-Stadt, 07/87

J. Bollmann, H. Klose und K. Maass: Zur Auswertung von DLT-Spektren bei hohen Konzentrationen tiefer Zentren in oberflächennahen Bereichen, 18. Tagung Physik der Halbleiteroberfläche, Binz, 04/87

H. Düsterhöft u.a.: Optimierung von Katodenmaterialien, Posterbeitrag zur Verteidigung wissenschaftl. Höchstleistungen und volkswirtschaftl. bedeutsamer Leistungen vor dem Wissenschaftl. Beirat Physik des MHF, Karl-Marx-Stadt, 02/87

M. Abbas, U. Benner: Kanalleitungsimplantationen in Silizium, 12. Arbeitstagung über Ionenimplantation und Ionenstrahltechnologie, Reinhardsbrunn, März/April 1987

M. Griepentrog: Ionenstrahlgestützte Modifizierung von Katodenmaterialien, Herbstschule des ZIE zu Elektrodenphänomenen, Bad Stuer, 12/87

H. Klose und J. Bollmann: Zur Bestimmung von Defektverteilungen in Silizium, gehalten in der MGU am 18. 06. 87

H. Klose: Channelingeffekte niederenergetischer Ionen in Silizium, IFP der SOAN, Novosibirsk, 24. 06. 1987

K. Lenkeit: Experimentelle und theoretische Untersuchungen zu richtungsabhängigen Effekten von leichten Ionen in Kristallen, Weiterbildungsveranstaltung zu modernen Problemen der Kern- und Atomphysik, MGU, Moskau, Januar 1987

B. Lukasch: Die Rutherford-Rückstreutechnik für halbleiterrelevante Probleme, Vortrag im HSE-Kolloquium, VEB WF Berlin, gehalten am 18. 09. 1987

H. Düsterhöft: Energieverteilungen und quantitative SIMS-Analyse, 2. SIMS-Seminar in Dresden am 15. 10. 1987

M. Griepentrog: Neue Werkstoffe, Verfahren und Temperaturstrahlen in der Lichtquellentechnologie, Ukley, 13./14.04.1987

BERGAKADEMIE FREIBERG, SEKTION PHYSIK, WB ANGEWANDTE PHYSIK

VERÖFFENTLICHUNGEN

Unterricker, S., Kim Jung Ho, W. Stolz, D. Degering: Investigations on the location and construction of a low background γ-spectrometer.
1) Proceedings 4th Meeting on Nuclear Analytical Methods, Dresden May 4 - 8, 1987, p. 584.
+ Vortrag

Degering, D., S. Unterricker, W. Stolz: Charged particle activation analysis of geological samples at the Rossendorf cyclotron. 1) p. 182. + Vortrag

Docekal, A., W. Stolz, O. Leeder: Spaltspurenalter natürlicher Gläser. 1) p. 190. + Vortrag

Leeder, O., S. Müller, D. Degering, S. Unterricker, W. Stolz: Rare earth element (REE) investigations in calcites of various origin by instrumental neutron activation analysis (INAA). 1) p. 270. + Vortrag

Stolz, W., S. Unterricker, J. H. Kim: Germanium als Detektor für ionisierende Strahlung. Freiberger Forschungshefte A 767 (1987) 89

Pietzsch, C., U. Thieme: RT-Mössbaueruntersuchungen zur Karbidbildung beim Anlassen des Stahls 62SiCr5. Wissenschaftliche Berichte der AdW der DDR, ZFW Nr. 34 (1987) 72 - 74

PROMOTIONEN A (DR. RER. NAT.)

Kim Jung Ho: Ein Beitrag zur low-level-γ-Spektrometrie und Bestimmung niedriger Aktivitäten. Bergakademie Freiberg, 2. 7. 1987

Sarenio, O.: Elektrochemisch geätzte Polycarbonatspurdetektoren zur Messung von Radon und Zerfallsprodukten. Bergakademie Freiberg, 11. 12. 1987

VORTRÄGE

Militzer, H., W. Stolz: Beobachtungen, physikalische und petrophysikalische Grundlagenuntersuchungen zur Radonfreisetzung an tiefreichenden Störungen. KAPG-Tagung, Neubrandenburg, 21. 4. 1987

Heinicke, J., H. Militzer, W. Stolz: Eine neue gerätetechnische Lösung zur Aufnahme und Auswertung anomaler Radonverteilungen im Verlaufe geodynamischer Prozesse. KAPG-Tagung, Neubrandenburg, 21. 4. 1987

Krbetschek, M., W. Stolz: Thermolumineszenzdatierung quartärer Sedimente; 34. Jahrestagung der Gesellschaft für Geologische Wissenschaften der DDR, Freiberg, 11. 9. 1987

Unterricker, S.: TDPAC-Untersuchungen zur Strahlenschädigung und zur Struktur von implantierten Halbleitern. Verteidigung wiss. Höchstleistungen, TU Karl-Marx-Stadt, 5. 2. 1987 (Poster)

Unterricker, S.: Possibilities of the TDPAC method for the diagnosis of radiation damage and annealing process in implanted semiconductors. EPM 87, Dresden, Sept. 7 - 11, 1987 (Poster).

Unterricker, S.: TDPAC investigations of implanted tetrahedrally coordinated semiconductors - structure of amorphized zones and correlation between binding type and annealing behaviour. XXII Zakopane School on Physics, Zakopane (Poland) May 8 - 15, 1987 (Poster)

Pietzsch, C., G. Schreiber, U. Thieme: Mössbauer- und Röntgenbeugungsuntersuchungen zur Karbidphasenbildung beim Anlassen des martensitischen Federstahls 62SiCr5.
5. Tagung Festkörperanalytik, TU Karl-Marx-Stadt, 30. 6. - 3. 7. 1987